

Development of crosslinkable, thermoplastic polyurethanes for cardiovascular prostheses

By

Jacobus Petrus Theron

Dissertation presented for the degree of
Doctor of Philosophy (Chemical Engineering)

In the
Department of Process Engineering
At the
University of Stellenbosch



Supervisors:



Prof. J.H. Knoetze
Department of Process Engineering
University of Stellenbosch



Dr. D. Bezuidenhout
Cardiovascular Research Unit
University of Cape Town



Prof. R.D. Sanderson
Institute for Polymer Science
University of Stellenbosch

Stellenbosch

December 2006

Declaration

I, the undersigned, hereby declare that the work contained in this dissertation is my own original work and that I have not previously in its entirety or in part submitted it at any university for a degree

.....

Jacobus Petrus Theron

.....

Date

Abstract

Existing thermoplastic polyurethanes (TPUs), used in the manufacturing of cardiovascular devices, still have unproven long-term biostability and may be prone to excessive plastic deformation when subjected to cyclic loading. These negative aspects can be attributed to, among other factors, the weak nature of virtual crosslinking through microphase separation. The modification and covalent crosslinking of existing medical grade polyurethanes with unsaturated acyl chlorides are thus proposed to improve these properties.

A model compound study was used to find a suitable acyl chloride (4-pentenoyl chloride), confirm the intended carbamate nitrogen as successful reaction site and to optimize the chemistry of the reaction. Two medical grade polyurethanes, Pellethane[®] 2363-80AE (Pellethane) and PurSil[®] 35-80A (PurSil), were subsequently successfully modified with 4-pentenoyl chloride. The degree of modification could be accurately controlled ($R^2 = 0.99$) to between 4.5% to 20.0% and between 11.5% to 18.5% for the respective polyurethanes.

The degree of modification and method of crosslinking were then optimized to obtain the required mechanical properties (i.e. minimum hysteresis). The hysteresis and creep of the modified and crosslinked Pellethane were reduced by 42.5% and 44.0%, respectively, while the hysteresis of the modified and crosslinked PurSil was reduced by 12.9%.

The chemical stability of Pellethane (control) modified Pellethane (15% modification) and crosslinked Pellethane (Pell15.0) was evaluated in an *in vitro* degradation study. The hysteresis of the crosslinked polymer was at least 27.5% better when compared to Pellethane, and showed a significant resistance to surface degradation (as studied with scanning electron microscopy). Although the soft phases in both polyurethanes are vulnerable toward degradation, it was not as pronounced in Pell15.0, mainly due to the restriction of chain movement resulting from the crosslinking.

Small-diameter tubular constructs, with similar fiber and wall thicknesses, were electrospun from Pellethane and the 15% modified Pellethane. A standard electrospinning technique was used in the case of the former while in the case of the latter a novel “reactive” electrospinning technique was used for the *in situ* crosslinking of the novel material, while simultaneously forming the tubular constructs.

It is suggested that the manufacturing of Pell15.0 be scaled up to produce adequate amounts of material to enable the extrusion and *in vivo* evaluation of e.g. pacemaker leads. A circulatory animal model, e.g. a senescent baboon model, could be used to evaluate and further optimize the electrospun tubular constructs.

Opsomming

Beskikbare termoplastiese poliuretane, wat gebruik word in die vervaardiging van kardiovaskulêre toestelle het nog nie 'n lang termyn rekord van biostabiliteit nie en is ook nog geneig tot geweldige plastiese deformatsie, wanneer dit blootgestel word aan sikliese lading. Hierdie negatiewe aspekte is te wyte aan onder andere, die swak virtuele kruisbinding wat bewerkstellig word deur mikrofase skeiding. Die modifikasie en kovalente kruisbinding van beskikbare mediese graad poliuretane deur die gebruik van asiel chloriede word dus voorgestel om die eienskappe daarvan te verbeter.

In 'n model komponent studie is 'n toepaslike asiel chloried (4-pentenoïel chloried) gevind, bewys is gelewer van die suksesvolle reaksie met die karbamaat stikstof en die betrokke chemie is geoptimeer. Twee mediese graad poliuretane Pellethane[®] 2363-80AE (Pellethane) en PurSil[®] 35-80A (PurSil) is daarop volgens gemodifiseer met die 4-pentenoïel chloried. Die graad van modifikasie kon akkuraat beheer word tussen 4.5% tot 20.0% vir Pellethane en tussen 11.5% tot 18.5% vir PurSil.

Die graad van modifikasie en kruisbinding is toe geoptimeer om die verlangde meganiese eienskappe (histerese) te verkry. Dit was moontlik om die histerese en kruip van die gemodifiseerde en gekruisbinde Pellethane met sowat 42.5% en 44.0%, onderskeidelik te verbeter, terwyl die histerese van die gemodifiseerde en gekruisbinde PurSil met sowat 12.9% verbeter is.

'n *In vitro* degradasie studie is gebruik om die chemiese stabiliteit van Pellethane (kontrole) en die gemodifiseerde (15% gemodifiseerd) en gekruisbinde Pellethane (Pell15.0) te vergelyk. Die histerese van die gekruisbinde polimeer was ten minste 27.5% beter in vergeleke met die Pellethane en het ook beduidende weerstand gebied teen oppervlak degradasie, soos bestudeer met skandering elektron mikroskopie. Alhoewel die sagte segmente in beide poliuretane vatbaar is vir degradasie, was dit nie so merkbaar in Pell15.0 nie, weens die beperkte beweging van die kettings a.g.v die kruisbinding.

Buisvormige konstruksies met klein diameter en met dieselfde draad en wanddikte is elektries gewef van Pellethane, deur van standaard tegnieke gebruik te maak. 'n Nuwe "reaktiewe" weef proses is vervolgens gebruik om die 15% gemodifiseerde Pellethane *in situ* te kruisbind, terwyl die buisvormige konstruksie gevorm is.

Dit word voorgestel dat die produksie van Pell15.0 opgeskaleer moet word om genoegsame produk te kan lewer om die ekstrusie van die materiaal moontlik te maak om sodoende die *in vivo* evaluering van bv. pasaangeër drade te kan ondersoek. 'n Sirkulerende diere model bv. 'n bobbejaan model, kan gebruik word in die veredere optimering van die gewefde pypagtige konstruksies.

Acknowledgements

I would like to express my sincere thanks to the following people and institutions:

Prof. J.H. Knoetze, Prof. R.D. Sanderson and Dr. D. Bezuidenhout, who supervised this dissertation, for their advice, guidance and encouragement throughout this study.

My friends and colleagues at the Cardiovascular Research Unit, University of Cape Town, especially Prof. Peter Zilla, for his limitless support and motivation, Lawrence Higham, Anel Oosthuysen and Johann Eygelaar.

Medtronic Inc. (Minneapolis, USA) for their financial support.

A very special word of thanks to Prof. R. Hunter and Dr. Gareth Arnott for their invaluable advice and support with the model urethane compound study and also to Dr. M. Bredenkamp, for his help and advice.

Mynhardt and Maretha Theron, my parents, and the rest of my family, for their motivation and support. I will be forever grateful to you and I would like to dedicate this thesis to you.

My friends who stood by me through thick and thin.

My Lord and Savior.

Contents

DECLARATION	i
ABSTRACT	ii
OPSOMMING	iii
ACKNOWLEDGEMENTS	iv
CHAPTER 1	1
INTRODUCTION	1
1.1 GENERAL INTRODUCTION.....	1
1.2 CONSIDERATIONS.....	2
1.3 OBJECTIVES.....	3
1.4 LAYOUT OF DISSERTATION.....	4
1.5 REFERENCES.....	6
CHAPTER 2	8
POLYURETHANES AS BIOMATERIAL: BACKGROUND AND THEORETICAL CONSIDERATIONS	8
ABSTRACT.....	8
2.1 INTRODUCTION.....	9
2.2 HISTORY.....	10
2.3 POLYURETHANE SYNTHESIS.....	11
2.3.1 <i>Reaction conditions</i>	11
2.3.2 <i>Raw materials</i>	12
2.4 BIOSTABILITY OF POLYURETHANES.....	12
2.4.1 <i>Hydrolysis</i>	13
2.4.2 <i>Oxidation</i>	14
2.4.2.1 <i>Autoxidation</i>	15
2.4.2.2 <i>Metal ion induced oxidation</i>	15
2.4.3 <i>Mineralization (calcification)</i>	16
2.4.4 <i>Sterilization</i>	16
2.4.5 <i>Biological catalysis of degradation</i>	16
2.4.5.1 <i>Enzymes</i>	16
2.4.5.2 <i>Cells</i>	17
2.4.6 <i>Environmental stress cracking</i>	17
2.5 MECHANICAL PROPERTIES OF MEDICAL GRADE POLYURETHANES.....	18
2.6 INFLUENCE OF POLYURETHANE CHEMISTRY ON BIOSTABILITY AND MECHANICAL PROPERTIES.....	20
2.6.1 <i>Diisocyanate</i>	20
2.6.2 <i>Polymeric diol</i>	21
2.6.3 <i>Chain extender</i>	21
2.7 PROPOSED POLYURETHANE REQUIREMENTS FOR THE MANUFACTURE OF CARDIOVASCULAR DEVICES.....	22
2.8 CONCLUSIONS.....	23
2.9 REFERENCES.....	23
CHAPTER 3	26
MODEL URETHANE COMPOUND STUDY	26
ABSTRACT.....	26
3.1 INTRODUCTION.....	27
3.2 HISTORICAL.....	28
3.2.1 <i>Synthesis and modification of the model urethane compound</i>	28
3.2.2 <i>Functionalization of carbamate-containing organic compounds</i>	29
3.3 THEORETICAL CONSIDERATIONS RELATED TO THE MODIFICATION OF THE CARBAMATE NITROGEN.....	30
3.3.1 <i>Basicity and nucleophilicity of the carbamate nitrogen</i>	30
3.3.2 <i>Acyl chlorides as possible modification reagent</i>	31
3.3.3 <i>Reaction approach</i>	32

3.3.3.1 Increasing the electrophilicity of the acyl chloride.....	32
3.3.3.2 Increasing the nucleophilicity of the carbamate nitrogen.....	33
3.4 EXPERIMENTAL	33
3.4.1 <i>Materials</i>	33
3.4.2 <i>Synthesis of the model urethane compound</i>	34
3.4.3 <i>Acylation of model urethane compound</i>	35
3.4.3.1 Small-scale reactions.....	35
3.4.3.2 Scale-up and purification of product.....	36
3.4.4 <i>Analyses</i>	37
3.4.4.1 Thin-layer chromatography.....	37
3.4.4.2 Preparative thin-layer chromatography.....	37
3.4.4.3 Nuclear magnetic resonance spectroscopy.....	38
3.4.4.4 High-resolution mass spectroscopy.....	38
3.4.4.5 Matrix-assisted laser desorption/ionization.....	38
3.5 RESULTS AND DISCUSSION	38
3.5.1 <i>Synthesis of the model urethane compound</i>	38
3.5.2 <i>Acylation of model compound</i>	41
3.5.2.1 Acylation using hexanoyl chloride.....	41
3.5.2.2 Acylation using unsaturated acyl chlorides.....	46
3.5.2.3 Acylation using 4-pentenoyl chloride.....	47
3.6 CONCLUSIONS	52
3.7 REFERENCES.....	53
CHAPTER 4.....	55
POLYURETHANE MODIFICATION.....	55
ABSTRACT	55
4.1 INTRODUCTION.....	56
4.2 HISTORICAL.....	57
4.2.1 <i>Modification of existing polyurethanes for enhanced biocompatibility</i>	57
4.2.2 <i>Heat processing of existing polyurethanes with reactive monomers</i>	58
4.2.3 <i>Synthesis of novel crosslinkable polyurethanes</i>	60
4.2.4 <i>Pellethane® 2363-80AE and PurSil® 35 80A</i>	62
4.3 EXPERIMENTAL	63
4.3.1 <i>Materials</i>	63
4.3.2 <i>Modification of Pellethane® 2363-80AE</i>	63
4.3.2.1 Purification.....	63
4.3.2.2 Acylation using 4-pentenoyl chloride.....	63
4.3.2.3 Isolation of the reaction product.....	64
4.3.2.4 Changing the degree of modification.....	64
4.3.3 <i>Modification of PurSil® 35-80A</i>	65
4.3.3.1 Acylation using 4-pentenoyl chloride.....	65
4.3.3.2 Isolation of the reaction product.....	65
4.3.3.3 Changing the degree of modification.....	66
4.3.4 <i>Analyses</i>	66
4.3.4.1 Fourier-transform infrared spectroscopy.....	66
4.3.4.2 Nuclear magnetic resonance spectroscopy.....	66
4.4 RESULTS AND DISCUSSION	67
4.4.1 <i>Modification of Pellethane® 2363-80AE</i>	67
4.4.1.1 Purification.....	67
4.4.1.2 Acylation using 4-pentenoyl chloride.....	68
4.4.2 <i>Modification of PurSil® 35-80A</i>	71
4.4.2.1 Acylation using 4-pentenoyl chloride.....	71
4.5 CONCLUSIONS	75
4.6 REFERENCES.....	75
CHAPTER 5.....	78
CROSSLINKING OF NOVEL MODIFIED POLYURETHANES.....	78
ABSTRACT	78
5.1 INTRODUCTION.....	79
5.2 HISTORICAL.....	79
5.3 THEORETICAL CONSIDERATIONS IN CROSSLINKING REACTIONS	80
5.3.1 <i>Initiation systems</i>	80
5.3.1.1 Thermal initiation	81
5.3.1.2 Photochemical initiation.....	81

5.3.1.3 Gamma irradiation.....	82
5.3.2 <i>Determination of crosslinking density</i>	82
5.3.2.1 Swelling index determination.....	82
5.3.2.2 Molecular mass between crosslinks.....	82
5.4 EXPERIMENTAL.....	83
5.4.1 <i>Materials</i>	83
5.4.2 <i>Methods</i>	84
5.4.2.1 Sample preparation for crosslinking.....	84
5.4.2.2 Ultraviolet light induced crosslinking.....	84
5.4.2.3 Heat induced crosslinking.....	85
5.4.2.4 Gamma irradiation.....	85
5.4.2.5 Optimization of initiator and monomer concentrations.....	85
5.4.3 <i>Analyses</i>	86
5.4.3.1 Swelling index determination.....	86
5.4.3.2 Calculation of molecular mass between crosslinks.....	86
5.4.3.3 Tensile testing.....	87
5.4.3.4 Dynamic mechanical analysis.....	88
5.4.3.5 Statistical analysis.....	89
5.5 RESULTS AND DISCUSSION.....	89
5.5.1 <i>Crosslinking of modified Pellethane® 2363-80AE</i>	89
5.5.1.1 Swelling index.....	89
5.5.1.2 Molecular mass between crosslinks.....	93
5.5.1.3 Tensile properties.....	95
5.5.1.4 Dynamic mechanical analysis.....	100
5.5.2 <i>Crosslinking of modified PurSil® 35-80A</i>	102
5.5.2.1 Swelling index determination.....	103
5.5.2.2 Molecular mass between crosslinks.....	104
5.5.2.3 Tensile properties.....	105
5.5.2.4 Dynamic mechanical analyses.....	106
5.6 CONCLUSIONS.....	108
5.7 REFERENCES.....	108
CHAPTER 6.....	110
<i>IN VITRO CHEMICAL STABILITY ASSAY</i>.....	110
ABSTRACT.....	110
6.1 INTRODUCTION.....	111
6.2 HISTORICAL.....	111
6.3 EXPERIMENTAL.....	113
6.3.1 <i>Materials</i>	113
6.3.2 <i>Methods</i>	114
6.3.2.1 Preparation of degradation solutions.....	114
6.3.2.2 Film casting.....	114
6.3.2.3 Sample preparation.....	114
6.3.3 <i>Analyses</i>	115
6.3.3.1 Tensile testing.....	115
6.3.3.2 Dynamic mechanical analysis.....	115
6.3.3.3 Fourier-transform infrared spectroscopy.....	115
6.3.3.4 X-ray photoemission spectroscopy.....	115
6.3.3.5 Scanning electron microscopy.....	115
6.3.3.6 Statistical analysis.....	116
6.4 RESULTS AND DISCUSSION.....	116
6.4.1 <i>Tensile testing</i>	116
6.4.2 <i>Dynamic mechanical analysis</i>	119
6.4.3 <i>Fourier-transform infrared spectroscopy</i>	121
6.4.4 <i>X-ray photoemission spectroscopy</i>	124
6.4.5 <i>Scanning electron microscopy</i>	125
6.5 CONCLUSIONS.....	129
6.6 REFERENCES.....	130
CHAPTER 7.....	132
<i>ELECTROSPINNING OF TUBULAR CONSTRUCTS</i>.....	133
ABSTRACT.....	133
7.1 INTRODUCTION.....	134
7.2 POLYURETHANE PROCESSING.....	134
7.3 ELECTROSPINNING.....	135

7.4 HISTORICAL.....	136
7.5 THEORETICAL.....	138
7.5.1 Determination of porosity by apparent volume method.....	138
7.5.2 Determination of porosity by Archimedes method.....	138
7.6 EXPERIMENTAL.....	139
7.6.1 Materials.....	139
7.6.2 Methods.....	139
7.6.2.1 Electrospinning set-up.....	139
7.6.2.2 Electrospinning procedure.....	140
7.6.2.3 Scanning electron microscopy.....	140
7.6.2.4 Architectural and structural evaluation.....	140
7.6.2.5 Porosity determination.....	141
7.7 RESULTS AND DISCUSSION.....	141
7.7.1 Fiber and wall thickness.....	142
7.7.2 Porosity evaluation.....	145
7.8 CONCLUSIONS.....	145
7.9 REFERENCES.....	145
CHAPTER 8.....	148
CONCLUSIONS AND RECOMMENDATIONS FOR FUTURE WORK.....	148
8.1 INTRODUCTION.....	148
8.2 CONCLUSIONS.....	148
8.2.1 Background and theoretical considerations of polyurethanes as biomaterial.....	148
8.2.2 Potential modification of the carbamate nitrogen with an acyl chloride.....	149
8.2.3 Model compound synthesis and optimization of acylation chemistry.....	149
8.2.4 Modification of existing polyurethanes.....	149
8.2.5 Optimization of the degree of modification and crosslinking.....	150
8.2.6 In vitro chemical stability assay.....	150
8.2.7 Manufacturing of tubular constructs.....	151
8.3 MAJOR CONTRIBUTIONS.....	151
8.4 RECOMMENDATIONS FOR FUTURE RESEARCH.....	152
APPENDICES.....	153
APPENDIX A RAW MATERIALS AND PROPERTIES OF POLYURETHANES.....	154
APPENDIX B SOLUBILITY OF SELECTED POLYURETHANES.....	158
APPENDIX C DETERMINATION OF SOLVENT SOLUBILITY PARAMETERS.....	159
APPENDIX D CROSSLINKING OF NOVEL MODIFIED POLYURETHANES.....	163
APPENDIX E LISTING OF POLYURETHANE IN VITRO DEGRADATION STUDIES.....	165
APPENDIX F ELECTROSPINNING OF CARDIOVASCULAR AND OTHER MEDICAL DEVICES.....	170
APPENDIX G COMMUNICATION OF WIDE-ANGLE X-RAY SCATTERING RESULTS.....	174
APPENDIX H SUMMARY OF BOOTSTRAP METHOD.....	175
REFERENCES.....	176

Glossary

Abbreviations	Description
1-D	One-dimensional
2-D	Two-dimensional
3-D	Three-dimensional
4-PCL	4-Pentenoyl chloride
AB	Generic polyurethane with hard and soft segments
ACA	Acetic acid
AcCl	Acryloyl chloride
AcSH	Thiolacetic acid
AFM	Atomic force microscopy
AIBN	2,2'-Azobisisobutyronitrile
AIDI	Generic aliphatic isocyanate
ArDI	Generic aromatic diisocyanate
ASTM	American standard test method
B	Base
BA	Buthylacrylate
BDO	1,4-Butanediol
BMP-2	Bone morphogenic protein 2
BnCl	Benzyl chloride
BPO	Benzoyl peroxide
BtOH	1-Butanol
BuDO	Butane diol
Caplry	Capillary
Cat	Catalogue
CB	Cathepsin B
CDCl ₃	Deuterated chloroform
CE	Cholesterol esterase
CHDI	1,4-cyclohexane diisocyanate
Co.	Company
CO	Colagenase
Conc	Concentration
CT	Computed tomography
d	Doublet
DA	Generic diamine
DAC	Diaminocyclohexane
DAMCH	1,4-Diamino cyclohexane
DBTDL	Dibutyltin dilaurate
DCM	Dichloromethane
DC	Direct current
DCP	Dicumyl peroxide
DEG	Diethylene diol
Dist	Distance
DMA	Dynamic mechanical analysis
DMAc	N,N-dimethyl acetamide
DMAP	Dimethylaminopyridine
DMF	N,N-dimethylformamide
DMPA	ω,ω -Dimethoxy- ω -phenylacetophenone
DMSO	Dimethyl sulfoxide
DNA	Deoxyribose nucleic acid
DO	Generic diol
DSC	Differential scanning calorimetry
EA	Ethyl acetate
EC	Endothelial cells
ECM	Extracellular matrices
EDA	Ethylene diamine
EDAX	Electron dispersive analysis by X-ray
EDGM	Ethylene glycol dimethacrylate
EDO	Ethane diol
EHMA	2-Ethylhexyl methacrylate
EI	Electrophile

Eq	Equation
ESCA	Electron spectroscopy for chemical analysis
ESEM	Environmental scanning electron microscopy
E-spun	Electrospun
EtOH	Ethanol
FA	Formic acid
Fiber.	Fiber thickness
FL	Florida
Flow.	Flow rate
FT-IR	Fourier-transform infrared
GPC	Gel permeation calorimetry
HBP	Hyperbranched polyamides
HDO	Hexane diol
HEMA	Hydroxy ethyl methacrylate
HEPM	Human embryonic palatal mesenchymal
HFIP	1,1,1,3,3,3-Hexafluoro-2-propanol
HLF	Human ligament fibroblast
HMDI	4,4-Methylenebis(cyclohexylisocyanate)
HMOD	Hydroxymethyl octadecanol
hMSCs	Human mesenchymal stem cells
HPLC	High-pressure liquid chromatography
HRMS	High-resolution mass spectroscopy
HTPBD	Hydroxy-terminated polybutadiene
HxCl	Hexanoyl chloride
HVK	Hoftyzer and Van Krevelen
I	Initiator
ID	Inside diameter
Inc	Incorporated
IPDI	3-isocyanatomethyl-3,5,5-trimethylcyclohexyl isocyanate
KK	Kallikrein
kV	Kilovolt
M	Monomer
MALDI	Matrix-assisted laser desorption/ionization
Mass 1	Mass of dry polymer
Mass 2	Submerged mass of dry polymer
Mass 3	Mass of swollen polymer gel
Mass 4	Submerged mass of swollen polymer gel
MbA	N,N'-methylenebisacrylamide
MC	Model compound
MDA	4,4-Methylenebis(phenylaniline)
MDI	4,4-Methylenebis(phenylisocyanate)
MeOH	Methanol
MIO	Metal ion induced oxidation
MN	Minnesota
MPC	2-methacryloylethyl phosphorylcholine
n	Number
NaH	Sodium hydride
n-BuLi	n-Butyllithium
NDI	1,5-Naphthalene diisocyanate
nHAP	Hydroxyapatite
NJ	New Jersey
NMR	Nuclear magnetic resonance spectroscopy
NRS	Non-recovered strain
Nuc	Nucleophile
p	Coefficient of statistical significance
PAA	Poly(acrylic acid)
PANi	Polyaniline
PBD	Hydrogenated polybutadiene
PBS	Phosphate buffer solution
PCDO	Polycarbonate diol
PCL	Polycaprolactone
PCLEEP	Poly(caprolactone-co-ethyl ethylene phosphate)
PCLG	Poly(caprolactone) glycol
PCN	Polycarbonate

PDMS	Poly(dimethyl siloxane)
PEA	Polyethylene adipate glycol
PED	Generic polyether diol
PEG	Poly(ethylene glycol)
PELA	Poly(ethylene-b-lactide)
Pellm	Modified Pellethane® 2363-80AE
Pellx	Modified and crosslinked Pellethane® 2363-80AE
PEO	Poly(ethylene oxide)
PesD	Generic polyester diol
PEUU	Poly(ester urethane) urea
PGA	Poly(glycolic acid)
PHMC	Poly(hexamethylene carbonate) glycol
PHECD	Poly(1,6-hydroxyl 1,2-ethyl carbonate) diol
PHMO	Poly(hexamethylene oxide)
phr	Parts per hundred resin
PIB	Hydroxy-terminated polyisobutylene
pKa	Acid dissociation constant
PKK	Prekallikrein
PLA	Poly(lactide)
PLCL	Poly(L-lactide-co-caprolactone)
PLGA	Poly(D,L-lactide-co-glycolide)
PMMA	Poly(methyl methacrylate)
PMN	Neutrophils
PO	Polyol
POADA	Poly(oxyalkylene) diamine
POPG	Poly(propylene oxide) glycol
PPG	Poly(propylene glycol)
PTG	Polymer Technology Group
PTLC	Preparative thin layer chromatography
PTMEG	Poly(tetramethylene oxide) glycol
PTMO	Poly(tetra methylene oxide)
PU	Polyurethane
Purm	Modified PurSil® 35-80A
Purx	Modified and crosslinked PurSil® 35-80A
PUU	Poly(urethane urea)
PVA	Poly(vinyl alcohol)
PVC	Poly(vinyl chloride)
PVDF	Poly(vinylidene fluoride)
q	Quartet
r	Linear regression coefficient
R	Alkyl or aryl
R ²	Regression coefficient
Ref	Reference
RT	Room temperature
s	Singlet
SAXS	Small-angle X-ray scattering
SEM	Scanning electron microscopy
SPU	Segmented polyurethane
SMC	Smooth muscle cells
std dev	Standard deviation
ST-gelatin	Styrenated gelatin
t	Triplet
TBAI	Tetrabutylammonium iodide
TDI	Toluene diisocyanate (2,4-2,6)
TGA	Thermal gravimetric analysis
THF	Tetrahydrofuran
TLC	Thin layer chromatography
TMPTA	Trimethylolpropane triacrylate
TMPTMA	Trimethylol propane trimethacrylate
TMS	Tetramethylsilane
TODI	Methylene bis(toluene isocyanate)
TPU	Thermoplastic polyurethane
USA	United States of America
UV	Ultraviolet

Volt	Voltage
WBC	White blood cells
X	Leaving group
XO	Xanthine oxidase
XPS	X-ray photoemission spectroscopy

Symbols	Description	Units
Δ	Difference	[-]
ΔG_M	Gibbs free energy of mixing	[J/mol]
ΔH_M	Enthalpy of mixing per unit volume	[J/cm ³]
Δh_M	Enthalpy of mixing	[J/mol]
ΔH_{vap}	Molar heat of evaporation	[J/mol]
ΔS_M	Entropy of mixing	[J/mol]
Δ_T	Lydersen correction for non-ideality	[-]
ΔU	Internal energy per mole	[J/mol]
α	Molar aggregation number	[-]
δ_1	Solvent solubility parameter	[MPa ^{1/2}]
δ_2	Polymer solubility parameter	[MPa ^{1/2}]
δ_C	Carbon shift	[ppm]
δ_{dij}	Contribution of dispersion of components i and j to the solubility parameter	[MPa ^{1/2}]
δ_{nij}	Contribution of hydrogen bonding of components i and j to the solubility parameter	[MPa ^{1/2}]
δ_H	Proton shift	[ppm]
δ_{ij}	Solvent solubility parameter of components i and j	[MPa ^{1/2}]
δ_{pij}	Contribution of polar forces of components i and j to the solubility parameter	[MPa ^{1/2}]
ϵ_b	Elongation at break	[%]
ϕ_{ij}	Volume fractions of components i and j	[-]
γ_w	Water contact angle	[-]
ρ	Density	[g/cm ³]
ρ_1	Density of the solvent in the swollen gel	[g/cm ³]
ρ_2	Density of the swollen gel	[g/cm ³]
σ_b	Stress at break	[MPa]
v_2	Volume fraction of the polymer in the swollen gel	[-]
[DCP]	Dicumyl peroxide concentration	[%]
[DMPA]	ω,ω -Dimethoxy- ω -phenylacetophenone concentration	[%]
B	Base value	[-]
e	Cohesive energy density in the amorphous state	[MPa]
E_{100}	Modulus at 100% elongation	[MPa]
E_γ	Young's modulus	[MPa]
E_{coh}	Cohesive energy	[J/mol]
E_d	Dispersion force	[J/mol]
E_h	Hydrogen bonding	[J/mol]
E_p	Polar forces	[J/mol]
F	Molar attraction coefficient	[J ^{1/2} /mol ^{1/2}]
F_d	Contribution of dispersion to the molar attraction coefficient	[J ^{1/2} /mol ^{1/2}]
F_h	Contribution of hydrogen bonding to the molar attraction coefficient	[J ^{1/2} /mol ^{1/2}]
F_p	Contribution of polar forces to the molar attraction coefficient	[J ^{1/2} /mol ^{1/2}]
G'	Storage modulus	[Pa]
M_c	Molecular mass between crosslinks	[g/mol]
M_{dry}	Dry scaffold mass	[g]
M_n	Number average molar mass	[g/mol]
M_r	Molecular mass of the linear polymer	[g/mol]
M_{sub}	Submerged scaffold mass	[g]
M_w	Mass average molecular mass	[g/mol]
M_{wet}	Wet scaffold mass	[g]
\bar{n}	Number of repeat units per polymer chain segment	[-]
p	Statistical significance coefficient	[-]
Q	Swelling index	[-]

R^2	Regression coefficient	[-]
R	Universal gas constant	[J/mol.K]
r	Linear correlation coefficient	[-]
t_0	Time at point 0	[min]
t_{90}	Time at point 90	[min]
T	Temperature	[K]
T_1	First polyurethane transition temperature	[°C]
T_2	Second polyurethane transition temperature	[°C]
V	Specific volume	[cm ³ /mol]
v_1	Specific volume of the solvent	[cm ³ /mol]
V_1	Volume of solvent in swollen polymer gel	[cm ³]
V_2	Volume of dry polymer	[cm ³]
V_3	Volume of swollen polymer gel	[cm ³]
V_a	Apparent scaffold cube volume	[cm ³]
V_g	Scaffold volume	[cm ³]
W_1	Mass of solvent in swollen gel	[g]
W_2	Mass of swollen gel	[g]
w%	Mass percentage	[%]
w/w	Mass per unit mass	[-]
X_1	Polymer-solvent interaction parameter	[-]

Chapter 1

Introduction

1.1 General introduction

The human body is inherently a very aggressive and hostile environment towards foreign objects, e.g. implantable cardiovascular devices [1]. The wide range of cardiovascular applications demands materials with versatile properties. It should be possible to process the material, using different manufacturing techniques (e.g. solvent casting or electrospinning), to economically and consistently manufacture uniform and high quality devices. While exhibiting excellent elastomeric properties, good suturability and general handling characteristics, the material should not be prone to excessive dilation (i.e. poor hysteresis). Chemical stability is one of the key demands and the material should not be susceptible to oxidation and hydrolysis, nor be prone to environmental stress cracking.

There are numerous thermoplastic polyurethanes exhibiting a unique combination of biocompatibility, toughness, biostability and surface functionality, which has led to their widespread use in implantable devices such as vascular grafts, pacemaker leads, blood bags, catheters, bladders and artificial hearts. The elastomeric properties of certain polyurethanes also make them good potential candidates for applications where interaction with, and mimicking of, soft tissue are required [2-4].

The properties of segmented polyurethanes (comprising hard and soft segments) depend not only on their chemical nature and constitutive elements, but also on the manner in which these hard and soft segments are arranged in the bulk of the polymer.

The chemical stability of polyurethanes is closely linked to the chemical nature of the macroglycol that constitutes the soft segment. Early polyurethane implants failed [5, 6] due to degradation of the hydrolytically unstable polyester macroglycols used in their synthesis. Replacement of the polyester-based soft segments with those based on polyethers provided the required *in vivo* hydrolytic stability, while retaining most of the desired mechanical properties. Subsequent studies have shown, however, that although hydrolytically stable, certain polyether urethanes are susceptible to oxidative degradation in the presence of metal ions and other strong oxidants.

Porous tissue engineered scaffolds (e.g. vascular grafts) have a large surface area to volume ratio. It is therefore important that any polyurethane used in such an application should have exceptionally good mechanical properties in order to cope with the resulting

weaker structure. As a result of the large surface area the prosthesis will also be more susceptible to *in vivo* degradation [2, 7]. Chemical stability is therefore a key issue.

Polyurethanes currently used in cardiovascular prosthesis mainly suffer from two drawbacks: 1) they still have unproven long-term biostability [4, 6, 8-19] and 2) they are prone to excessive plastic deformation [20-27], especially when used as porous implants [28]. These negative aspects can be attributed to (among other factors) the weak nature of virtual crosslinking of thermoplastic polyurethanes, through microphase separation.

In order to improve on the above the following aspects had to be considered.

1.2 Considerations

The chemical/bio-stability and the elastic response (the plastic deformation) of existing or new thermoplastic polyurethanes, especially those intended for a medical application, could be increased by chemically modifying the thermoplastic polyurethane with functional groups (pendent groups) capable of undergoing crosslinking reactions. The crosslinking reactions could be induced during (e.g. by extrusion processing) or after (e.g. by solvent casting techniques) the manufacturing of the required device so that the positive aspects of the thermoplastic materials (ease of processing and recycling) are combined with the positive aspects of thermoset materials (high elastic response and increased chemical stability resulting from the high molecular mass).

Controlling the degree of chemical modification, and therefore the crosslinking is critical when polyurethanes are considered to mimic soft tissue, such as in peripheral and coronary porous vascular graft applications, where the mechanical properties, like elastic response and compliance, and the long-term chemical stability, are among the key issues in the healing response [29-34].

Polyurethanes that are used for medical applications are often large ($M_n \geq 30\ 000$ g/mole) and very complex molecules. Hence monitoring the extent of modification, involving small molecules ($M_r = 80 - 120$ g/mole), using standard analytical techniques like nuclear magnetic resonance spectroscopy (NMR) is not a trivial task. The synthesis and use of a smaller, less complex molecule i.e. a model compound, which resembles the same hard segment of the intended medical grade polyurethane, e.g. Pellethane[®] 2363-80AE, would enable a more accurate investigation of the chemistry involved, using standard analytical techniques such as nuclear magnetic resonance spectroscopy (NMR), high resolution mass spectroscopy (HRMS) and matrix-assisted laser desorption/ionization (MALDI).

The chemistry and reaction conditions optimized in such a model urethane study could then be transferred and scaled up, in an effort to modify the polyurethanes successfully. Initial work could be focused on a well-known and existing medical grade polyurethane e.g. Pellethane[®] 2363-80AE (academic standard), whereafter other polyurethanes (e.g. PurSil[®]

35 80A) could be considered. Controlling the degree of chemical modification and hence the crosslinking accurately and reproducibly would be a key issue, as the different resulting crosslinked polyurethanes could find application in a wide range of medical products that may require different mechanical properties.

The chemical stability of the novel modified and crosslinked materials could be tested together with the untreated materials (controls) in an *in vitro* degradation study. An accelerated degradation study could be conducted at elevated temperature (higher than physiological temperature, e.g. 65 °C) using very aggressive chemicals like hydrogen peroxide and silver nitrate to simulate the oxidative conditions in the body, and especially in the presence of metal ions (e.g. found in pacemaker leads). Such conditions are frequently used to accelerate degradation conditions (see Table E1, Appendix E).

Pending the successful modification and crosslinking, Pellethane® 2363-80AE and the novel modified polyurethane material could then be used to manufacture small-diameter (1.6 mm ID) tubular constructs using an electrospinning technique, for example. An ultraviolet light source and initiator could be used to crosslink the modified polyurethane while electrospinning the tubular construct.

1.3 Objectives

The overall goal of this study was to develop crosslinkable, thermoplastic polyurethanes for cardiovascular application. In order to achieve this the following objectives were proposed:

1. Conduct a literature survey of the chemical and mechanical properties of polyurethanes available for the use as biomaterials in the development of cardiovascular prostheses.
2. Study the hard segment structure of typical existing medical grade polyurethanes (preferably an academic polyurethane standard) and the nucleophilic character of the carbamate nitrogen, then investigate the use of acyl chlorides as potential modification reagents.
3. Synthesize a model urethane compound, based on the hard segment structure of the academic polyurethane standard, in order to determine the proposed reaction between the carbamate nitrogen and an acyl chloride, find a suitable acylating agent, and then optimize the chemistry of the reaction (to later be transferred to existing medical grade polyurethanes).
4. Modify Pellethane® 2363-80AE (an existing academic standard medical grade polyurethane) and a second polyurethane (PurSil® 35 80A), for post-process crosslinking.

5. Optimize the degree of modification and method of crosslinking of the two modified polyurethanes to obtain the required mechanical properties (i.e. minimum hysteresis).
6. Evaluate the chemical stability of Pellethane[®] 2363-80AE (control) and compare it with that of the novel modified and crosslinked polyurethane material (Pellx) in an *in vitro* degradation study.
7. Manufacture tubular constructs from Pellethane[®] 2363-80AE (control) and from the novel modified polyurethane using a standard electrospinning technique in the case of the former and, in the latter, a novel “reactive” electrospinning technique for the *in situ* crosslinking of the novel material, while simultaneously forming the tubular constructs.

This dissertation is multi-disciplinary; it covers aspects of several subject areas, including: polymer science, synthetic and analytical organic chemistry and process engineering.

1.4 Layout of dissertation

This dissertation consists of eight chapters, five of which are experimental. The layout is illustrated in the flow diagram presented in Figure 1.1. Chapter 2 provides a brief background to the synthesis, degradation, mechanical properties and general medical application of polyurethanes as biomaterial.

The reactivity of the carbamate nitrogen of polyurethanes towards nucleophilic addition reactions was studied and the use of acyl chlorides as modification reagents investigated. The complexities involved in the acylation of the proposed carbamate nitrogen of medical grade polyurethanes necessitated the synthesis and use of a model compound. This is described in Chapter 3. The synthesized model compound was then used in studies to find suitable unsaturated acyl chlorides, identify the successful acylated reaction site and to optimize the reaction conditions.

In Chapter 4 the chemistry optimized in the model compound study (Chapter 3) was first transferred to Pellethane[®] 2363-80AE (an academic standard) and then to a second medical grade polyurethane, PurSil[®] 35 80A. The control of the modification reactions was also studied.

The novel modified polyurethanes were then used to study different methods of crosslinking, including heat, ultraviolet light and gamma irradiation, using different initiators and crosslinking enhancing monomers. This is described in Chapter 5. The measured swelling indices and mechanical properties (tensile testing) were used to find the optimum

degree of modification and crosslinking (i.e. lowest hysteresis) for the novel modified polyurethanes.

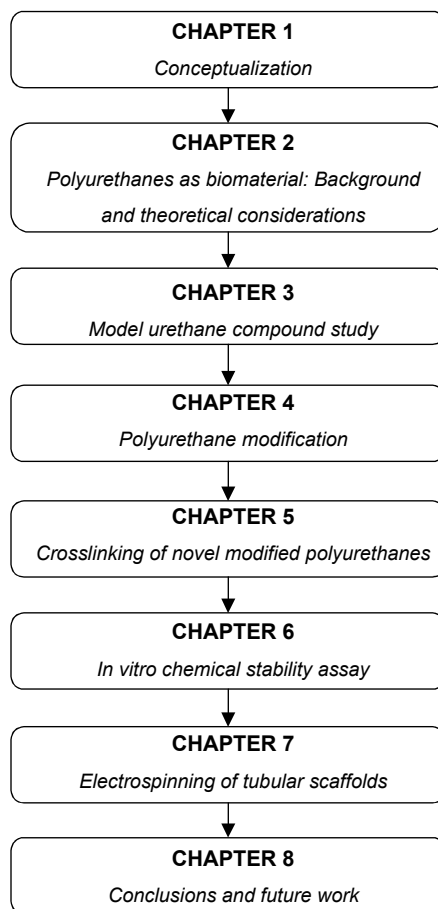


Figure 1.1 Flow diagram of thesis layout

Pellethane[®] 2363-80AE (control) and the modified and crosslinked polyurethane (PelIx) were then subjected to an *in vitro* degradation study. Changes in mechanical properties (as determined by tensile and dynamic mechanical analysis) and chemical properties (as determined by scanning electron microscopy, Fourier transform infrared spectroscopy etc.) were investigated. This is described in Chapter 6.

The electrospinning of small-diameter tubular constructs (1.6 mm ID), manufactured from Pellethane[®] 2363-80AE, was studied and then a novel “reactive” electrospinning technique was developed for the *in situ* crosslinking of the novel modified polyurethane developed in Chapter 4. This is described in Chapter 7.

In Chapter 8 the main conclusions are presented and some recommendations for future research are given.

Results of this study contribute to the fields of both the development and optimization of the mechanical properties and the *in vitro* chemical stability of crosslinkable thermoplastic polyurethanes and the fabrication of tubular constructs.

1.5 References

1. Ramakrishna, S., J. Mayer, E. Wintermantel, and K. Leong, *Biomedical applications of polymer-composite materials: A review*. Comp. Sci. and Techn., 2001. **61**: p. 1189-1224.
2. Tiwari, A., H. Salacinski, A. Seifalian, and G. Hamilton, *New prosthesis for use in bypass grafts with special emphasis*. Cardiovasc. Surg., 2001. **10**: p. 191-197.
3. Coury, A., K. Stokes, P. Cahalan, and P. Slaikou, *Biostability considerations for implantable polyurethanes*. Life Support Syst., 1987. **5**(1): p. 25-39.
4. Stokes, K., A. Coury, and P. Urbanski, *Autooxidative degradation of implanted polyether polyurethane devices*. J. Biomater. Appl., 1987. **1**(4): p. 411-448.
5. Szycher, M., *Biostability of polyurethanes: A critical review*, in *Blood Compatible Materials and Devices*, C. Sharma, Editor. 1991, Technomic: Lancaster, PA. p. 33-85.
6. Stokes, K., W. Berthelsen, and M. Davis, *Metal catalyzed oxidative degradation on implanted polyurethane devices*. ACS Division of Polymeric Materials: Science and Engineering, 1985. **6**: p. 159-169.
7. Coury, A., R. Levy, C. McMillin, Y. Pathak, B. Ratner, F. Schoen, D. Williams, and R. Williams, *Degradation of Materials in the Biological Environment*, in *Biomaterials Science: An Introduction to Materials in Medicine.*, B. Ratner, et al., Editors. 1996, Academic Press: San Diego. p. 243-281.
8. Stokes, K. and K. Cobian, *Polyether polyurethanes for implantable pacemaker leads*. Biomaterials, 1982. **3**: p. 225-231.
9. Zhao, Q., M. Agger, M. Fitzpatrick, J. Anderson, A. Hiltner, K. Stokes, and P. Urbanski, *Cellular interactions with biomaterials: in vivo cracking of pre-stressed Pellethane 2363-80A*. J. Biomed. Mater. Res., 1990. **24**(5): p. 621-637.
10. Stokes, K., P. Urbanski, and J. Upton, *The in vivo auto-oxidation of polyether polyurethane by metal ions*. J. Biomater. Sci. Polym Ed., 1990. **1**(3): p. 207-230.
11. Capone, C., *Biostability of a non-ether polyurethane*. J. Biomater. Appl., 1992. **7**(2): p. 108-129.
12. Szycher, M., A. Reed, and A. Siciliano, *In vivo testing of a biostable polyurethane*. J. Biomater. Appl., 1991. **6**(2): p. 110-130.
13. Reed, A., J. Potter, and M. Szycher, *A solution grade biostable polyurethane elastomer: ChronoFlex AR*. J. Biomater. Appl., 1994. **8**(3): p. 210-236.
14. Sutherland, K., J. Mahoney, A. Coury, and J. Eaton, *Degradation of biomaterials by phagocyte-derived oxidants*. J. Clin. Invest., 1993. **92**(5): p. 2360-2367.
15. Brandwood, A., G. Meijis, P. Gunatillake, K. Noble, K. Schindhelm, and E. Rizzardo, *In vivo evaluation of polyurethanes based on novel macrodiols and MDI*. J. Biomater. Sci. Polym. Ed., 1994. **6**: p. 41-54.
16. Joshi, R., T. Underwood, J. Frautschi, R. Phillips, F. Schoen, and R. Levy, *Calcification of polyurethanes implanted subdermally in rats is enhanced by calciphylaxis*. J. Biomed. Mater. Res., 1996. **31**: p. 201-207.
17. McCarthy, S., G. Meijis, N. Mitchell, P. Gunatillake, G. Heath, A. Brandwood, and K. Schindhelm, *In-vivo degradation of polyurethanes: transmission-FTIR microscopic characterization of polyurethanes sectioned by cryomicrotomy*. Biomaterials, 1997. **18**(21): p. 1387-1409.
18. Duguay, D., R. Labow, J. Santerre, and D. McLean, *Development of a mathematical model describing the enzymatic degradation of biomedical polyurethanes. 1. Background, rationale and model formulation*. Polym. Degr. & Stab., 1995. **47**: p. 229-249.
19. Wu, L., B. You, D. Li, and F. Qian, *The in vitro and in vivo stability of poly(urethaneurea)s as biomedical materials*. Polym. Degr. & Stab., 2000. **70**: p. 65-69.
20. Yi, J., M. Boyce, G. Lee, and E. Balizer, *Large deformation rate-dependent stress-strain behaviour of polyurea and polyurethanes*. Polymer, 2006. **47**: p. 319-329.
21. Sheth, J., E. Yilgor, B. Erenturk, H. Ozhalici, I. Yilgor, and G. Wilkes, *Structure-property behaviour of poly(dimethylsiloxane) based segmented polyurea copolymers modified with poly(propylene oxide)*. Polymer, 2005. **46**: p. 8185-8193.
22. Qi, H. and M. Boyce, *Stress-strain behaviour of thermoplastic polyurethanes*. Mech. of Mat., 2005. **37**: p. 817-839.

23. Prisacariu, C., C. Buckley, and A. Caraculacu, *Mechanical response of dibenzyl-based polyurethanes with diol chain extension*. *Polymer*, 2005. **46**: p. 3884-3894.
24. Fray, M. and V. Alstadt, *Fatigue behaviour of multiblock thermoplastic elastomers. 2. Dynamic creep of poly(aliphatic/aromatic-esters) copolymers*. *Polymer*, 2003. **44**: p. 4643-4650.
25. Abdel-Magid, B., R. Lopez-Anido, G. Smith, and S. Trofka, *Flexure creep properties of E-glass reinforced polymers*. *Comp. Struct.*, 2003. **62**: p. 247-253.
26. Zhu, H. and N. Mills, *Modelling the creep of open cell polymer foams*. *J. Mech. Phys. Solids*, 1999. **47**: p. 1437-1457.
27. Bershtein, V., P. Yakushev, N. Peschanskaya, A. Sinani, and P. Pissis, *Segmental relaxations in complex polymer system as studied by high resolution laser-interferometric creep rate spectroscopy*. *J. Non-Crystal Solids*, 1998: p. 584-586.
28. Coury, A., *Biostable Polymers as Durable Scaffolds for Tissue Engineered Vascular Prostheses*, in *Tissue Engineering of Vascular Prosthetic Grafts*, Zilla, P and Greisler, HP, Editors. 1999, R.G. Landes: Texas. p. 469-480.
29. Kidson, I. and W. Abbott, *Low compliance and arterial graft occlusion*. *Circulation*, 1978. **58**: p. 11-14.
30. Walden, R., G. L'Italien, J. Megerman, and W. Abbott, *Matched elastic properties and successful arterial grafting*. *Arch. Surg.*, 1980. **115**: p. 1166-1169.
31. Kinley, C. and A. Marble, *Compliance: a continuing problem with vascular surgery*. *J. Vasc. Surg.*, 1980. **21**: p. 163-170.
32. Abbott, W., J. Megerman, J. Hasson, G. L'Italien, and DF. Warnock, *Effect of compliance mismatch on vascular graft patency*. *J. Vasc. Surg.*, 1987. **5**: p. 376-382.
33. Stewart, S. and D. Lyman, *Effects of a vascular graft/natural artery compliance mismatch on pulsatile flow*. *J. Biomech.*, 1992. **25**: p. 297-310.
34. Weston, M., K. Rhee, and J. Tarbell, *Compliance and diameter mismatch affect the wall shear rate distribution near end-to-end anastomosis*. *J. Biomech.*, 1996. **29**: p. 187-198.

Chapter 2

Polyurethanes as biomaterial: Background and theoretical considerations

Abstract

The great variety in their chemical and physical properties makes thermoplastic polyurethanes very attractive candidates as biomaterials, especially for the mimicking of soft tissue. They are therefore generally accepted as materials of choice in many cardiovascular applications. Although not useful when first introduced in 1937 by Prof. Otto Beyer, polyurethanes have since had a long history filled with a number of historical milestones. They have also emerged as very attractive materials for use in the medical industry because of the numbers of available raw materials and reaction conditions. Thermoplastic polyurethanes also have very good processability properties. They do however have an unproven long-term biostability and suffer from plastic deformation due to the weak nature of virtual crosslinking. This chapter will provide a general background to medical grade polyurethanes.

2.1 Introduction

Due to the almost endless number of formulations that may be used to prepare polyurethanes, they offer the greatest variety of chemical and physical properties of any family of polymers. Their physical properties range from hard, rigid thermosetting materials to those of softer thermoplastic elastomers, while their chemical properties may be tailored to control durability and chemical stability. Polyurethanes have been extensively studied over the past four decades and this has led to the development of a number of medical devices, such as complaint vascular grafts and low profile pacemaker leads (see Table 2.1) [1-3], which would otherwise not have been possible.

Table 2.1: *Biomedical applications of polyurethanes* [4]

Blood bags, closures, fittings
Blood oxygenation tubing
Breast prostheses
Cardiac assist pump bladders, tubing, housing, coatings
Catheters
Dental cavity liners
Endotracheal tubes
Heart pacemaker connectors, coatings, lead insulators, fixation devices
Hemodialysis tubing, membranes, connectors
Heart valve leaflets
Mechanical heart valve coatings
Orthopedic splints, bone adhesives
Percutaneous shunts
Reconstructive surgery materials
Skin dressing and tapes
Surgical drapes
Suture material
Synthetic bile ducts
Vascular grafts and patches

The number of candidate materials available for long-term implant applications, especially those elastomeric materials required for the mimicking of soft tissue, is limited due to design, biocompatibility and availability constraints [4]. The only alternative elastomeric material to polyurethanes (PU) that has enjoyed some degree of success in the body is silicone rubber. Fluoroelastomers, such as Fluorel® (3M Co., Minneapolis, MN), which could have been a likely candidate, unfortunately require additives such as fillers and initiators which could leach out into the body over time [4].

According to Pinchuk [4] there are mainly two families of elastomers with tensile strengths in the range of that of polyurethanes (28 – 62 MPa): the amorphous nylons and the glycolated polyester terephthalates. It is well known that polyamides (nylons) are biodegradable and that the glycolated polyesters suffer from a predisposition that ester groups are susceptible to both hydrolysis and esterase enzyme activity in the body. This leaves only polyurethanes for high tensile strength applications.

2.2 History

Professor Otto Bayer introduced the first polyurethanes in 1937 (Leverkusen, Germany) when he was trying to synthesize novel fibers not covered in the polyamide (Nylon) patents held by Carothers at E.I. du Pont de Nemours & Co (1935). His first attempts involved the reactions between diamines and aliphatic diisocyanates [5, 6]. The resulting polyurea materials could not compete with the existing Nylons, mainly due to their hydrophilic nature, and were dismissed as impractical by his superiors at I.G. Farbenindustrie. Further research led to the use of high molecular mass glycols and aromatic diisocyanates, and yielded the first polyurethane elastomers. A brief summary of the milestones in polyurethane development is presented in Table 2.2.

Table 2.2: Historical milestones in polyurethane development

1937	First polyurethane patent application (I.G. Farbenindustrie)	[5]
1938	First US patent application (Rinke <i>et al.</i>)	[5]
1941	Reaction of glycols and diisocyanates	[6]
1942	Introduction of Igamid U & UL and Perlon U in Germany	[5]
1943	Vulcollan – introduction of linear polyesters to PU manufacture	[5]
1947	First rigid foams (Bayer)	[6]
1952	First flexible polyurethanes	[6]
1954	Lycra® patent (Langerak)	[5]
1955	Patent for Estane® (B.F. Goodrich)	[5]
1957	Polyether urethane foams commercially available	[6]
1958	Thermoplastic polyurethanes (TPU's) discovered	[6]
1960	US Lycra® patent awarded to Steuber (DuPont)	[5]
1971	Avcothane® patent awarded to E. Nyilas (Avco)	[5]
1972	Biomer® ((Lycra T-126)	[5]
1977	Pellethane® materials introduced (Upjohn)	[5]
1979	Second generation aliphatic polyurethanes (PU) disclosed	[5]
1984	Patent on thermoplastic elastomers awarded (M Szyzher)	[2]
1989	Biostable PU (M48) patent awarded (Coury <i>et al.</i>)	[7]
1992	Bionate® patent awarded (L. Pinchick)	[8]
1993	Chronoflex® patent awarded (M. Szyzher)	[9]
2001	Elast-Eon patent awarded (Meijs <i>et al.</i>)	[10]

It is not exactly known when polyurethanes were first introduced to the market for medical applications [4]. According to Pinchuk [4] the introduction of these materials might have come from three independent paths. The first might have been as early as the 1950s when Pangman [11] patented composite polyurethane breast prosthesis, unfortunately consisting of hydrolytically unstable polyester foams, the only commercially available polyurethane foams at the time. He continued with his research and it led to the development of the Natural-Y breast prosthesis patented in 1971 [12].

The second path might have been in the mid-1960s, when Cordis Corporation (Miami, FL) began marketing the polyurethane diagnostic catheter. The third came in 1967 with the publication by Boretos and Pierce [13], which may have stimulated the introduction of aromatic polyether urethanes, such as Biomer™ (Ethicon, Somerville, NJ) and aromatic polyether urethane pacemaker lead insulators and pacemaker connector modules by Medtronic (Minneapolis, MN) in 1977 [14].

Pacemakers require sensing and stimulation in both the ventricle and atrium and therefore multiple insulated wires have to be maneuvered to the inside of the heart. Silicone rubber as lead insulation material was found to be too bulky and it was difficult to slide one lead over another. Polyurethanes offered a solution to both the dimensional constraint and lubricity problem [4], and they had tensile strengths five times that of silicone rubber.

2.3 Polyurethane synthesis

2.3.1 Reaction conditions

In order to discuss the material properties of polyurethanes and the effect of polymer structure on such properties, a brief introduction to segmented polyurethane synthesis is required. Polyurethanes are commercially synthesized via either a “one-step” or a “multi-step” process. A “two-step” process is generally preferred in the manufacturing of medical-grade polyurethanes as greater control over the chemistry is possible, influencing the structure, physical properties, reactivity, and processability of the finished product.

In the first step of the two-step process a prepolymer (M_n up to 15000 – 20000) is synthesized from the reaction of a macromolecular diol with excess diisocyanate (Figure 2.1). In the second step, the prepolymer (and the remaining unreacted diisocyanate from the first step) is then further reacted with a diol or diamine chain extender to produce the desired segmented multiblock copolymer of type $(AB)_n$, where A denotes the soft segment and B represents the hard segment.

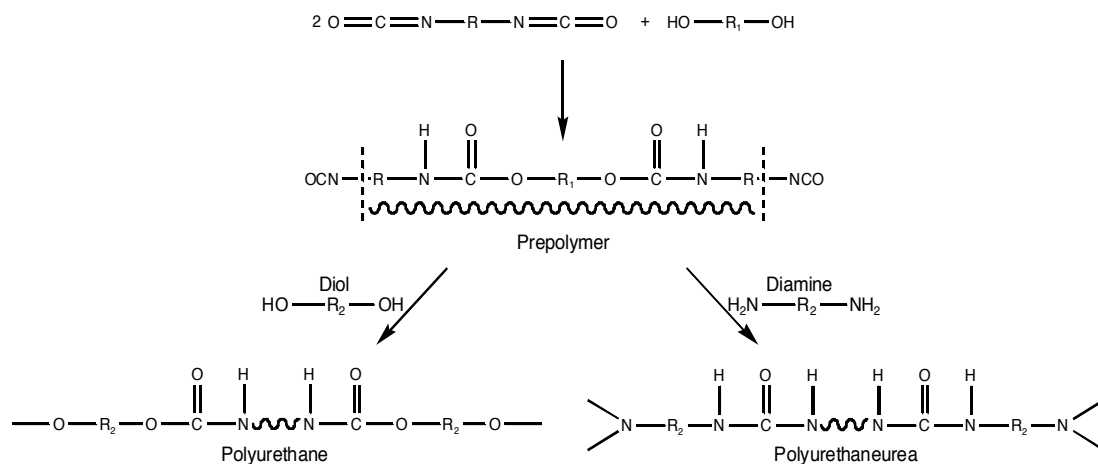


Figure 2.1: Synthesis of segmented polyurethanes and polyurethaneureas

During the synthesis the reactive diisocyanate may be involved in a number of side reactions, including [6]:

- Allophanate reactions (reaction with a urethane group)
- Biuret formation (reaction with a urea group)

- c) Acylurea (intermolecular interaction with an amide)
- d) Isocyanurate formation (trimerization of isocyanate groups)
- e) Uretidione formation (dimerization of isocyanate groups)
- f) Carbodiimide formation (reaction with another diisocyanate).

Processing considerations that also have an influence on the reaction product include: reaction temperature, stirring speed, reactor geometry, addition rates of raw materials and catalyst, choice of catalyst, and reaction medium. For example, chain extension is generally favored at temperatures below 50 °C, while higher temperatures (50 – 150 °C) will promote crosslinking and branching reactions. Reaction temperatures above 150 °C lead to dissociation of biuret and allophanate linkages and degradation of aromatic polyurethanes, while temperatures above 220 °C will result in the degradation of aliphatic polyurethanes. Catalysts commonly used in polyurethane synthesis include sodium hydroxide, sodium acetate and triamines, and transition metals (tin compounds) [6].

2.3.2 Raw materials

An almost endless number and combination of different chain extenders, diisocyanates and polymeric diols are used in the manufacturing of medical grade polyurethanes. The generic structure and some examples of commonly used raw materials used to prepare medical grade polyurethanes are summarized in Table A.1, and a non-exhaustive list of medical grade polyurethanes, including some of their physical properties, is given in Table A.2, in Appendix A.

2.4 Biostability of polyurethanes

Polyurethanes undergo a variety of degradation reactions. Polyurethane surfaces are “mobile”: in an effort to minimize free energy the hard and soft segments can rearrange in response to the biological environment [5]. If the polyurethane is hydrophobic, the degradation is usually limited to the surface, while hydrophilic polyurethanes will absorb water, leading to bulk degradation [5].

It is now generally accepted that the degradation of polyurethanes exposed to blood and extracellular fluids includes the following processes: (1) adsorption of the medium (e.g. lipids and proteins) on the polymer surface, (2) diffusion and absorption of the medium into the bulk of the polymer, (3) chemical reactions with the unstable chemical bonds in the polymer, and (4) desorption and transport of the degradation products out of the polymer matrix. Not necessarily all of the above processes occur in every case. Chemical degradation is often associated with the scission of covalent bonds, but may also involve

ionic bond transformations or even covalent crosslinking [1] and will thus lead to a compromise in the chemical and/or physical performance.

In applications of tissue-engineered scaffolds (e.g. vascular grafts) where structural integrity is required, the physical changes (swelling, crystallization, melting/crystallization loss, plasticization, fatigue fracture, creep and stress cracking) that might occur could be detrimental.

Biodegradation will be defined here as the changes in the mechanical and/or chemical properties of a biomaterial that are initiated or accelerated by the activity of the host environment. In the following sections the major factors (hydrolysis, oxidation and mineralization) involved in the biostability/biodegradation of polyurethanes are discussed.

2.4.1 Hydrolysis

Hydrolysis is the scission of susceptible molecular functional groups (e.g. ester bonds typically found in some polyurethanes) by reaction with the aqueous environment of the body. Hydrolysis may also be facilitated by polar groups in side chains of the polymer backbone [15, 16] and be catalyzed by acids, bases, salts or enzymes [17].

The urethane and urethane-urea bonds, found in poly(ether urethanes) and poly(ether urethane-ureas), although capable of hydrolyzing under accelerated conditions (e.g. months in boiling water), appear to be more stable and are not considered susceptible to hydrolysis under normal implant conditions [18]. These conditions could however occur during manufacturing processes, such as extrusion and injection molding [6]. Other bonds considered to be very stable to hydrolysis are tabulated in Table 2.3.

Table 2.3: Groups considered to be very stable to hydrolysis [17]

Structure	Group
$\begin{array}{c} \text{---CH}_2\text{---CH---} \\ \\ \text{R} \\ \text{R = H, Alkyl, Aryl} \end{array}$	Hydrocarbon
$\begin{array}{c} \text{---CX}_2\text{---CX}'_2\text{---} \\ \text{X = F, Cl, H} \\ \text{X}' = \text{F, Cl} \end{array}$	Halocarbon
$\begin{array}{c} \text{CH}_3 \\ \\ \text{---SiO---} \\ \\ \text{CH}_3 \end{array}$	Dimethylsiloxane
$\begin{array}{c} \text{O} \\ \\ \text{---S---} \\ \\ \text{O} \end{array}$	Sulfone

Factors that could suppress hydrolysis kinetics include hydrophobic moieties (e.g. hydrocarbon or fluorocarbon), crosslinking, high crystallinity due to chain order, thermal annealing or orientation, low stress and compact shape [17]. Porous hydrolyzable structures, however, undergo especially rapid property loss because of their high surface area to volume ratio.

Lamba et al. [6] illustrated the hydrolysis reactions of bonds typically involved in polyurethane degradation, as shown in Figure 2.2. As hydrolysis reactions are facilitated by water, hydrophilic polyurethanes are therefore more susceptible to hydrolytic degradation than hydrophobic polyurethanes. Extensive hydrolysis will result in the presence of deep, usually random cracks on the surface of the material, resulting from significant reduction in molecular mass [6, 17].

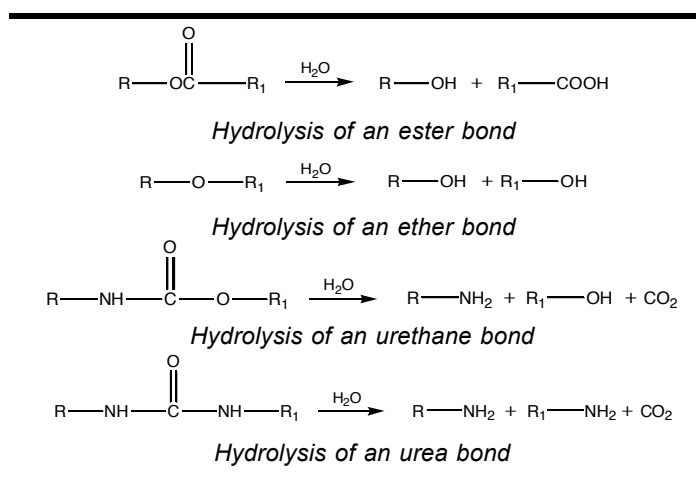


Figure 2.2: Hydrolysis reactions of polyurethanes [6]

2.4.2 Oxidation

Poly(ether urethanes) are susceptible to oxidative degradation processes. This usually requires a continuous source of oxidants (e.g. oxygen) and a means of generating free radicals [1]. Two powerful sources of free radicals are heat and ultraviolet light. There are several mechanisms of oxidation, including autoxidation and metal ion induced oxidation (MIO) (§2.4.2.2), oxidation by peroxides, free radicals, enzymes and cells (§2.4.5).

It had been suggested [4, 6] that oxidation occurs in the polyether soft segment at the α -methylene position. Degradation can also occur in the soft segment by abstraction of a hydrogen atom from the methylene carbon by free radicals. Anions and cations could catalyze the oxidation reaction in a similar manner to that in which they catalyze hydrolysis [4].

2.4.2.1 Autoxidation

Most polyurethanes undergo autoxidation, but it is considered to occur at a negligibly slow rate. Overheating (e.g. as occurring during processing or sterilization) could catalyze the reaction, resulting in the cleavage of the urethane bond between the isocyanate and the diol (Figure 2.3), ultimately leading to the formation of shallow ($\leq 10 \mu\text{m}$) “mud-cracks”.

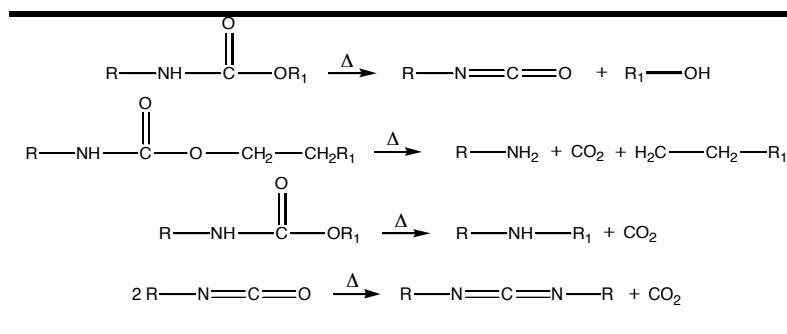


Figure 2.3: Thermal degradation of polyurethanes [6]

Autoxidation (considered as thermal oxidation) is believed to take place by a free-radical process at temperatures above 150°C [6]. A detailed description of the reactions involved is given by Stokes et al. [19]. Initiation, propagation and termination result in chain cleavage, which could be self-propagating once initiated.

2.4.2.2 Metal ion induced oxidation

The process of metal ion induced oxidation, thus far only reported in the pacemaker literature, requires a very specific set of conditions. Metal ion induced oxidation takes place on the enclosed inner surface of the pacing lead insulation near corroded metallic components and their entrapped corrosion products. Metal ions are often found at the sites of degradation: cobalt and molybdenum have been implicated as particularly vigorous promoters of metal ion induced oxidation [3]. Smooth crack walls and a microscopically random crack orientation are indicative of brittle fracture [17].

Several mechanisms have been proposed for metal ion induced oxidation, involving cell encapsulation with high concentrations of hydrogen peroxide or superoxides from cells [6]. Stokes et al. [20] have suggested that metal ion induced oxidation can possibly occur by anaerobic processes as well as autoxidation.

In the anaerobic mechanism, polymer oxidation is initiated by the abstraction of hydrogen by oxidized transition metal ions [20], but it is possible that other mechanisms could also be involved, given the complex biological environment [6].

2.4.3 Mineralization (calcification)

Mineralization is the attachment and incorporation of inorganic crystalline materials to implanted structures [1]. Micro defects (induced or enhanced by intensive flexing), neointernal surfaces or fabrication imperfections catch debris, which can nucleate the formation and growth of crystals rich in forms of calcium phosphate [1].

It predominantly occurs in devices subjected to dynamic flexing in soft tissue or in the bloodstream where mechanical activity is most pronounced. Polyurethanes subjected to gentle motion in vivo are less likely to show overt calcification [18]. Mineralization in polyurethane insulated pacemaker leads has not yet been observed, even after 3.5 years implantation [1, 18]. Mineralization of the fibrotic sheath surrounding the leads have been observed, but it had no effect on the leads [6].

2.4.4 Sterilization

The use of high-energy radiation is generally considered an attractive form of sterilization, because of the resistance that polyurethanes exhibit [6]. Extremely high doses could however have a detrimental effect and result in progressive degradation [21].

Shintani and Nakamura [22] found that γ radiation could lead to the release of MDA (methylene bis (p-phenyl aniline)) in MDI (methylene bis (p-phenyl isocyanate)) based polyurethanes, with correlation between the radiation levels and the release of MDA.

Steam sterilization has also been indicated as a contributing factor in polyurethane degradation, resulting in the formation of MDA in MDI-based polyurethanes, and suppliers have therefore cautioned the use of steam for sterilization purposes [6, 23]. Ethylene oxide treatment is usually preferred, as it causes essentially no change in the properties of the polyurethanes [24].

2.4.5 Biological catalysis of degradation

The biological degradation of polyurethanes occurs as a result of direct cellular and enzymatic interaction or by the production of oxidative or hydrolytic components. The mechanisms of enzyme and cell associated degradation can be the basic mechanisms of oxidation and hydrolysis, as described above [6]. Calcification (§2.4.3) and environmental stress cracking (§2.4.6) have been found in association with cells and enzymes [6].

2.4.5.1 Enzymes

Enzymes, whether secreted from cells or from the blood, are now known to be involved in both the hydrolysis and oxidative degradation of many different polymers,

including polyurethanes [6, 25-28]. Enzymes, including esterase, trypsin, chymotrypsin, collagenase, cathepsin B, xanthine oxidase and lysosomal liver enzymes, just to name a few, have been implicated.

A well-known and extensively studied polyurethane, Pellethane[®] 2363-80A (Dow Chemicals), is highly sensitive to especially chymotrypsin, papain and trypsin, resulting in the cleavage of the ether bond [29-31]. The exact mechanism and enzyme involved is however highly dependent on the specific polyurethane [6].

2.4.5.2 Cells

Many different cells release active compounds that affect the degradation of polyurethanes. In an extensive study conducted by Labow et al. [32] both macrophages and neutrophils have been directly implicated in polyurethane degradation. Phagocytes, macrophages and neutrophils will try to engulf the foreign material in an attempt to digest or “kill” it. It has been speculated [5, 6, 20, 31, 33] that this could occur through an oxygen-dependent or oxygen-independent mechanism.

In the oxygen-dependent mechanism, cells release superoxide anions, hydrogen peroxide, hydroxyl radicals and a host of halogenating substances, which will result in oxidative degradation. The oxygen-independent mechanism appears to involve hydrolytic enzymes.

2.4.6 Environmental stress cracking

Environmental stress cracking requires an “active chemical agent” and tensile stress. The biological environment is a particularly aggressive one and thus provides a number of possible active chemical agents [5, 6, 18, 31, 34]. Stress could be introduced during the manufacturing (e.g. extrusion or injection molding) of the specific device or due to phase separation in response to the biological environment [5].

The attachment of cells onto the surface of a polymeric material may provide an interfacial area where the cell/polymer interactions are possibly accentuated, thereby initiating surface microcracks propagated by residual (internal) stress. Applied external stress results in the elongation and enlargement of the cracks for cells to enter, thus facilitating degradation, and which can propagate deeper into the bulk [31]. Environmental stress cracking is characterized by deep ragged fractures within the polyurethane, perpendicular to the direction of the applied stress (Figure 2.4). In more advanced cases the polyurethane has three-dimensional cracks, referred to as mud-cracks [6].

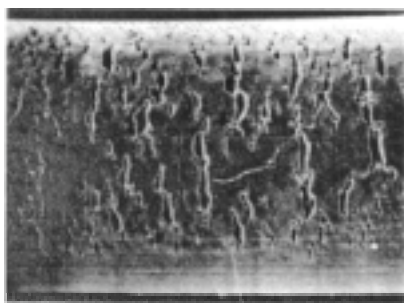


Figure 2.4: Scanning electron microscope image showing environmental stress cracking in Pellethane® 2363 80A [4]

2.5 Mechanical properties of medical grade polyurethanes

Some of the most important mechanical properties of selected medical grade polyurethanes, as summarized in Table A.2 (Appendix A), will briefly be discussed in this section.

The Pellethane 2363 medical grade polyurethane family (Dow Chemicals, USA) has been widely used since its introduction as biomaterial in 1977 [1, 3, 5, 18, 19, 24, 34, 35]. It is an aromatic poly(ether urethane) with a hard segment consisting of 4,4-methylenebis(phenylisocyanate) (MDI) and 1,4-butanediol (BDO), while its soft segment consists of poly(tetramethylene oxide) glycol (PTMEG) ($M_n = 1000$ g/mole) [18, 36-39].

It is available in a shore hardness range of (80A, 80AE, 90A, 90AE) and (55D, 55DE, 65D, 75D). The former, which is the softer, has a stress and strain at break ranging from 28.9 to 41.3 MPa and from 500 to 650%, respectively. In contrast, the harder Pellethane (D shore hardness) has a significantly higher stress at break (40.0 - 47.5 MPa), but a much lower strain at break (380 - 450%). The difference in tensile properties between the Pellethane A and D series is further evident in the large difference in their Young's moduli (13.2 MPa and 87 MPa, respectively).

Techothane TT (Thermedics, USA) is another example of a aromatic poly(ether urethane) and, like Pellethane, have hard and soft segments consisting of MDI and PTMEG, respectively, although the exact chain extender used is not known [40, 41]. Techothane TT is also available in a shore hardness of A and D, but has a much higher stress at break (41.3 - 68.9 MPa) and significantly lower strain at break (150 - 450%), when compared to Pellethane.

Tecoflex EG (Thermedics, USA) is an aliphatic poly(ether urethane) with a soft segment and chain extender consisting of PTMEG and BDO, respectively, but is based on the fully hydrogenated version of MDI namely HMDI (4,4-methylenebis (cyclohexyl isocyanate)) [18, 37, 40]. Tecoflex EG is available in a shore hardness of (80A, 85A, 93A and 100A) and (60D, 65D, 68D and 72D), respectively. Tecoflex generally has a much higher stress at break (40.0 - 57.2 MPa), but a significantly lower strain at break (310 -

660%) when compared to the Pellethane 2363 series. The stress at 100% elongation (E_{100}) of Tecoflex EG however compares very well with Pellethane 2363 for both the A and D shore hardness series.

Biospan (Polymer Technology Group, USA) is an aromatic poly(ether urethane urea) based on MDI and PTMEG, but is chain extended with a diamine [37, 42]. Biospan is only available in a shore hardness of 70A and has a stress at break of 41.3 MPa, which is comparable with Pellethane and Techothane. The strain at break of Biospan (850%) is among the highest of all polyurethanes studied, while its Young's modulus (5.9 MPa) is among the lowest.

Bionate (Polymer Technology Group, USA), an aromatic polycarbonate polyurethane, has a hard segment and chain extender, comprising MDI and BDO, respectively. Poly(1,6-hydroxyl 1,2-ethyl carbonate) diol is used as the soft segment [37, 41, 42]. It is available in a softer grade (80A and 90A) and a harder grade (55D and 75D). The stress (48.1 - 68.9 MPa) and strain (260 - 570%) at break of the Bionate series is comparable to the aromatic polyether urethane, Techothane, but has a much higher stress and lower strain at break when compared to Pellethane. The stress (37.9 - 55.2 MPa) and strain (255 - 490%) at break of Chronoflex C (Cardiotech Inc., USA) (80A, 55D, 75D), also an aromatic polycarbonate polyurethane, is more comparable to Pellethane [43].

In general, the aliphatic polycarbonate polyurethanes Chronoflex AL (Cardiotech Inc., USA) and Carbothane (Thermedics, USA) have lower stress and strain at break when compared to the aromatic polycarbonate polyurethanes Bionate and Chronoflex C [37, 40, 41, 43].

Silicones have long been known to be biostable and biocompatible in most implants [42]. Conventional silicone elastomers can have very high ultimate elongations, but unfortunately have low tensile strengths [36, 42]. Elast-Eon 3 (Aortecbio, USA), PurSil and CarboSil (Polymer Technology Group, USA) are thermoplastic copolymers containing polysiloxanes in the soft segment. These polyurethanes are prepared by a multi-step bulk synthesis where poly(dimethyl siloxane) (PDMS) is incorporated into the polymer soft segment with PTMEG (PurSil), an aliphatic hydroxyl-terminated polycarbonate (CarboSil), or poly(hexamethylene oxide) (PHMO) (Elast-Eon 3).

The hard segment of PurSil is either based on MDI (PurSil AR) or an aliphatic aromatic diisocyanate (AIDI) (PurSil AL). The stress and strain at break of PurSil AR and AL are comparable, and in the range of 24.8 MPa to 36.5 MPa and 620% to 900%, respectively. The Young's modulus of PurSil AL (1.9 MPa) is significantly lower than for PurSil AR (5.6 - 7.2 MPa). Although the stress at break of CarboSil (29.6 - 42.6 MPa) is of the same order of magnitude as that of PurSil, CarboSil has a significant lower strain at break and much higher Young's modulus than PurSil.

In the following section the influence of the raw materials on the biostability and mechanical properties of the polyurethanes will be discussed.

2.6 Influence of polyurethane chemistry on biostability and mechanical properties

Polyurethanes used in the manufacturing of medical devices are generally elastomers consisting of hard and soft chain segments. These segments are to some degree thermodynamically incompatible, resulting in a heterophase microstructure [24]. The physical and chemical properties of segmented polyurethanes depend therefore not only on the chemical nature of the raw materials and relative ratios used, but also on the structure of the resulting microphases and the interaction between these phases. The hard segments form glassy or semi-crystalline domains dispersed in the amorphous soft segment matrix. Virtual crosslinking is achieved through hydrogen bonding of the respective hard segments (glassy hardness, and where applicable, crystallinity), resulting in a material exhibiting high modulus and elastic behavior normally associated with covalently crosslinked polymers.

2.6.1 Diisocyanate

One of the main considerations in the choice of the hard segment is the use of an aromatic versus an aliphatic isocyanate. This has been a topic of much discussion over the past few years. The most frequently used aromatic isocyanate in the medical industry to date has been methylene bis(p-phenyl isocyanate) (MDI) while methylene bis(p-cyclohexyl isocyanate) (HMDI) has been the most frequently used aliphatic isocyanate [4].

Organic chemistry dictates that aromatic isocyanates should be more stable than aliphatic ones. Aromatic isocyanates are stabilized by resonance, an effect involving the sharing of π -electrons by adjacent atoms. The bond strengths of the resonance stabilized aromatic isocyanates are significantly higher than in the equivalent aliphatic molecule, thus requiring more energy to break or degrade [4, 6]. Aromatic diisocyanates (e.g. MDI) also have a rigid planar structure that provides stiffness, strength and hard-segment character to polyurethanes, while the fully hydrogenated version of MDI, namely HMDI (4,4-methylenebis(cyclohexyl isocyanate)), provides for weaker hard-segment aggregation and yields weaker polyurethanes with poorer dynamic performance, such as shorter flex life, larger stress hysteresis, lower impact and abrasion resistance [24].

Aromatic isocyanates have greater intermolecular bond strengths than aliphatic isocyanates, because of their semicrystalline nature. Crystallization of the hard segment is favored with increasing symmetry of the isocyanate, resulting in an increase in phase

separation, modulus, hardness and abrasion resistance [6]. Cycloaliphatic isocyanates, e.g. HMDI, cannot crystallize due to the configurational isomers present. HMDI can change from a boat form to a chair form, which disturbs its crystallinity [4] and will generally result in polyurethanes with poorer high-temperature properties and lower solvent resistance.

Polyurethanes based on aliphatic diisocyanates do however have certain advantages. They have been shown by Frisch et al. [44] to be more stable to alkaline hydrolysis and to have greater thermal stability [45]. They also do not yellow when exposed to light for prolonged periods of time, whereas aromatic polyurethanes may yellow. This is however only a cosmetic difference, and has no bearing on the performance of the respective polyurethanes [4].

2.6.2 Polymeric diol

The flexibility (especially at low temperatures) and the elongation at break of polyurethanes are to a large degree dependent on the polymeric diol used as the soft segment. The glass transition temperature will decrease with an increase in molecular mass of the diol and a higher degree of microphase separation is achieved, which also increases the ease of the backbone rotation in the soft segment, which ultimately results in a more extensible material [6].

The chemical stability of polyurethanes is closely linked to the chemical nature of the polymeric diol that constitutes the soft segment. Although polyurethanes synthesized from polyester-containing soft segments possess good mechanical properties, they are very sensitive to hydrolytic cleavage of the ester linkage. As an alternative, polyether soft segments provide the required *in vivo* hydrolytic stability, while maintaining most of the desired mechanical properties [1]. They have however been shown to be susceptible to oxidative degradation in the presence of metal ions and other strong oxidants [3, 18]. Poly(tetramethylene oxide) glycol (PTMEG) containing polyurethanes have comparable mechanical properties to the polyester counterparts and further possess relatively good hydrolytic stability [45].

This finding had prompted further research into possible soft segment replacement, resulting today in the incorporation of polymeric carbonates [37, 40, 41, 43, 46-50], siloxanes [36, 42, 51-53], hydrocarbons [52] and fluorinated ethers [54-56].

2.6.3 Chain extender

Polyurethanes are also strongly influenced by the chemical nature and ratio of the chain extender incorporated. An increase in the ratio of the chain extender will result in a harder, stiffer and stronger material with higher tear strength, but with lower abrasion resistance and elongation [24]. Generally, the use of aliphatic extenders leads to polymers

that are softer than those obtained with aromatic extenders [6]. The molecular mass of the extenders also has a strong influence on the crystallinity of the hard segment, which in turn will affect the physical properties of the resulting polyurethane [6].

The most commonly used chain extenders are: 1,4-butanediol used in Pellethane®, Tecoflex® and Corethane™ polyurethanes, while amine terminated chain extenders such as ethylene diamine (EDA) and 1,4-diamino cyclohexane (DAMCH) are used in polyurethanes such as Lycra®, Biomer™ and Coremer™. The resulting urea linkage renders the polyurethane difficult to extrude or mold, therefore limiting application in dip-coating or fiber production [4].

2.7 Proposed polyurethane requirements for the manufacture of cardiovascular devices

It is therefore proposed that, depending on the particular application, the polyurethane used should have the following required properties:

(A) Processability:

- It should be possible to use different manufacturing techniques (e.g. solvent casting, extrusion, electrospinning etc) to economically and consistently manufacture uniform and high quality devices.
- The use of conventional methods of sterilization should not have a negative impact on material integrity and other properties.

(B) Mechanical properties

- The intended material should be elastomeric.
- It should display good suturability and general handling characteristics.
- The material should not be prone to excessive dilation (unrecovered energy loss) when subjected to continuous cyclic stresses as in a vascular graft application.

(C) Chemical stability (biostability)

- The material should not be susceptible to oxidation and hydrolysis, nor be prone to environmental stress cracking and calcification.
- It should further not be toxic, inflammatory or thrombogenic, either in itself or upon the release of possible degradation products.

The required material should therefore preferably contain:

- Aromatic hard segments for good microphase separation

- Hydrocarbon- or siloxane-based soft segments for oxidative and stress cracking resistance
- Permanent covalent crosslinks as opposed to weak hydrogen bonds.

Two polyurethanes were selected as starting materials in this study: Pellethane[®] 2363-80AE (Dow Chemicals, USA) and PurSil[®] 35 80A (Polymer Technology Group Inc, USA). The hard segments of both these polyurethanes consist of MDI. The soft segment of the former is poly(tetramethylene oxide) glycol (PTMEG), and chain extended with 1,4-butanediol, while the latter has a soft segment consisting of 35% polydimethylsiloxane.

2.8 Conclusions

Thermoplastic polyurethanes are very attractive candidates as biomaterials due to their great flexibility in chemical and physical properties (e.g. processability) and are therefore widely used for the manufacture of a great variety of medical devices.

The body is a very aggressive environment and polyurethanes have not yet been shown to have the long-term biostability required for use as a long-term medical implants.

Polyurethanes further suffer from large energy losses (hysteresis) when subjected to continuous cyclic loading, due to the transient (weak) nature of virtual crosslinking by physical associations.

2.9 References

1. Coury, A., K. Stokes, P. Cahalan, and P. Slaikeu, *Biostability considerations for implantable polyurethanes*. Life Support Syst., 1987. **5**(1): p. 25-39.
2. Szycher, M., *Extrudable polyurethane for prosthetic devices prepared from a diisocyanate, a polytetramethylene ether polyol and 1,4 butane diol*. United States Patent Office. US 4,447,590, 1984: USA.
3. Stokes, K., A. Coury, and P. Urbanski, *Autooxidative degradation of implanted polyether polyurethane devices*. J. Biomater. Appl., 1987. **1**(4): p. 411-448.
4. Pinchuk, L., *A review of the biostability and carcinogenicity of polyurethanes in medicine and the new generation of 'biostable' polyurethanes*. J. Biomater. Sci. Polym Ed., 1994. **6**(3): p. 225-267.
5. Szycher, M., *Biostability of polyurethanes: A critical review*, in *Blood Compatible Materials and Devices*, C. Sharma, Editor. 1991, Technomic: Lancaster, PA. p. 33-85.
6. Lamba, N., K. Woodhouse, and S. Cooper, *Polyurethanes in Biomedical Applications*. 1998, Boca Raton: CRC Press.
7. Coury, A., C. Hobot, and K. Carlson, *Biostable, segmented aliphatic polyurethanes and process therefor*. United States Patent Office. US 4,873,308, 1989: USA.
8. Pinchuk, L., *Crack-resistant polycarbonate urethane polymer prostheses*. United States Patent Office. US 5,133,742, 1992: USA.
9. Szycher, M. and A. Reed, *Biostable polyurethane products*. United States Patent Office. US 5,254,662, 1993: USA.
10. Meijis, G., P. Gunatillake, and S. McCarthy, *Polysiloxane-containing polyurethane elastomeric compositions*. United States Patent Office. US 6,313,254, 2001: USA.

11. Pangman, W., *Compound prosthesis device*. United States Patent Office. US 2,842,775, 1958: USA.
12. Pangman, W., *Compound prosthesis*. United States Patent Office. US 3,559,214, 1971: USA.
13. Boretos, J. and W. Pierce, *Segmented polyurethane - a new elastomer for biomedical applications*. Science, 1967. **158**: p. 1481-1505.
14. Stokes, K. and K. Cobian, *Polyether polyurethanes for implantable pacemaker leads*. Biomaterials, 1982. **3**: p. 225-231.
15. Ossefort, Z. and Z. Testroet, *Hydrolytic stability of urethane elastomers*. Rubber Chem. Technol., 1966. **37**(17): p. 1308-1327.
16. Gahimer, F. and F. Nieske, *Hydrolytic stability of urethane and polyacrylate elastomers in the human environment*. J. Elast. Plast., 1969. **1**: p. 266-280.
17. Coury, A., R. Levy, C. McMillin, Y. Pathak, B. Ratner, F. Schoen, D. Williams, and R. Williams, *Degradation of Materials in the Biological Environment*, in *Biomaterials Science: An Introduction to Materials in Medicine.*, B. Ratner, et al., Editors. 1996, Academic Press: San Diego. p. 243-281.
18. Coury, A., P. Slaikeu, P. Cahalan, and K. Stokes, *Medical applications of implantable polyurethanes: current issues*. Prog. in Rub. & Plast. Techn., 1987. **3**(4): p. 24-37.
19. Stokes, K., W. Berthelsen, and M. Davis, *Metal catalyzed oxidative degradation on implanted polyurethane devices*. ACS Division of Polymeric Materials: Science and Engineering, 1985. **6**: p. 159-169.
20. Stokes, K., R. McVenes, and J. Andersen, *Polyurethane elastomer biostability*. J. Biomater. Appl., 1995. **9**: p. 321-354.
21. Lela, M. and S. Cooper, *Polyurethanes in Medicine*. 1986, Boca Raton, FL.: CRC Press.
22. Shintani, H. and N. Nakamura, *Formation of 4,4'-methylenedianiline in polyurethane potting materials by either gamma-ray or autoclave sterilization*. J. Biomed. Mater. Res., 1991. **25**: p. 1275-1286.
23. Szycher, M. and A. Siciliano, *An assessment of 2,4-TDA formation of a polyurethane foam under simulated physiological conditions*. J. Biomater. Appl., 1991. **5**: p. 323-351.
24. Coury, A., P. Slaikeu, P. Cahalan, K. Stokes, and C. Hobot, *Factors and interactions affecting the performance of polyurethane elastomers in medical devices*. J. Biomater. Appl., 1988. **3**: p. 130-176.
25. Santerre, J., R. Labow, and G. Adams, *Enzyme-biomaterial interactions: effect of biosystems on degradation of polyurethanes*. J. Biomed. Mater. Res., 1993. **27**(1): p. 97-109.
26. Smith, R., C. Oliver, and D. Williams, *The enzymatic degradation of polymers in vitro*. J. Biomed. Mater. Res., 1987. **21**: p. 991-1003.
27. Marchant, R., A. Hiltner, C. Hamlin, A. Rabinovitch, R. Slobodkin, and J. Andersen, *In vivo biocompatibility studies: I. The cage implant system and a biodegradable hydrogel*. J. Biomed. Mater. Res., 1983. **17**: p. 301-325.
28. Takahara, A., R. Hergenrother, A. Coury, and S. Cooper, *Effect of soft segment chemistry on the biostability of segmented polyurethanes. II. In vitro hydrolytic stability*. J. Biomed. Mater. Res., 1992. **26**: p. 801-818.
29. Ratner, B., K. Gladhill, and T. Horbett, *Analysis of in vitro enzymatic and oxidative degradation of polyurethanes*. J. Biomed. Mater. Res., 1988. **22**: p. 509-527.
30. Bouvier, M., A. Chawla, and I. Hinberg, *In vitro degradation of a poly(ether urethane) by trypsin*. J. Biomed. Mater. Res., 1991. **25**: p. 773-789.
31. Zhao, Q., M. Agger, M. Fitzpatrick, J. Anderson, A. Hiltner, K. Stokes, and P. Urbanski, *Cellular interactions with biomaterials: in vivo cracking of pre-stressed Pellethane 2363-80A*. J. Biomed. Mater. Res., 1990. **24**(5): p. 621-637.
32. Labow, R., D. Erfle, and J. Santerre, *Neutrophil-mediated degradation of segmented polyurethanes*. Biomaterials, 1995. **16**: p. 51-59.
33. Stokes, K., P. Urbanski, and J. Upton, *The in vivo auto-oxidation of polyether polyurethane by metal ions*. J. Biomater. Sci. Polym. Ed., 1990. **1**(3): p. 207-230.
34. Stokes, K., *Polyether polyurethanes: biostable or not?* J. Biomater. Appl., 1988. **3**: p. 228-259.

35. Coury, A., *Biostable Polymers as Durable Scaffolds for Tissue Engineered Vascular Prostheses.*, in *Tissue engineering of vascular prosthetic grafts*, Zilla, P and Greisler, HP, Editors. 1999, R.G. Landes: Texas. p. 469-480.
36. Martin, D., L. Warren, P. Gunatillake, S. McCarthy, G. Meis, and K. Schindhelm, *Polydimethylsiloxane/polyether-mixed macrodiol-based polyurethane elastomers: biostability.* *Biomaterials*, 2000. **21**: p. 1021-1029.
37. Zdrahala, R. and I. Zdrahala, *Biomedical applications of polyurethanes: a review of past promises, present realities, and a vibrant future.* *J. Biomater. Appl.*, 1999. **14**(1): p. 67-90.
38. Tanzi, M., D. Mantovani, P. Petrini, R. Guidoin, and G. Laroche, *Chemical stability of polyether urethanes versus polycarbonate urethanes.* *J. Biomed. Mater. Res.*, 1997. **36**(4): p. 550-559.
39. www.dowchemicals.com, *Typical physical properties of Pellethane.* [accessed: 8 June 2006].
40. www.thermedics.com, *Medical grade resins- A selection guide.* [accessed: 8 June 2006], Thermedice Inc, USA.
41. Yang, M., Z. Zhang, C. Hahn, G. Laroche, M. King, and R. Guidoin, *Totally implantable artificial hearts and left ventricular assist devices: selecting impermeable polycarbonate urethane to manufacture ventricles.* *J. Biomed. Mater. Res.*, 1999. **48**(1): p. 13-23.
42. www.polymertech.com, *The polymer technology group.* [accessed: 8 June 2006].
43. www.cardiotech-inc.com, *Polyurethane biomaterials from CT biomaterials.* [accessed: 8 June 2006].
44. Matuzak, M., K. Frisch, and S. Reegen, *Hydrolysis of linear polyurethanes and model monocarbamates.* *J. Pol. Sci., Pol. Chem. Ed.*, 1973. **11**: p. 1683-1690.
45. Fabris, H., *Thermal and oxidative stability of polyurethanes*, in *Advances in urethane science and technology*, K. Frisch and S. Reegen, Editors. 1976, Technomic: Lancaster, PA.
46. Salacinski, H., N. Tai, R. Carson, A. Edwards, G. Hamilton, and A. Seifalieu, *In vitro stability of a novel compliant poly(carbonate-urea)urethane to oxidative and hydrolytic stress.* *J. Biomed. Mater. Res.*, 2001. **59**: p. 207-218.
47. Reed, A., J. Potter, and M. Szycher, *A solution grade biostable polyurethane elastomer: ChronoFlex AR.* *J. Biomater. Appl.*, 1994. **8**(3): p. 210-236.
48. Salacinski, H., M. Odlyha, G. Hamilton, and A. Seifalian, *Thermo-mechanical analysis of a compliant poly(carbonate-urea)urethane after exposure to hydrolytic, oxidative, peroxidative and biological solutions.* *Biomaterials*, 2002. **23**: p. 2231-2240.
49. Labow, R., E. Meek, and J. Santerre, *Hydrolytic degradation of poly(carbonate)-urethanes by monocyte-derived macrophages.* *Biomaterials*, 2001. **22**: p. 3025-3033.
50. Khan, I., N. Smith, E. Jones, D. Finch, and R. Cameron, *Analysis and evaluation of a biomedical polycarbonate urethane tested in an in vitro study and an ovine arthroplasty model. Part I: materials selection and evaluation.* *Biomaterials*, 2005. **26**: p. 621-631.
51. Gunatillake, P., G. Meijs, S. McCarty, and R. Adhikari, *Poly(dimethylsiloxane)/Poly(hexamethylene oxide) mixed macrodiol based polyurethane elastomers. 1. Synthesis and properties.* *J. Appl. Polym. Sci.*, 2000. **76**: p. 2026-2040.
52. Takahara, A., A. Coury, R. Hergenrother, and S. Cooper, *Effect of soft segment chemistry on the biostability of segmented polyurethanes. I. In vitro oxidation.* *J. Biomed. Mater. Res.*, 1991. **25**(3): p. 341-356.
53. www.elastomedic.com, *Guide to Elast-Eon medical polymers.* [accessed: 15 August 2001].
54. Tonelli, C., T. Trombetta, M. Scicchitano, G. Simeone, and G. Ajroldi, *New fluorinated thermoplastic elastomers.* *J. Appl. Polym. Sci.*, 1996. **59**: p. 310-327.
55. del Guerra, R., L. Lelli, C. Tonelli, T. Trombetta, M. Cascone, M. Taveri, P. Narducci, and P. Giusti, *In vitro biocompatibility of fluorinated polyurethanes.* *J. Mater. Sci.: Materials in Medicine*, 1994. **5**: p. 452-456.
56. Simmons, A., J. Hyvarinen, R. Odell, D. Martin, P. Gunatillake, K. Noble, and L. Poole-Warren, *Long-term in vivo biostability of poly(dimethylsiloxane)/poly(hexamethylene oxide) mixed macrodiol-based polyurethane elastomers.* *Biomaterials*, 2004. **25**: p. 4887-4900.

Chapter 3

Model urethane compound study

Abstract

Difficulties in following the chemistry of the modification reactions of large, complex polyurethanes involving small molecules, prompted the synthesis of a model urethane compound as a smaller, less complex structure, but representative of the hard segment of Pellethane® 2363-80AE (academic polyurethane standard). The resulting molecule was then reacted with different acyl chlorides (including hexanoyl, acryloyl and 4-pentenoyl chloride). Reactions with hexanoyl chloride confirmed the proposed reaction site to be the carbamate nitrogen. Reaction conditions were optimized and good conversions were achieved when the nucleophilicity of the carbamate nitrogen was increased using either sodium hydride (53.3%) or butyllithium (79.1%). Reactions with 4-pentenoyl chloride simulated the introduction of latent crosslinking groups. The highest conversion was again achieved using nucleophilic enhancement with sodium hydride (51.5%) and butyllithium (63.1%). The model compound could be used to simulate and optimize the reaction between the carbamate nitrogen and selected acyl chlorides for future application to polyurethane modification via crosslinking.

3.1 Introduction

The accurate control of the modification of polyurethanes with latent crosslinking groups, and thus control over the structural crosslinking, is a critical consideration for materials intended for medical or biological applications.

Polyurethanes are large and complex molecules. The number average molecular mass (M_n) of Pellethane[®] 2363-80AE, a well-known medical grade polyurethane (PU), is approximately 45 000 g/mole. Many commercial thermoplastic polyurethanes (TPU) comprise a hard segment consisting of 4,4-methylenebis(phenylisocyanate) (MDI) and 1,4-butanediol (BDO) [1]. Pellethane[®] 2363-80AE has a soft segment consisting of poly(tetramethylene oxide) glycol (PTMEG) ($M_n = 1000$ g/mole) [2].

The size and complexity of such polyurethane molecules therefore make it almost impossible to study modification reactions involving small molecules by standard analytical techniques (including nuclear magnetic resonance spectroscopy (NMR)), due to e.g. dynamic range problems (i.e. limited concentration ranges, especially with proton NMR).

The utilization of a smaller, less complicated molecule, a so-called model compound, could hence enable more accurate investigation of the chemistry involved in modification reactions, by enabling the monitoring of reactions using standard organic chemistry techniques, such as thin layer chromatography. Quantitative analyses of the product using nuclear magnetic resonance spectroscopy (NMR), high-resolution mass spectrometry (HRMS) and matrix-assisted laser desorption/ionization (MALDI) is then also possible.

Thus, in order to avoid the complexities of macromolecules and the difficulties associated with their characterization, a model urethane compound with similar structure to the repeating hard segment of Pellethane[®] 2363-80AE (see Figure 3.1) was synthesized via the reaction between MDI and 1-butanol (BtOH) and the product then isolated, purified and characterized.

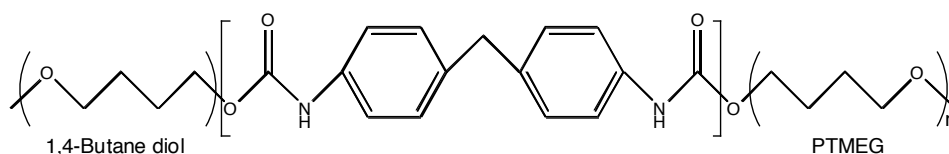


Figure 3.1: Chemical structure of Pellethane[®] 2363-80AE showing hard segment structure in square brackets

The synthesized model compound was then used to study and evaluate the acylation reaction to be used on the polymer by reaction with different candidate acyl chlorides. As the reaction may be achieved by either increasing the strength of the nucleophile (carbamate nitrogen), or by improving the electrophilicity of the modification agent (acyl chloride), both routes were investigated. The complicating factor, however, lay in the fact

that the concept requires the modification reagent to also contain a second group that is unaffected by the modification reaction, but is capable of crosslinking the modified material at a later stage (in this case, an acrylate or a vinyl was desirable). It was therefore hoped that results of the model compound study would identify an effective acylating agent and appropriate acylation conditions, which would yield a product that would still be effective in crosslinking.

These two aspects were separated such that optimized acylation conditions were initially identified using an acyl chloride with a long saturated aliphatic tail (e.g. hexanoyl chloride). Reactions were subsequently carried out with other acyl chlorides containing unsaturated groups capable of remaining stable during the N-acylation reaction in order to address the crosslinking aspect.

3.2 Historical

3.2.1 Synthesis and modification of the model urethane compound

As the hard segments of most commercial TPUs are based on MDI and BDO, it is no surprise that model compounds containing MDI and BDO have been investigated by a number of authors [1, 3-8]. Most have focused on either the kinetics involved in the reaction between various diisocyanates and alcohols, including MDI and BDO [8], or the physical properties of these materials [3-5, 8], while one study [1] has investigated reactions between model compounds and several common functional groups.

Although the references mentioned above do not include the acylation reactions intended in the current study, it is considered useful to describe the most applicable reactions in some further detail.

Caraculacu and Agherghinei [8] described a new method of following the kinetics of uncatalyzed reactions between diisocyanates and alcohols (including MDI and BtOH). Their method allowed for the determination of the concentration of all species occurring during the reaction by means of high-performance liquid chromatography. It was found that the relationship between the unchanged fraction and the fraction that reacts, theoretically inferred for ideal systems (null catalytic effect), is validated over the whole reaction for real systems. The rate constant for the reaction between MDI and BtOH was found to be equal to 1.36 in comparison to 3.07 when a mixture of methanol and 1-butanol was used instead.

Yang et al. [3] found that terminal hydroxyl groups facilitated the thermal degradation of carbamate groups. Lu et al. [1] therefore chose model urethanes with hydrocarbon end groups in the high temperature reaction studies. They first prepared a model compound by capping MDI with BtOH. The reactions between the model compound and various mono-functional compounds, as well as two model poly(ethylene glycols), were studied at elevated temperatures (170 – 200 °C). Carbamate conversion was measured, by NMR, in

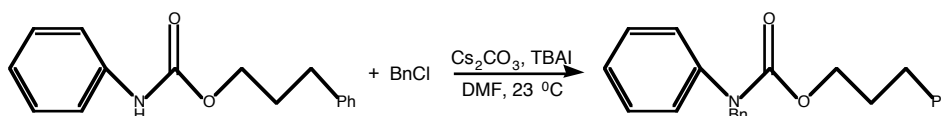
this kinetic study. The ranking of reactivity of the functional groups with the model compound was found to be: primary amine > secondary amine >>> hydroxyl ~ acid ~ anhydride >>> epoxide.

Model compounds (similar to the one used in the current study) were successfully synthesized and characterized. The rate constant for the uncatalyzed reaction between MDI and BtOH was found to be low, while model compounds with terminal hydroxyl groups would not only surely lead to polymerization, but also facilitate thermal degradation. Modification reactions involving the carbamate moiety of the model compound were carried out under vigorous reaction conditions (high temperatures), not necessarily suitable for the intended future modification of polyurethanes.

Functionalization of the carbamate moiety, an important structural element of biological active compounds, has played a crucial role in synthetic organic chemistry [9]. It offers great potential e.g. in the generation of large combinatorial libraries for rapid screening and drug design [9]. Reactions with other small organic compounds containing carbamate moieties not necessarily similar to the specific one under investigation in this dissertation are considered useful and a brief overview will be given.

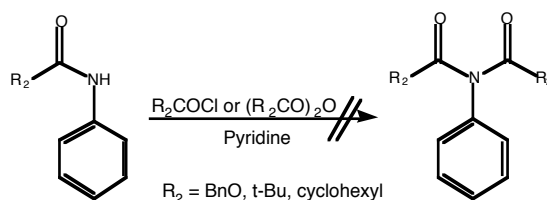
3.2.2 Functionalization of carbamate-containing organic compounds

Salvatore et al. [9] reported on the use of cesium carbonate (Cs_2CO_3) and tetrabutylammonium iodide (TBAI), which serve as base and catalyst, respectively, in the chemoselective alkylation of various aliphatic and aromatic carbamates. In one such an example (Scheme 3.1) an aromatic carbamate was alkylated and a yield of up to 98% was achieved using benzyl chloride (BnCl) as alkylating agent (at room temperature) in N,N-dimethylformamide as solvent. In a further example, however, the reaction with cyclooctyl carbamate (aliphatic carbamate) was not successful and the developed method proved to be very sensitive to the chemical structure of the carbamate.



Scheme 3.1: N-Alkylation of an aromatic carbamate using benzyl chloride [9]

Similarly, also in the context of N-acylation of a nitrogen molecule attached to a carbonyl group, Kondo et al. [10] attempted to synthesize N-acylanilides (Scheme 3.2), using acyl chloride or anhydride in pyridine, as a potentially good leaving group for the chemoselective acylation of amino groups, but did not succeed.



Scheme 3.2: Attempted synthesis of *N*-acylanilides [10]

Surprisingly, no successful examples could be found in the open literature on the acylation of small carbamate containing organic molecules. It can only be concluded that the proposed *N*-acylation of the carbamate moiety, as described in this dissertation, is not a trivial problem and that it may require the use of harsh reaction conditions, involving e.g. the use of a strong base like sodium hydride or *n*-butyllithium, to enhance the nucleophilicity of the carbamate nitrogen.

3.3 Theoretical considerations related to the modification of the carbamate nitrogen

3.3.1 Basicity and nucleophilicity of the carbamate nitrogen

Nucleophilicity is the ability of a donor atom (nitrogen) to form a bond by electron donation (δ^-). The lone pair of electrons on the nitrogen atom thus generally renders amines basic and nucleophilic. The pK_a values of the conjugated acids of simple amines increase (i.e. increase in basicity) with increasing alkyl substitution; this is due to the electron release from the alkyl groups, up to the di-alkylamine level [11]. The pK_a values of some conjugated acids in water at 25 °C are given in Table 3.1.

Table 3.1: pK_a values for some conjugated acids in water at 25 °C [11]

Amine	pK_a
NH_3	9.25
$\text{C}_2\text{H}_5\text{NH}_2$	10.80
$(\text{C}_2\text{H}_5)_2\text{NH}$	16.09
$(\text{C}_2\text{H}_5)_3\text{N}$	10.85
$\text{C}_6\text{H}_4\text{NH}_2$	4.58
$\text{C}_6\text{H}_4\text{N}(\text{C}_2\text{H}_5)_2$	6.56

Aromatic amines are generally less basic, and nucleophilic, than their alkyl counterparts because of back donation of the nitrogen lone pair into the aromatic p system, therefore rendering it less available for direct reaction (+R effect).

Carbamates, on the other hand, are even less basic, and nucleophilic, than aromatic amines [11]. Not only is the lone electron pair (on the nitrogen) compromised by back donation into the aromatic p system (as described above), but also because of

delocalization into the carbonyl group, rendering the nitrogen atom even less available for direct reaction (Figure 3.2).

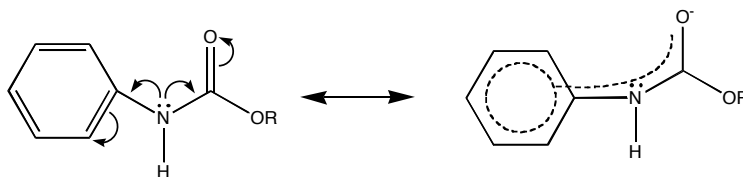


Figure 3.2: Resonance structure of the carbamate nitrogen

3.3.2 Acyl chlorides as possible modification reagent

Many important functional groups used in organic chemistry contain a carbonyl group (CO): aldehydes, ketones, carboxylic acids, esters, amides, etc.

The carbon of a C=O bond is sp^2 hybridized and, further, lies in the same plane as the atoms attached to it, with bond angles around 120° . The carbon – oxygen bond length is typically ≈ 120 pm in aldehydes and ketones compared to ≈ 140 pm in alcohols and ethers. Oxygen is more electronegative than carbon and the C=O bond is polarized accordingly (Figure 3.3).

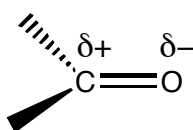


Figure 3.3: Polarization of the carbonyl bond

As a result, substrates of the type $R(CO)X$ (where X is referred to as the leaving group and R forms part of the substrate) are very reactive towards nucleophilic substitution. They are, for example, much more reactive than the corresponding RCH_2X type substrates. The three main reasons for the enhanced reactivity of $R(CO)X$ can be given as follows. (1) The carbonyl carbon has a sizeable partial positive charge that makes it very attractive to nucleophiles. (2) In a tetrahedral mechanism (mechanism involved in substrates of the type $R(CO)X$) π electrons shift, which requires much less energy than in the SN_2 reactions (RCH_2X) where a σ bond must break in the rate-determining step. (3) A trigonal carbon offers less steric hindrance to a nucleophile than a tetrahedral carbon [11]. An illustration of the generalized mechanism for the addition step is given in Figure 3.4.

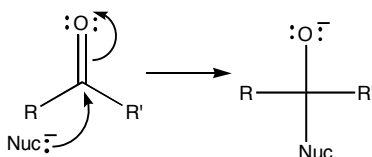


Figure 3.4: Generalized mechanism for the nucleophilic addition step

The leaving group (X) has a direct influence in the success and rate of the nucleophilic substitution reaction and affects the reactivity of the substrate. It alters the electron density at the carbonyl carbon, which affects the rate of the reaction. The greater the electron withdrawing character of X, the greater the partial positive charge on the carbon atom and the more rapid the attack by the nucleophile. The following sequence in reactivity is hence obtained: $R(CO)Cl$ (acid chloride) $>$ $R(CO)O(CO)R'$ $>$ $R(CO)OAr$ $>$ $R(CO)OR'$ $>$ $R(CO)NH_2$ $>$ $R(CO)NR'_2$ $>$ $R(CO)O^-$ [11].

Hydrogen atoms alpha to the carbonyl are acidic and may be abstracted by a strong base or an anion, resulting in the formation of an enolate ion, as illustrated in Figure 3.5.

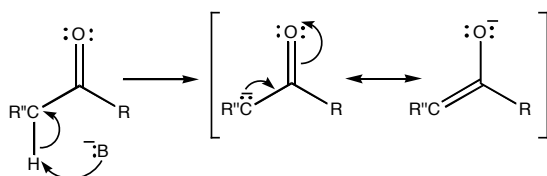


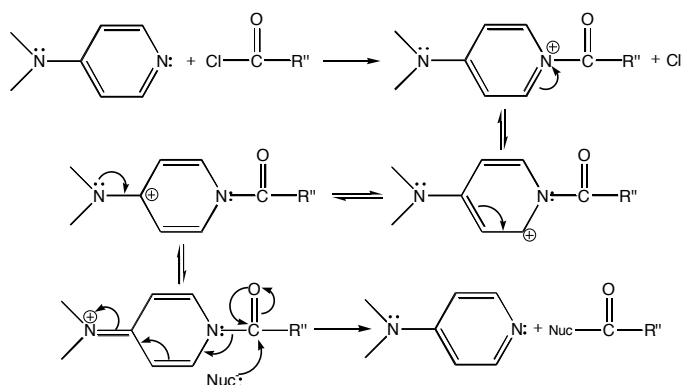
Figure 3.5: Resonance structure showing formation of the enolate atom

The proton is acidic because the carbonyl group can stabilize the negative charge. The pKa of an alpha proton in a ketone is ≈ 20 and a strong base such as n-butyllithium can remove it. The pKa of an alpha proton in a 1,3-dicarbonyl compound is ≈ 10 and a base such as an ethoxide ion can remove it [11].

3.3.3 Reaction approach

3.3.3.1 Increasing the electrophilicity of the acyl chloride

Although acyl chlorides are generally good electrophiles (as discussed in §3.3.2) their electrophilic character can further be enhanced by increasing its leaving group potential. Acylpyridinium salts e.g. enhance the acylating potential of acyl chlorides, because pyridine is a better leaving group and it is neutral compared to e.g. anionic chloride.



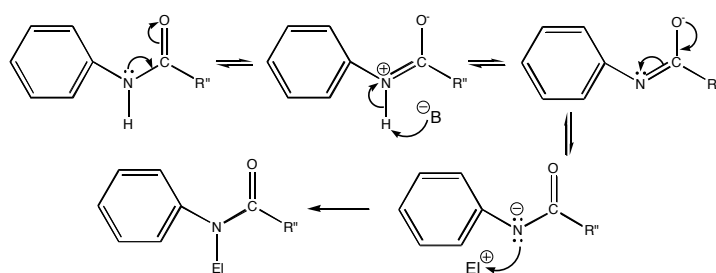
Scheme 3.3: Resonance structures of the dimethylaminopyridine-acylpyridinium salt, illustrating electrophilic enhancement

Delocalizing the cationic charge of the acylpyridinium species can further enhance this character, as is illustrated in Scheme 3.3. A good example of such a species is dimethylaminopyridine-acylpyridinium salt. Other species could also include imidazole.

3.3.3.2 Increasing the nucleophilicity of the carbamate nitrogen

The nucleophilic character of the nitrogen of carbamates can be enhanced by ionizing the carbamate. A strong base can be used to deprotonate the amide, rendering a strong base and also enhancing the nucleophilicity of the amide (Scheme 3.4).

Strong bases that have the potential to deprotonate the amide include n-butyllithium and sodium hydride.



Scheme 3.4: Resonance structures of the carbamate, illustrating nucleophilic enhancement

3.4 Experimental

3.4.1 Materials

The following materials were used for the preparation of the model urethane compound. Methylenebis(p-phenylisocyanate) (Aldrich, Cat: 25,643-9) and 1-butanol (Riedel-de Haën, Cat: 34931) were used as the only two reagents. Tetrahydrofuran (THF) (Merck, Cat: AB009731) was used as solvent and dibutyltin dilaurate (DBTDL) (Aldrich, Cat: 29,123-4) as catalyst. n-Hexane was obtained from Merck (Cat: 152496G). Molecular sieves (Riedel-de Haën Cat: 31812) were used as drying agent for the tetrahydrofuran, which was freshly distilled.

The following materials were used for the acylation, extraction and purification of the model urethane compound. A number of acyl chlorides were investigated, including: acryloyl chloride (Aldrich, Cat: A2,410-9), hexanoyl chloride (Aldrich, Cat: 29,465-9) and 4-pentenoyl chloride (Aldrich, Cat: 46,847-9). N,N-dimethylformamide (DMF) (Aldrich, Cat: 27,054-7) and dichloromethane (DCM) (Aldrich, Cat: 27,099-7) were used as solvents. n-Butyllithium (Aldrich, Cat: 18,617-1), 60% (w%) sodium hydride (Fluka, Cat: 71620) (strong bases) and dimethylaminopyridine (DMAP) (Aldrich, Cat: 10,770-0) (acyl transfer agent).

Diisopropylethylamine (Hünig's base) (Aldrich, Cat: 49,621-9) and pyridine (Aldrich, Cat: 27,040-7) were used as acid acceptors.

Thin-layer chromatography plates (TLC) with aluminum support (Merck, Cat: 1.05554.0001) were used for monitoring purposes, and preparative thin-layer chromatography plates (PTLC) with glass support (Merck, Cat: 5717) for the separation of reaction products. A mixture of ethyl acetate (Merck (SA), Cat: 2235020) and petroleum ether (Merck (SA), Cat: 4947040) were used as mobile phases.

3.4.2 Synthesis of the model urethane compound

The experimental formulation for the preparation of 50 g (theoretical yield) of the model compound (chemical structure which is given later in Scheme 3.5) is summarized in Table 3.3. A fifty percent excess of 1-butanol was used.

A 1000-ml round-bottomed flask was fitted with a thermometer, inert gas (He) inlet, gas outlet, magnetic follower, a cooled condenser and a heating mantle.

Table 3.3: Formulation of model compound synthesis

Reactants	Mass (g)
1-Butanol (BtOH)	27.96
Tetrahydrofuran (THF)	280.00
4,4-Methylenebis(phenylisocyanate)	31.46
Dibutyltin dilaurate (DBTDL)	0.10

The reaction vessel was charged with the 1-butanol, and water was removed by azeotropic distillation (93 °C). The condenser was then removed and the helium flow rate set at 3 l/min. After cooling to 40 °C and addition of 120 g of THF, DBTDL (0.10 g) (catalyst) was added and the reaction mixture re-heated to 50 °C.

Pre-dissolved MDI (31.46 g in 160 g THF) was subsequently added to the vessel over 5 - 10 min, from a dropping funnel. After 5 h of reaction at 50 °C the heating source was removed. The reaction mixture was allowed to cool to room temperature (RT, ≈20 °C) and thereafter reacted for an additional 17 h. The reaction was performed throughout under constant stirring and inert (He) atmosphere.

Excess solvent was removed by bubbling with helium gas, and the concentrated product recovered by precipitation in a 10-fold excess of cold n-hexane (-10 °C). After drying (under vacuum, RT, 24 h) the product was purified by redissolving in THF and precipitating with n-hexane, before calculation of the yield.

3.4.3 Acylation of model urethane compound

Reactions involving an array of different reagents and solvents were first performed on small scale (0.5 mmol) involving two reaction approaches (see §3.4.3.1A and §3.4.3.1B) and the reactions were qualitatively analyzed using thin-layer chromatography (TLC). Selected reactions were scaled up (§3.4.3.2) and products separated by preparative thin-layer chromatography. The products were then quantitatively analyzed by nuclear magnetic resonance spectroscopy, high-resolution mass spectroscopy and matrix-assisted laser desorption/ionization.

3.4.3.1 Small-scale reactions

A: Increasing the nucleophilicity of the carbamate nitrogen

A 25-ml round-bottomed reaction vessel was supplied with a septum and inert gas supply. Reactions were carried out under anhydrous conditions using freshly distilled solvents under an inert atmosphere (helium gas). Either sodium hydride or n-butyllithium was selected as base.

Sodium hydride (1.25 mmol) and THF (2 ml) were added to the reactor and cooled to below 0 °C, using a mixture of ice and ethanol. The model compound, pre-dissolved in 1 ml of THF, was then slowly added to the reactor over 5 min and the resulting mixture was left for 30 min to allow the formation of the anion.

When n-butyllithium was used as base, the pre-dissolved model compound was first added to the reactor, whereafter the contents were cooled down (below 0 °C), followed by the addition of the n-butyllithium (dropwise over 5 min) (see Table 3.4 for list of reactants and formulation used).

Table 3.4: Formulation for acylation reactions of the model compound (compound 1) to increase nucleophilicity

Components	Reactants	Quantity	Mass
1. Strong base	1.1 Sodium hydride (NaH)	1.25 mmol	0.05 g
	1.2 n-Butyllithium (n-BuLi)	1.25 mmol	0.53 g
2. Solvent	2.1 Tetrahydrofuran (THF)	3.0 ml	2.64 g
3. Starting material	3.1 Model compound (MC)	0.5 mmol	0.20 g
4. Acyl chloride	4.1 Acryloyl chloride (AcCl)	2.0 mmol	0.18 g
	4.2 Hexanoyl chloride (HxCl)	2.0 mmol	0.27 g
	4.3 4-Pentenoyl chloride (4-PCI)	2.0 mmol	0.24 g

Four molar equivalents (two-fold excess) of acyl chloride were added dropwise over a period of 15 - 20 min using a syringe and the resulting mixture was left for 30 min at 0 °C, whereafter the ice-bath was removed and the reaction mixture allowed to warm to room temperature (≈ 20 °C). Reactions were monitored using TLC, and stopped after 60 min.

B: Increasing the electrophilicity of the acyl chloride

A 25-ml round-bottomed reaction vessel was supplied with a septum and inert gas supply. Reactions were carried out under anhydrous conditions using freshly distilled solvents under an inert atmosphere (helium gas).

Table 3.5: Formulation for acylation reactions of the model compound (compound 1) to increase electrophilicity

Components	Reactants	Quantity	Mass
1. Acid acceptor	1.1 Hunig's base	2.0 mmol	0.26 g
	1.2 Pyridine	2.0 mmol	0.16 g
2. Acyl transfer agent	2.1 Dimethylaminopyridine (DMAP)	0.2 mmol	0.03 g
3. Solvent	3.1 Tetrahydrofuran (THF)	3.0 ml	2.64 g
	3.2 Dichloromethane (DCM)	3.0 ml	3.96 g
4. Starting material	4.1 Model compound (MC)	0.5 mmol	0.20 g
5. Acyl chloride	5.1 Acryloyl chloride (AcCl)	2.0 mmol	0.18 g
	5.2 Hexanoyl chloride (HxCl)	2.0 mmol	0.27 g
	5.3 4-Pentenoyl chloride (4-PCI)	2.0 mmol	0.24 g

The reactor was charged with the acyl transfer agent, acid acceptor (base for HCl) and 2 ml of solvent. The model compound (which was pre-dissolved in 1 ml of solvent) was then added to the reactor over 5 min, and the resulting mixture was cooled down to below 0 °C using a bath containing a mixture of ice and ethanol.

Four molar equivalents (two times excess) of acyl chloride were then added dropwise over a period of 15 - 20 min using a syringe. The resulting mixture was left for 30 min at 0 °C, whereafter the ice-bath was removed and the reaction mixture allowed to warm to room temperature (≈ 20 °C). See Table 3.5 for a list of the reactants and the formulation used. Reactions were monitored using TLC, and stopped after 24 h.

3.4.3.2 Scale-up and purification of product

The selected reactions were then scaled up (by a factor of 5) in order to produce sufficient crude product for separation into the respective fractions using gravity columns

and preparative TLC, and for subsequent characterization. The synthesis method as described in §3.3.3.1 was used for the initial reactions, followed by the following additional steps.

The reaction product was diluted with 150 ml of diethyl ether and transferred to a 250-ml separating funnel. The excess base was neutralized using 50 ml of saturated ammonium chloride and washed four times with water (4 x 50 ml) to remove most of the unreacted reagents (including the salt formed during the reaction with the free metal ion of the strong base). After an additional wash with a saturated sodium chloride solution, the product-rich phase was transferred to a beaker, dried with anhydrous magnesium sulphate, filtered, and the solvent removed *in vacuo* on a rotary evaporator.

The dried product was dissolved in a sparing volume of diethyl ether and carefully transferred to a gravity column pre-packed with silica-gel. A product to silica-gel ratio of approximately 1:50 was used with a 15% ethyl acetate/petroleum ether mixture as mobile phase to elute the product. The fractions were evaporated on a Büchi rotary-evaporator.

3.4.4 Analyses

3.4.4.1 Thin-layer chromatography

Approximately 0.3 - 0.5 ml of sample was withdrawn from the reactor during reactions and quenched in saturated ammonium chloride, after which the product was extracted into ethyl acetate. TLC was used to monitor the progress of the reaction. The TLC plates were spotted and allowed to develop in a 15% ethyl acetate/petroleum ether mixture, whereafter the plates were visualized with 254-nm ultraviolet light (UV).

3.4.4.2 Preparative thin-layer chromatography

No more than 100 mg of product was dissolved in a sparing volume of diethyl ether. A syringe and needle was used and the product was applied to the preparative-TLC plate as a very thin line, approximately 20 mm from the bottom of the plate.

A 5% mixture of ethyl acetate/petroleum ether was used as mobile phase. After the plate was allowed to run in the mobile phase, it was removed and carefully dried. This was repeated five times or until good separation was achieved.

The regions on the plate where the different fractions were observed by UV were carefully marked and scraped off the plate, whereafter they were extracted, with ethyl acetate, and vacuum dried.

3.4.4.3 Nuclear magnetic resonance spectroscopy

Approximately 40 - 60 mg of product was dissolved in deuterated chloroform. ^1H and ^{13}C NMR spectra of the sample were obtained from a Varian Unity 400 spectrometer at 400 and 100 MHz frequency respectively. Chemical shifts are reported as δ (ppm) - values relative to tetramethylsilane (TMS) as internal reference.

3.4.4.4 High-resolution mass spectroscopy

High-resolution mass spectroscopy was performed at the University of the Witwatersrand, South Africa, on a Micromass VG 70SEQ MS. A direct insertion probe with sample introduction was used with a positive polarity. Four scans/decade were used and the mass range was 3000 amu/8 kV.

3.4.4.5 Matrix-assisted laser desorption/ionization

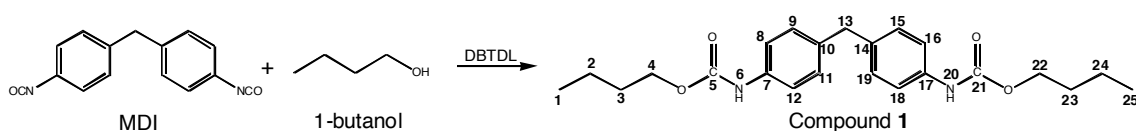
Approximately 1 – 2 mg of product was diluted 1:100 with tetrahydrofuran. A saturated solution of 2,5-dihydroxybenzoic acid in deuterated water was used as matrix. One microliter of the matrix was applied to a MALDI P100 gold sample plate and 1 μl of sample added by mixing it with a micropipette. The spot was then allowed to completely dry under a gentle stream of air in order to crystallize the matrix and trap the sample in the crystals. After crystal formation was confirmed by light microscopy, the plate was then inserted into a Perspective Biosystems Voyager DE-PRO Biospectrometry Workstation (which possesses delayed extraction technology) for analysis.

The sample was analyzed using the positive ion method, with an accelerating voltage of 20 kV, grid voltage of 94%, guide wire voltage of 0.05%, delayed extraction at 250 ns, and laser intensity of 2600. Spectra were captured using Perspective Grams/32(R) v.4.14.

3.5 Results and discussion

3.5.1 Synthesis of the model urethane compound

The reaction scheme for the synthesis of the urethane model compound (compound 1) is presented below (Scheme 3.5).



Scheme 3.5: Synthesis of model urethane compound (compound 1)

A final yield of 93% (mass %) was calculated. The signals of the recorded ^1H and ^{13}C NMR spectra (Figure 3.6 and Figure 3.7) were assigned on the basis of chemical shifts and multiplicities.

The characteristic signal at 6.62 ppm in the ^1H NMR spectrum (Figure 3.6) was assigned to the N-H hydrogen of the carbamate group while the resonance at 3.87 ppm was attributed to the methylene protons between the two aryl rings (Ar_2CH_2). These signals are important and sensitive signatures for monitoring structured changes within the model urethane compound on acylation [1].

The methylene protons (H -4, 22) α to oxygen were observed at 4.15 ppm (expected at 4.1 - 4.2 ppm) [12] and the absence of a signal at 3.6 ppm indicated full conversion of 1-butanol.

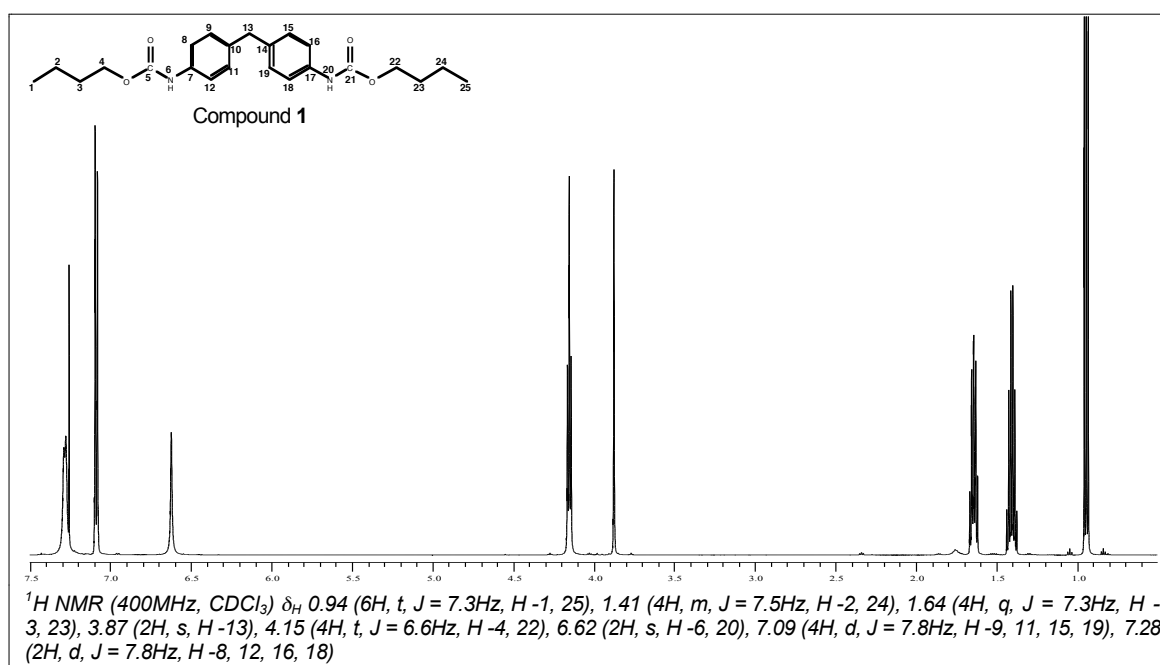


Figure 3.6: ^1H NMR spectrum of compound 1 showing structure and assignment of signals

The signals of the ^{13}C spectrum were assigned and found to be consistent with the proposed product (compound 1). The distinctive signals of deuterated chloroform (CDCl_3) solvent were observed at 77.3 ppm (Figure 3.7), the terminal methyl (C -1, 25) at 13.9 ppm, the carbonyl carbons (C -5, 21) at 154.0 ppm, while the characteristic methylene carbon signal (for the carbon attached to the oxygen of the ester) (C -4, 22) was observed at 65.3 ppm [13].

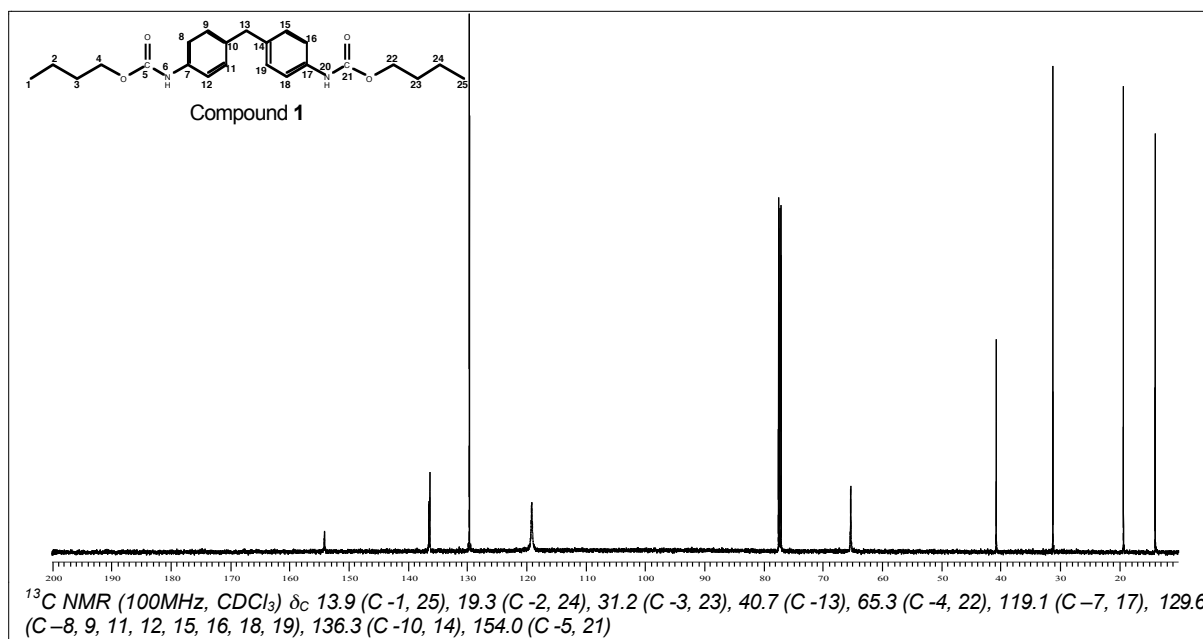


Figure 3.7: ^{13}C NMR spectrum of compound 1 showing assignment of signals

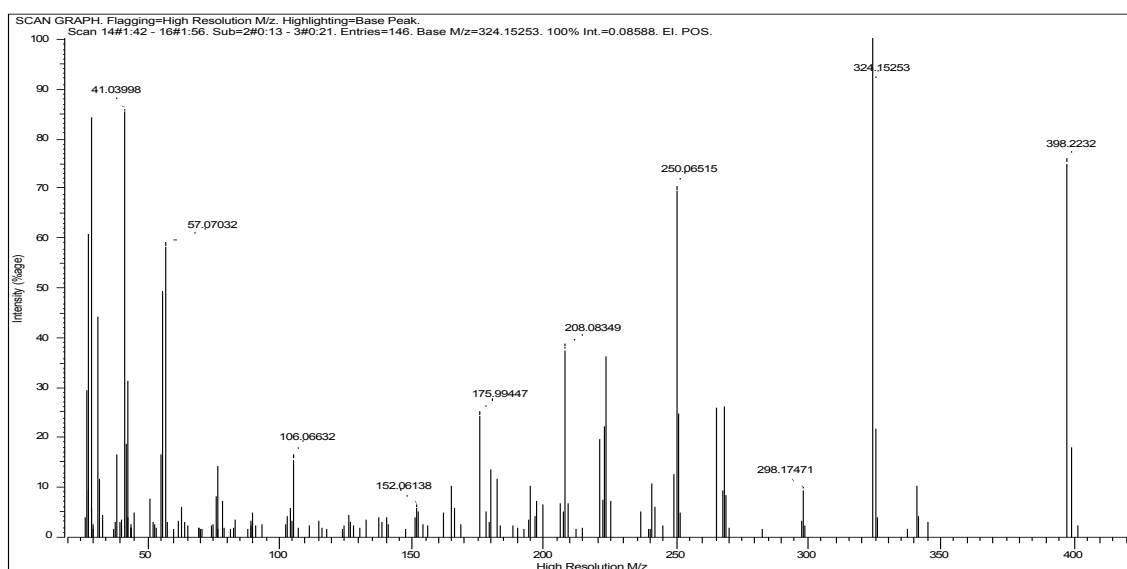


Figure 3.8: High-resolution mass spectrometry of compound 1

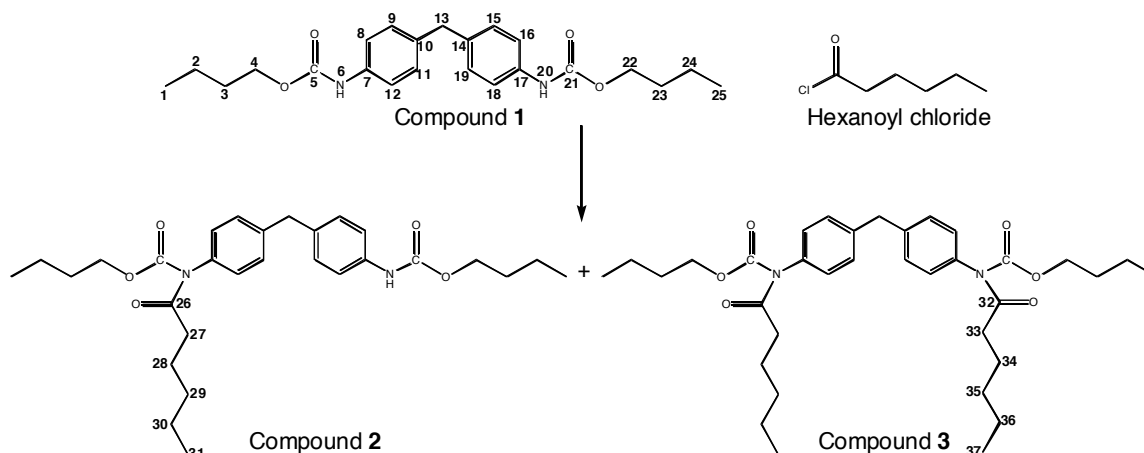
The returned mass obtained from the HRMS (Figure 3.8) (mass for compound 1. HRMS: 398.22) was compared with the theoretically calculated mass (calculated for $\text{C}_{23}\text{H}_{30}\text{O}_4\text{N}_2 = 398.22$) and found to compare well. The calculated error (6.6 ppm) was well below the instrument's allowable error (10 ppm).

Thus, in conclusion, the model urethane compound was considered successfully synthesized, purified and characterized. The returned mass (HRMS) and NMR spectra were found to be consistent with the structure of compound 1 and the latter was also found to be consistent with reported spectra [1, 3-5].

3.5.2 Acylation of model compound

3.5.2.1 Acylation using hexanoyl chloride

The reaction scheme for the reaction between the synthesized model urethane compound (compound **1**) and hexanoyl chloride is presented in Scheme 3.6, showing the possible formation of the mono- and di-acylated products. Acylation was anticipated to proceed at the nitrogen rather than the oxygen, in view of literature precedent.



Scheme 3.6: Acylation of compound **1** with hexanoyl chloride

The first approach investigated was to try and increase the electrophilicity of the hexanoyl chloride using different acyl transfer agents (e.g. DMAP) and acid acceptors (e.g. Hünig's base). Extensive trials were performed and the best results (monitored by TLC) obtained when Hünig's base was used with catalytic amounts (10%) of DMAP in DCM or THF. Thin-layer chromatography revealed two spots, the starting material (compound **1**) and a second, faintly observed, less polar spot. This was believed to be the mono-acylated urethane compound (compound **2**) (confirmed later, see below).

Reactions were then carried out for different reaction times and temperatures in an attempt to increase the conversion. Minor influences, as monitored with TLC, were observed and the best results were obtained when the reaction temperature was moderately increased (from room temperature to 55 °C), following the addition of hexanoyl chloride, and maintained for 24 h.

In the alternative approach, attention was focused on enhancing the nucleophilicity of the donor by using the carbamate anion. This was achieved by either using sodium hydride or *n*-butyllithium (25% molar excess). TLC revealed the formation of three fractions, the starting material (compound **1**) (faintly observed) and two distinctive less polar fractions, believed to be the mono- and di-acylated products. This observation led to the scale-up of the reaction.

It was found to be possible to separate and isolate the product fractions by using preparative TLC plates following column chromatography (which only gave a band of

compounds). The two new, less polar fractions, assigned as compound **2** and compound **3**, in order of decreasing polarity (each as single spots on TLC), were submitted for ^1H and ^{13}C NMR analyses and HRMS. The returned spectra were found to be identical, irrespective whether the reactions were carried out with NaH or n-BuLi. The ^1H and ^{13}C NMR spectra, as well as the HRMS of the isolated fractions (**2** & **3**), for the reactions carried out with n-BuLi are presented below (see Figures 3.9 - 3.14).

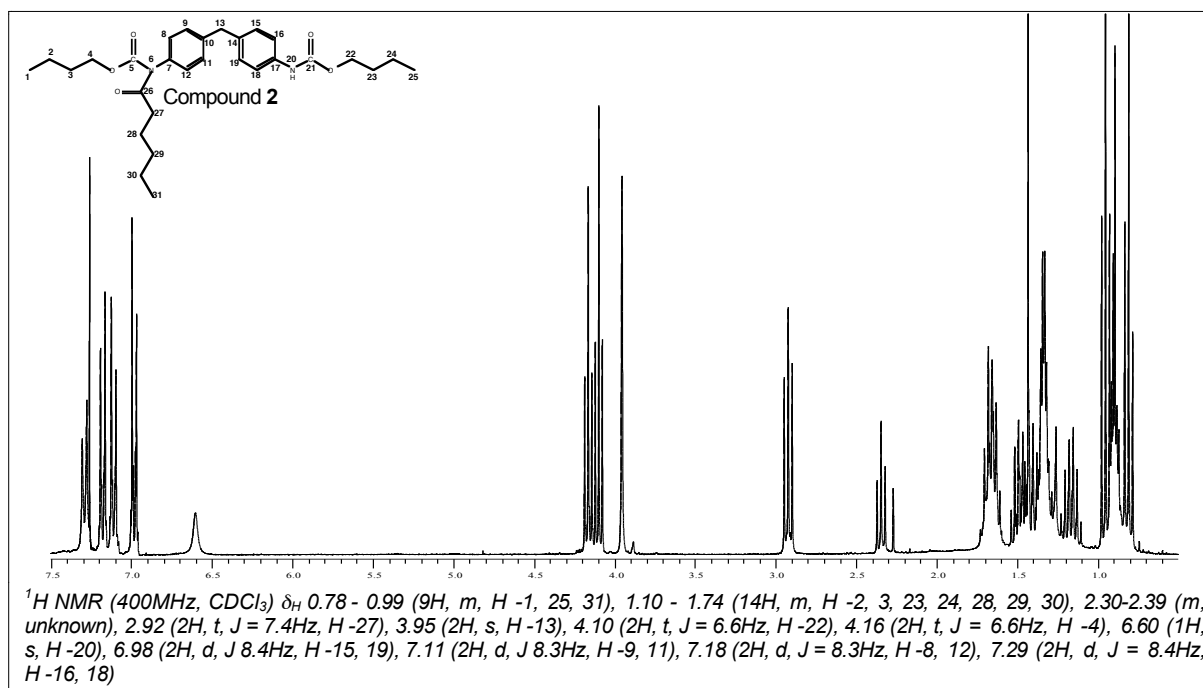


Figure 3.9: ^1H NMR spectrum of compound **2** showing structure and assignment of signals

The following observations were made regarding the ^1H NMR spectrum (Figure 3.9) of the first less polar fraction (assigned as compound **2**). The carbamate N-H proton integrated for only half of those of compound **1** (Figure 3.6), signifying that mono acylation had taken place. The introduction of one hexanoyl group was corroborated by high-field aliphatic signals as well as a downfield (2.92 ppm) triplet for the protons adjacent to the new carbonyl group (assigned as H -27), integrating for two protons. The dissimilarity observed for the chemical shift pattern of the aromatic ring protons at δ_{H} = 6.98 - 7.29 (H -9,11 ; H -15,19 and H -8,12 ; H -16,18) served as further evidence that disymmetrization had taken place.

A downfield shift in the signal corresponding to the methylene protons (Ar_2CH_2) of compound **2**, from δ_{H} = 3.87 ppm (compound **1**) to δ_{H} = 3.95 ppm (Figure 3.9), was observed compared to compound **1** (Figure 3.6). This corresponds to an expected downfield shift due to the stronger electron-withdrawing effect imparted by the latent mono-acylated group.

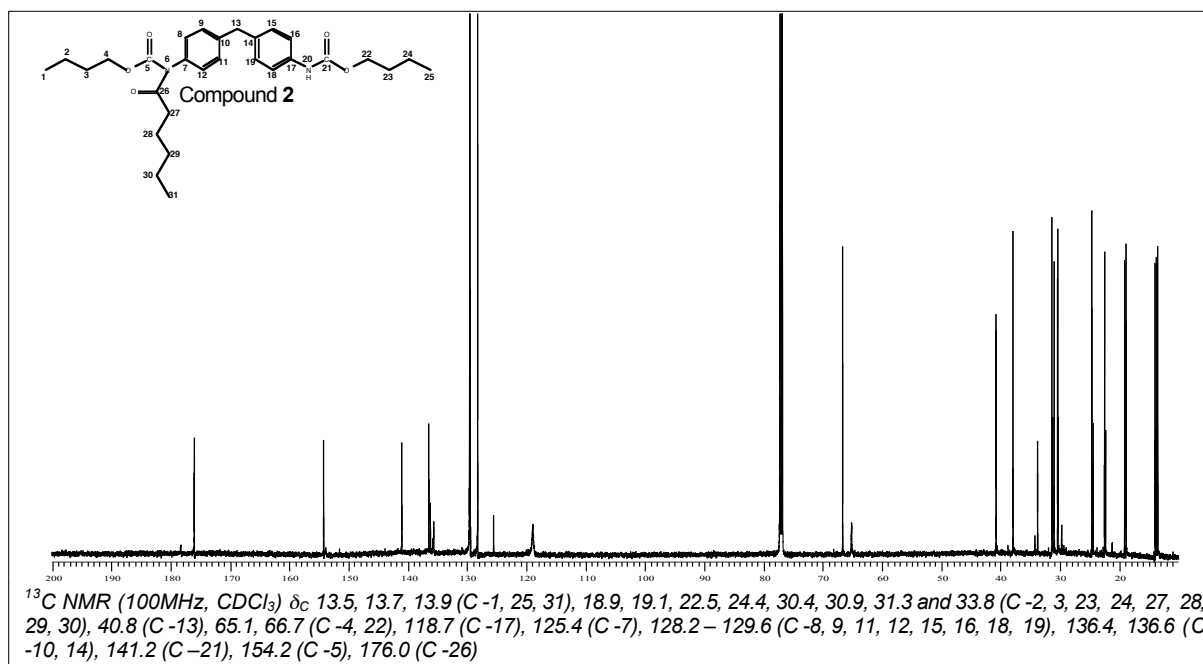


Figure 3.10: ^{13}C NMR spectrum of compound 2 showing assignment of signals

The signals of the ^{13}C spectrum of compound 2 (Figure 3.10) were assigned and found to be consistent with the proposed product. The correct number of aliphatic carbons (14) was found to be present. The presence of a third carbonyl signal (assigned as C -26), resulting from the introduction of the hexanoyl group, was also observed. The electronic environments of the two respective aromatic rings were different, as is evident from the observed signals at 128.2 - 129.6 ppm (when compared to compound 1 see Figure 3.7) supporting dissymmetrization by mono-acylation. Minimal impurities (trace amounts of compound 1) were found to be present and are due to imperfect separation.

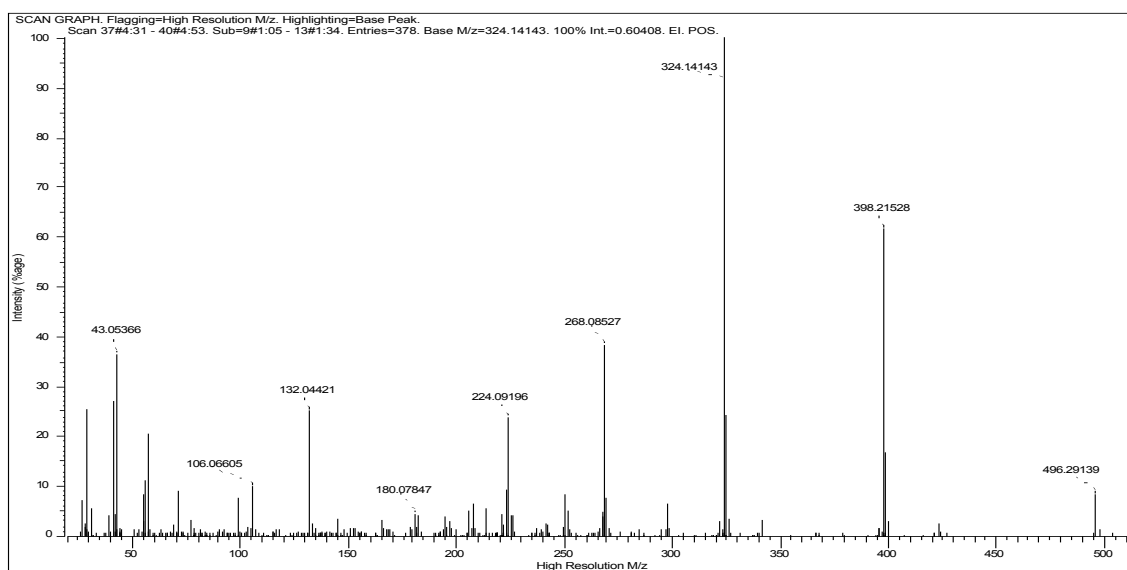


Figure 3.11: High-resolution mass spectrometry of compound 2

The returned mass for compound **2** obtained from the HRMS (Figure 3.11) (HRMS: 496.29) was again within the allowable error range (error less than 4.7 ppm) when compared with the theoretically calculated mass ($C_{29}H_{40}O_5N_2 = 496.29$).

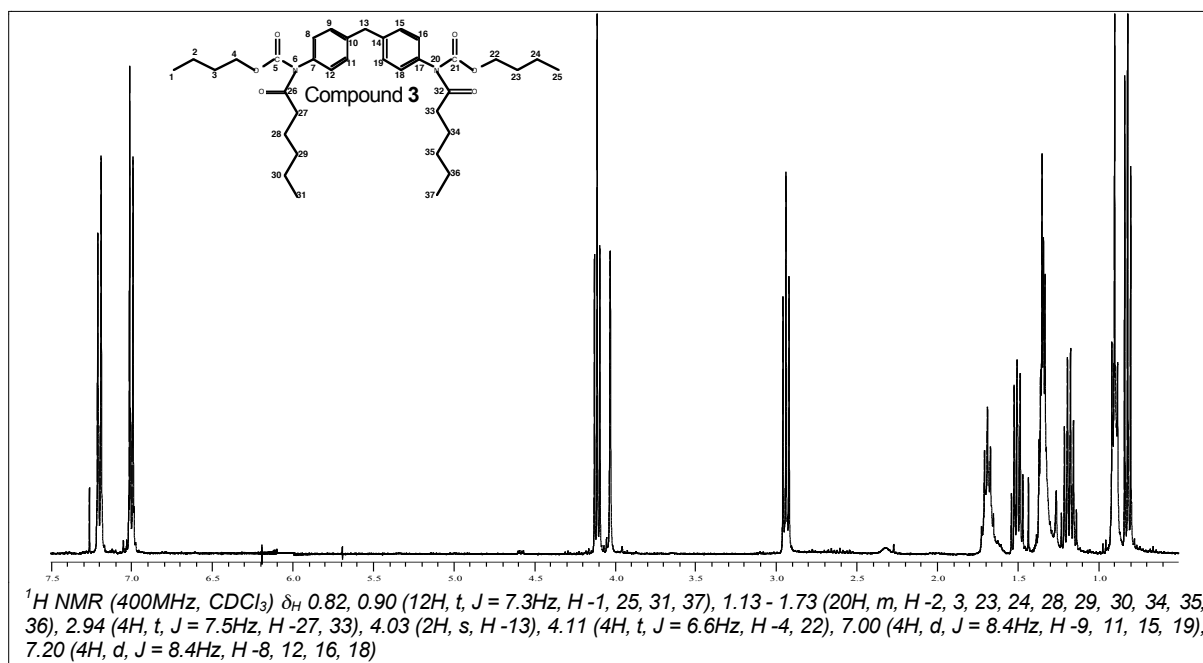


Figure 3.12: 1H NMR spectrum of compound **3** showing structure and assignment of signals

In the 1H NMR spectrum of the least polar fraction (Figure 3.12), the protons of the carbamate nitrogen were completely absent, indicating full substitution of both nitrogen atoms as a result of di-acylation. In accordance with this was the similarity of the ring protons $\delta_H = 7.00$ (H -9,11,15,19) and $\delta_H = 7.20$ (H -8,12,16,18) due to restoration of symmetry, i.e. both aromatic rings are now equivalent.

The observed downfield shift in the signal corresponding to the methylene protons (H -13) of compound **3** (Figure 3.12) to $\delta_H = 4.03$ ppm compared to those for both compound **1** ($\delta_H = 3.87$ ppm) as well as mono-acylated compound **2** ($\delta_H = 3.95$ ppm), due to the even stronger electron-withdrawing effect imparted by the two acylated carbonate functionalities, was further evidence for di-acylation.

The signals of the ^{13}C spectrum of compound **3** (Figure 3.13) were assigned and the signals observed at 13.9 ppm and 176.0 ppm attributed to the terminal methyl (C -31, 37) and the amide carbonyl carbons (C -26, 32) of the newly introduced acyl functionality, respectively. Once again, restoration of symmetry reduced the number of signals to 10 : 4 : 2 for aliphatic : aromatic : carbonyl.

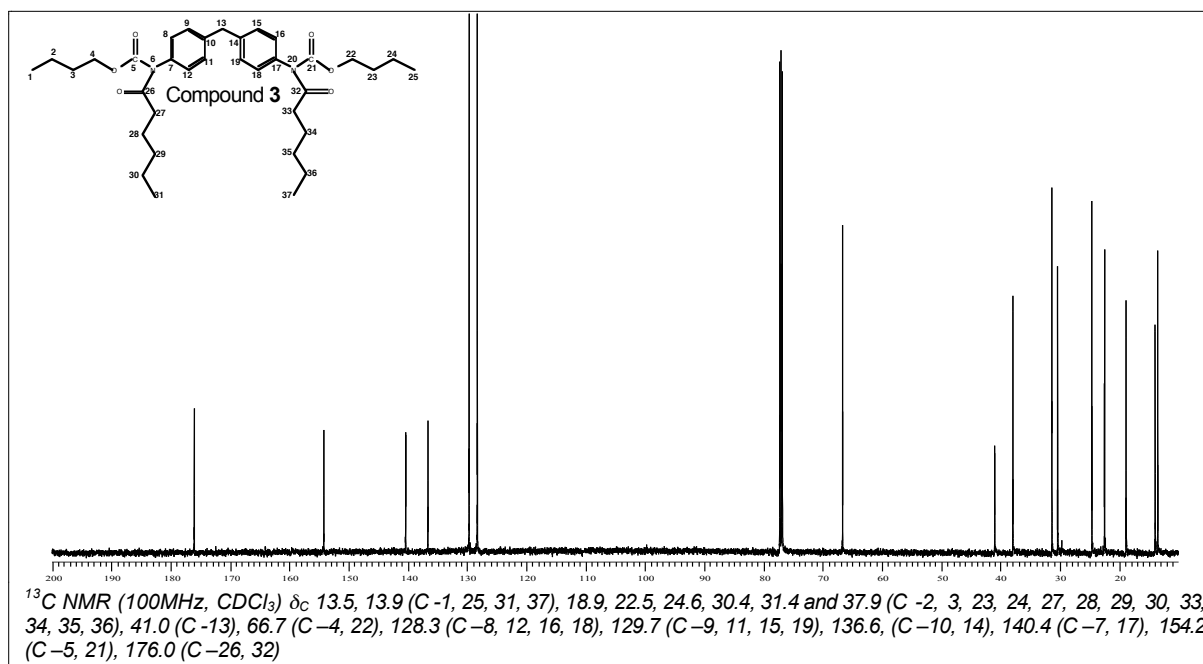


Figure 3.13: ¹³C NMR spectrum of compound 3 showing structure and assignment of signals

High-resolution mass spectroscopy (Figure 3.14) returned an exact mass for compound 3 (HRMS: 594.37) compared to the theoretically calculated mass (C₃₅H₅₀O₆N₂ = 594.37).

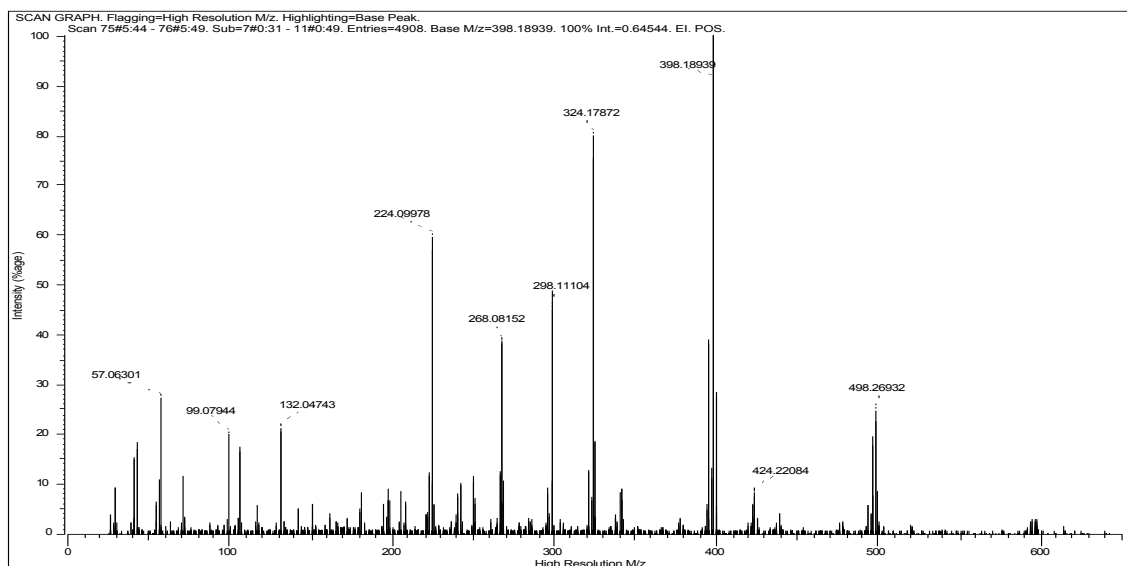


Figure 3.14: High-resolution mass spectrum of compound 3

The percentage yield (mole %) for each individual fraction was calculated for the products of the reactions carried out with sodium hydride (25% molar excess) and n-

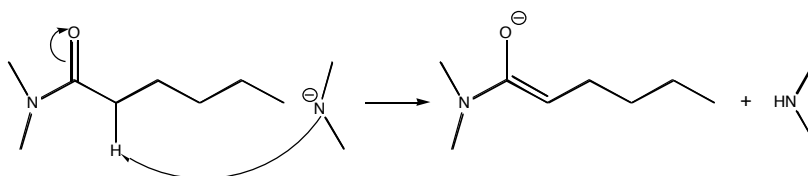
butyllithium (25% molar excess), and presented in Table 3.6. The overall yield was found to be 25.8% higher when n-butyllithium was used instead of sodium hydride.

The use of sodium hydride (solid) resulted in a heterogeneous reaction mixture, which might not have been as effective when compared to the use of n-butyllithium (miscible liquid). n-Butyllithium is also a stronger base than sodium hydride [11].

Table 3.6: Calculated yields of individual fractions 2 & 3

Compound	NaH	n-BuLi
2 (mono-acylated)	36.5%	24.6%
3 (di-acylated)	35.0%	66.8%
Yield	53.3%	79.1%

In summary, the reaction between the model urethane compound (compound **1**) and hexanoyl chloride was shown to be successful. Full conversion (although not a primary objective of this part of the study) was however not achieved, even when a strong base like n-butyllithium was used. This phenomenon could be attributed to either the incomplete deprotonation of compound **1** or side reactions with hexanoyl chloride, as indicated in Scheme 3.7.



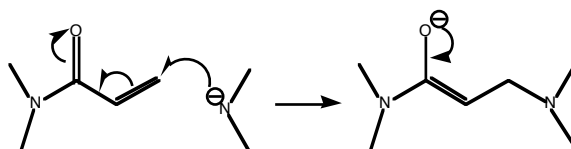
Scheme 3.7: Possible side reactions involving the pendant hexanoyl adduct of the urethane group

3.5.2.2 Acylation using unsaturated acyl chlorides

In order to address the objectives of the project concept, as outlined in Chapter 1, a number of acyl chlorides were then “screened” in trials to find one containing an acrylic or a vinyl group that is unaffected during the N-acylation of compound **1**, but capable of crosslinking the modified material at a later stage.

No discernible product was, however, observed on a TLC plate when acryloyl chloride was used, neither for the reactions when the nucleophilicity of the N-atom (urethane nitrogen) was enhanced (using sodium hydride or n-butyllithium) or when an attempt was made to increase the electrophilicity of acryloyl chloride by introducing different acid acceptors and acyl-transfer agents. NMR analysis of the crude reaction product revealed the unreacted model urethane compound (compound **1**).

It has been reported [14] that the use of a strong base (e.g. NaH) to de-protonate the carbamate nitrogen (hence rendering it more nucleophilic) followed by the introduction of acryloyl chloride results in the dimerization of the primary-formed product. Travnicek et al. [14] used a Cu/Cu₂Cl₂ system in an attempt to prevent dimerization, but it proved to be unsuccessful. Although they did not propose a possible mechanism by which the proposed dimerization could be taking place [14], it is likely to involve the Michael-type addition between the α,β -unsaturated latent acryloyl group and the carbamate anion (Scheme 3.8) [11].



Scheme 3.8: Michael-type addition between the α,β -unsaturated latent acryloyl group and the carbamate anion

From the foregoing results and discussion it is proposed that the successful unsaturated acyl chloride candidate would have to be one lacking the α,β -unsaturated arrangement and therefore have the generic structure as illustrated in Figure 3.15, in which R₁ would have to be at least one carbon in size (e.g. -CH₂-).

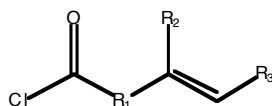
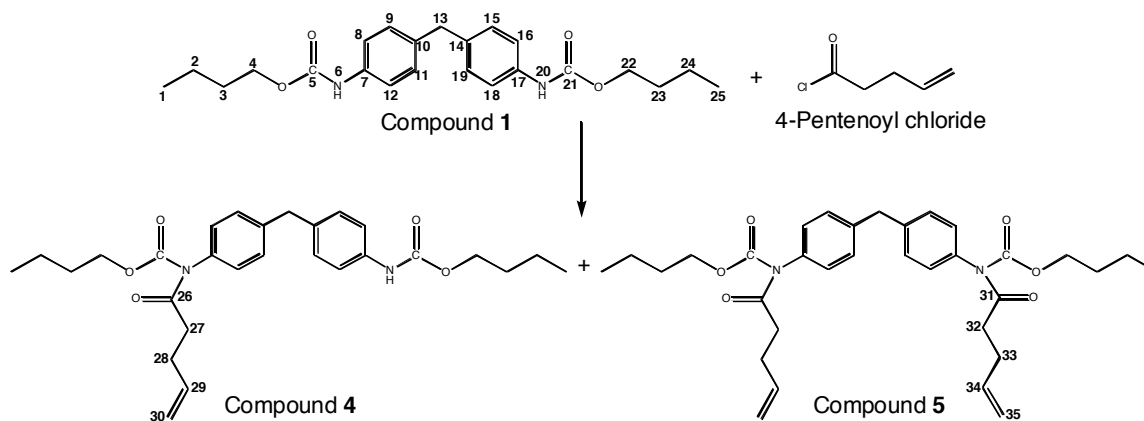


Figure 3.15: Proposed generic structure for candidate unsaturated acyl chloride

3.5.2.3 Acylation using 4-pentenoyl chloride

The author subsequently decided to study the reaction of 4-pentenoyl chloride with the model urethane compound (compound 1). Scheme 3.9 shows the possible formation of the mono- and di-acylated products. 4-Pentenoyl chloride was chosen in order to separate the double bond from the carbonyl group, to prevent conjugation promoted by the basic conditions.



As in the acylation of compound **1** using hexanoyl chloride (§3.5.2.1), acylation under acyl-transfer conditions was first studied involving electrophilicity enhancement of the acyl chloride and then reacting with the neutral carbamate. The best results (monitored with TLC) were obtained when Hünig's base was used with catalytic amounts of DMAP (10%) in THF. TLC revealed two fractions: the starting material (compound **1**) and one new, faintly visible, less polar fraction. The latter was believed to be the monoacylated (compound **4**) urethane compound (later confirmed, see below). Several attempts were then made to try to increase the conversion by increasing the reaction temperature and time of reaction, but TLC results indicated little or no improvement. The best TLC results were obtained at room temperature and a 24-h reaction time.

Attention was then directed at nucleophilicity enhancement of the carbamate anion (using either sodium hydride or *n*-butyllithium). Promising TLC results were obtained, revealing the formation of three spots: the starting material (compound **1**) (faintly visible fraction) and two distinctive, less polar fractions (**4** & **5**) (Figure 3.16). The reactions (using sodium hydride or *n*-butyllithium) were then scaled up to produce suitable quantities of product.

Numerous attempts were then made to separate the scaled-up reaction product into its respective fractions using a gravity column packed with silica-gel. It was however not possible to obtain pure fractions, either by reduction of the polarity of the mobile phase (ethyl acetate/petroleum ether) or by increasing the silica to product ratio.

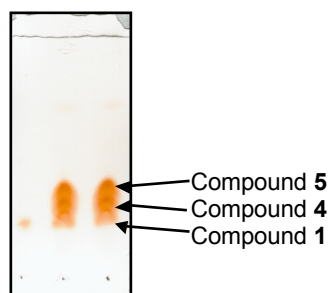
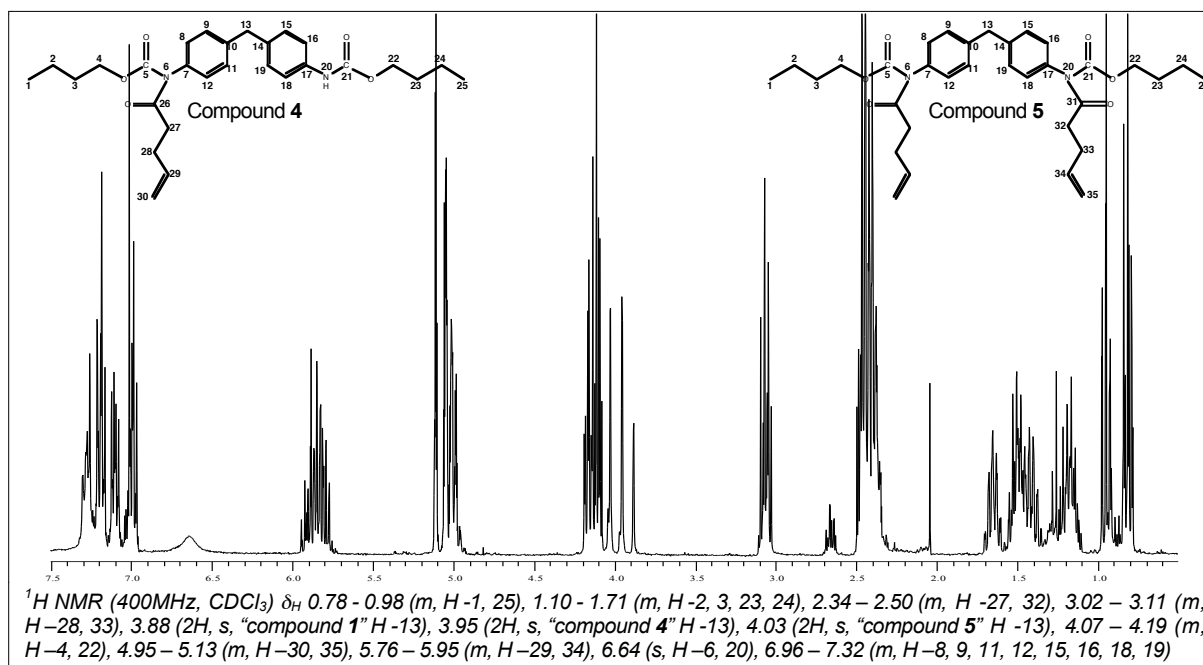


Figure 3.16: TLC plate of a mixture of compounds 1, 4 & 5

The small difference in polarity between the three fractions, as is evident from the TLC plate in Figure 3.16, also prevented successful separation by PTLC. The purified (but unseparated) reaction product was analyzed by NMR and HRMS.



Although it was not possible to assign all of the individual signals of the returned ^1H and ^{13}C NMR spectra (Figures 3.17 & 3.18) sufficient assignments could be made to enable elucidation of the reaction product.

The introduction of a 4-pentenoyl unit resulted in the appearance of characteristic signals between 4.95 - 5.13 ppm and 5.76 - 5.95 ppm in the ^1H NMR spectrum (Figure 3.17). These were attributed to the vinyl protons (H -30, 35) and (H -29, 34), respectively. The acyl group further resulted in the appearance of extra high-field aliphatic signals (2.35 - 2.50 ppm) for the protons adjacent to the new carbonyl group (assigned H -27 and H -32), integrating for four protons. The three singlet proton signals of the methylene protons (Ar_2CH_2) corresponding to compounds 1, 4 and 5 were observed at 3.88, 3.95 and 4.03 ppm, respectively, and could be used to estimate relative amounts as approximately 1 : 2 : 2 for compound 1 : compound 4 : compound 5.

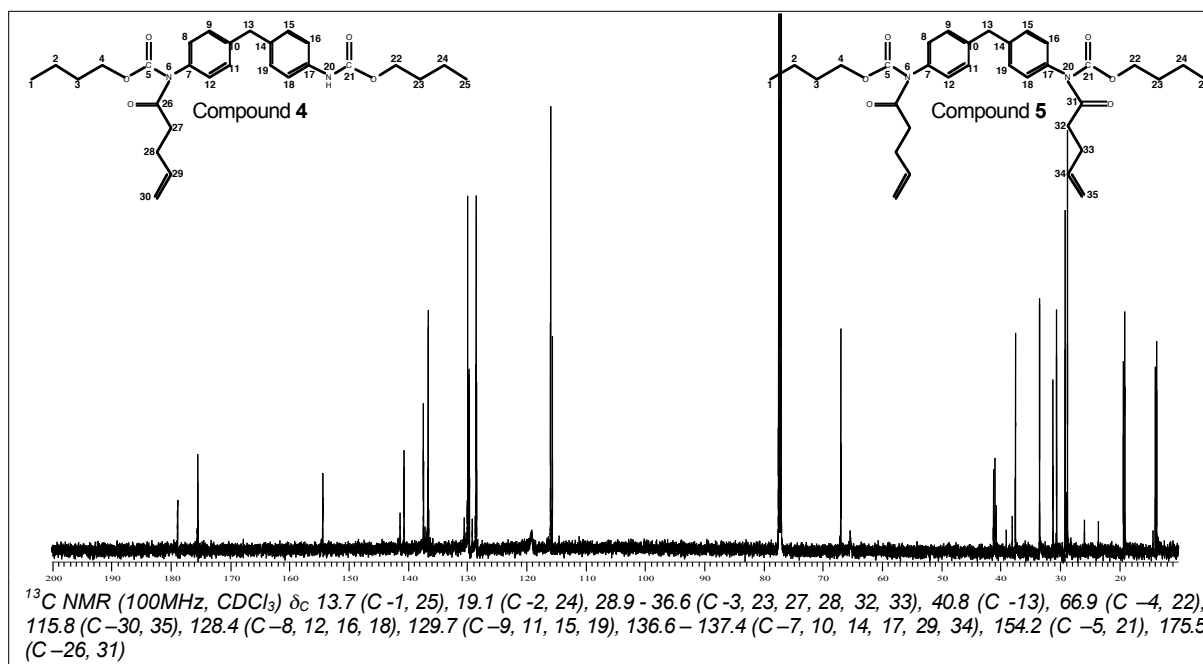


Figure 3.18: ^{13}C NMR spectrum of a mixture of compounds 1, 4 & 5

The presence of the terminal vinyl carbon signals (C -30, 35), assigned at 115.8 ppm in the ^{13}C spectrum (Figure 3.18), served as further evidence of successful acylation. The presence of two carbonyl signals (assigned as C -26, 31) for the two amide carbonyl carbons of compounds 4 and 5 (C -26 and C -26, 31) further supported the presence of the mono- and di-acylated products.

The methylene proton signals attributed to compounds 1, 4 and 5 were integrated for the respective reactions carried out with sodium hydride and n-butyllithium, and used to calculate the following yields (see Table 3.7).

Table 3.7: Calculated yields of the mono- (compound 4) and di-acylated (compound 5) compounds

Compound	NaH	n-BuLi
4 (mono-acylated)	49.1%	39.1%
5 (di-acylated)	24.3%	43.5%
Yield	51.5%	63.1%

The overall product yield was found to be 11.6% higher when n-butyllithium was used instead of sodium hydride. This is consistent with the results obtained with hexanoyl chloride, and can be ascribed to the relative strength of n-butyllithium and the homogeneous nature of the reaction mixture.

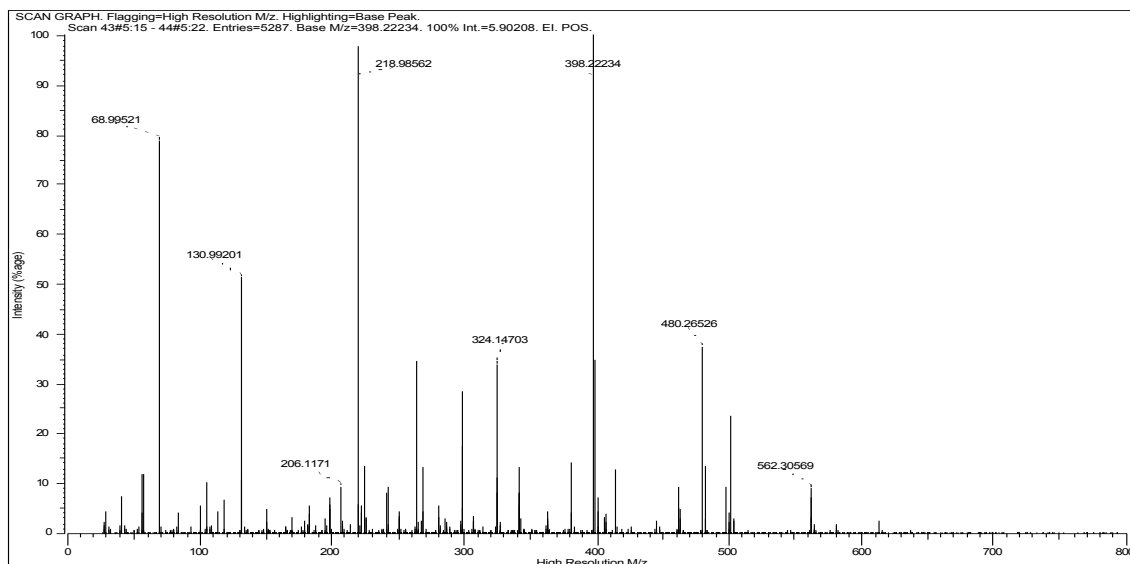


Figure 3.19: HRMS of a mixture of compounds **1**, **4** & **5**

High-resolution mass spectroscopy (Figure 3.19) returned correct masses for the individual compounds in the mixed sample when compared to the theoretically calculated masses, as summarized in Table 3.8.

Table 3.8: Summary of the molecular masses of compounds **1**, **4** and **5** obtained from HRMS

Components	Compound 1	Compound 4	Compound 5
Mass from HRMS (g/mole)	398.22	480.27	562.31
Molecular formula	C ₂₃ .H ₃₀ .O ₄ .N ₂	C ₂₈ .H ₃₆ .O ₅ .N ₂	C ₃₃ .H ₄₂ .O ₆ .N ₂
Calculated mass (g/mole)	398.22	480.26	562.31
Error (ppm)	4.5	5.9	2.5

The spectrum obtained from MALDI analysis is presented in Figure 3.20. Although MALDI is generally not a suitable analytical method for molecules with such low molecular masses as the ones under investigation, useful results were obtained by optimization of the assay conditions, as described earlier (§3.4.5.3).

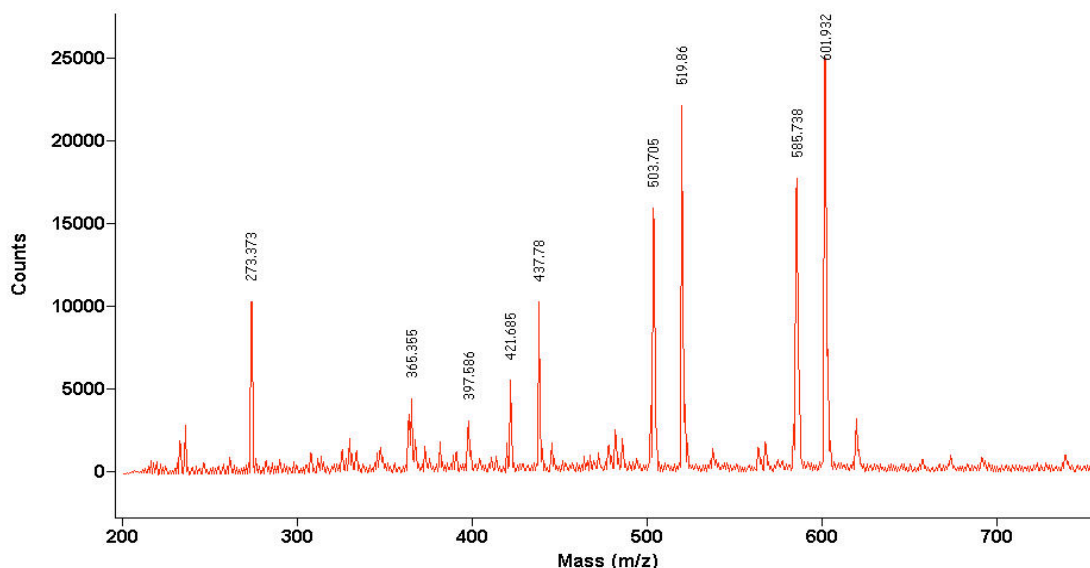


Figure 3.20: MALDI analysis of a mixture of compounds **1**, **4** & **5**

Compounds **1**, **4** and **5** were observed at molecular masses of (421.685, 437.78), (503.705, 519.86) and (585.738, 601.392) corresponding to the Na- and K- adducts (inherent to the method used). The molecular masses of Na and K were deducted and the results are presented in Table 3.9.

Table 3.9: Summary of the molecular masses of compounds **1**, **4** and **5** obtained from MALDI analysis

Components	Compound 1	Compound 4	Compound 5
Na-adduct (g/mole)	398.69	480.72	562.74
K-adduct (g/mole)	398.68	480.76	562.83
Molecular formula	C ₂₃ .H ₃₀ .O ₄ .N ₂	C ₂₈ .H ₃₆ .O ₅ .N ₂	C ₃₃ .H ₄₂ .O ₆ .N ₂
Calculated mass (g/mole)	398.22	480.26	562.30

Although the MALDI results were not as accurate as the results obtained with HRMS, they were nonetheless useful. The signals at molecular masses of 273.37, 365.35 and 397.57 are distinctive of the matrix used.

3.6 Conclusions

The conceptualized urethane model compound was successfully synthesized, purified and then characterized by nuclear magnetic resonance and high-resolution mass spectroscopy. The results (signals of NMR spectra and returned masses) were found to be consistent with reported and theoretical values.

Acylation of compound **1** with hexanoyl chloride was achieved by both nucleophilic and electrophilic enhancement. The former was the more effective method, with the stronger base n-butyllithium resulting in a significantly higher conversion. Separation of the product fractions was achieved using preparative thin-layer chromatography. High-resolution mass spectroscopy returned masses consistent with the mono- and di-acylated compounds, while NMR data showed that the successful reaction site was indeed the proposed carbamate nitrogen.

A range of reactions of compound **1** with acryloyl chloride proved to be unsuccessful, most likely due to the promotion of oligomerization via Michael addition of the primary formed product. This indicates the importance of the consideration in choosing a suitable unsaturated acyl chloride.

The success of the hexanoyl chloride coupling could be emulated with 4-pentenoyl chloride, thereby introducing a non- α,β -unsaturated C=C bond for potential future crosslinking. Although the coupling could be achieved by either nucleophilic or electrophilic enhancement, the former (especially when n-butyllithium was used) was again the more effective method. Although pure products could not be isolated, spectroscopic analyses of the mixed product (compound **1**, **4** and **5**) provided satisfactory support for their formation.

3.7 References

1. Lu, Q.-W., T. Hoye, and C. Macosko, *Reactivity of common functional groups with urethanes: Models for reactive compatibilization of thermoplastic polyurethane blends*. J. Pol. Sci., Part A: Polym. Chem., 2002. **40**: p. 2310-2328.
2. Martin, D., L. Warren, P. Gunatillake, S. McCarthy, G. Meis, and K. Schindhelm, *Polydimethylsiloxane/polyether-mixed macrodiol-based polyurethane elastomers: biostability*. Biomaterials, 2000. **21**: p. 1021-1029.
3. Yang, W., C. Macosko, and S. Wellinghoff, *Thermal degradation of urethanes based on 4,4'-diphenylmethane diisocyanate and 1,4-butanediol (MDI/BDO)*. Polymer, 1986. **27**: p. 1235-1240.
4. Camberlin, Y. and J. Pascault, *Synthesis and DSC study of model hard segments from diphenyl methane diisocyanate and butane diol*. J. Pol. Sci., Polym. Chem. Ed., 1982. **20**: p. 383-392.
5. Qin, Z., C. Macosko, and S. Wellinghoff, *Synthesis and characterization of model urethane compounds*. Macromolecules, 1985. **18**: p. 553-557.
6. Dyer, E. and G. Newborn, *Thermal degradation of carbamates of methylene bis (4-phenyl isocyanate)*. J. Am. Chem. Soc., 1958. **80**: p. 5495-5497.
7. Boutevin, B. and J. Hugon, *Synthese de polyurethanes fluores*. Tetrahedron Lett., 1978. **2**: p. 129-132.
8. Caraculacu, A. and I. Agherghinei, *A new method for a kinetic study of reactions between di-isocyanates and alcohols. Part 1. Symmetrical di-isocyanates*. J. Chem. Soc. Perkin Trans. 2, 1990. **8**: p. 1343-1348.
9. Salvatore, R., S. Shin, V. Flanders, and K. Jung, *Efficient and selective N-alkylation of carbamates in the presence of Cs₂CO₃ and TBAI*. Tetrahedron Lett., 2001. **42**: p. 1799-1801.
10. Kondo, K., E. Sekimoto, J. Nakao, and Y. Murakami, *Studies on development of sufficiently chemoselective N-acylation reagents: N-Acyl-N-(2,3,4,5,6-pentafluorophenyl)methanesulfonamides*. Tetrahedron, 2000. **56**: p. 5843-5856.

11. Smith, B. and J. March, *Advanced Organic Chemistry*. 5th ed. 2001, New York: John Wiley & Sons, Inc.
12. Pouchert, C. and J. Behnke, *The Aldrich Library of ¹³C and ¹H FT NMR Spectra*. Vol. 1. 1993, New York: Aldrich.
13. Pouchert, C. and J. Behnke, *The Aldrich Library of ¹³C and ¹H FT NMR Spectra*. Vol. 3. 1993, New York: Aldrich.
14. Travnicek, M. and M. Potacek, *A new routine for the synthesis of N-substituted-N-(sulfonyl) bromoacetamides with ZnCl₂ as a catalyst*. *Molecules*, 1999. **4**: p. 238-244.

Chapter 4

Polyurethane modification

Abstract

The acylation chemistry of a carbamate nitrogen, optimized in a model compound study (Chapter 3), was transferred to Pellethane[®] 2363-80AE (academic polyurethane standard) using 4-pentenoyl chloride (unsaturated acyl chloride), sodium hydride (for nucleophilic enhancement of the unreactive carbamate nitrogen) and an aprotic solvent, N,N-dimethylformamide (DMF), capable of stabilizing the resulting polyanion. Treatment, using an initial sodium hydride concentration of 10% molar equivalent to carbamate nitrogens (as suggested in the literature) followed by the addition of 4-pentenoyl chloride, isolation and purification, resulted in an average degree of modification of 4.5% (based on the carbamate nitrogens), calculated using proton nuclear magnetic resonance spectroscopy (¹H NMR). The degree of modification was accurately and reproducibly controlled ($R^2 = 0.99$) between 4.5% - 20% (maximum determined) by changing the sodium hydride concentration. Modification of a second, technologically much more advanced polyurethane, PurSil[®] 35 80A, was also achieved. A maximum degree of modification of 18.5% was calculated, based on ¹H NMR, after successful deprotonation (using sodium hydride), purification and isolation. The degree of modification was accurately and reproducibly controlled ($R^2 = 0.99$) between 11.5% - 18.5% by changing the sodium hydride concentration. The novel modified, isolated and purified polyurethanes can be used to study crosslinking reactions and to optimize their mechanical properties.

4.1 Introduction

The modification of medical grade polyurethanes at the carbamate nitrogen with unsaturated modification agents, rendering the polyurethanes (PUs) crosslinkable whilst they remain stable during the modification and subsequent purification stages, is not a trivial task.

The harsh reaction conditions that are required to effect nucleophilic addition reactions of the relatively unreactive carbamate nitrogen of the respective polyurethanes could result in *in situ* crosslinking reactions of the unsaturated pendent groups. Finding a suitable unsaturated acyl chloride and optimizing the reaction conditions was thus crucial.

In the model compound study described in Chapter 3 the reaction site at which acylation occurs, namely the carbamate nitrogen, was confirmed. 4-Pentenoyl chloride was found to be an ideal modification reagent and sodium hydride could be used for nucleophilic enhancement of the carbamate nitrogen. The knowledge gained in that section of the work was now transferred to medical grade polyurethanes.

Pellethane[®] 2363-80AE (an academic polyurethane standard) was the first candidate polyurethane that was selected with which to study the transfer of the chemistry developed with the model compound. Reactions were carried out with Pellethane[®] 2363-80AE and 4-pentenoyl chloride. A sodium hydride concentration equivalent to 10 molar percentage of the carbamate nitrogens, as suggested in the literature [1], and an aprotic solvent, DMF, capable of stabilizing the resulting polyanion [2] were used. Nuclear magnetic resonance spectroscopy (NMR) was used to confirm the presence of vinyl signals in the products of the acylation reactions.

The maximum degree of modification could then be determined by increasing the sodium hydride concentration whilst maintaining a reaction temperature well below 0 °C (-4 °C), as suggested by Adibi et al. [2]. The degree of modification was then studied by varying the sodium hydride concentration.

Focus was then directed at using a technologically much more advanced medical grade polyurethane PurSil[®] 35 80A (advanced in terms of synthetic chemistry and raw materials used). The maximum degree of modification was determined after the presence of vinyl signals was confirmed by NMR. Changing the sodium hydride concentration was again used to alter or improve the degree of modification.

4.2 Historical

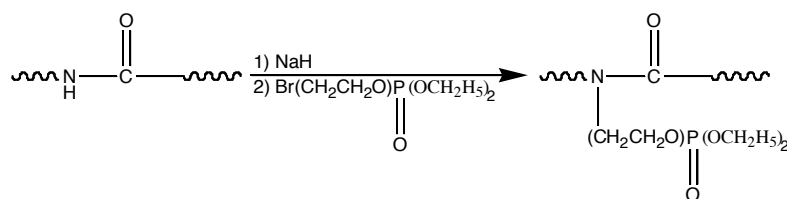
4.2.1 Modification of existing polyurethanes for enhanced biocompatibility

N-alkylation reactions of polyurethanes have been extensively investigated (from as early as 1949 [3]), initially to try and improve the fire resistance of the urethanes [3-10]. It was however only much later that their medical use became evident [1, 11-13].

It is thus no surprise that there is a rich literature and patent reference database available describing different reaction conditions, including the use of sodium hydride, to enhance the nucleophilic character of the carbamate nitrogen, which is of specific interest in this dissertation. Although improving the mechanical and chemical properties of the polyurethanes was not the objective of this study, but rather enhancing the biocompatibility, a brief summary of the most relevant work will be given here.

A number of investigations [3-10] have demonstrated the successful N-alkylation (alkylhalogenides) of polyurethanes and polyamides (in the presence of a strong base e.g. NaH), mainly to improve the fire resistance of these polymers. These reactions were carried out at temperatures not exceeding 0 °C and using DMF as solvent.

In one such an investigation [4] the N-alkylation reaction of a polyurethane (based on MDI) was studied using sodium hydride to first abstract the labile carbamate proton (at 0 °C in DMF). Hydrogen gas was immediately observed, whereafter the reported mixture showed a green color, caused by the urethane polyanion - thus showing successful deprotonation [4]. Diethyl 2-bromoethyl phosphate was used as alkylation reagent, as illustrated in Scheme 4.1.



Scheme 4.1: *N-alkylation of a polyurethane using diethyl 2-bromoethyl phosphate* [4]

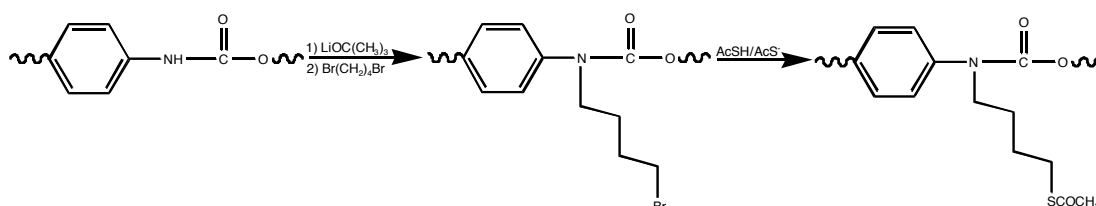
In an effort to increase the biocompatibility of polyurethanes, molecules with reactive groups (to which substituents can be added after polymer synthesis) have been incorporated into the polymer backbone [14-16]. The molecular mass and mechanical properties of the polymers obtained in this manner may however preclude their medical use [1].

In an alternative approach to increase the biocompatibility [2], N-alkylation of polyurethanes was considered. It has been demonstrated that the reaction of moderate

grades of metallation of polyurethanes (based on MDI) and toluene diisocyanate (2,4-2,6) (TDI)) with sodium hydride at temperatures not significantly exceeding 0 °C do not induce significant polymer degradation [2]. According to Adibi et al. [2] the “polyanions” further remain soluble in aprotic solvents, e.g. DMF.

The first application of this N-alkylation method to medical grade polyurethanes involved N-alkylation of “sodium hydride-activated” polyurethanes using alkyl iodides to attach C₂ - C₁₈ alkyl chains to the polymer backbone [12] in an effort to improve the blood compatibility of the polymers. The polyurethanes were pretreated with sodium hydride at 0 - -5 °C and the reaction of the activated polymer with alkyl iodides was performed at a temperature of 50 °C. The stability of the polyanion is however questionable at this temperature, especially in the light of the work conducted by Adibi et al. [2].

Alferiev et al. [1, 11, 13] modified polyurethanes with pendant acylated thiol groups, which resist oxidative crosslinking (often characteristic of molecules containing multiple thiol groups), and thus managed to decrease the alkylation temperature. The resulting polymer was prepared from a polyether-urethane pre-modified with bromobutyl groups, which were reacted with an excess of thiolacetic acid (AcSH) in the presence of a thioacetate ion (AcS⁻) (Scheme 4.2).



Scheme 4.2: Low temperature N-alkylation of a polyurethane with thiolacetic acid (AcSH) in the presence of a thioacetate ion (AcS⁻) [11]

Although crosslinking of the polyurethanes was not one of the main objectives of the aforementioned studies, valuable information was gained regarding the susceptibility of the carbamate nitrogen to proton abstraction using sodium hydride. DMF was generally used as solvent and it was shown that the polyanions of polyurethanes based on MDI would remain stable in aprotic solvents (e.g. DMF). Adibi et al. [2] further demonstrated that the resulting polyurethane anion would remain stable at temperatures below 0 °C.

4.2.2 Heat processing of existing polyurethanes with reactive monomers

The first evidence that was found involving the “crosslinking of polyurethanes” came mainly from the patent literature, where heat processing (mainly extrusion) of

thermoplastic polyurethanes with “reactive” monomers is described. Some of the most relevant references are briefly discussed below.

The technology described by the Babolat Sports Company (manufacturers of tennis and badminton rackets, etc.) [17] involves the crosslinking of a semi-crystalline ester-based polyurethane for the manufacturing of tennis and badminton racket strings with enhance flow/creep resistance at room temperature.

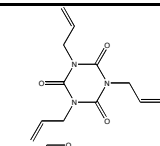
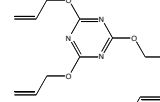
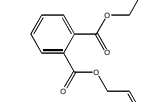
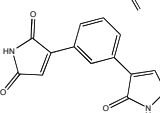
The inventors [17] first developed a “two-step” process to achieve crosslinking functionality, whereafter crosslinking was induced. The modification process involves use of a “grafting agent” (e.g. TDI) and a “crosslinking precursor” (e.g. hydroxy ethyl methacrylate (HEMA)), which are mixed together with the thermoplastic polyurethane (TPU) in an extruder. Crosslinking was induced during the extrusion process either using irradiation or an ultraviolet light (UV) source.

In a second example the inventors [17] tried to use just a “grafting agent” (trimethylol propane trimethylacrylate, (TMPTMA)), which they mixed together with a thermoplastic polyurethane, in a single screw extruder. Crosslinking was achieved by irradiation (75 kGy).

No evidence could be found as to whether or where this technology had been successfully used to modify other polyurethanes, or where a description is given to the degree of reproducibility and control over the required degree of modification and crosslinking. A possible limitation is that it does not offer much control over the degree of modification.

Sardanopoli and Stonehouse [18] from BASF claim the use of an isocyanate-terminated pre-polymer (based on e.g. MDI), which is then mixed in an extruder with the TPU, whereafter crosslinking is induced by the heat in the extruder.

Table 4.1: Crosslinkers for enhance crosslinking [19]

Group	Structure
Triallylisocyanurate (TAIC)	
Triallylcyanurate (TAC)	
Diallyl phthalate (DAP)	
Meta-phenylene dimaleimide (MPDM)	

Beyer and Steckenbiegler [20] added a tri-functional methacrylate (5 – 15 phr) during the synthesis of a polyether polyurethane and a polyester. Plates were then injection molded, during which the films were irradiated with electrons of 150 kGy. No mention was made as to how exactly it was incorporated into the polyurethanes, or the exact structure of the polyisocyanates used.

Zamore [19] claimed to have improved the technology of Beyer and Steckenbiegler [20] by using more “reactive crosslinkers”. A list of the crosslinkers used or suggested by Zamore is included in Table 4.1. The TPU and the respective monomers were mixed in a twin-screw extruder and crosslinked using irradiation.

Zamore [19] was unable to successfully modify and crosslink a TPU based on an aromatic polyisocyanate including Pellethane[®] 2363-55D, one of the Pellethane[®] 2363-80AE family, which is also based on the aromatic polyisocyanate, MDI.

The lack of evidence describing control over the degree of modification and crosslinking during these heat-processing methods indicates that the usefulness in any cardiovascular application is questionable. The versatility of this technology is also limited to extrusion only.

Crosslinkability can alternatively be introduced in a post-polyurethane-synthesis step (as will be followed in this dissertation), or during synthesis of the respective polyurethanes, a brief discussion of which will follow.

4.2.3 Synthesis of novel crosslinkable polyurethanes

The literature describes three main approaches that have been followed during polyurethane synthesis to introduce crosslink functionality i.e. to render the resulting novel polyurethanes crosslinkable. It has been achieved either through the choice of isocyanate [21-24], or chain extender or soft segment [25-29], or by the synthesis of novel urethane oligomers [30].

Reitel and Goethlick [22] included an unsaturated isocyanate (vinyl isocyanate) during the synthesis of a pre-polymer, whilst others like Muhfeld et al. [23] introduced crosslink functionality using a multi-functional isocyanate (e.g. di- and triisocyanate) to develop a polyurethane with improved light and temperature stability. Their method involved mixing polycaprolactone, 1,6-hexane diol and 1,6-hexamethylene together in a reaction vessel at 180 °C for 12 min [23], whereafter the polymer was processed into a granular material. A triisocyanate (8% w/w) was then added and the resulting material sintered according to the “conventional” powder-slush method in an open-heated mold at 225 °C, to form a 1-mm-thick crosslinked film. Only qualitative improvements, in light and temperature stability, were reported in some cases.

In a second approach the use of unsaturated [25, 28], hydroxy functional [29] or hyperbranched pre-polymers [27] were investigated as possible chain extenders.

Le Roy and Pattein [28] developed novel crosslinkable polyurethanes using but-2-ene-1,4-diol as chain extender. Crosslinking was achieved using a heat press or extrusion process at temperatures and times ranging from 120 – 200 °C and 5 – 60 min, respectively. The intended application was not mentioned, nor was any mention made regarding improvements in either chemical or mechanical properties.

A novel poly(ether urethane amide) was synthesized by Stern et al. [25], by chain-extending the prepolymer with fumaric acid, resulting in a polymer containing chemically active derivatization sites, stemming from the fumaramide double bond. Although crosslinking was not the main objective of this specific study, but rather the grafting of polyethylene oxide onto the active double bond, the authors did however test the reactivity of the double bonds by studying crosslinking reactions, using hexamethylene diamine and diethylene triamine; crosslinking was only achieved at 60 °C overnight.

Gordon [29] aimed to develop latexes and aqueous polyurethane dispersions for use in the manufacture of health care devices such as protective gloves, condoms, tourniquets and dental dams. Crosslinking was achieved by means other than sulfur vulcanization of double bonds. One of the patented methods is by means of including crosslink functionality, using hydroxy functional diamines (e.g. 1,3-diamino-2-hydroxy propane) as chain extenders. Multi-functional isocyanates are used as crosslinkers and heat-induced crosslinking is then achieved at 260 °C. Amine-terminated AB₂-type hyperbranched polyamides (HBP) of different molecular masses (3516 – 13063 g/mole) were prepared from 3,5-bis-(4-aminophenoxy)benzoic acid and used as crosslinkers in the preparation of different polyurethanes [27]. The HBPs were mixed in different ratios with 1,4-butanediol, which were then used as chain extenders. A control (no HBPs) and nine other different polymers were prepared in this manner and the mechanical properties (tensile strength and elongation) of only two of the nine were significantly improved, when compared with the control.

In the third approach, vinyl-containing oligomers were synthesized [30] by reacting TDI with 4-hydroxybutyl vinyl ether and three different diols, namely poly(ethylene glycol), poly(propylene glycol) (PPG) and α - ω -hydroxy terminated organofunctional poly(dimethyl siloxane) (PDMS). The resins were cationically polymerized by UV irradiation in the presence of a diaryliodonium photoinitiator. Of the three, PDMS oligomers gave the highest tensile strength and elongation and char yield when analyzed thermal gravimetrically.

Crosslink functionality has successfully been introduced during polyurethane synthesis using unsaturated [22] or multi-functional [23] isocyanates. Although successful crosslinking was achieved, only qualitative improvements were reported. Unsaturated [25, 28], hydroxy functional [29] and hyperbranched pre-polymers [27] have also been

successfully used as chain extenders during polyurethane synthesis to incorporate crosslink functionality. The derivation sites incorporated by Stern et al. [25] seemed unreactive towards crosslinking reactions and this would not be a practical approach.

Although the synthesis of novel crosslinkable polyurethanes was not an objective of this dissertation, but rather the modification and post-process crosslinking of existing medical grade TPUs, a rich literature pertaining to the former is available, as is evident from the aforementioned discussion.

4.2.4 Pellethane[®] 2363-80AE and PurSil[®] 35 80A

Pellethane[®] 2363-80AE (a polyether urethane) was developed by Dow Chemicals, USA. Poly(tetramethylene oxide) glycol is used in the soft segment and the hard segment consists of 4,4-methylenebis(phenylisocyanate), with 1,4-butanediol as chain extender [31].

The extruded pellets are coated with a waxy extrusion processing aid [32-35]. In the Fourier-transform infrared analysis the presence of peaks at 1635 cm⁻¹, 1563 cm⁻¹ and 1250 cm⁻¹ refer to amide I, amide II and amide III vibrational modes, respectively, while the peaks at 3302 cm⁻¹, 2918 cm⁻¹, 2850 cm⁻¹ are related to the stretching mode vibration of unbonded N-H groups and to the antisymmetric and symmetric stretching modes of methylene groups, respectively. This data would support the assumption that the extrusion processing aid is most likely an aliphatic amide (bis-stearamide) [32-34] and could be removed by ethanol [32, 33].

PurSil[®] 35 80A (a silicone-polyether-urethane) was developed by the Polymer Technology Group Inc. (PTG), USA. It is prepared by a multi-step bulk synthesis in which 35% polydimethylsiloxane is incorporated into the polymer soft segment with poly(tetramethylene oxide) glycol. The hard segment consists of MDI, with a low molecular mass glycol chain extender [36]. This very advanced and superior material (in terms of chemical resistance and mechanical properties) could potentially be used in the manufacturing of pacemaker leads.

4.3 Experimental

4.3.1 Materials

Pellethane[®] 2363-80AE and PurSil[®] 35-80A were obtained from Dow Chemicals (USA) and Polymer Technology Group, Inc. (USA), respectively. Tetrahydrofuran (THF) (Merck, Cat: AB009731) and N,N-dimethylformamide (Aldrich, Cat: 27,054-7) were used as solvents and 60% (w/w) sodium hydride (Fluka, Cat: 71620) served as strong base. 4-Pentenoyl chloride (Aldrich, Cat: 46,847-9) was used as acylation reagent. Water, ethanol (EtOH) (Merck, Cat: BB10107), n-hexane (Merck, Cat: 152496G), di-ethyl ether (Riedel-de Haën, Cat: 32203), iso-propanol (Aldrich, Cat: 15,497-0) and cyclohexane (Aldrich, Cat: 15,474-1) were used as non-solvents.

4.3.2 Modification of Pellethane[®] 2363-80AE

4.3.2.1 Purification

A 10% solution (w/w) of Pellethane[®] 2363-80AE and THF was slowly poured into a glass beaker containing a 10-fold excess of vigorously stirring ethanol at room temperature, as suggested in the literature [33, 35], to effect the precipitation of the polymer. After decanting most of the ethanol, the remaining ethanol was removed from the polymer by vacuum drying for 24 h at room temperature. This was repeated at least twice or until the satisfactory removal of the processing aid was observed by FT-IR analysis. The purified polymer was then vacuum dried at room temperature for 4 days and stored in a dark bottle under an inert atmosphere (helium) for later use.

In an attempt to isolate the processing aid 300 ml of ethanol was added to 200 g of Pellethane[®] 2363-80AE pellets and shaken on a laboratory shaker for 12 hours. The resulting solution was then filtered, the solvent removed *in vacuo* on a rotary evaporator and vacuum dried for 24 h. Samples were then submitted for FT-IR analysis.

4.3.2.2 Acylation using 4-pentenoyl chloride

Dried, purified Pellethane[®] 2363-80AE (hereafter referred to as Pellethane) was weighed off and dissolved (under an inert atmosphere) in N,N-dimethylformamide (DMF) (over night at 50 °C). Helium was used to maintain an inert atmosphere in all experiments. The formulation for a typical experiment is summarized in Table 4.1.

A 1000-ml round-bottomed reaction vessel was fitted with a septum, thermometer and inert gas supply. Reactions were carried out under anhydrous conditions, using dry solvents, under an inert atmosphere.

Table 4.1: Typical formulation used for the modification of Pellethane

Reactants	Mass (g)
Pellethane [®] 2363-80AE	25.00
Dimethyl formamide (DMF)	550.00
Sodium hydride (NaH)	0.40
4-Pentenoyl chloride (4-PCI)	1.77

The pre-dissolved Pellethane (25 g in 550 g DMF) was added to the reactor and cooled down to below 0 °C, using a mixture of ice and ethanol. A suspension of NaH (0.4 g) in DMF (10 g) was then slowly added to the reactor over 20 min and the resulting mixture was left for 60 min to allow the formation of the anion.

A 50% molar excess of 4-pentenoyl chloride (1.77 g) in DMF (10 g) was added drop-wise over a period of 20 min, using a syringe. The resulting mixture was left for 30 min at a temperature of below 0 °C, whereafter the ice-bath was removed and the reaction mixture allowed to warm to room temperature (≈ 20 °C). The reaction was allowed to continue for an additional 30 min. The reaction product was then isolated.

4.3.2.3 Isolation of the reaction product

The reaction mixture was slowly poured into a glass beaker (over a period of 10 minutes) containing a 10-fold excess of vigorously stirring water (non-solvent) at room temperature to effect the precipitation of the modified polymer. After decantation of most of the water, the remaining water was removed from the polymer by vacuum drying for 24 h in the dark, at room temperature. The dried polymer was re-dissolved in THF and re-precipitated in a 10-fold excess of ethanol, and vacuum dried under the same conditions.

4.3.2.4 Changing the degree of modification

The modification of Pellethane was studied by first adding 5.0 mmol (0.20 g) NaH to a pre-dissolved Pellethane solution (25 g in 550 g DMF) in an amount equal to 10 mole percent (relative to the nominal molar amount of carbamate nitrogens) in the polymer solution [1]. The molar amount of NaH was then increased to above 20.0 mmol (0.80 g) (over a period of 60 min), while the temperature was kept well below 0 °C. This was done in an effort to determine the maximum degree of modification possible for Pellethane.

Pellethane (25 g) was subsequently modified with different quantities of NaH, in six separate reactions, as described in §5.3.2.2: 0.20 g (5.0 mmol), 0.30 g (7.5 mmol), 0.40 g (10.0 mmol), 0.50 g (12.5 mmol), 0.60 g (15.0 mmol) and 0.80 g (20.0 mmol). After addition of the 4-pentenoyl chloride followed by isolation and purification, the respective yields were calculated and the samples submitted for NMR analyses.

4.3.3 Modification of PurSil® 35-80A

4.3.3.1 Acylation using 4-pentenoyl chloride

Dried PurSil® 35-80A (hereafter referred to as PurSil) was weighed off and dissolved (under an inert atmosphere) in DMF (overnight at 50 °C). The formulation for a typical experiment is summarized in Table 4.2.

Table 4.2: Typical formulation for the modification of PurSil

Reactants	Mass (g)
PurSil® 35 80A	25.00
Dimethyl formamide (DMF)	550.00
Sodium hydride (NaH)	0.75
4-Pentenoyl chloride (4-PCI)	3.18

A 1000-ml round-bottomed reaction vessel was fitted with a septum, thermometer and inert gas supply. Reactions were carried out under anhydrous conditions, using dry solvents under an inert atmosphere.

The pre-dissolved PurSil (25 g in 550 g DMF) was added to the reactor and cooled down to below 0 °C (0 - -4 °C), using a mixture of ice and ethanol. A suspension consisting of NaH (0.75 g) in DMF (10 g) was then slowly added to the reactor over 20 min and the resulting mixture was left for 90 min to allow the formation of the anion.

A 50% molar excess of 4-pentenoyl chloride (3.18 g) in DMF (10 g) was added dropwise over a period of 20 min, using a syringe. The resulting mixture was left for 30 min at a temperature of below 0 °C, whereafter the ice-bath was removed and the reaction mixture allowed to warm to room temperature (≈ 20 °C). The reaction was allowed to continue for an additional 30 min. The reaction product was then isolated.

4.3.3.2 Isolation of the reaction product

A number of non-solvents at different temperatures (-20 - +22 °C) were evaluated to effect the precipitation of the modified PurSil (from the reaction solution). These included water, ethanol, n-hexane, di-ethyl ether, iso-propanol and cyclohexane (see list of non-solvents in Appendix A1). The polymer solution was added dropwise to the vigorously stirring non-solvents (10-fold excess) and the recovered polymer dried and weighed.

After determination of a suitable non-solvent the reaction product could be recovered by slowly pouring it into a glass beaker containing a 10-fold excess of the vigorously stirring non-solvent. Remaining non-solvent was removed from the polymer by vacuum drying. The dried polymer was re-dissolved in THF and different non-solvents

again evaluated (as described above), after which the polymer could be recovered and vacuum dried for 24 h in the dark at room temperature.

4.3.3.3 Changing the degree of modification

The modification of PurSil was studied by first adding 0.40 g (10.0 mmol) NaH to a pre-dissolved PurSil solution (25 g in 550 g DMF). In an effort then to determine the maximum degree of modification possible, up to 1.50 g NaH was added to the pre-dissolved PurSil solution.

PurSil (25g) was then modified in three different reactions with 0.75 g (18.8 mmol), 1.13 g (28.3 mmol) and 1.50 g (37.5 mmol) NaH. After isolation and purification, the respective yields were calculated and the samples submitted for NMR analyses.

4.3.4 Analyses

4.3.4.1 Fourier-transform infrared spectroscopy

Samples were analyzed by means of photo acoustic FT-IR. The photo acoustic detector (MTEC model 300) was coupled to a Thermo Nicolet Avatar 370 spectrophotometer. The parameters used for the determination of each spectrum were the following:

Mirror velocity:	0.4 cm/s	Spectral range:	400 - 4000 cm^{-1}
Resolution:	8 cm^{-1}	Number of scans:	512
Source aperture:	maximum	Detector gas:	helium

A core sample (10 mm in diameter) was punched out from the pre-cast disk and placed in the sample holder cup, allowing as little air into the sample compartment as possible. A typical scan required fifteen minutes scan time. This allowed enough time for the sample temperature to equilibrate, and hence, to obtain a quantitative measurement.

4.3.4.2 Nuclear magnetic resonance spectroscopy

Approximately 30 mg of product was dissolved in deuterated THF (d-THF). Proton (^1H) and carbon (^{13}C) NMR spectra of the modified and control samples were obtained from a Varian Unity 600 spectrometer at 600 and 100 MHz frequency respectively. Chemical shifts are reported as δ (ppm) - values relative to tetramethylsilane (TMS) as internal reference. The degree of modification was calculated as a fraction of the integrated, vinyl proton signals (keeping in mind that it integrates for three protons) and the total number of carbamate nitrogens (i.e. the unmodified carbamate protons plus those modified (vinyl protons)).

4.4 Results and discussion

4.4.1 Modification of Pellethane® 2363-80AE

4.4.1.1 Purification

FT-IR analysis of the unpurified Pellethane pellets confirmed the presence of peaks at 3302 cm^{-1} (1), 2918 cm^{-1} (2) and 1635 cm^{-1} (3) (Figure 4.1, --blue), indicative of a bis-stearamide processing aid [32-35]. Extractions carried out according to the literature [32, 33], using ethanol to remove the processing aid, however, highlighted a second impurity that remained (Figure 4.1, --red) [37]. This impurity appears to be an imine [38] and is seen together with many other peaks, typical of a urethane in Figure 4.2 to be short molecular mass or cyclized isocyanate by-products [38].

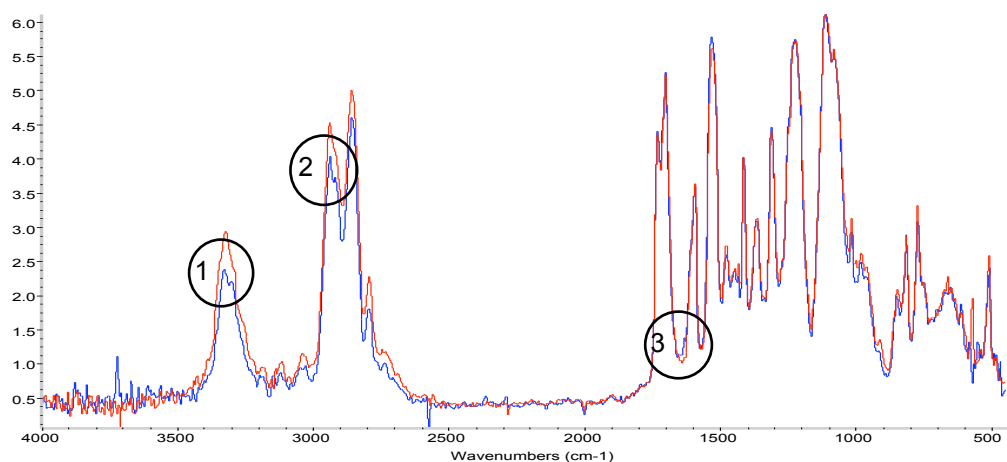


Figure 4.1: FT-IR analyses of (--) unpurified and (--) purified Pellethane

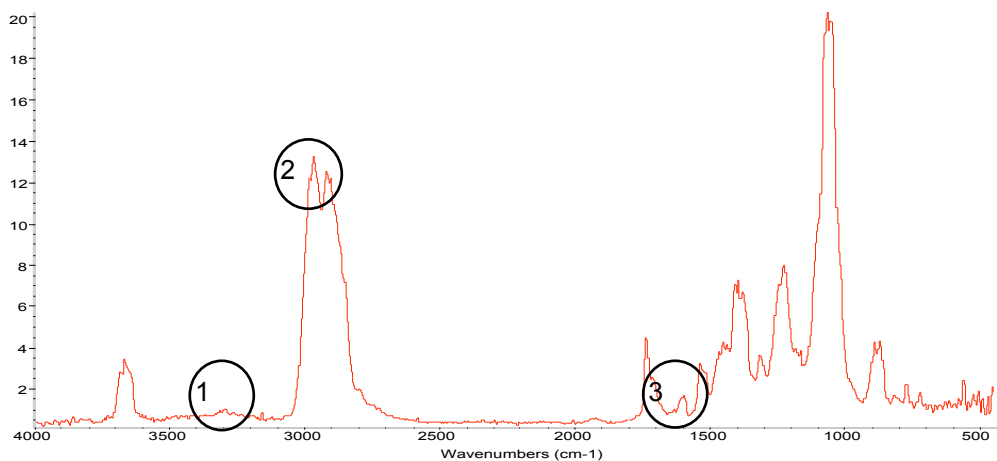


Figure 4.2: FT-IR analyses of the recovered processing aid corresponding with the peak numbers presented in Figure 4.2

The sensitivity was not strong enough to see the wax components in Figure 4.1, but there is a much stronger evidence of the wax in Figure 4.2, especially in peak 2. Approximately 0.35 g of processing aid was recovered from the 200 g Pellethane pellets used.

4.4.1.2 Acylation using 4-pentenoyl chloride

Evolution of hydrogen gas was immediately observed after the addition of the sodium hydride (5.0 mmol). After 5 - 10 min the solution had a slight yellowish-green color caused by the urethane polyanion, showing successful deprotonation. This observation was consistent with the literature [2, 4].

After reaction with 4-PCI, followed by isolation and purification, the resulting polymer was submitted, together with a Pellethane control sample, for ^1H NMR analysis. The results are presented in Figures 4.3 and 4.4 respectively.

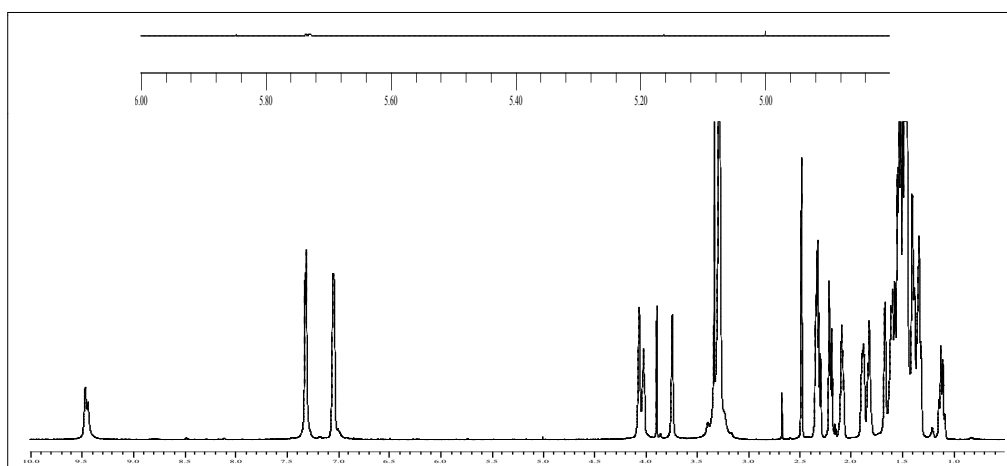


Figure 4.3: ^1H NMR spectrum of Pellethane (control)

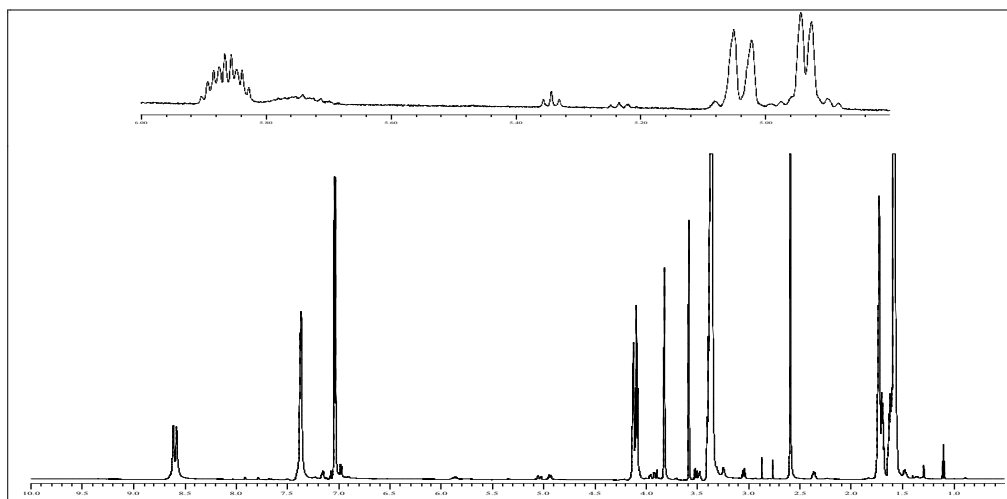


Figure 4.4: ^1H NMR spectrum of modified Pellethane

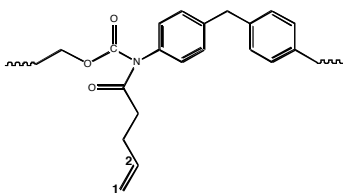


Figure 4.5: Partial structure of modified Pellethane

The introduction of a 4-pentenoyl unit resulted in the appearance of characteristic signals between 4.91 - 5.07 ppm and 5.81 - 5.92 ppm (Figure 4.4), when compared to Figure 4.3 (Pellethane control). These are attributed to the vinyl protons (H -1) and (H -2), respectively (Figure 4.5), indicating successful modification of Pellethane.

An average degree of modification of 4.5% was calculated, based on the proton-NMR spectrum data (Figure 4.4). The degree of modification indicates the percentage of carbamate hydrogens (at 8.5 - 8.7 ppm) substituted with the modification reagent.

Pellethane was thus successfully modified with 4-pentenoyl chloride after deprotonation, using sodium hydride. Hence the chemistry was successfully transferred from the model compound (Chapter 3) to a medical grade polyurethane (Pellethane[®] 2363-80AE). This was considered significant and meaningful.

When the molar amount of NaH was increased to above 20.0 mmol NaH per 25 g Pellethane the color of the mixture changed from a slight yellowish-green to a brownish color, whereafter the polymer started precipitating out of solution, forming brown sludge at the bottom of the reactor. It was not possible to recover the polymer after addition of 4-pentenoyl chloride. At high sodium hydride concentrations it is believed that the polyanion could become unstable, resulting in the degradation of the polymer chains [2].

Thereafter only 20.0 mmol NaH was added to a Pellethane solution, reacted with 4-pentenoyl chloride, the product isolated and purified, and submitted for proton nuclear magnetic resonance spectroscopy. The ¹H NMR spectrum of the modified Pellethane is presented in Figure 4.6.

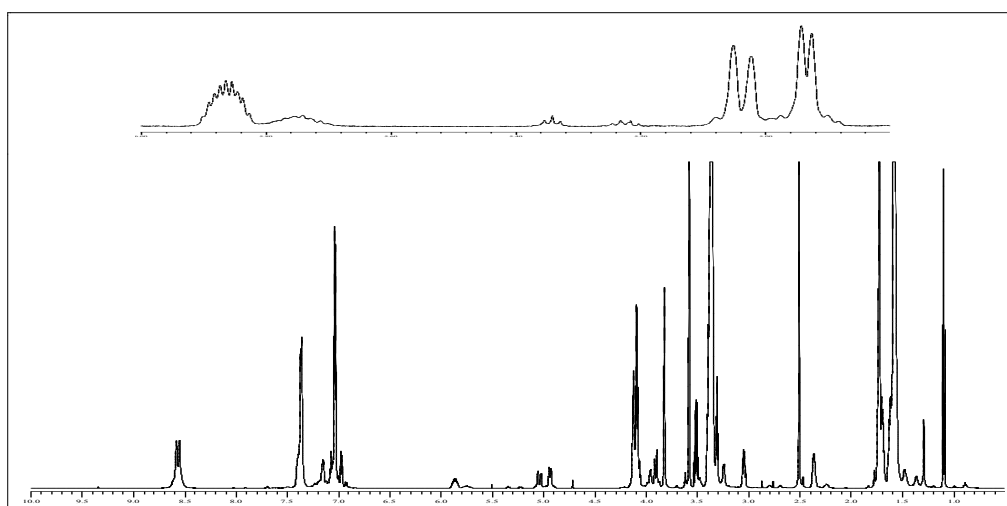


Figure 4.6: ¹H NMR spectrum of modified Pellethane

The appearance of the characteristic vinyl proton signals between 4.90 - 5.07 ppm and 5.81 - 5.91 ppm was once again evident. The maximum degree of modification was found to be 20.0%, based on calculations of the ^1H NMR spectrum (Figure 4.6).

Calculations from ^1H NMR spectra revealed an increase in the modification extent with increasing NaH concentration (Table 4.4). The yields (w/w), on the other hand, randomly varied between 85 to 88% for the Pellethane samples.

Table 4.4: Control of extent of modification of Pellethane using different quantities of NaH

NaH (mmol)	5.0	7.5	10.0	12.5	15.0	20.0
Modification (%) (Theoretical)	5.0	7.5	10.0	12.5	15.0	20.0
Modification (%) (Experimental)	4.7	7.0	10.1	11.7	14.7	19.8

The degrees of modification at the lower end (4.5% & 4.7%) as well as at the higher end (20.0% & 19.8%) were found to be reproducible ($n = 2$). Very good correlation ($R^2 = 0.99$) and a very tight 95% confidence interval (see Figure 4.7) were obtained between the theoretically calculated (based on calculations assuming 1:1 reaction of NaH with carbamate hydrogen) and experimentally (% modification indicates % of hydrogens on carbamate substituted with modification reagent) obtained degrees of modification, for the five reactions (as presented in Table 4.4) and the two repeat experiments (i.e. a total of eight experiments). The Bland Altman plot (Figure 4.8) further shows a positive difference between the theoretical and experimentally obtained degrees of modification (i.e. experimental values always lower than theoretical values), probably due to trace amounts of water present during the reaction.

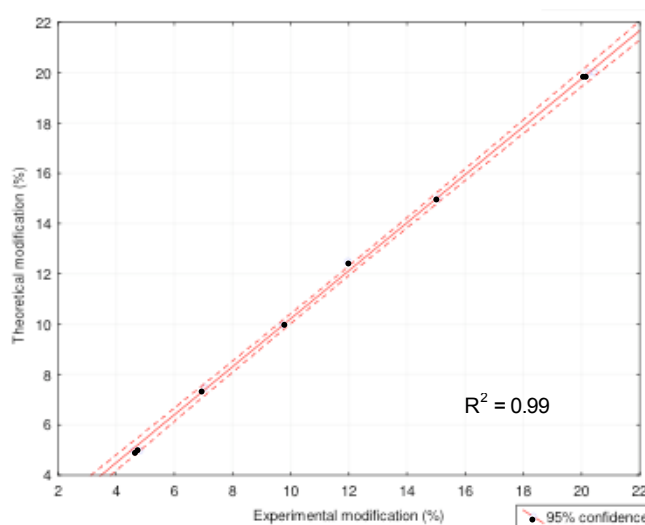


Figure 4.7: Correlation between theoretical and experimental degrees of modification of Pellethane

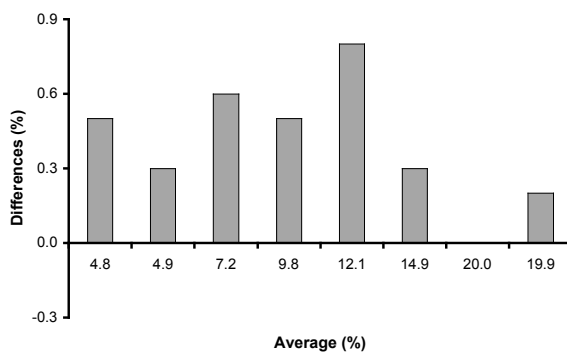


Figure 4.8: Bland Altman plot showing the differences between theoretically and experimentally obtained degrees of modification of Pellethane

The relationship between the degrees of modification obtained experimentally (Table 4.4) was tested against the sodium hydride concentration using linear regression. A linear regression coefficient (R^2) equal to 0.99 was obtained, signifying linearity, the result of which is shown in Figure 4.9. It was hence found to be possible to accurately control the degree of modification (between 4.5% - 20%) by changing the molar amount of NaH.

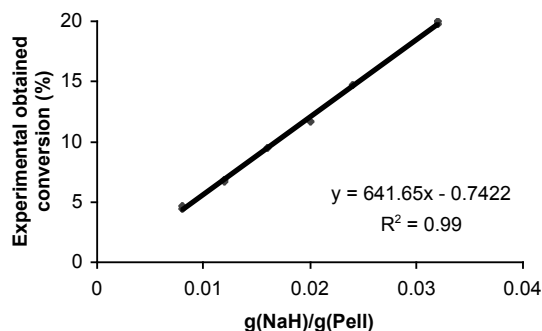


Figure 4.9: Change in degrees of modification of Pellethane with change in NaH concentration

4.4.2 Modification of PurSil® 35-80A

4.4.2.1 Acylation using 4-pentenoyl chloride

Water (1 - 4 °C) was found to be the best non-solvent to effect the precipitation of modified PurSil from the reaction mixture when DMF was used as solvent and in the second precipitation, n-hexane (-20 °C) was best when tetrahydrofuran was used as solvent.

Immediately after the addition of NaH (10.0 mmol) the solution showed a greenish color. This, in addition to the evolution of hydrogen, indicated successful deprotonation, and was consistent with the literature [2, 4].

After addition of 4-PCI, isolation and purification, the resulting polymer was submitted, with a PurSil control sample, for ^1H NMR analysis. Spectra are shown in Figures 4.10 and 4.11 respectively.

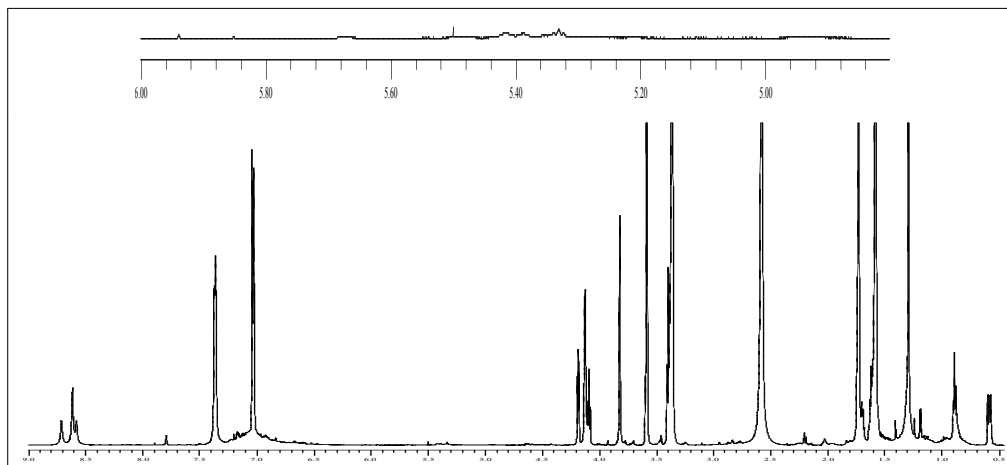


Figure 4.10: ^1H NMR spectrum of PurSil (control)

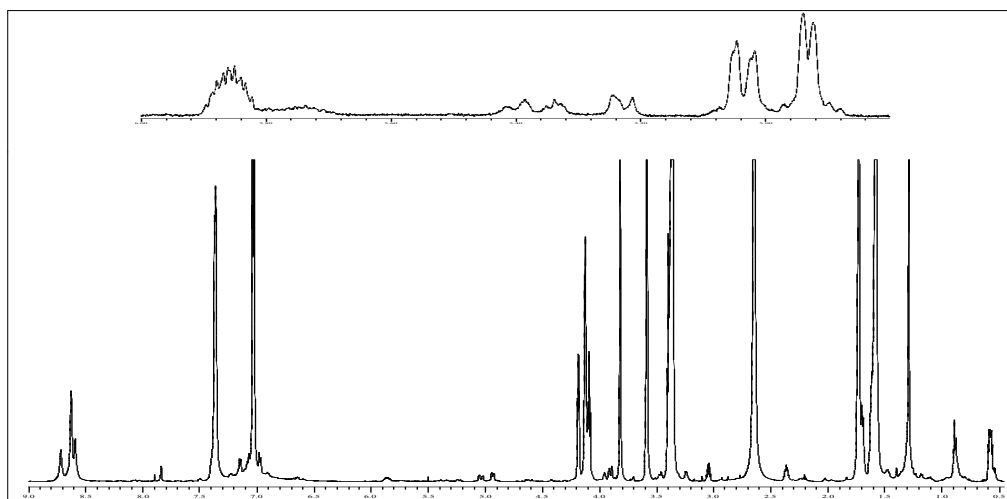


Figure 4.11: ^1H NMR spectrum of modified PurSil

The introduction of a 4-pentenoyl unit resulted in the appearance of characteristic signals between 4.90 - 5.07 ppm and 5.81 - 5.91 ppm in Figure 4.11, when compared to Figure 4.10 (PurSil control). These signals are attributed to the vinyl protons, indicating successful modification of a second medical grade polyurethane, PurSil[®] 35-80A.

An average degree of modification of 8.1% (% modification indicates the % of carbamate hydrogens (at 8.5 - 8.8 ppm) substituted with modification reagent) was calculated based on the ^1H NMR data (Figure 4.11).

PurSil[®] 35-80A was thus successfully modified with 4-pentenoyl chloride, although the degree of modification was slightly lower compared to modified Pellethane[®] 2363-

80AE (using the same NaH concentration). This can be attributed to the difference in chemical structure (and thus stoichiometry) between Pellethane[®] 2363-80AE and PurSil[®] 35-80A.

It was found that increasing the molar amount of NaH beyond 37.5 mmol had very little or no further effect on the degree of modification. The appearance of the characteristic vinyl proton signals between 4.91 - 5.07 ppm and 5.81 - 5.91 ppm in Figure 4.12 was once again evident. The maximum degree of modification was thus found to be 18.5%, calculated from ¹H NMR data (Figure 4.12).

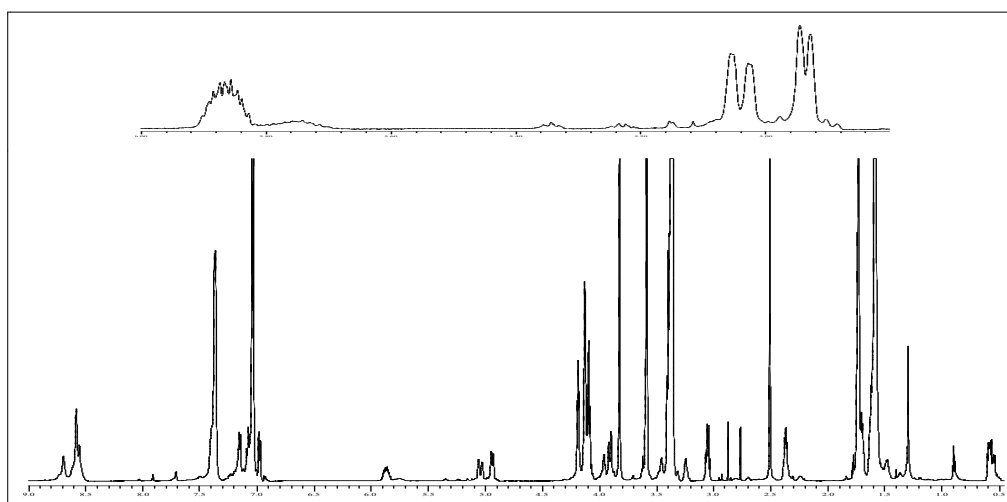


Figure 4.12: ¹H NMR spectrum of modified (18.5%) PurSil

The yields obtained after the treatment of PurSil with the range of NaH concentrations (Table 4.5) varied randomly between 50 and 60%, which were much lower than for the Pellethane samples. It was very difficult to effect the precipitation of PurSil when drastic conditions (temperatures as low as -20 °C) were not used. Calculations from ¹H NMR spectra of the three modified PurSil samples revealed an increase in the extent of modification with increasing NaH addition (Table 4.5).

Table 4.5: Control of extent of modification of PurSil with increase in NaH addition

NaH (mmol)	18.8	28.3	37.5
Modification (%) (Theoretical)	11.5	15.0	18.5
Modification (%) (Experimental)	11.7	15.2	17.9

The reproducibility of the reaction (n = 2) to obtain a theoretical degree of modification of 18.5% was tested and found to be reproducible (18.7%). A very good correlation ($R^2 = 0.99$, see Figure 4.13) was obtained between the theoretically calculated and experimentally obtained degrees of modification, for the three experiments (as

presented in Table 4.4) and the repeat experiment (i.e. a total of four experiments). An expected wider 95% confidence interval was obtained and can most likely be attributed to the very small sample size (n = 4).

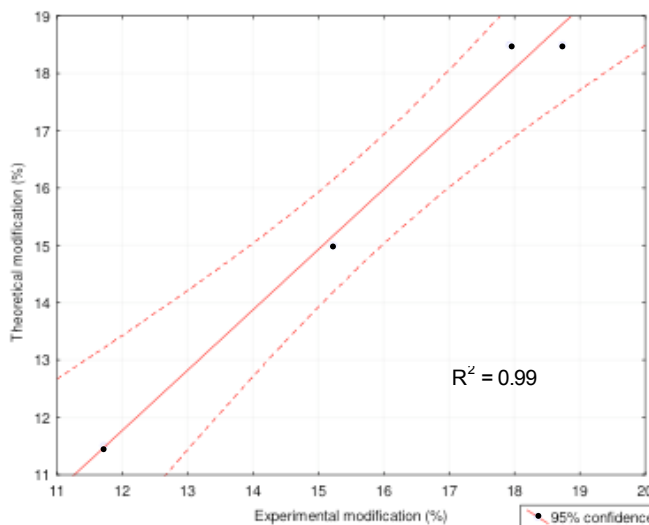


Figure 4.13: Correlation between theoretical and experimental degrees of modification of PurSil with NaH

The relationship between the degrees of modification obtained experimentally (Table 4.5) was tested against the sodium hydride concentration using linear regression. A linear regression coefficient (R^2) equal to 0.99 was obtained, signifying linearity (see Figure 4.15). It is thus possible to accurately control the degree of modification (between 11.5 - 18.5%) by changing the molar amount of NaH.

The Bland Altman plot shows small random differences between the theoretical and experimentally obtained degrees of modification. These differences could be due to experimental and/or analytical errors.

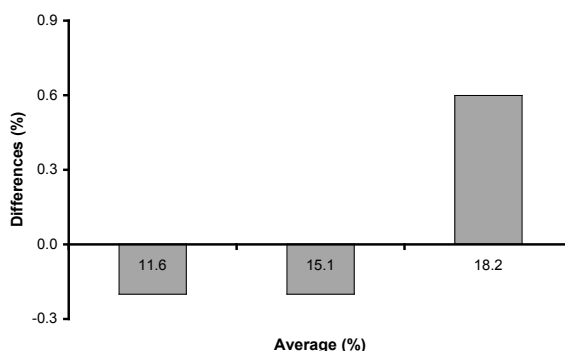


Figure 4.14: Bland Altman plot

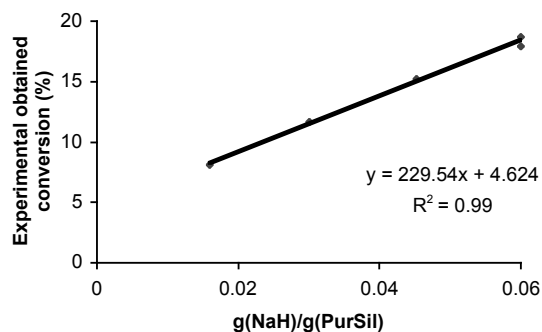


Figure 4.15: Change in degree of modification with change in NaH concentration

4.5 Conclusions

Pellethane[®] 2363-80AE could be purified by precipitation using ethanol at room temperature and then successfully modified with 4-pentenoyl chloride. The model compound chemistry could thus be successfully transferred to a medical grade polyurethane. A maximum degree of modification of 20.0% could be obtained and the degree of modification could be accurately ($R^2 = 0.99$) and reproducibly ($n = 2$) controlled, to between 4.5% and 20%, by changing the sodium hydride and 4-pentenoyl chloride concentrations accordingly.

A second medical grade polyurethane, with a different chemical structure and stoichiometry, namely PurSil[®] 35-80A, could also be successfully modified with 4-pentenoyl chloride. The maximum degree of modification was determined by proton-NMR spectroscopy and found to be 18.5%. The degree of modification could accurately be controlled to between 11.5% and 18.5% by changing the sodium hydride and 4-pentenoyl chloride concentrations, respectively.

4.6 References

1. Levy, R. and I.S. Alferiev, *Derivated polyurethane compositions which exhibit enhanced stability in biological systems and methods of making the same*. United States Patent Office. US 6,320,011 B1, 2001: USA
2. Adibi, K., M. George, and J. Barrie, *Anionic synthesis of poly(urethane-g-acrylonitrile)*. *Polymer*, 1979. **20**: p. 483-487.
3. Cairns, T., H. Foster, A. Larchar, A. Schneider, and R. Schreiber, *Preparation and properties of N-methylol, N-alkoxymethyl and N-alkylthiomethyl polyamides*. *J. Am. Chem. Soc.*, 1949. **71**: p. 651-655.
4. Liaw, D.-J. and S.-P. Lin, *Phosphorus-containing polyurethanes based on bisphenol-s, prepared by N-alkylation*. *Eur. Polym. J.*, 1996. **32**: p. 1377-1380.
5. Sivriev, H., S. Georgiev, and G. Borissov, *Phosphorus-containing polyurethanes, prepared by N-modification*. *Eur. Polym. J.*, 1990. **26**(1): p. 73-76.
6. Tesoro, G., *Chemical modification of polymers with flame-retardant compounds*. *J. Pol. Sci. Macromol. Rev.*, 1978. **13**: p. 283-353.

7. Espenschied, B. and R. Schulz, *Metalation and N-alkylation of some polyamides*. Poly. Bull, 1981. **5**: p. 489-495.
8. Beachell, H. and C. Ngoc Son, *Stabilization of polyurethane to thermal degradation*. J. Appl. Polym. Sci., 1964. **8**: p. 1089-1096.
9. Takayangi, M. and T. Katayose, *N-substituted poly(p-phenyl terephthalamide)*. J. Polym. Sci., Polym. Chem. Ed., 1981. **19**: p. 1133-1145.
10. Kashani, H., J. Barrie, and M. George, *Synthesis of vinyl graft copolymers of poly(hexamethylene adipamide) and poly(m-phenylene isophthalamide)*. J. Polym. Sci.: Polym. Chem. Ed., 1978. **16**: p. 533-537.
11. Alferiev, I. and I. Fishbein, *Activated polyurethane modified with latent thiol groups*. Biomaterials, 2002. **23**: p. 4753-4758.
12. Grasel, T., J. Pierce, and S. Cooper, *Effects of alkyl grafting on surface properties and blood compatibility of polyurethane block copolymers*. J. Biomed. Mater. Res., 1987. **21**: p. 815-842.
13. Alferiev, I., N. Vyavahare, C. Song, J. Connolly, J. Hinson, Z. Lu, S. Tallapragada, R. Bianco, and R. Levy, *Biophosphonate derivatized polyurethanes resist calcification*. Biomaterials, 2001. **22**: p. 2683-2693.
14. Baumgartner, J. and S. Cooper, *Bacterial adhesion on polyurethane surfaces conditioned with thrombus components*. ASAIO J., 1996. **42**(5): p. M476-9.
15. Mikroyannidis, J., *Phosphorus-containing polyurethanes and copolyurethanes based on 1,2-dihydroxy-1,2-bis(diethoxyphosphinyl)*. J. Pol. Sci., Pol. Chem. Ed., 1984. **22**: p. 891-903.
16. Li, Y.-J., N. Nakamura, Y.-F. Wang, M. Kodaman, and T. Nakaya, *Synthesis and hemocompatibilities of new segmented polyurethanes and poly(urethane urea)s with poly(butadiene) and phosphatidylcholine analogues in the main chains and long-chain alkyl groups in the side chains*. Chem. Mater., 1997. **9**: p. 1570-1577.
17. Pascault, J. and M. Dumon, *Method for obtaining a crosslinkable polyurethane and its uses*. World Patent Office. WO 02/44239 A1, 2002: France.
18. Sardanopoli, A. and J. Stonehouse, *Cross-linking thermoplastic polyurethane*. United States Patent Office. US 6,258,310, 2001: USA.
19. Zamore, A., *Irradiation conversion of thermoplastic to thermoset polymers*. United States Patent Office. US 6,596,818, 2003: USA.
20. Beyer, G. and B. Steckenbiegler, *Radiation crosslinked thermoplastic polyurethanes*. J. Int. Polym. Sci. Techn., 1991. **19**(1): p. T6-T10.
21. Goyert, W., J. Winkler, H. Perrey, and H. Heidingsfield, *Process for the production of radiation-crosslinked thermoplastic polyurethanes*. United States Patent Office. US 4,762,884, 1988: USA
22. Reitel, C. and L. Goethlich, *Curable coating composition*. United States Patent Office. US 4,239,866, 1980: USA.
23. Muhfeld, H., T. Schaubert, and S. Wagener, *Molded polyurethane bodies*. United States Patent Office. US 6,573,341, 2003: USA.
24. Jung, H., J. Kang, W. Kim, Y.-B. Lee, K. Choe, S.-H. Hong, and S.-B. Kim, *Properties of crosslinked polyurethanes synthesized from 4,4'-diphenylmethane diisocyanate and polyester polyol*. J. Appl. Polym. Sci., 2000. **78**: p. 624-630.
25. Stern, T., A. Penhasi, and D. Cohn, *Derivatization of a new poly(ether urethane amide) containing chemically active sites*. Biomaterials, 1995. **16**: p. 17-23.
26. Petrovic, Z., M. Ilavsky, K. Dusek, M. Vidakovic, I. Javni, and B. Banjanin, *The effect of crosslinking on properties of polyurethane elastomers*. J. Appl. Polym. Sci., 1991. **42**: p. 391-398.
27. Nasar, A., M. Jikei, and M.-A. Kakimoto, *Synthesis and properties of elastomers crosslinked with amine-terminated AB2-type hyperbranched polyamides*. Eur. Polym. J., 2003. **39**: p. 1201-1208.
28. Le Roy, P. and J. Pattein, *Crosslinkable thermoplastic polyurethane resins containing ethylenic side groups*. United States Patent Office. US 4,366,301, 1982: USA.
29. Gordon, J., *Non-allergenic medical and health care devices made from crosslinked synthetic elastomers*. United States Patent Office. US 5,997,969, 1991: USA.

30. Kayaman-Apohan, N., A. Amanoel, N. Arsu, and A. Gungor, *Synthesis and characterization of UV-curable vinyl ether functionalized urethane oligomers*. Prog. Org. Coat., 2004. **49**: p. 23-32.
31. www.dowchemicals.com, *Typical physical properties of Pellethane*. [accessed: 8 June 2006].
32. Coury, A., P. Slaikeu, P. Cahalan, K. Stokes, and C. Hobot, *Factors and interactions affecting the performance of polyurethane elastomers in medical devices*. J. Biomater. Appl., 1988. **3**: p. 130-176.
33. Tanzi, M., D. Mantovani, P. Petrini, R. Guidoin, and G. Laroche, *Chemical stability of polyether urethanes versus polycarbonate urethanes*. J. Biomed. Mater. Res., 1997. **36**(4): p. 550-559.
34. Stokes, K., A. Coury, and P. Urbanski, *Autooxidative degradation of implanted polyether polyurethane devices*. J. Biomater. Appl., 1987. **1**(4): p. 411-448.
35. Stokes, K., P. Urbanski, and J. Upton, *The in vivo auto-oxidation of polyether polyurethane by metal ions*. J. Biomater. Sci., Polym. Ed., 1990. **1**(3): p. 207-230.
36. www.polymertech.com, *The polymer technology group*. [accessed: 8 June 2006].
37. Han, D., K. Park, and Y. Kim, *Sulfonated poly(ethylene oxide)-grafted polyurethane copolymer for biomedical applications*. J. Biomater. Sci., Polym. Ed., 1998. **9**(2): p. 163-174.
38. Christian, G. and J. O'Reilly, *Instrumental Analysis*. 2nd ed. 1986, Boston: Allyn and Bacon, Inc. p. 238-239

Chapter 5

Crosslinking of novel modified polyurethanes

Abstract

A number of existing thermoplastic polyurethanes (TPUs) exhibit poor creep and large hysteresis (energy losses) when subjected to static or dynamic loading. The mechanical drawbacks of these existing TPUs have prompted the modification and crosslinking of such materials, replacing weak hydrogen bonding with permanent covalent crosslinks. Crosslinking of the two novel modified polyurethanes (Chapter 4) were studied using different initiation sources (ultraviolet light (UV), heat and gamma irradiation), initiators and crosslinking enhancing monomers. The swelling behavior (determined gravimetrically) of the crosslinked films allowed for the calculation of the swelling index (Q) and, in turn, the molecular mass between crosslinks. The mechanical properties (specifically hysteresis, creep and $\tan \delta$) of the respective controls and crosslinked films were then evaluated using uniaxial tensiometric testing and dynamic mechanical analysis. Successful UV and heat induced crosslinking of the two novel modified polyurethanes (Pellethane and PurSil) was achieved, using ω,ω -dimethoxy- ω -phenylacetophenone (DMPA) and dicumyl peroxide (DCP), respectively, although only UV initiation was investigated as a method of crosslinking for modified PurSil. The swelling index values, used to calculate the molecular mass between crosslinks, were used to optimize the initiator concentrations. The optimum initiator concentration, i.e. the smallest Q value, was found to be between 1.5% and 2.0% (both for DMPA and DCP) for modified Pellethane, and between 2.0% and 2.5% (DMPA) for modified PurSil. The lowest Q value (i.e. the lowest molecular mass between crosslinks) was obtained for the 15.0% and 18.5% modified and crosslinked Pellethane (Pell15.0) and PurSil samples (Pur18.5), respectively. The best mechanical properties (e.g. hysteresis) were also obtained for Pell15.0 and Pur18.5, with respective improvements of up to 42.5% in hysteresis and 44.3% in creep for Pell15.0 and improvements of up to 12.9% in hysteresis for Pur18.5. The use of the crosslinking enhancing monomer, MBA, resulted in lower swelling index values, but had a detrimental effect on the hysteresis. It was therefore not included in further investigations.

5.1 Introduction

The drawbacks associated with the mechanical and chemical properties of existing medical grade polyurethanes (e.g. they may be prone to excessive dilation and still have unproven long-term biostability) [1-10], prompted the modification and crosslinking of these existing polyurethanes, replacing labile hydrogen bonding with permanent covalent crosslinks.

Crosslinking of the two novel modified polyurethanes (Chapter 4) were evaluated using different crosslinking systems (ultraviolet light, thermal and gamma irradiation) and various initiators. In an attempt to further enhance crosslinking, the addition of a number of crosslinking enhancing monomers was also investigated.

Quantification (i.e. the efficiency of crosslinking) of all the crosslinked films was first determined using the swelling behavior (determined gravimetrically), which allowed for the calculation of the swelling index (Q). The swelling index was specifically used as an analytical tool to quantify the degree of crosslinking (i.e. the lowest Q results in the highest crosslink density) and was not used to try and simulate *in vivo* behavior. The swelling index values were then used to calculate the molecular mass between crosslinks [11-14]. Due to complexity and uncertainty of the exact structure of the polymerized system only the films where no monomer was added were considered in these calculations.

The mechanical properties of the controls and crosslinked polyurethane films were then evaluated using uniaxial tensiometric testing and dynamic mechanical analysis (DMA) to determine the effect of crosslinking on the energy losses. The parameters studied included hysteresis, creep and $\tan \delta$. Correlation between the mechanical properties (e.g. hysteresis) and swelling index values was then investigated.

5.2 Historical

Thermoplastic polyurethanes (TPU) are known to suffer from excessive plastic deformation when subjected to cyclic loading. Due to their wide range of applications, the mechanical properties of existing and new TPUs, when subjected to cyclic loading (hysteresis) [3-6] or static loads (creep) [7-10], have been studied extensively.

A number of polyurethanes, comprising different hard and soft segments and chain extenders, have been studied. In one such a study a poly(urethane urea) and three polyurethanes were synthesized, comprising 4,4-methylenebis(phenylisocyanate) (MDI), poly(tetramethylene oxide) glycol (PTMEG) and 1,4-butanediol (BDO) (in different ratios) [3]. The main objective of the study was to minimize the hysteresis. The lowest hysteresis results were obtained with the TPU having an amorphous, well-dispersed hard segment structure. This led to the development of a complex mathematical model [5] describing the

important mechanical properties of the polyurethanes under investigation. In other studies, large hysteresis of new poly(dimethylsiloxane) based segmented polyurea copolymers [4] and dibenzyl-based polyurethanes [6] have also been reported.

The dynamic [7] and static [8] creep behavior of polyurethanes have also been studied. The dynamic creep behavior of novel poly(aliphatic/aromatic-ester) urethanes was compared with an existing medical grade polyurethane (Pellethane[®] 2363-80AE) [7]. Pellethane exhibited poor creep, especially when compared to the ester-based polyurethanes. Unfortunately, the latter are known to be hydrolytically unstable (as discussed in Chapter 2) and this precludes their use as biomaterial.

The crosslinking of polyurethanes has been achieved by various pathways, as discussed in Chapter 4 (§4.2). Although the main objective of most of the studies was not necessarily to improve the mechanical properties, many researchers used solubility and the swelling index (Q) [11-13, 15-17] in the former to indicate successful crosslinking or in the latter to optimize crosslinking. Swelling index values were then further used to calculate the molecular mass between crosslinks [11-14] according to the well-known Flory-Rehner [16] equation. As Q decreases, the molecular mass between crosslinks is reduced, resulting in a more densely crosslinked structure [11, 13, 14, 16]. A complex theory, based on rubber elasticity, has also been used to calculate the molecular mass between crosslinks [18].

In the Flory-Rehner equation the polymer solubility parameter (δ_2) is however needed to calculate the polymer-solvent interaction parameter (X_1). The polymer solubility parameter can be obtained by group contribution methods [11, 19] or by the method of Hansen [17, 19, 20] (also see Appendix C for a summary of the relevant theory and methods used). Jayabalan and co-workers [13] made the assumption of mutual solubility (ideal scenario) [13], in which it is assumed that the solvent (δ_1) and polymer solubility parameters (δ_2) are equal, resulting in X_1 being equal to 0.34 (Eq. 5.4). This was done due to the sensitivity in the calculation of the polymer-solvent interaction parameters to uncertainty in the determination of the polymer interaction parameter.

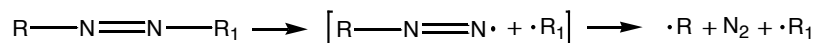
5.3 Theoretical considerations in crosslinking reactions

5.3.1 Initiation systems

The modification agent used in this study, 4-pentenoyl chloride, has a pendent vinyl group, and in order to induce crosslinking of the modified polyurethane a suitable free radical initiation source was required. Possible initiation methods include thermal, photochemical, and gamma irradiation methods. The following discussion is based on the very comprehensive book by Moab et al. [21].

5.3.1.1 Thermal initiation

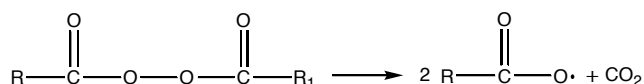
Azo-compounds and peroxides are generally used as initiators in thermal induced polymerization reactions. The initiator decomposes into free radicals, resulting in the evolution of nitrogen gas (Scheme 5.1). The decomposition rate is highly dependent on the reaction temperature and the solvent used [21].



Scheme 5.1: Illustration of the decomposition of an azo-compound [21]

Azo-compounds can be subdivided into dialkyldiazenes, which are a high-temperature (65 - 200 °C) source of alkyl radicals, and dialkyl hyponitrites, which are a low-temperature (40 - 70 °C) source of alkoxy or acyloxy radicals. In the former, 2,2-azobis(2-methylpropanenitrile) (AIBN) is commonly encountered, while dialkyl hyponitrites have not found wide application due to difficulties associated with their synthesis and commercial availability.

The most commonly used peroxide initiators include: diacyl peroxides, dialkyl peroxydicarbonates, peresters, dialkyl peroxides, hydroperoxides and inorganic peroxides. The decomposition of the peroxide molecule is illustrated in Scheme 5.2.

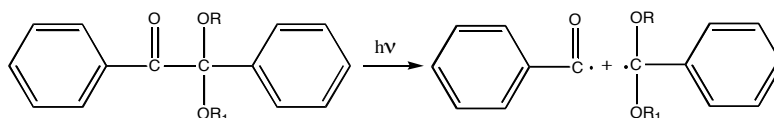


Scheme 5.2: Illustration of the decomposition of the peroxide molecule [21]

Dialkyl peroxydicarbonates and peresters (e.g. di-*t*-butyl peroxalate (DBPOX)) are used in low temperature (35 - 55°C) applications and diacyl peroxides (e.g. benzoyl peroxide, BPO and dilauroyl peroxide, LPO) in moderate reaction temperature ranges (35 - 80°C). Dialkyl peroxides, e.g. dicumyl peroxide (DCP), are a high-temperature source of alkoxy radicals. In general, the decomposition rate of dialkyl peroxides is not sensitive to the solvent when compared to most other peroxides. Persulfates are primarily used in emulsion polymerization.

5.3.1.2 Photochemical initiation

Photochemical initiation is commonly used in curing or crosslinking processes and in initiating graft copolymerization [21]. The initiators used are often aromatic carbonyl containing compounds, including benzoin derivatives.



Scheme 5.3: Decomposition of an acetophenone chromophore [21]

The acetophenone chromophore absorbs in the near UV (300 - 400 nm) and usually decomposes by α -scission, as presented in Scheme 5.3. Benzoin ethers ($R = \text{alkyl}$; $R_1 = \text{H}$) and the α -alkyl benzoin derivatives ($R = \text{H}$, alkyl ; $R_1 = \text{alkyl}$) (e.g. ω,ω -dimethoxy- ω -phenylacetophenone, DMPA) are primarily used. The α -scission process is extremely facile and is not quenched by oxygen, which means it can be used for UV-curing in air.

5.3.1.3 Gamma irradiation

Gamma rays are ultra-short electromagnetic waves. They involve the transfer of sufficient energy to a bound electron located in an atomic or molecular orbital of the irradiated material so that the electron becomes free [22]. Polymerization initiated by gamma rays most often occurs via a free radical mechanism [22].

5.3.2 Determination of crosslinking density

5.3.2.1 Swelling index determination

The swelling index is determined by Eq. 5.1 [13, 14, 16, 23].

$$Q = \frac{V_1}{V_2} \quad (5.1)$$

where V_1 and V_2 are the volumes of solvent in the swollen gel and the polymer, respectively, which can be obtained using a gravimetric method (§5.3.3.1) [13, 16, 23, 24].

5.3.2.2 Molecular mass between crosslinks

The most widely used, and essentially the standard, method for determining crosslink density of crosslinked polymers (3-D networks) depends upon knowledge of their swelling properties [14], i.e. the swollen volume of the crosslinked polymer is measured and used to calculate the crosslink density.

When the crosslinked polymer sample is placed in contact with a suitable solvent, imbibition of the solvent takes place, resulting in swelling of the polymer. The three-dimensional network is extended until, due to deformation stresses, the rate of imbibition of solvent equals the rate of expulsion. This equilibrium swelling can be related to the well-

known Flory-Rehner equation to calculate the number of effective network chains per unit volume of crosslinked polymer [14]. The modified form of this equation is [14]:

$$\frac{1}{M_c} - \frac{2}{M_r} = -\frac{\ln(1 - v_2) + v_2 + X_1 v_2^2}{\rho_2 v_1 (v_2^{1/3} - v_2/2)} \quad (5.2)$$

where M_c is the molecular mass between crosslinks; M_r , the molecular mass of the linear polymer; v_2 , the volume fraction of the polymer in the swollen gel; X_1 , the polymer-solvent interaction parameter; and v_1 , the specific volume of solvent. The volume fraction of the polymer in the swollen gel (v_2) can be calculated by the reciprocal of the swelling (Q).

$$v_2 = \frac{1}{(1 + Q)} \quad (5.3)$$

X_1 is obtained from the solubility parameters by the following equation:

$$X_1 \approx 0.34 + \frac{V_1}{RT} (\delta_1 - \delta_2)^2 \quad (5.4)$$

where δ_1 and δ_2 are the solubility parameters of the solvent and polymer respectively; R is the universal gas constant; T is the temperature. The polymer solubility parameter is often not known, but can be estimated using the well known group contribution methods of Hansen, Hoy, and Hoftyzer and Van Krevelen (HVK). The relevant theory is summarized in Appendix C.

Newer theory of rubber elasticity could potentially be used in the interpretation of swelling [11, 24]. However, network parameters such as cycle rank, entanglement constraints, the average junction functionality, the number of chains and the molecular mass of chains between two junctions are required. Due to the complexities of these methods, as described by others [11, 24], this was considered outside the scope of this dissertation.

5.4 Experimental

5.4.1 Materials

The following polyurethanes were used, Pellethane[®] 2363-80AE (Pellethane), modified Pellethane (degree of modification ranging from 4.5 – 15%, Chapter 4), PurSil[®] 35-80A (PurSil) and modified PurSil (degree of modification ranging from 11.5 – 18.5%, Chapter 4). Tetrahydrofuran (THF) (Merck, Cat: AB009731) was used as solvent and ω,ω -dimethoxy- ω -phenylacetophenone (DMPA) (Aldrich Cat: 19,611-8) as UV initiator. The thermal initiators that were evaluated included 2,2'-azobisisobutyronitrile (AIBN) (Aldrich Cat: 44,109-0), benzoyl peroxide (BPO) (Aldrich Cat: 17,998-1), cumene hydroperoxide (Aldrich Cat:

24,750-2), dicumyl peroxide (DCP) (Aldrich Cat: 32,954-1) and lauroyl peroxide (Aldrich Cat: 29,078-5).

A number of crosslinking enhancing monomers were used, including ethylene glycol dimethacrylate (EDGM) (Aldrich Cat: 33,568-1), trimethylolpropane trimethacrylate (TMPTMA) (Aldrich Cat: 24,684-0), trimethylolpropane triacrylate (TMPTA) (Aldrich Cat: 24,680-8) and N,N'-methylenebisacrylamide (MbA) (Aldrich Cat: 14,607-2). n-Hexane was obtained from Merck (Cat: 152496G).

5.4.2 Methods

5.4.2.1 Sample preparation for crosslinking

The crosslinking of modified Pellethane (degree of modification ranging from 4.5 – 15%, Chapter 4) and modified PurSil (degree of modification ranging from 11.5 – 18.5%, Chapter 4) was studied. The following abbreviations will hereafter be used:

Pellm	Modified Pellethane (uncrosslinked)	Purm	Modified PurSil (uncrosslinked)
Pellm15.0	15% modified Pellethane (uncrosslinked)	Purm15.0	15% modified PurSil (uncrosslinked)
Pellx	Modified and crosslinked Pellethane	Purx	Modified and crosslinked PurSil
Pell15.0	15% modified and crosslinked Pellethane	Pur15.0	15% modified and crosslinked PurSil

The three polyurethanes Pellethane (control), Pellm and Purm were dissolved in tetrahydrofuran, and the PurSil (control) in cyclohexanone (10% solution (w/w)). To the novel modified polyurethanes (Pellm and Purm) different initiators (e.g. DCP and DMPA) and, in selected experiments, crosslinking enhancing monomers (e.g. BA, MbA and TMPTMA), were added.

Solid films were cast from the solutions by standard solvent casting and evaporation techniques and dried *in vacuo* for at least 18 hours. Crosslinking of the dried films (≈ 0.5 mm thick) using an ultraviolet light (UV initiation), a heat source (thermal initiation) or gamma irradiation, respectively, were studied.

5.4.2.2 Ultraviolet light induced crosslinking

The films were exposed to a 315 - 400 nm UV light source (Sylvania, 100 W) at a distance of 500 mm for a period of 5 - 20 min (depending on the size of the samples and the film thickness) to induce crosslinking (see Figure 5.1). After crosslinking, the samples were dried for an additional 72 hours *in vacuo*, before any mechanical tests were performed.

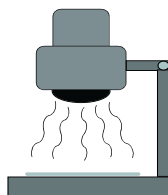


Figure 5.1: Illustration of UV initiation set-up used

5.4.2.3 Heat induced crosslinking

The films were placed between two plates of a heat press (Figure 5.2), fitted with two spacers, equal to the required film thickness, which ensured a constant film thickness when a pressure of approximately 30 MPa was applied to the plates.

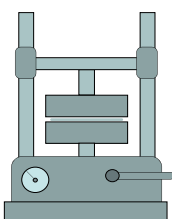


Figure 5.2: Illustration of thermal initiation set-up used

The films were exposed to temperatures ranging between 60 - 180 °C for time periods of 0.5 - 6 h, depending on the specific initiator in the film sample used. The heat press was then switched off and the film allowed to slowly cool down to room temperature (22 °C). The average rate of cooling over the higher temperature ranges used (>100 °C), was approximately 15 - 20 °C/h. The cooling rate was relatively constant due to the construction of the heat press (large, thick heating blocks). After crosslinking, the samples were dried for an additional 72 hours *in vacuo*, before any mechanical tests were conducted.

5.4.2.4 Gamma irradiation

Films were exposed to a Co⁶⁰ source with a half-life of 5.3 years (HEPRO, South Africa). Irradiation dosages ranging between 10 - 250 kGy were used to impart crosslinking.

5.4.2.5 Optimization of initiator and monomer concentrations

First the initiator concentration used in the crosslinking reaction was varied between 0 - 3% (max). The swelling indexes (Q) of the crosslinked films were determined and an optimum (lowest Q) found, which was desirable in this dissertation to illustrate the highest degree of crosslinking. The different crosslinking-enhancing monomers were then included separately, using the optimum initiator concentration as determined above and was then

varied between 0 - 3% (max). Q was determined and an optimum (lowest Q) found. This was repeated for the whole range of novel modified Pellethane[®] 2363-80AE (Pellx) and PurSil[®] 35-80A (Purx) samples.

5.4.3 Analyses

5.4.3.1 Swelling index determination

The swelling index (Q) was determined ($n = 3$) using a gravimetric method [13, 16, 23, 24]. Round disks (15 mm diameter) were punched from the dried films, their weight measured in air (mass 1) and as submerged in n-hexane (non-solvent immiscible with DMF [14]) (mass 2) (Figure 5.3) and the dry volume (V_2) determined according to Eq. 5.5, where ρ_{air} and $\rho_{\text{n-Hexane}}$ are the densities of air and n-hexane, respectively. The films were then allowed to swell in dimethylformamide (DMF) (for at least 18 hours) and weighed again in air (mass 3) and as submerged in n-hexane (mass 4) and the swollen volume determined (V_3) (Eq 5.6). DMF was used as solvent to achieve the sufficient swelling required, minimizing the possible experimental error [14]. The swelling index (Q) was calculated according to Eq. 5.7 [13, 14, 16, 23]:

$$V_2 = (\text{Mass1} - \text{Mass2}) / (\rho_{\text{n-Hexane}} - \rho_{\text{air}}) \quad (5.5)$$

$$V_3 = (\text{Mass3} - \text{Mass4}) / (\rho_{\text{n-Hexane}} - \rho_{\text{air}}) \quad (5.6)$$

$$Q = (V_3 - V_2) / V_2 = V_1 / V_2 \quad (5.7)$$

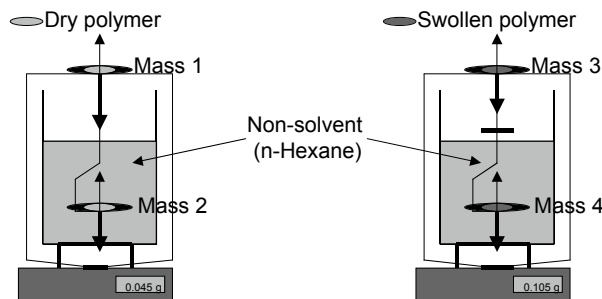


Figure 5.3: Illustration of the procedure used to obtain the swelling index (Q)

5.4.3.2 Calculation of molecular mass between crosslinks

Although the exact molecular structures of Pellethane[®] 2363-80AE or PurSil[®] 35-80A are not known, some limited knowledge of Pellethane[®] 2363-80AE enabled an estimation of its polymer solubility parameter (δ_2), not only experimentally using the method by Hansen (as in the case of PurSil[®] 35-80A), but also theoretically, using the group contribution methods of Hoy, and Hoftyzer and Van Krevelen (HVK). The calculated molecular mass between crosslinks (M_c) was then compared with that of the "ideal", where it is assumed that the solvent (δ_1) and polymer solubility parameters are equal ($\delta_1 = \delta_2$ resulting in $X_1 = 0.34$) (Eq. 5.4), i.e. mutual solubility [19].

The solubility parameter of Pellethane[®] 2363-80AE and PurSil[®] 35-80A, respectively, (as described by Hansen, Appendix C) was determined by placing 0.10g of dried polyurethane in ampoules with 1.00 ml of solvent and then shaking for 7 days at room temperature. The liquids were then classified as good solvents, good swelling agents, poor swelling agents, and non-solvents, by visual assessment. The polymer interaction was then also estimated using the group contribution methods (outlined in Appendix C). The Flory-Rehner equation was then ultimately used to calculate M_c (Eq 5.2).

5.4.3.3 Tensile testing

Test specimens (≈ 0.5 mm thick) were cut from the dried films using an ASTM D638 (Type V) cutter. The tensile testing was performed at room temperature (20 - 22 °C) using an Instron model 5544, equipped with a 1 kN load cell. Each test was repeated at least three times ($n \geq 3$). Testing was performed on the dry films to gain basic knowledge first, which allowed for direct comparisons with published results. The results could be slightly influenced by the absorption of moisture *in vivo* [26].

(A) Tensile stress and strain at break

Once a preload of 0.005 N was achieved at a crosshead speed of 2 mm/min, samples were pulled to failure at a crosshead speed of 200 mm/min. The tensile stress and strain at break were recorded ($n = 4$).

(B) Cyclic tensile testing

Once a preload of 0.005 N was achieved at a crosshead speed of 2 mm/min, samples ($n = 4$) were subjected to four extension cycles to an extension of 200% of the samples' original length (200 mm/min). The second cycle was consistently used throughout [4] to calculate the hysteresis and non-recovered strain (NRS), as illustrated in Figure 5.4.

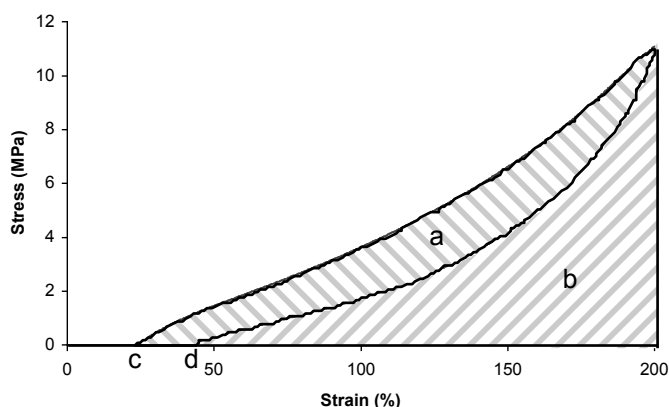


Figure 5.4: Illustration of cyclic tensile testing calculations

The areas (a and b), as illustrated in Figure 5.4, were numerically integrated (trapezium rule) and the hysteresis calculated as the energy loss (a) per total input energy (a+b) (Eq. 5.8) [4, 6].

$$\text{Hysteresis} = a/(a + b) \quad (5.8)$$

Non-recovered-strain (NRS) (also called instantaneous residual strain [4]) was calculated according to Eq. 5.9 [4].

$$\text{NRS} = (d - c) \quad (5.9)$$

(C) Creep

The samples (n = 3) were pulled at a crosshead speed of 50 mm/min to a tensile stress of 8 MPa (t_0), where the tensile strain of Pellethane and Pell15.0 are comparable, and the stress maintained for a period of 90 min (t_{90}). The creep was calculated according to Eq. 5.10 (see Figure 5.5) as the ratio between the difference between measured strains at t_{90} and t_0 (e) and the strain measured at t_0 (f).

$$\text{Creep} = e/f \quad (5.10)$$

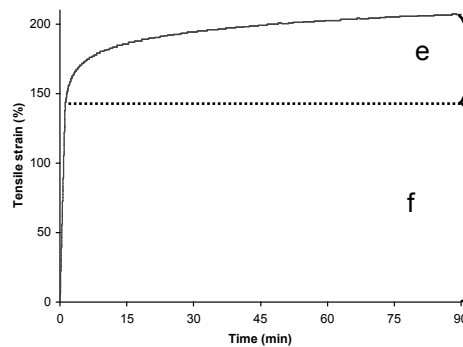


Figure 5.5: Illustration of variables used to calculate the creep

5.4.3.4 Dynamic mechanical analysis

Dynamic mechanical analyses (n = 1) were performed with a Perkin Elmer DMA 7e equipped with a parallel plate measuring system and 3-mm disc probe. A temperature scan mode was used and the temperature was ramped at a rate of 5 °C/min from -100 to 220 °C under a nitrogen atmosphere. Scans were performed at a frequency of 1 Hz with initial static and dynamic forces of 110 mN and 100 mN, respectively. A static tension control (120%) and amplitude dynamic control of 10 μm were used.

The transition temperatures (T_1 and T_2) were obtained from the $\tan \delta$ curves [4, 18], at the onset of the respective peaks. The storage moduli will be reported at 37 °C (physiological temperature).

5.3.4.5 Statistical analysis

Statistical analyses were performed using either (a) student t-test (unpaired 2-tailed, assuming equal variance), (b) 1-way analysis of variance (ANOVA) and (c) 2-way ANOVA. Bonferroni corrections were applied in cases of multiple comparisons. A significance level of 0.05 or less was accepted as being statistically significant. Standard assumptions of normality were made, but in cases where it was suspected that the assumptions were violated the results were verified using non-parametric (bootstrap) techniques (see Appendix H for a summary).

5.5 Results and discussion

5.5.1 Crosslinking of modified Pellethane® 2363-80AE

5.5.1.1 Swelling index

Successful UV induced crosslinking was achieved after 5 - 20 min, using DMPA or, alternatively, using DCP at 120 °C for 5 hours. The evolution of nitrogen gas during thermal initiation produced bubbles in the polyurethane films, which rendered the azo-containing initiators (e.g. 2,2'-azobisisobutyronitrile) unusable. Crosslinking was not achieved in the temperature range (60 - 180 °C) and time range (0.5 - 6 h) studied when benzoyl peroxide, cumene hydroperoxide or lauroyl peroxide were used.

The change in $Q \pm$ standard deviation with change in initiator (DMPA and DCP) concentration (0 - 2%) for a typical example (Pell8.5) is presented in Figure 5.6.

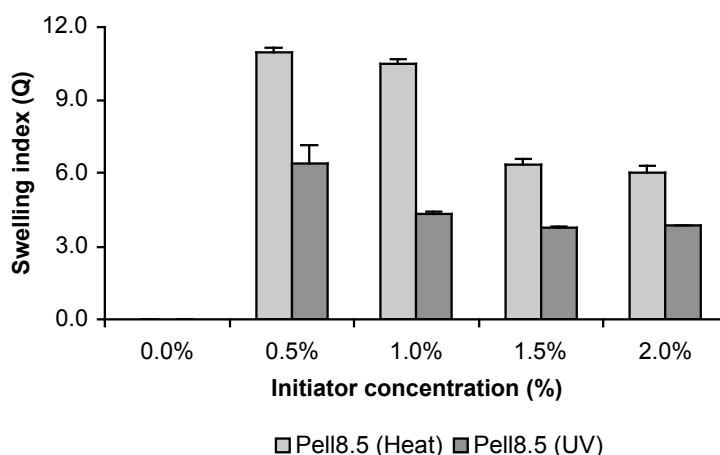


Figure 5.6: Change in $Q \pm$ standard deviation ($n = 3$) with change in DMPA and DCP concentration for Pell8.5 using UV and heat induced crosslinking, respectively

Crosslinking was not achieved without using initiator ("0%", Figure 5.6), even after the samples were subjected to the UV source for 30 min or the heat source (150 °C) for up to 6 hours. This finding was consistent over the whole range of Pellx samples.

The swelling index at a DCP concentration of 1.5% (w/w) was found to be significantly lower compared to a concentration of 1.0% ($p < 0.01$), but did not change significantly when compared to a concentration of 2.0% ($p = 1.0$). Similarly, the swelling index at a DMPA concentration of 1.5% (w/w) was found to be significantly lower than at a concentration of 1.0% ($p = 0.01$), but did not change significantly ($p = 0.28$) when compared to 2.0%. The swelling indices obtained for the UV initiation system were significantly lower than the heat induced initiation system ($p < 0.01$) for all the samples in the initiator range. The lowest swelling index (optimum initiator concentration) was thus achieved at an initiator concentration of 1.5% (w/w) (in this specific example) using either DMPA or DCP as initiator. The DMPA and DCP concentrations were similarly optimized for the range of Pellx samples (i.e. Pell4.5, Pell6.5, etc.), the swelling indices of which are presented in Figure 5.7 and summarized in Table 5.1.

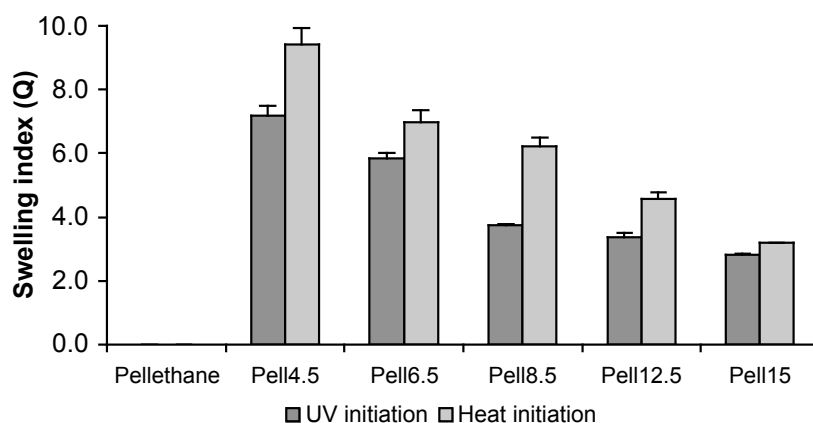


Figure 5.7: Change in $Q \pm$ standard deviation ($n = 3$) for Pell8.5 with optimized initiator concentration

Table 5.1: Optimized initiator concentrations for the Pellx range

Pellx	Pell4.5	Pell6.5	Pell8.5	Pell12.5	Pell15.0
[DMPA] (w/w)	1.5%	1.5%	1.5%	2.0%	2.0%
Q \pm std dev	7.17 \pm 0.31	5.85 \pm 0.15	3.77 \pm 0.01	3.39 \pm 0.12	2.82 \pm 0.05
[DCP] (w/w)	1.5%	1.5%	1.5%	2.0%	2.0%
Q \pm std dev	9.44 \pm 0.50	6.99 \pm 0.38	6.24 \pm 0.27	4.58 \pm 0.20	3.20 \pm 0.03

The Pellethane control samples ("Pellethane") did not crosslink after subjection to either the UV or heat sources. As expected, a decrease in the swelling index was observed with an increase in the degree of modification (in the range tested, i.e. Pell4.5 – Pell15.0) for both UV and heat induced crosslinking (Figure 5.7 and Table 5.1). The lowest swelling index was obtained for Pell15.0 (when compared to Pell12.5, Pell8.5, Pell6.5 and Pell4.5) for both UV ($p < 0.02$) and heat ($p < 0.01$) initiation. This was expected, as a higher degree of modification (e.g. Pell15.0) would lead to a more densely crosslinked structure

(i.e. the molecular mass between crosslinks would be lower, see §5.4.1.2), thus increasing the elastic response and limiting the solvent uptake in the resulting tighter three-dimensional polymer structure, resulting in the lowest swelling index [14].

This finding was consistent for both UV and thermal induced crosslinking although the swelling index was consistently significantly higher in the latter ($p < 0.03$) (Table 5.1), except for Pell6.5 where the difference was found to be non-significant ($p = 0.11$). Heat induced crosslinking was achieved at the onset of the melt region of Pellethane (see Figure 5.19, DMA) most probably resulting initially in free chain movement and “pre-mature” crosslinking, which in turn then restricted full micro-phase separation. This is in contrast to UV induced crosslinking, which was achieved at room temperature and thus after complete micro-phase separation.

In a control study of the influence of the respective initiators (ranging in concentration between 0 - 2%) on the swelling index of Pellethane it was found that neither DMPA nor DCP (at concentrations as high as 2%) resulted in crosslinking reactions, even after exposure of the films to the UV light source for more than 30 min or temperatures of 120°C for periods of up to 6 hours.

Gamma irradiation induced crosslinking was only achieved at very high radiation dosages (250 kGy) for Pellm12.5 and Pellm15.0. The samples swelled excessively in solvent (e.g. DMF) and unfortunately the mechanical integrity of the resulting crosslinked structures was so weak that it was not possible to determine the swelling indices. Pellm films were also prepared with a wide range of initiators (as listed in §5.4.1), at different concentrations, but crosslinking using gamma irradiation was not achieved in any of the samples. In a control study, Pellethane did not crosslink, even after being subjected to the very high irradiation dosages. This is most likely due to a combination of the low degree of modification of the other samples and scission that occurs during the irradiation process.

Table 5.2: Swelling index \pm standard deviation of Pell8.5 with variation in initiator (I) and monomer (M) concentrations

Pell8.5	0.0%I	0.5%I	1.0%I	1.5%I	2.0%I
0.0%M	-	6.39 \pm 0.72	4.29 \pm 0.11	3.76 \pm 0.05	3.84 \pm 0.01
0.5%M	-	4.60 \pm 0.41	4.22 \pm 0.16	3.58 \pm 0.04	3.65 \pm 0.08
1.0%M	-	4.51 \pm 0.05	4.10 \pm 0.04	3.45 \pm 0.07	3.61 \pm 0.08
1.5%M	-	4.47 \pm 0.13	3.78 \pm 0.04	3.05 \pm 0.06	3.33 \pm 0.25
2.0%M	-	4.45 \pm 0.32	4.16 \pm 0.31	3.93 \pm 0.12	3.96 \pm 0.15

Although a number of potential crosslinking enhancing monomers was originally evaluated it was decided to proceed with MbA, because of its long and proven history in the field of biomedical polymers.

To illustrate the effect that the DMPA and MbA concentrations (with UV initiation) have on the swelling index of Pell8.5, a matrix consisting of the swelling index results ($Q \pm$ standard deviation) ($n = 3$) for the full initiator (I) (DMPA, 0 - 2%) and monomer (M) (MbA, 0 - 2%) ranges is presented in Table 5.2, and illustrated in Figure 5.8.

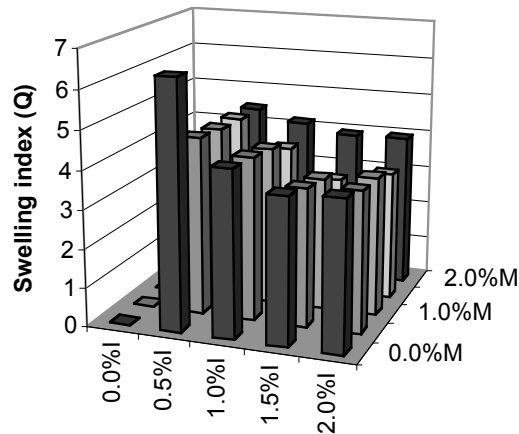


Figure 5.8: 3-D plot of swelling index (I:0-2%, M:0-2%) results obtained for Pell8.5

Again no crosslinking was achieved without initiator (“0.0%I”). A small decrease in Q with an increase in monomer concentration (M) was observed for the full initiator concentration (I) range studied. A decrease in Q was further observed with an increase in initiator concentration, for the monomer concentration range studied. The lowest swelling index was observed with both monomer and initiator concentrations at 1.5%.

Figure 5.9 compares $Q \pm$ standard deviation ($n = 3$) values obtained with both optimum initiation systems, both with (Table 5.3) and without optimized monomer (MbA) concentration.

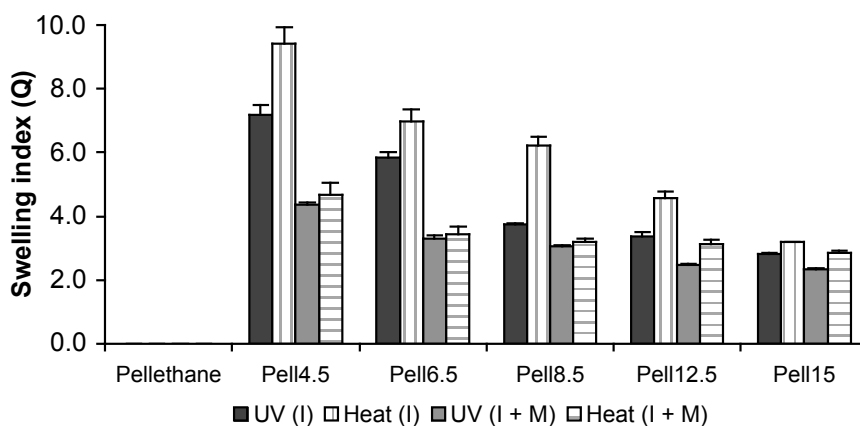


Figure 5.9: Effect of modification percentage of crosslinked Pellethane on swelling index for UV and thermal initiation, both with and without MbA monomer ($n = 3$)

Similarly, a decrease in Q (when using either UV or heat) was observed with the additional inclusion of the crosslinking enhancing monomer MbA (i.e. “UV(I+M)” & Heat(I+M)”, Figure 5.9). A significant reduction in the swelling index was observed when monomer was included compared to the cases when only initiator was included, using either UV ($p < 0.01$) or heat ($p < 0.02$), over the whole range (i.e. Pell4.5 - Pell15.0). The only significant difference between the UV and heat initiation systems, when monomer was added, was found between Pell12.5 ($p = 0.03$) and Pell15.0 ($p < 0.01$). The inclusion of the MbA molecule presumably reduced Q by forming “linking bridges” between the spaced reactive 4-pentenoyl pendent groups during their polymerization.

When the swelling indices of samples ($n = 3$) initiated using UV (DMPA) are compared with those initiated using heat (DCP) (Table 5.3) (when MbA was included), those of the former were found to be significantly lower for Pell8.5, Pell12.5 and Pell15.0.

Table 5.3: $Q \pm$ standard deviation ($n = 3$) for optimized initiator and MbA concentrations for Pellx

Pellx	Pell4.5	Pell6.5	Pell8.5	Pell12.5	Pell15.0
[DMPA] (w/w)	1.5%	1.5%	1.5%	2.0%	2.0%
[MbA] (w/w)	0.5%	1.5%	1.5%	2.0%	2.0%
Q \pm std dev	4.35 \pm 0.09	3.32 \pm 0.10	3.05 \pm 0.06	2.47 \pm 0.05	2.35 \pm 0.03
[DCP] (w/w)	1.5%	1.5%	1.5%	2.0%	2.0%
[MbA] (w/w)	0.5%	1.5%	1.5%	2.0%	2.0%
Q \pm std dev	4.65 \pm 0.38	3.46 \pm 0.24	3.21 \pm 0.11	3.13 \pm 0.14	2.86 \pm 0.07

In the following section the swelling index values will be used to calculate the molecular mass between crosslinks for Pellx. Swelling index results obtained with MbA will not be considered due to the complexity and uncertainties involved in the degree of polymerization and possible other side reactions involving MbA.

5.5.1.2 Molecular mass between crosslinks

The calculation of the polymer solubility parameter (δ_2) using the group contribution method of Hoy [19] was found to be the closest to mutual solubility (“Ideal”, Table 5.5), where the solubility parameter of the solvent (DMF) ($\delta_1 = 24.8 \text{ MPa}^{1/2}$) is equal to the solubility parameter of the polymer ($\delta_1 = \delta_2 = 24.8 \text{ MPa}^{1/2}$). This equates to a polymer-solvent interaction parameter (X_1) equal to 0.34 (Eq. 5.4). Table 5.4 compares this result with those obtained using the methods of Hoy, Hansen, and of Hoftyzer and Van Krevelen (HVK) (Table 5.4).

Table 5.4: Calculation of the polymer and polymer-solvent interaction parameters by various methods

	Ideal	Hoy	Hansen	HVK
δ_2 (MPa ^{1/2})	24.80	24.01	21.80	19.11
X_1 ()	0.34	0.36	0.62	1.36

The polymer-solvent interaction parameter (X_1) is very sensitive to changes in δ_2 (and thus the differences between δ_1 and δ_2) as it is a quadratic function of the latter (Eq. 5.4). The sensitivity of X_1 to changes in δ_2 , ranging between 0 - 15%, on the solubility parameter of the polymer is shown in Figure 5.10.

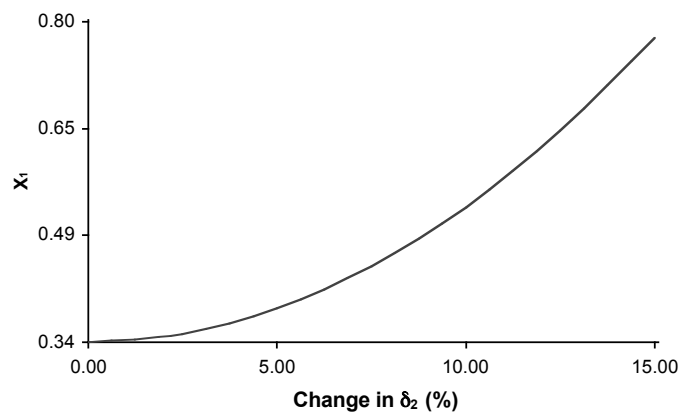


Figure 5.10: Sensitivity of the solvent-polymer interaction parameter (X_1) to changes in the polymer solubility parameter (δ_2)

Figure 5.11 shows the effect of the sensitivity of X_1 on the molecular mass between crosslink (M_c) determinations for Pellx.

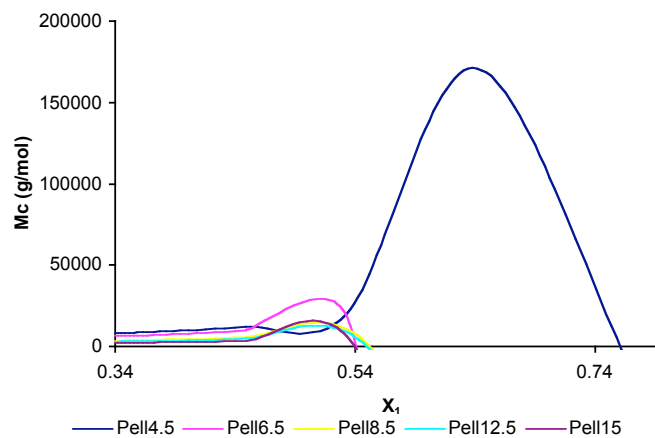


Figure 5.11: Change in M_c with change in X_1 for Pellx

The calculated molecular masses between crosslinks (M_c) are relatively stable for changes in X_1 only between values of 0.34 and 0.39, which equates to a change in δ_2 of 5%. This was found to be consistent over the whole range of Pellx (i.e. Pell4.5, Pell6.5, etc.) presented in Figure 5.11.

Only the method of Hoy was thus found to be useful in the determination of the polymer interaction parameter (δ_2). The calculated molecular mass between crosslinks for mutual solubility (“Ideal”), and using the method of Hoy for both the UV and heat initiation systems, is presented in Figure 5.12, with a summary of the exact values in Table D.1 (Appendix D).

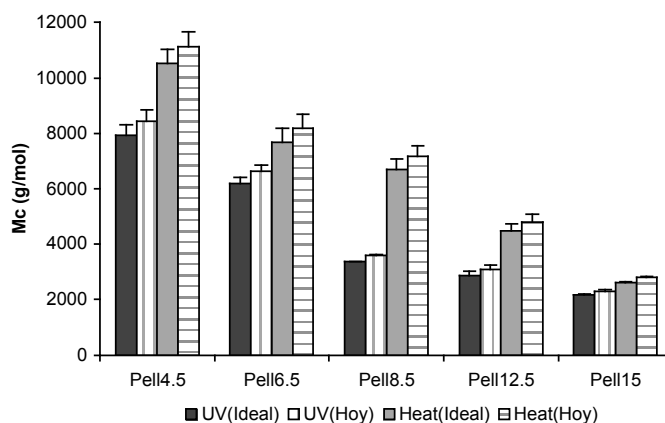


Figure 5.12: Comparison of $M_c \pm$ standard deviation ($n = 3$) for UV and heat initiation of Pellx

A decrease in M_c was observed with an increase in the degree of modification (in the range tested, i.e. Pell4.5 - Pell15.0) for both the UV and heat induced crosslinking (Figure 5.12). The trends in the M_c values for both the UV and heat initiation systems are consistent with those obtained for the swelling indexes, as presented in Figure 5.7 (see Table D.1, Appendix D, for the exact values), which was expected, since the swelling index values were used to calculate M_c .

There will still be an uncertainty because of the microphase separation and since crosslinking is only in the hard phase. As the soft phase is not crosslinked a certain swellability must persist. At present, there is no method to take this variability of block crosslinking into account.

5.5.1.3 Tensile properties

The hysteresis for Pellethane (control) and for Pell8.5 (typical example) and as a function of initiator (DMPA and DCP) concentration (0 – 2%) is presented in Figure 5.13.

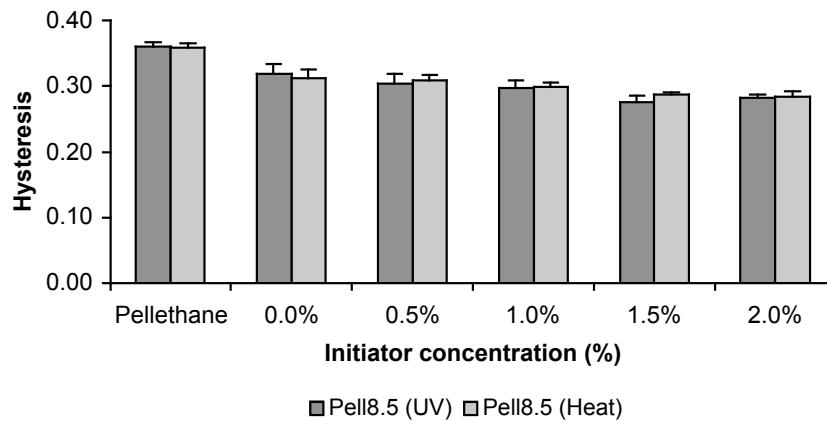


Figure 5.13: Hysteresis \pm standard deviation ($n = 4$) of Pell8.5 as function of DMPA and DCP concentrations

A decrease in the hysteresis was observed with an increase in initiator concentration (DMPA and DCP), over the initiator concentration range studied. The hysteresis for the UV and heat initiation systems were found to be a minimum at an initiator concentration of 1.5% (w/w), for both DMPA ($p=0.04$) and DCP ($p=0.03$), when compared to initiator concentrations of 1.0%, but with no significant change when compared to initiator concentrations of 2.0%. The lowest hysteresis (optimum) was thus achieved at initiator concentrations of 1.5% (w/w) (for both UV and heat). This is in good agreement with swelling index values, where the lowest Q value for Pell8.5 (§5.4.1.1) was also obtained at initiator concentrations of 1.5% (w/w).

The DMPA concentration was similarly optimized for Pell15.0. The initiator concentrations (DMPA and DCP) as optimized for Pell8.5 (Figure 5.13), and the DMPA concentration as optimized for Pell15.0, compared well with the swelling results. The hystereses \pm standard deviation ($n = 4$) of Pellethane (control) and Pellx (Figure 5.14) are summarized in Table 5.5 at the initiator concentrations, as optimized in the swelling experiments, and verified for the selected ones, as mentioned above.

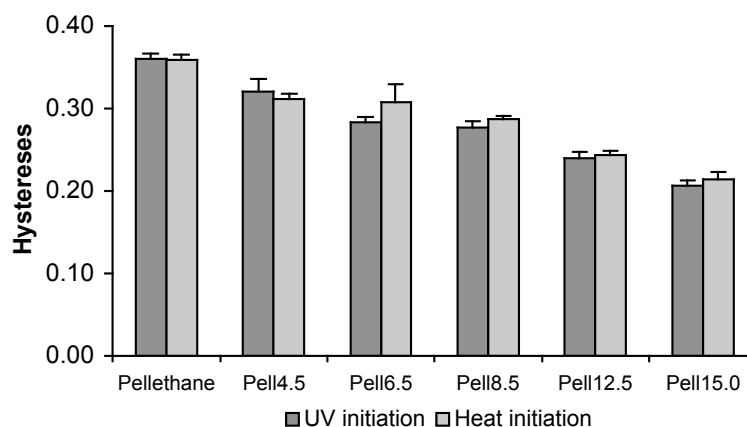


Figure 5.14: Change in hysteresis with change in degree of modification of Pellx

A decrease in hysteresis was observed with an increase in the degree of modification for both thermal and UV initiation, with a minimum obtained for Pell15.0 ($p < 0.01$), when compared to their respective controls, i.e. a marked improvement of more than 40% in hysteresis was achieved over the Pellethane control. The difference between UV and heat initiation on the hysteresis (Figure 5.14) was found to be non-significant ($p > 0.05$) over the Pellx range tested.

Table 5.5: Measured and calculated mechanical properties \pm standard deviation for Pellx ($n = 4$)

Pellx	Pellethane	Pell4.5	Pell6.5	Pell8.5	Pell12.5	Pell15.0
[DMPA] (w/w)		1.5%	1.5%	1.5%	2.0%	2.0%
Hysteresis (-)	0.36 \pm 0.01	0.32 \pm 0.02	0.28 \pm 0.01	0.28 \pm 0.01	0.24 \pm 0.01	0.21 \pm 0.01
% Change		11.0%	21.4%	23.3%	33.6%	42.5%
NRS (-)	16.74 \pm 0.97	16.30 \pm 0.77	13.31 \pm 0.61	12.70 \pm 0.68	11.78 \pm 1.11	8.75 \pm 0.88
% Change		2.6%	20.5%	24.1%	29.6%	47.7%
Stress (MPa)	46.97 \pm 2.44	42.63 \pm 1.96	35.81 \pm 3.13	38.70 \pm 1.07	31.07 \pm 1.58	29.23 \pm 1.92
% Change		9.2%	23.8%	17.6%	33.9%	37.8%
Strain (%)	571.6 \pm 19.3	488.6 \pm 15.1	498.1 \pm 25.1	475.5 \pm 15.4	435.5 \pm 5.2	411.5 \pm 18.4
% Change		12.8%	12.9%	16.8%	23.8%	28.0%
[DCP] (w/w)		1.5%	1.5%	1.5%	2.0%	2.0%
Hysteresis (-)	0.36 \pm 0.11	0.31 \pm 0.01	0.31 \pm 0.02	0.29 \pm 0.00	0.24 \pm 0.00	0.21 \pm 0.01
% Change		13.0%	14.2%	19.9%	32.0%	40.2%
NRS (-)	21.70 \pm 0.83	14.34 \pm 0.75	14.84 \pm 0.96	14.42 \pm 1.18	11.88 \pm 0.48	9.16 \pm 0.68
% Change		33.9%	31.6%	33.5%	45.2%	57.8%
Stress (MPa)	47.82 \pm 3.13	46.66 \pm 2.74	43.79 \pm 4.93	36.34 \pm 4.44	35.12 \pm 1.18	29.43 \pm 4.27
% Change		2.4%	8.4%	24.0%	26.6%	38.5%
Strain (%)	619.9 \pm 21.4	550.5 \pm 18.3	566.5 \pm 36.6	445.9 \pm 34.2	491.1 \pm 14.0	402.1 \pm 32.1
% Change		11.2%	8.6%	28.1%	20.8%	35.1%

Figure 5.15 shows the linear correlation between the swelling index and hysteresis for Pellx (UV initiation).

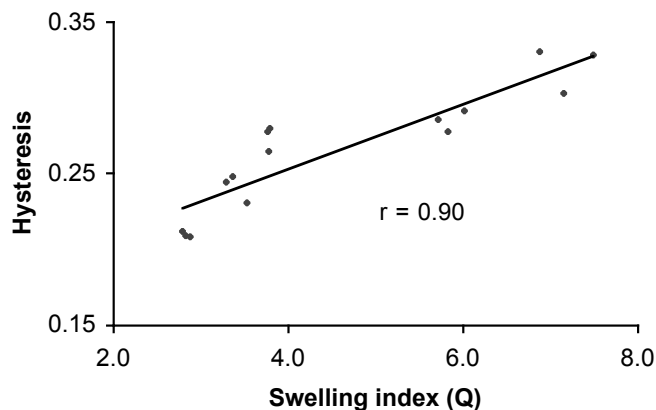


Figure 5.15: Correlation between the swelling index and hysteresis of Pellx

A linear correlation coefficient (r) equal to 0.90 was calculated, indicating (from table of correlation coefficients with degree of freedom equal to 13) that the swelling index and hysteresis are positively correlated ($p=0.01$).

A decrease in NRS (i.e. improvement in recovered strain) was also observed with an increase in the degree of modification, for both UV and heat initiation, when compared to the Pellethane control sample (Table 5.5). As expected, a decrease in the strain at break was observed, due to the restriction of chain movement caused by the resulting crosslinked network [12]. A decrease in the stress at break was also observed with an increase in the degree of crosslinking, with the lowest value obtained for Pell15.0. Similar observations have been made in the literature [12, 14]. According to Ania and Calleja [25], the wide angle X-ray scattering analysis of Pellethane and Pell15.0 (Figure D.1, Appendix D) shows no clear evidence of crystalline peaks in any of the two polymers. It means that, from the point of view of X-ray scattering, the crystallinity is negligible [25]. See Appendix G for Ania and Calleja's comments). Crosslinking through the 4-pentenoyl pendent group is the main changing variable. Figure 5.16 shows the stress-strain curves (typical) for Pellethane (control) and Pell15.0.

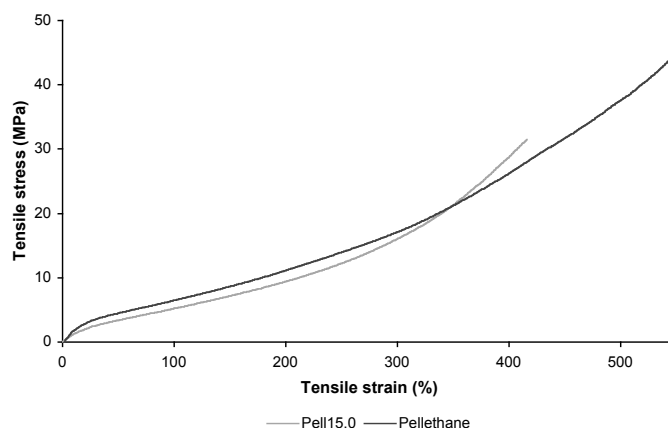


Figure 5.16: Tensile stress and strain at break for Pellethane and Pell15.0

The introduction of the pendent groups during the polyurethane modification step would not replace the existing hydrogen bonds in a stoichiometrical ratio but would rather have a more disruptive effect, possibly due to the size of the pendent group. Weak hydrogen bonds are however replaced by strong and permanent covalent crosslinks, resulting in a drastic improvement (>40%) in reducing energy losses (hysteresis), due to flow. The uncrosslinked Pellethane control will, under large strain and large stress, show deformation (large) of the hard segments. The crosslinked Pellx will begin to show deformation of the hard segment but this will obey the law of a crosslinked material, which will restrict the flow (causing less strain at break) and more rapidly increase stress on the sample (lower flow is less accommodating to relieve stress), as seen in Figure 5.16. This

will also start crack formation sooner (i.e. lower stress at break, typical of increased crosslinking of the blocked domains [12]).

Typical creep results for Pellethane and Pell15.0 are presented in Figure 5.17 and the calculated values (Eq. 5.7) summarized in Table 5.6.

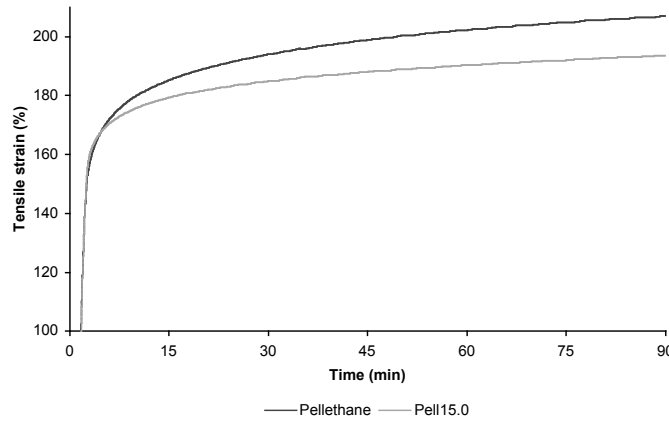


Figure 5.17: Creep results for Pellethane and Pell15.0

Table 5.6: Calculated creep values \pm standard deviation ($n = 3$) obtained for Pellethane and Pell15.0

	Pellethane	Pell15.0
Creep \pm stdev	0.65 \pm 0.01	0.36 \pm 0.01
Improvement (%)		44.3%

The tested Pell15.0 samples showed a 44.3% reduction in creep when compared to Pellethane ($p < 0.01$).

Table 5.7 summarizes the hysteresis results (hysteresis \pm standard deviation) obtained for the full initiator (I) (DMPA, 0 - 2%) and monomer (M) (MbA, 0 - 2%) concentration ranges for Pell8.5 (typical example). This is illustrated in Figure 5.18.

Table 5.7: Hysteresis \pm standard deviation of Pell8.5 for variation in monomer (M) and initiator (I) concentrations

Pell8.5	0.0%I	0.5%I	1.0%I	1.5%I	2.0%I
0.0%M	0.32 \pm 0.02	0.30 \pm 0.02	0.30 \pm 0.00	0.28 \pm 0.01	0.28 \pm 0.00
0.5%M	0.34 \pm 0.00	0.31 \pm 0.01	0.31 \pm 0.01	0.29 \pm 0.01	0.29 \pm 0.01
1.0%M	0.34 \pm 0.01	0.30 \pm 0.01	0.30 \pm 0.01	0.29 \pm 0.00	0.30 \pm 0.01
1.5%M	0.35 \pm 0.03	0.32 \pm 0.01	0.31 \pm 0.00	0.30 \pm 0.01	0.30 \pm 0.02
2.0%M	0.37 \pm 0.02	0.34 \pm 0.02	0.31 \pm 0.01	0.33 \pm 0.01	0.32 \pm 0.01

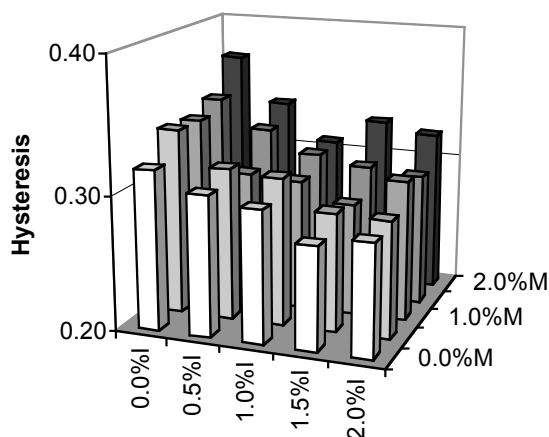


Figure 5.18: 3-D illustration of hysteresis for Pell8.5

The introduction of the crosslinking-enhancing monomer had a detrimental effect on the hysteresis. An increase in hysteresis with increase in monomer concentration (M) was observed for the full initiator (I) concentration range studied. The best result, i.e. the lowest hysteresis, was still obtained when no monomer (“0.0%M”) was used (Figure 5.18), thus as optimized and presented in Figure 5.13. Although the swelling indices were lower when crosslinking-enhancing monomer was used (Figure 5.3), an increase in the hysteresis (i.e. greater energy losses) was however observed. This was consistent over the entire Pellx range and use of the crosslinking enhancing monomer (MbA) was therefore not further considered in this dissertation.

The following hypothesis is offered to explain this seemingly contradictory result. The crosslinking monomer forms a stable radical, which does not easily add to the pendent vinyl bond, i.e. it shows a propensity to homopolymerize and produce long bulky crosslinked links between pendant modification groups. This defeats the purpose of achieving short-range crosslinks, even if more crosslinks are achieved.

5.5.1.4 Dynamic mechanical analysis

Typical $\tan \delta$ curves obtained for Pellethane and Pell15.0, and storage moduli (G') for Pellethane and Pell15.0 are presented in Figures 5.19 and 5.20, respectively.

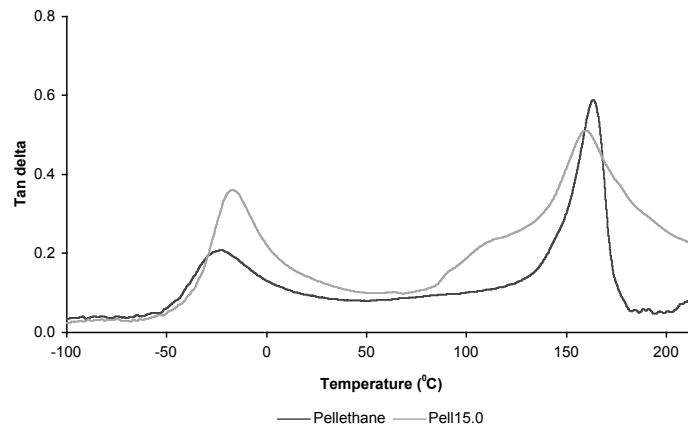


Figure 5.19: *Tan δ curves obtained for Pellethane and Pell15.0*

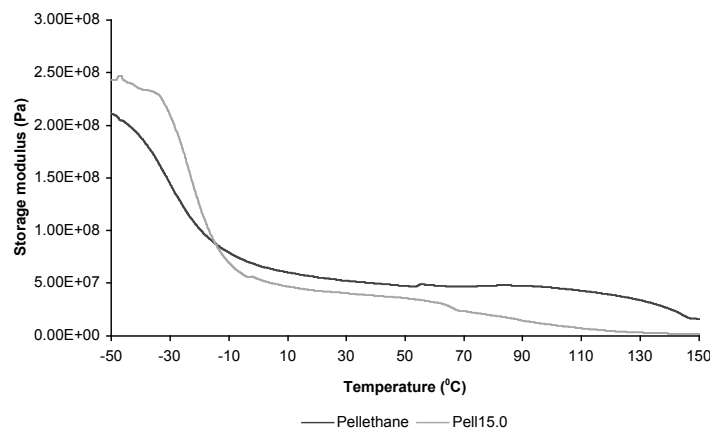


Figure 5.20: *Storage moduli (G') for Pellethane and Pell15.0*

The DMA behavior corresponds to a distinct two-phase elastomeric structure, as opposed to a network structure [11], as is evident from the two main transitions at an onset temperature in the first phase at approximately -48°C to -55°C (transition temperature, T_1 , of the amorphous PTMEG) and in the second phase 85°C to 132°C (transition temperature, T_2 , of hard block) (Figure 5.19 & 5.20) [26, 27].

Pell15.0 has a significantly higher T_1 and much lower T_2 (Figure 5.19), coinciding with a much smaller but broader second transition temperature, compared to Pellethane.

Table 5.9 compares the two transition temperatures, as well as the storage moduli, of Pellethane (control) with Pell4.5, Pell8.5 and Pell15.0.

Table 5.8: Summary of DMA results of Pellethane and Pell4.5, Pell8.5 and Pell15.0

	Pellethane	Pell4.5	Pell8.5	Pell15.0
T ₁ (°C)	-55.1	-54.9	-51.8	-48.6
ΔT ₁ (°C)	0	0.2	3.3	6.5
T ₂ (°C)	131.9	111.5	110.7	84.7
ΔT ₂ (°C)	0	-20.4	-21.2	-42.7
T ₂ (width) (°C)	48.7	71.8	86.2	144.0
G' (Pa)	5.0x10 ⁷	5.0x10 ⁷	4.8x10 ⁷	3.9x10 ⁷

The increase in the first transition temperature with an increase in the degree of crosslinking is clearly illustrated in Table 5.8, with Pell15.0 showing an increase of 6.5 °C when compared to Pellethane. In general, crosslinking minimizes the sliding of polymer chains past one another (viscous flow) (i.e. it restricts the mobility of the chains), with a resulting increase in T₁ [11, 14, 16]. Yet the crosslinking is in the hard phase, not the soft phase, therefore the only way the soft phase can change transition temperature or can increase in storage modulus is if part of the crosslinked hard phase becomes compatible in the soft phase. The T₁ of a mixture is the sum of the volume fractions of individual T₁ values of mixing components, (i.e. adding higher the T₁ components increases the T₁ of mixture). Since the hard phase will consist of small to large domains it may be possible that many of the smaller phases mix after crosslinking. Conversely, the outer sheaths of the hard phases may become compatible and, by mixing into the soft phase, show the behavior seen in the tan δ and storage moduli curves.

A significant decrease in the onset of the second transition temperature, coinciding with an increase in the peak width, with an increase in the degree of crosslinking, was observed for Pell4.5, Pell8.5 and Pell15.0, when compared to Pellethane.

The storage moduli of the crosslinked polymers compared well with that of Pellethane, although a slightly lower value was obtained for Pell15.0 at 37 °C. Similar observations with an increase in degree of crosslinking have been described in the literature [14, 16]. If the argument above is accepted, then the integrity of the hard phases must be compromised (they will change from a hard phase to a crosslinked domain that would be softer, more compatible). Then the storage modulus decreases significantly on crosslinking. This can be seen for Pell15.0 at 150 °C where it has a storage modulus of approximately zero, showing no remaining hard phase as was present in Pellethane.

5.5.2 Crosslinking of modified PurSil® 35-80A

The crosslinking of the second novel modified polyurethane (PurSil) (Chapter 4) was investigated using a UV initiation system.

5.5.2.1 Swelling index determination

Ultraviolet light (UV) induced crosslinking was achieved after 5 - 20 min using DMPA. The initiator concentration was varied over the range 0 - 3% (w/w). The swelling indices were determined and results for a typical example (Pur18.5) are presented in Figure 5.21.

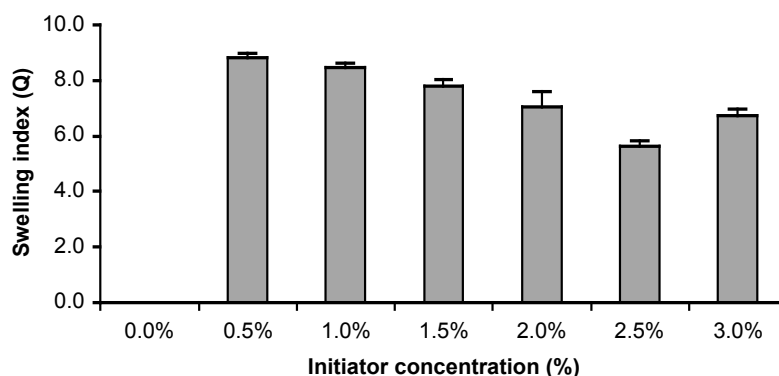


Figure 5.21: Change in $Q \pm$ standard deviation ($n = 3$) with change in DMPA concentration for Pur18.5

Crosslinking was not achieved without initiator ("0%", Figure 5.21), not even after the samples were subjected to the UV source for 30 min. This finding was consistent for the PurSil control and the whole range of modified PurSil (Purm) samples.

The swelling index was found to be the lowest at an initiator concentration of 2.5%. The swelling index at this concentration was found to be significantly lower compared to the swelling index at initiator concentrations of 2.0% ($p=0.03$) and 3.0% ($p<0.01$), respectively. The DMPA concentration was similarly optimized for all the Purx samples (i.e. Pur11.5, Pur15.0 and Pur18.5), the swelling indexes of which are presented in Figure 5.22 and summarized in Table 5.10.

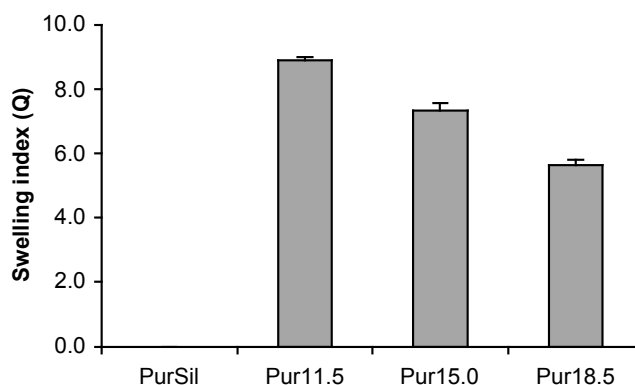


Figure 5.22: $Q \pm$ standard deviation ($n = 3$) for PurSil and Purx samples with optimized DMPA concentrations

Table 5.9: Optimized DMPA concentration for Purx range ($Q \pm$ standard deviation)

Purx	Pur11.5	Pur15.0	Pur18.5
[DMPA] (w/w)	2.0%	2.0%	2.5%
$Q \pm$ std dev	8.91 \pm 0.08	7.35 \pm 0.23	5.64 \pm 0.18

As expected, a decrease in the swelling index was observed with an increase in the degree of modification (Figure 5.22 and Table 5.9) in the Purx range studied. Pur18.5 had the lowest swelling index when compared to Pur15.0 ($p < 0.01$) and Pur11.5 ($p < 0.01$). A higher degree of modification (e.g. Pur18.5) leads to a more densely crosslinked structure (i.e. lower molecular mass between crosslinks), limiting swellability [14].

In a control study to illustrate the influence of the DMPA (ranging in concentration from 0 – 3%) on the swelling index of PurSil it was found that DMPA (at concentrations as high as 3%) did not result in crosslinking reactions, even after exposure of the films to the UV light source for more than 30 min.

5.5.2.2 Molecular mass between crosslinks

The molecular mass between crosslinks for the Purx samples are presented in Figure 5.23, with the exact values presented in Table D.2, Appendix D.

The interaction between the methods of Hansen and assuming mutual solubility ('Ideal') were found to be non-significant ($p = 0.65$). There is a decrease in the M_c (i.e. increase in crosslinking density) with an increase in degree of modification of Purx, for both the methods of Hansen and assuming mutual solubility ('Ideal'). The lowest M_c was calculated for Pur18.5 ($p < 0.01$) when compared to Pur15.0 and Pur11.5.

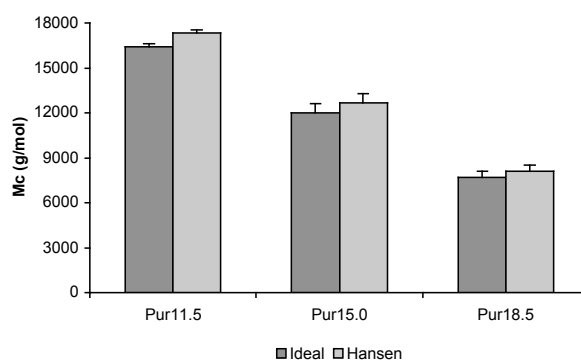


Figure 5.23: Molecular mass between crosslinks \pm standard deviation ($n = 3$) for Purx samples

5.5.2.3 Tensile properties

An example (Pur18.5) of the hysteresis of polyurethane samples as a function of initiator (DMPA) concentration (0 – 3%) is presented in Figure 5.24.

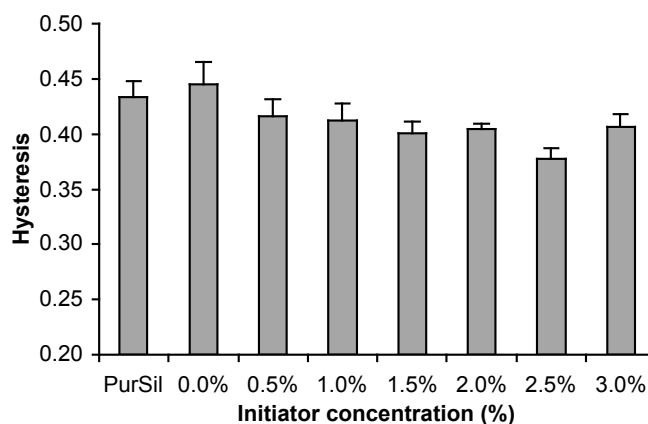


Figure 5.24: Hysteresis \pm standard deviation ($n = 4$) of Pur18.5 as function of DMPA concentration

The lowest hysteresis was achieved at an initiator concentration of 2.5% (w/w). The hysteresis at the latter concentration was found to be significantly lower compared to hysteresis values at initiator concentrations of 2.0% ($p < 0.01$) and 3.0% ($p = 0.02$), respectively

The DMPA concentration was similarly optimized for each Purx sample (i.e. Pur11.5 etc.), the hysteresis of which is presented in Figure 5.25. A summary of all the other measured (stress and strain at break) and calculated (non-recovered strain, NRS) mechanical properties is presented in Table 5.10.

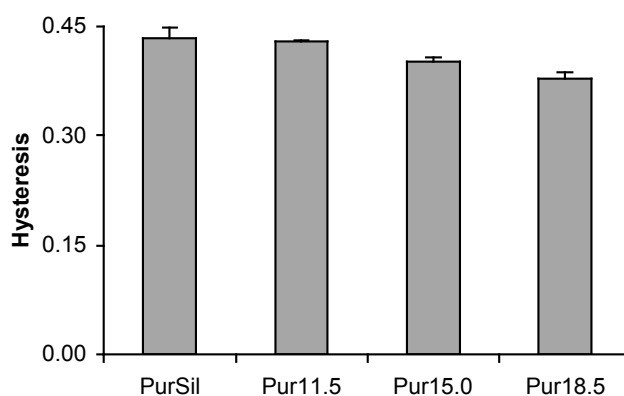


Figure 5.25: Change in hysteresis \pm standard deviation ($n = 4$) with change in degree of modification for Purx

Table 5.10: Measured and calculated mechanical properties \pm standard deviation ($n = 4$) for Purx

Purx	PurSil	Pur11.5	Pur15.0	Pur18.5
[DMPA] (w/w)		2.0%	2.0%	2.5%
Hysteresis (-)	0.43 \pm 0.01	0.43 \pm 0.00	0.40 \pm 0.00	0.38 \pm 0.01
% Change		1.0%	7.2%	12.9%
NRS (-)	26.77 \pm 1.14	24.53 \pm 0.03	23.18 \pm 1.57	20.33 \pm 1.17
% Change		8.3%	13.4%	24.0%
Stress (MPa)	28.34 \pm 0.99	29.04 \pm 0.85	29.53 \pm 1.72	21.39 \pm 1.72
% Change		2.4%	1.7%	27.6%
Strain (%)	469.7 \pm 5.57	288.3 \pm 12.91	305.8 \pm 8.69	311.9 \pm 28.16
% Change		38.6%	34.9%	33.6%

A decrease in hysteresis (Figure 5.25) and non-recovered strain (Table 5.11) was observed with an increase in the degree of modification when compared to the PurSil control sample. The lowest hysteresis and non-recovered strain was obtained for Pur18.5. The hysteresis for Pur18.5 (Figure 5.25) was found to be significantly ($p < 0.01$) the lowest when compared to Pur15.0, Pur11.5 and the PurSil control.

These results are in accordance with the measured swelling index (Q) for Purx, where the lowest swelling indexes were obtained at similar initiator concentrations for the whole range of Purx.

As expected a decrease in the strain at break was observed, due to the restriction of chain movement imparted by the crosslinking. A similar decrease, as with Pellx, in the stress at break was observed, with an increase in the degree of modification. The same explanation offered earlier (§5.5.1.3) is given here.

5.5.2.4 Dynamic mechanical analyses

Typical $\tan \delta$ curves and storage moduli (G') obtained for PurSil and Pur11.5 are presented in Figures 5.26 and 5.27, respectively.

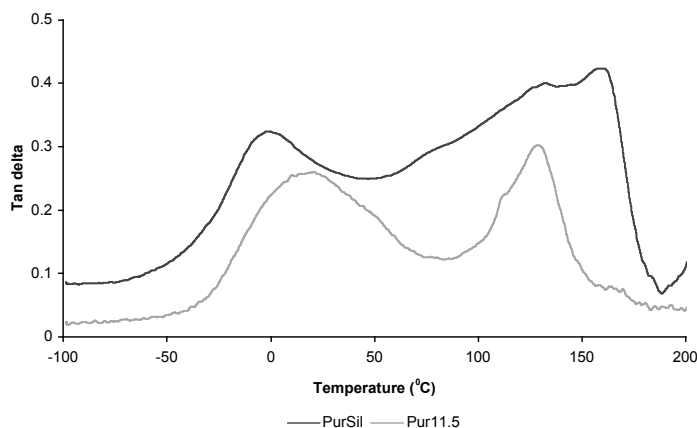


Figure 5.26: $\tan \delta$ curves obtained for PurSil and Pur11.5

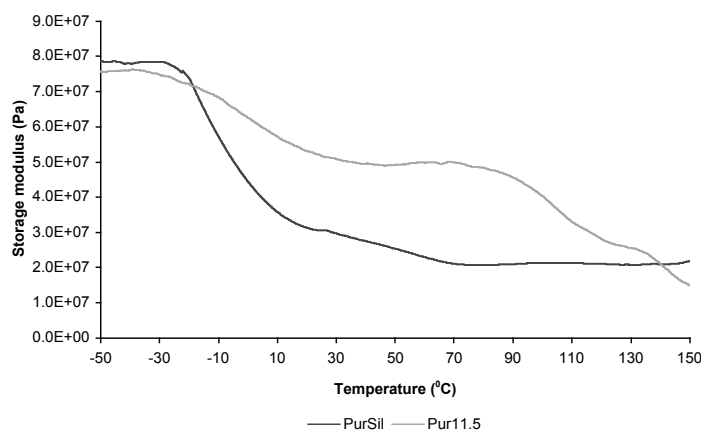


Figure 5.27: Storage moduli (G') for PurSil and Pur11.5

Two main transitions are again observed from the results presented in Figure 5.26, showing the typical two-phase structure of polyurethanes [11]. The storage modulus of Pur11.5 (Figure 5.27) was found to be significantly higher than that of PurSil over the temperature range of -10 to 140°C . The DMA results are summarized in Table 5.11.

Table 5.11: Summary of DMA results of PurSil and Purx

	PurSil	Pur11.5	Pur15.0	Pel18.5
T_1 ($^{\circ}\text{C}$)	-50.6	-33.9	-31.4	-30.0
ΔT_1 ($^{\circ}\text{C}$)	0	16.7	19.2	20.6
G' (Pa)	2.8×10^7	5.0×10^7	5.3×10^7	2.5×10^7

The increase in the first transition temperature with an increase in the degree of crosslinking is again clearly illustrated in Table 5.11, with Pur18.5 showing an increase of 20.6°C compared to PurSil. Here the possible explanation needs a modification compared to Pellx, as the 35% siloxane soft block will be less likely to mix with a modified hard block. This would imply less change to storage modulus at low temperature but more change in the intermediate zone between T_1 and T_2 (as was found).

A substantial increase in storage modulus was obtained for Pur11.5 and Pur15.0, compared to PurSil, while the value obtained for Pur18.5 was found to be comparable with the PurSil control. Concerning the storage modulus, if the degree of compatibilization with the soft block is severely restricted by the siloxane segments then the higher temperature $\tan \delta$ will not diminish; it will be modified, and can either increase (better flow), become more spread (less homogeneous phase after crosslinking), or decrease (less hard phase due to mixing with soft phase). The results point to minor mixing with part of the soft phase. The results also show typical expectations for a crosslinked hard phase that loses

stiffness, gaining flow and increased $\tan \delta$, but does not lose integrity (will not mix with siloxane block).

5.6 Conclusions

Successful crosslinking of two novel modified polyurethanes (Pellm and Purm) (Chapter 5) could be achieved using an ultraviolet light source and the initiator DMPA, a heat source (120°C) and the initiator DCP, and gamma irradiation

The swelling indices, used to calculate the molecular mass between crosslinks, could be used successfully to optimize the initiator concentrations for the Pellx and Purx samples, respectively. The lowest swelling indexes (i.e. lowest molecular mass between crosslinks) were obtained for Pell15.0 and for Pur18.5.

The best mechanical properties (in terms of hysteresis and NRS) were obtained for Pell15.0 and Pur18.5, with respective improvements in hysteresis (up to 42.5%) and creep (44.0%) for Pell15.0. The hysteresis and swelling indexes of Pellx are positively correlated ($r=0.90$, $p=0.01$).

The use of crosslinking enhancing monomers (e.g. MbA) resulted in lower swelling index values, but had a detrimental effect on the hysteresis. They were therefore not included in further investigations.

5.7 References

1. Adibi, K., M. George, and J. Barrie, *Anionic synthesis of poly(urethane-g-acrylonitrile)*. *Polymer*, 1979. **20**: p. 483-487.
2. Liaw, D.-J. and S.-P. Lin, *Phosphorus-containing polyurethanes based on bisphenol-s, prepared by N-alkylation*. *Eur. Polym. J.*, 1996. **32**: p. 1377-1380.
3. Yi, J., M. Boyce, G. Lee, and E. Balizer, *Large deformation rate-dependent stress-strain behaviour of polyurea and polyurethanes*. *Polymer*, 2006. **47**: p. 319-329.
4. Sheth, J., E. Yilgor, B. Erenturk, H. Ozhalici, I. Yilgor, and G. Wilkes, *Structure-property behaviour of poly(dimethylsiloxane) based segmented polyurea copolymers modified with poly(propylene oxide)*. *Polymer*, 2005. **46**: p. 8185-8193.
5. Qi, H. and M. Boyce, *Stress-strain behaviour of thermoplastic polyurethanes*. *Mech. of Mat.*, 2005. **37**: p. 817-839.
6. Prisacariu, C., C. Buckley, and A. Caraculacu, *Mechanical response of dibenzyl-based polyurethanes with diol chain extension*. *Polymer*, 2005. **46**: p. 3884-3894.
7. Fray, M. and V. Alstadt, *Fatigue behaviour of multiblock thermoplastic elastomers. 2. Dynamic creep of poly(aliphatic/aromatic-esters) copolymers*. *Polymer*, 2003. **44**: p. 4643-4650.
8. Abdel-Magid, B., R. Lopez-Anido, G. Smith, and S. Trofka, *Flexure creep properties of E-glass reinforced polymers*. *Comp. Struct.*, 2003. **62**: p. 247-253.
9. Zhu, H. and N. Mills, *Modelling the creep of open cell polymer foams*. *J. Mech. Phys. Solids*, 1999. **47**: p. 1437-1457.
10. Bershtein, V., P. Yakushev, N. Peschanskaya, A. Sinani, and P. Pissis, *Segmental relaxations in complex polymer system as studied by high resolution laser-interferometric creep rate spectroscopy*. *J. Non-Crystal. Solids.*, 1998: p. 584-586.

11. Jung, H., J. Kang, W. Kim, Y.-B. Lee, K. Choe, S.-H. Hong, and S.-B. Kim, *Properties of crosslinked polyurethanes synthesized from 4,4'-diphenylmethane diisocyanate and polyester polyol*. J. Appl. Polym. Sci., 2000. **78**: p. 624-630.
12. Petrovic, Z., M. Ilavsky, K. Dusek, M. Vidakovic, I. Javni, and B. Banjanin, *The effect of crosslinking on properties of polyurethane elastomers*. J. Appl. Polym. Sci., 1991. **42**: p. 391-398.
13. Jayabalan, M., P. Lizymol, and V. Thomas, *Synthesis of hydrolytically stable low elastic modulus polyurethane-urea for biomedical applications*. Polym. Int., 2000. **49**: p. 88-92.
14. Mark, H., *Encyclopedia of Polymer Science and Technology: plastics, resins, rubbers, fibers*. Crosslinking. Vol. 4. 1966, New York: Wiley Chapman & Hall. p. 331-392.
15. Nasar, A., M. Jikei, and M.-A. Kakimoto, *Synthesis and properties of elastomers crosslinked with amine-terminated AB₂-type hyperbranched polyamides*. Eur. Polym. J., 2003. **39**: p. 1201-1208.
16. Shibata, M. and T. Ito, *Metallization of cross-linked polyurethane resins by reduction of polymer-incorporated metal ion*. Polymer, 2003. **44**: p. 5617-5623.
17. Eroglu, M., B. Baysal, and O. Guven, *Determination of solubility parameters of poly(epichlorohydrin) and poly(glycidyl azide) networks*. Polymer, 1997. **38**: p. 1945-1947.
18. Stanciu, A., V. Bulacovschi, M. Lungu, S. Vlad, S. Balint, and S. Oprea, *Mechanical behaviour of crosslinked poly(ester-siloxane) urethanes*. Eur. Polym. J., 1999. **35**: p. 2039-2044.
19. Van Krevelen, D., *Properties of Polymers*. 1990, Amsterdam: Elsevier Science. p. 189-224
20. Terada, M. and R. Marchessault, *Determination of solubility parameters for poly(3-hydroxyalkanoates)*. Int. J. Biol. Macromol., 1998. **25**: p. 207-215.
21. Moad, G. and D. Solomon, *The Chemistry of Free Radical Polymerization*. 1st ed. 1995, New York: Elsevier Science Ltd. p. 43-95
22. Frahn, M., *Radiation-induced polymerization monitored with fluorogenic molecular probes*, PhD dissertation, *Department of Science*. 2003, Technical University of Delf: Delft. p.1-28
23. Department of polymer Science, University of Southern Mississippi, *Macrolab experiment: Determination of crosslink density*. 2004. p. 1-8
24. www.campoly.com, *Swelling measurements of crosslinked polymers*. [accessed: 5 December 2004].
25. Ania, F. and B. Calleja, *Personal communication, discussing wide angle X-ray scattering results*. 26 July 2006: Instituto de Estructura de la Materia, C.S.I.C, Madrid, Spain.
26. Tanzi, M., D. Mantovani, P. Petrini, R. Guidoin, and G. Laroche, *Chemical stability of polyether urethanes versus polycarbonate urethanes*. J. Biomed. Mater. Res., 1997. **36**(4): p. 550-559.
27. Harrison, H., *Synthetic materials as vascular prostheses. Ia. A comparative study in small vessels of nylon, dacron, orlon, ivalon sponge and teflon*. Amer. J. Surg., 1958. **95**: p. 3-15.

Chapter 6

In vitro chemical stability assay

Abstract

Laboratory experiments (*in vitro*) involving aggressive reagents and high temperatures (exceeding physiological) are generally first used to evaluate the chemical stability of new or modified polyurethanes, before such materials are evaluated in animals (*in vivo*). In such a study, the chemical stability of Pellethane[®] 2363-80AE (control) was compared to Pell15.0 using silver nitrate, hydrogen peroxide and a phosphate buffer solution at 65 °C for periods ranging from 4 to 8 weeks. Changes in mechanical properties of the respective polyurethanes, (determined using tensile testing and dynamic mechanical analysis (DMA)) and chemical properties (determined using Fourier transform infrared spectroscopy (FT-IR), scanning electron microscopy (SEM) and X-ray photoemission spectroscopy (XPS)) were subsequently compared. Degradation of the two respective polyurethanes was already evident after 4 weeks, as evident from their measured tensile properties (e.g. hysteresis and non-recovered strain (NRS)). The hysteresis and NRS of Pell15.0 was better by at least 27.5% and 21.0%, respectively, when compared to Pellethane[®] 2363-80AE. The latter also showed a decrease in the hard phase integrity when compared to Pell15.0 (DMA) due to the absence of the imparted oxidative stable crosslinks. FT-IR results mainly confirmed the degradation of the “more vulnerable, less ordered” soft segment, in both Pellethane[®] 2363-80AE and Pell15.0. XPS results confirmed the degradation of the ether soft phase in both Pellethane[®] 2363-80AE and Pell15.0, although this effect was more pronounced in the former, because the hard phases are more free to rearrange. Pellethane[®] 2363-80AE showed much more surface degradation (SEM), in both silver nitrate and hydrogen peroxide, when compared to Pell15.0, although the difference was statistically significant only for the samples incubated in silver nitrate. It can finally be concluded, from the extensive *in vitro* degradation study, that Pell15.0 generally showed a higher resistance toward degradation because of the imparted, stable covalent crosslinks. The soft phases of both polyurethanes are however vulnerable towards degradation, but this is not as pronounced in Pell15.0, mainly due to the restriction of chain movement, resulting from crosslinking.

6.1 Introduction

Time, cost and moral issues necessitate that the chemical stability of new biomaterials first be tested in the laboratory (*in vitro*) before they are evaluated in animals (*in vivo*). Aggressive reagents (e.g. hydrogen peroxide and silver nitrate) and temperatures exceeding physiological temperature ($>37^{\circ}\text{C}$) are often used to accelerate possible chemical degradation reactions (see Appendix E) in the former case.

The chemical stability of Pellethane[®] 2363-80AE (control) was compared to Pell15.0 (modified and crosslinked as described in Chapters 4 & 5, using ω,ω -dimethoxy- ω -phenylacetophenone and an ultraviolet light source) in such an *in vitro* degradation study. Samples were placed separately in silver nitrate, hydrogen peroxide (to simulate metal ion induced oxidation and oxidation reactions, respectively) and phosphate buffer solutions (PBS) and incubated at 65°C for periods ranging from 4 to 8 weeks.

Tensile testing of the specimens was performed after 4 weeks to accommodate cyclic testing. Dynamic mechanical analysis (DMA), Fourier-transform infrared spectroscopy (FT-IR), scanning electron microscopy (SEM) and X-ray photoemission spectroscopy (XPS) analyses were performed at the end of the degradation study (8 weeks). Changes in mechanical and chemical properties of the respective polyurethanes were subsequently compared.

6.2 Historical

From the almost infinite number of possible polyurethane compositions, relatively few have demonstrated successful performance in implantable devices [1]. In the 1960's published clinical reports of implantable polyurethanes described excellent initial properties but severe chemical breakdown in the body within months. It was then believed that polyurethanes were not suitable for implantation, but this erroneous attitude was mainly based on the lack of appreciation of the tremendous number of chemical polyurethane formulations possible.

Since then, there has been a widespread investigation into finding polyurethanes that are chemically stable, as well as *in vitro* testing methods that could simulate *in vivo* conditions. This has led to a much better understanding of the sensitivity of the method of processing and the sensitivity of certain raw materials to chemical degradation. Some of these studies will now be briefly discussed (also see Table E.1, Appendix E for a more complete list).

Polyurethanes, especially the Pellethane family, have been extensively used in the manufacturing of the first pacemaker leads [1, 2]. It was however not until the first reported

clinical failure that *in vitro* test methods had to be devised in order to create an understanding of the possible mechanisms involved in order to prevent such occurrences.

A. Coury and K. Stokes were the pioneers in evaluating the chemical stability of especially pacemaker leads, and have published widely. Whole pacemaker leads [2, 3], pre-stressed tubing [1, 2] and flat sheets [1, 2, 4, 5] were incubated in different oxidative metal ion solutions (metals typically used in the manufacture of the wires inside the leads, such as platinum, silver, ferrous chloride, copper, nickel and cobalt) and other oxidative media such as hydrogen peroxide. The samples were typically kept at temperatures ranging between 37 - 90 °C for periods of up to 6 months and then analyzed mainly using Fourier transform infrared spectroscopy and tensile testing.

Severe cracking of Pellethane 80A (Dow Chemicals, USA) was observed after a 30-day incubation period in hydrogen peroxide at 37 °C [3]. Pellethane 80A was compared with Pellethane 55D (Dow Chemicals, USA), Techoflex EG80A (Thermedics, USA), Biomer (Ethicon, USA) and Cardiothane-51 (Avcothane, USA). It was found that the susceptibility to degradation is directly proportional to the oxidative potential of the metal ions present and the ether content of the respective polyurethanes, with Pellethane 80A (highest ether content) performing significantly the worst [2].

This inspired the syntheses of “custom-made” polyurethanes, using different raw materials (especially different soft segments) and at different concentrations, to subsequently create an understanding of the underlying degradation mechanisms involved.

In efforts to improve commercially available polyurethanes, Takahara [6], Santerre, [7, 8], Petrovic [9], del Guerra [10], Labow [11], Schubert [12] and their co-workers synthesized polyurethanes containing different soft segments, such as poly(ethylene oxide), poly(tetra methylene oxide), poly(butane) diol and poly(dimethyl siloxane).

Polyurethane samples were incubated in various media, including metal ion solutions and other oxidative media e.g. cholesterol esterase at physiological temperatures (37 °C), for periods of up to 30 days. Flat films were formed either by solvent casting techniques or extruded to thicknesses of up to 0.3 mm.

Degradation of the surface of polyurethanes with high ether soft segment content, resulting from an autoxidation mechanism, was again observed. Much less degradation was observed in the polyurethanes synthesized from e.g. poly(dimethyl siloxane) and hydrogenated poly(butadiene), respectively. It was concluded that high resistance could be obtained from highly linear aliphatic polyol soft segments with a saturated hydrocarbon content and siloxanes.

Due to the high number of formulations possible and their great versatility as biomaterial, the demand for chemically stable polyurethanes increased in the late 1980s. This resulted in a change of focus in terms of the methods of *in vitro* chemical stability

evaluation, from the use of mainly metal ions and oxidative media to *in vitro* degradation media that could more accurately simulate physiological conditions [13-25].

Technologically more advanced commercially available polyurethanes (e.g. Corethane 80A, Biospan, Techoflex and MyoLink) were subsequently used in comparative studies. Flats sheets, tubing (strained and unstrained) and even porous grafts [16, 20] were evaluated at physiological temperatures (for up to 4 months) in a wide range of media. These included: cholesterol, steroids (e.g. cortisone), different enzymes (e.g. papain), human macrophages, human plasma, mouse fibroblast cells and immunoglobulin. Differential scanning calorimetry, gel permeation calorimetry, dynamic mechanical analyses, atomic force microscopy (AFM) and environmental scanning electron microscopy were commonly used to evaluate degradation.

It was found that although poly(carbonate) urethanes are less susceptible to oxidative degradation than poly(ether) urethanes, they are more prone to hydrolytic degradation [16, 22]. Polar steroids (e.g. cortisone) have strong interactions, especially with Pellethane 55D (as opposed to Pellethane 80A), and environmental stress cracking was observed at moderate strains [24]. Poly(urea) urethanes showed higher calcification and white blood cell consumption when compared to poly(ether) urethanes [18].

It is clear from the summary presented in Table E.1 (Appendix E) and the discussion above that polyurethanes are strongly influenced by the aging media, raw materials that constitute the urethane, temperature and incubation time. The most commonly used *in vitro* degradation conditions (from the extensive list, in Appendix E) were chosen and used in this study.

6.3 Experimental

6.3.1 Materials

Pellethane was obtained from Dow Chemicals, while Pell15.0 was synthesized and crosslinked as described in Chapters 4 & 5. Tetrahydrofuran (THF) (Merck, Cat: AB009731) was used as solvent and ω,ω -dimethoxy- ω -phenylacetophenone (DMPA) (Aldrich Cat: 19,611-8) as UV initiator

The following reagents were used to prepare the degradation media: silver nitrate (Aldrich Cat: 20,913-9), hydrogen peroxide (30% wt%) (Riedel-de Haën cat: 31642), disodium hydrogen orthophosphate (Saarchem, Cat: 5822900), potassium dihydrogen orthophosphate (Saarchem, Cat: 5043600), potassium chloride (Aldrich, Cat: 20,800-0), sodium chloride (Aldrich, Cat: 22,351-4) and double-distilled ultra-pure water (17 $\mu\Omega$).

6.3.2 Methods

6.3.2.1 Preparation of degradation solutions

The degradation solutions were prepared to volumes of 1500 ml, with concentrations and pH values as presented in Table 6.1.

Table 6.1 *Reactants used in degradation study*

Reactants	Concentration
Silver nitrate (AgNO ₃)	0.1 mol/l
Hydrogen peroxide (H ₂ O ₂)	20% (w/w)
Phosphate buffer solution (PBS)	pH = 7.4

The phosphate buffer solution was prepared by dissolving di-sodium hydrogen orthophosphate (14.48 g), potassium dihydrogen orthophosphate (1.00 g), potassium chloride (1.00 g) and sodium chloride (40.00 g) in 1400 ml of double-distilled ultra-pure water (17 μΩ) and adjusting the pH to 7.4. Hydrogen peroxide was diluted with water to obtain the required concentration, while 25.48 g of silver nitrate was dissolved in 1500 ml water to obtain a concentration of 0.1 mol/l.

6.3.2.2 Film casting

Pellethane and Pellm15.0 were dissolved in tetrahydrofuran to obtain 10% (w/w) solutions. To the Pellm15.0 solution 2.0% DMPA was added. Solid films were cast of all the polymer solutions (to thicknesses of 0.5 mm) by standard solvent casting and evaporation techniques, then dried *in vacuo* for 12 h. Pellm15.0 was subsequently crosslinked (Pell15.0) using a 315 - 400 nm ultraviolet light source (UV initiation) for 15 min, whereafter all the films were dried for an additional 72 h *in vacuo*.

6.3.2.3 Sample preparation

Dumbbell samples for tensile testing (≈0.5 mm thick) (ASTM D638, Type V) (n = 4) and a strip (10-mm wide) were cut from the dried polymer films as prepared in §6.3.2.2 and placed in 30 ml glass tubes filled with the three respective solutions (see Table 6.1).

The tensile samples were placed in a constant-temperature laboratory oven at 65 °C for 4 weeks, while the other samples were left at 65 °C for 8 weeks. The solutions were replaced twice weekly. After the respective study periods the samples were thoroughly washed with double distilled water, slowly air dried overnight and then dried *in vacuo* for 4 days (room temperature).

6.3.3 Analyses

6.3.3.1 Tensile testing

Cut samples were tested for tensile behavior, as described in §5.4.3.3 (Chapter 5).

6.3.3.2 Dynamic mechanical analysis

Dynamic mechanical analyses (DMA) were performed as described in §5.4.3.4 (Chapter 5).

6.3.3.3 Fourier-transform infrared spectroscopy

The degraded and control samples were analyzed by means of photo acoustic Fourier-transform infrared spectroscopy (FT-IR), as described in §4.3.4.1 (Chapter 4).

Ratios of peaks at wavenumbers of: 1075 cm^{-1} (urethane ether), 1105 cm^{-1} (aliphatic ether), 1175 cm^{-1} (new peak), 1220 cm^{-1} (Amide III), 1703 cm^{-1} (bonded carbonyl), 1730 cm^{-1} (unbonded carbonyl), 2860 cm^{-1} (asymmetrical PTMEG CH_2 stretch) and 2940 cm^{-1} (symmetrical PTMEG CH_2 stretch) were studied and compared.

6.3.3.4 X-ray photoemission spectroscopy

The surface chemistry of the test samples, subjected to the degradation study for 8 weeks, and their respective controls (Pellethane and Pell15.0) were analyzed using XPS. Samples ($n = 1$) were analyzed using a Quantum 2000 (PHI) scanning X-ray microprobe, which employs a monochromate AL $\text{K}\alpha$ source. The X-ray gun was operated at a take-off angle of 45° and at 20 W with pass energy of 118 eV for the wide scans and 23 eV for the narrow scans. All calculations (e.g. integration) were performed by the built-in software.

6.3.3.5 Scanning electron microscopy

The surfaces of the samples subjected to the degradation study for 8 weeks and control samples of Pellethane and Pell15.0 were investigated using a LEO (1450EP) scanning electron microscope (SEM). Test pieces ($n = 3$) were cut from each sample with a sharp blade, mounted on aluminum stubs, sputter coated with gold-palladium (AuPd), and viewed in the SEM at an accelerating voltage of 7 kV.

Complete areas were investigated and captured at different magnifications (x2000 & x5000). Representative images ($n = 5$) from the different treatment groups were then compared at similar positions (e.g. close to the edges) and magnification (x2000) and scored by seven independent blinded observers. The control samples (not subjected to the degradation media) were used as references and scores of between 0 and 5 were given

depending on the degree of degradation, where 5 indicated a sample that was most degraded (i.e. deep, open cracks).

6.3.3.6 Statistical analysis

Statistical analyses were performed using either (a) student t-test (unpaired 2-tailed, assuming equal variance), (b) Kruskal-Wallis (non-parametric test) (c) 1-way analysis of variance (ANOVA) and (d) 2-way ANOVA. Bonferroni corrections were applied in cases of multiple comparisons. A significance level of 0.05 or less was accepted as being statistically significant. Standard assumptions of normality were made, but in cases where it was suspected that the assumptions were violated the results were verified using non-parametric (bootstrap) techniques (see Appendix H for a summary).

6.4 Results and discussion

6.4.1 Tensile testing

The measured and calculated tensile properties of the controls (Pell & Pell15.0) and samples degraded in the various degradation media are presented in Table 6.2.

Table 6.2: Summary of tensile properties \pm standard deviation ($n = 3$) of Pellethane and Pell15.0 degraded in the various media

	Controls		AgNO ₃		H ₂ O ₂		PBS	
	Pell	Pell15.0	Pell	Pell15.0	Pell	Pell15.0	Pell	Pell15.0
Hysteresis (-)	0.36 \pm 0.01	0.21 \pm 0.01	0.38 \pm 0.01	0.27 \pm 0.01	0.38 \pm 0.01	0.26 \pm 0.01	0.37 \pm 0.01	0.20 \pm 0.01
p	p < 0.01		p < 0.01		p < 0.01		p < 0.01	
Δ (%)	42.5%		27.5%		30.9%		45.3%	
NRS (%)	16.74 \pm 0.97	8.75 \pm 0.88	18.70 \pm 2.78	14.79 \pm 1.26	8.90 \pm 2.12	14.52 \pm 1.88	17.91 \pm 1.33	9.17 \pm 0.75
p	p < 0.01		p = 0.06		p = 0.02		p < 0.01	
Δ (%)	47.7%		21.0%		23.3%		48.8%	
Stress (MPa)	46.97 \pm 2.44	29.23 \pm 1.92	56.84 \pm 4.75	16.73 \pm 1.20	41.63 \pm 4.07	27.80 \pm 2.84	50.45 \pm 1.16	32.88 \pm 1.57
p	p < 0.01		p < 0.01		p < 0.01		p < 0.01	
Δ (%)	37.8%		70.6%		31.1%		34.8%	
Strain (%)	571.6 \pm 19.3	411.5 \pm 18.4	665.3 \pm 43.0	527.0 \pm 51.7	618.8 \pm 49.3	537.3 \pm 45.6	630.4 \pm 14.6	522.9 \pm 34.5
p	p < 0.01		p < 0.01		p = 0.04		p < 0.01	
Δ (%)	28.0%		20.8%		13.2%		17.0%	

An increase in hysteresis was observed for Pellethane and Pell15.0 samples all treated in the degradation media except in PBS (Figure 6.2). The increase was significant for Pellethane ($p=0.02$) and Pell15.0 ($p<0.01$) degraded in silver nitrate, and for Pell15.0 in hydrogen peroxide ($p<0.01$). The hysteresis of all the degraded Pell15.0 samples was significantly lower (at least 27.5%) than the degraded Pellethane ($p<0.01$) samples.

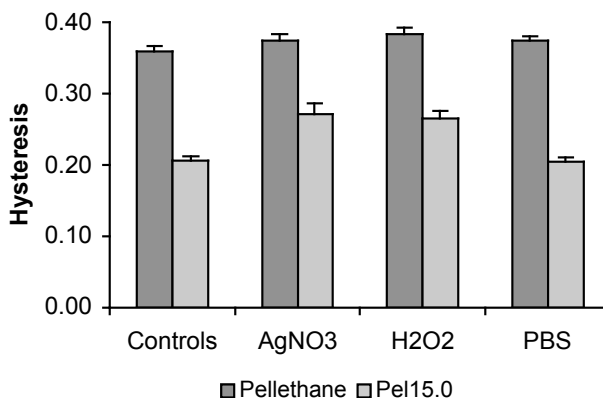


Figure 6.2: *Hysteresis ± standard deviation (n = 3) of Pellethane and Pel15.0 in the various degradation media*

A similar trend was observed for the non-recovered strain (Figure 6.3). Here, however, the NRS of the Pel15.0 samples was at least 21.0% better compared to the Pellethane control sample. The differences between Pellethane and Pel15.0 were significant for the samples degraded in hydrogen peroxide ($p=0.03$) and PBS ($p<0.01$).

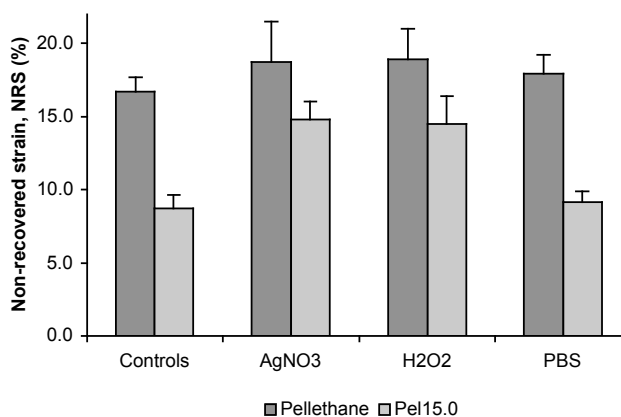


Figure 6.3: *NRS ± standard deviation (n = 3) of Pellethane and Pel15.0 with change in degradation media*

The apparent slower degradation of Pellethane in silver nitrate and hydrogen peroxide compared to Pel15.0 may be a result of re-ordering of the polyurethane's conformation and better phase separation, due to the absorption of the degradation media [26]. The oxidation attack is said to be at the ether linkage of the soft section [1, 27, 28]. However, it is also known that amide and urethane groups are susceptible to oxidation [3, 28] and one of two effects could occur: either loss of crosslinks at the carbamate coupling or the introduction of the modification making the hard segment more penetrable to the oxidants, allowing chain scission at nascent urethane groups. In the authors view, the latter would be more plausible and in keeping with the findings of the above references.

This effect is clearly illustrated in Figures 6.4 and 6.5, where an unexpected significantly higher stress ($p < 0.01$) and strain at break ($p = 0.04$) was obtained for Pellethane incubated in silver nitrate, compared to the Pellethane control.

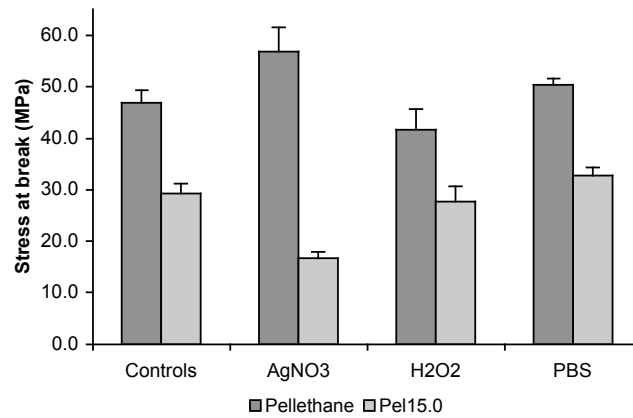


Figure 6.4: Comparison of stress at break \pm standard deviation ($n = 3$) of Pellethane with Pel15.0

These results are consistent with tensile results obtained by Stokes et al. [26], where Pellethane initially showed very little loss in stress and strain at break in a silver nitrate medium (Figure 6.5), but dramatically degraded after a longer period of time.

The stress at break (Figure 6.4) remained fairly constant for Pel15.0 (except for the decrease in AgNO_3 , $p < 0.01$), but degradation was clearly evident for Pellethane incubated in hydrogen peroxide, where a decrease in stress at break was observed (Figures 6.4), compared to the Pellethane control. This is probably due to localized chain scission in the soft segment of Pellethane, possibly near the interphase bonding, as was reported by Pinchuk [27].

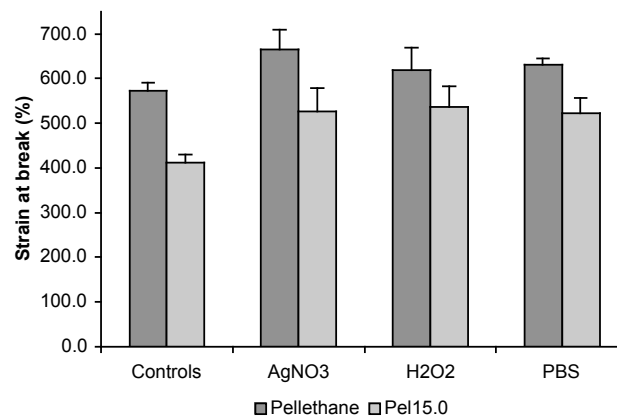


Figure 6.5: Change in strain at break \pm standard deviation ($n = 3$) with change in degradation medium

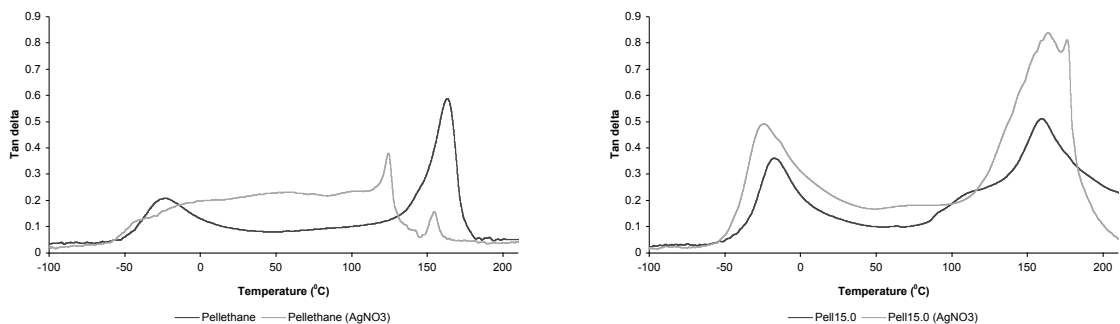
A significant increase ($p < 0.01$) in strain at break was observed for the degraded Pell15.0 samples, compared to the Pell15.0 control. As discussed earlier, the increase in strain at break was only significant for the Pellethane sample degraded in silver nitrate ($p = 0.04$).

Although results obtained under these accelerated in vitro degradation conditions, are not directly translatable to the in vivo environment, they have been extensively used [1-6] to compare the degradation resistance of polyurethanes and to offer a certain degree of prediction of the long-term behavior in the body.

The hysteresis and non-recovered strain of Pell15.0, compared to Pellethane, was still better on average by between 21.0% to 48.8%, even after the 4-week incubation period in the various degradation media. The stress and strain at break of Pell15.0 remained relatively constant, although a slight decrease in stress at break was observed for Pell15.0 in silver nitrate. On average, the tensile properties of Pell15.0 remained superior to Pellethane even after subsection of the samples to the harsh conditions.

6.4.2 Dynamic mechanical analysis

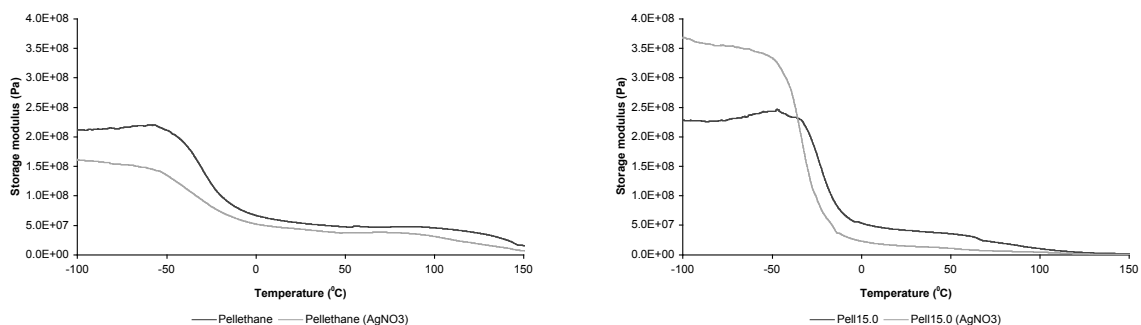
Figures 6.6a and 6.6b exhibit the mechanical loss tangents ($\tan \delta$) for Pellethane and Pell15.0 control samples and degraded samples in silver nitrate.



a) $\tan \delta$ of Pellethane (control) and a Pellethane sample degraded in silver nitrate

b) $\tan \delta$ of Pell15.0 (control) and a Pell15.0 sample degraded in silver nitrate

Figure 6.6: Comparison of $\tan \delta$ for control and degraded samples



c) Storage modulus (G') of Pellethane (control) and a Pellethane sample degraded in silver nitrate

d) Storage modulus (G') of Pell15.0 (control) and a Pell15.0 sample degraded in silver nitrate

Figure 6.7: Comparison of storage modulus (G') for control and degraded samples

The storage moduli (G') for typical samples degraded in silver nitrate with their respective controls, are presented in Figures 6.7a and 6.7b.

The distinct two-phase polyurethane elastomeric structure is still clearly evident for Pell15.0 (Figure 6.6b), even after exposure of the sample to silver nitrate. This result was consistent for Pell15.0 samples exposed to all the respective degradation media. If scission occurs in the polyether this would not affect phase separation, while scission in the hard polyurethane domain would. However, the $\tan \delta$ data in Figure 6.6b shows that the crosslinking keeps this phase intact. The author therefore suggests that the crosslinks are impervious to the silver nitrate, but that the urethane groups can still be attacked on the periphery of the hard segments, leading to scission and some compatibility with the soft segment, as is seen in the increased storage modulus, Figure 6.7d [20]. A small decrease in T_1 was further observed for the degraded sample (Figure 6.6b and Table 6.3) when compared to the control (Pell15.0), indicative of scission in the soft segment. A decrease in storage modulus in the temperature range of 0 - 100°C (Figure 6.7d) was also observed. This is in keeping with scission at the periphery of the hard segments.

The $\tan \delta$ of the Pellethane sample degraded in silver nitrate (Figure 6.6a) exhibited polyphase properties. The second transition is evident, indicating degradation of part of the polyurethane hard segment. There also is a very slight lower onset of the first transition temperature when compared to the Pellethane control (Table 6.3), which indicates chain scission in the soft segment (more chain ends lower T_1) [15, 17, 29]. The lower storage modulus reinforces the concept of chain scission in both phases (Figure 6.7c).

Table 6.3: Summary of DMA results of Pellethane and Pell15.0

	Controls		AgNO ₃		H ₂ O ₂		PBS	
	Pell	Pell15.0	Pell	Pell15.0	Pell	Pell15.0	Pell	Pell15.0
T_1 (°C)	-55.1	-48.8	-59.1	-51.6	-61.5	-59.1	-57.1	-50.8
d T_1 (°C)		+6.5		+7.5		+2.4		+6.3
T_2 (°C)	131.9	84.7	124.4	116.3	118.9	93.6	134.7	113.5
d T_2 (°C)		-47.2		-8.1		-25.3		-21.2
G' (Pa)	5.0×10^7	3.9×10^7	4.0×10^7	1.3×10^7	5.2×10^7	2.8×10^7	4.8×10^7	2.0×10^7
d G' (Pa)		1.1×10^7		2.7×10^7		2.5×10^7		2.8×10^7

The data presented in Table 6.3 clearly show the slight decrease in T_1 for both Pellethane and Pell15.0 samples after degradation. The first transition temperature of the Pell15.0 samples is however a few degrees higher (Table 6.3), possibly due to the restriction of the mobility of the polymer chains imparted by the covalent crosslinking.

The decrease in hard segment integrity (T_2) for Pellethane degraded in silver nitrate and hydrogen peroxide, also described by Tanzi et al. [17], is proposedly caused by chemically induced disruption of the hard segment domains [17]. The opposite effect was

observed for the Pell15.0 samples, and can be attributed to the restriction of chain movement, again as a result of the imparted oxidatively stable crosslinks.

6.4.3 Fourier-transform infrared spectroscopy

FT-IR analysis may not be the best analytical method by which to investigate degraded surfaces, as the beam penetrates the sample, averaging between very thin degraded material on the surface and underlying non-degraded polymer [26]. A summary of some important ratio of absorbances ($\text{cm}^{-1}/\text{cm}^{-1}$) for Pellethane (Pell) and Pell15.0 is however given in Table 6.4, with graphical illustrations of selected ratios in Figures 6.8 - 6.11.

Table 6.4: Ratios of absorbance ($\text{cm}^{-1}/\text{cm}^{-1}$) \pm standard deviation ($n = 4$) for Pellethane (Pell) and Pell15.0

	Controls		AgNO ₃		H ₂ O ₂		PBS	
	Pell	Pell15.0	Pell	Pell15.0	Pell	Pell15.0	Pell	Pell15.0
1703/1730	2.280	1.611	2.715	2.285	3.147	4.529	1.913	1.848
Stdev	0.331	0.418	0.645	0.559	0.279	0.744	0.219	0.230
1175/1220	0.000	0.000	0.158	0.230	0.028	0.000	0.000	0.000
Stdev	0.000	0.000	0.026	0.029	0.021	0.000	0.000	0.000
1105/1220	0.447	0.457	0.406	0.458	0.398	0.381	0.438	0.417
Stdev	0.025	0.025	0.031	0.020	0.041	0.035	0.030	0.013
1075/1220	0.133	0.147	0.268	0.272	0.182	0.225	0.137	0.179
Stdev	0.005	0.007	0.025	0.013	0.004	0.028	0.008	0.010
1105/1075	3.368	3.226	1.530	1.688	2.191	1.726	3.205	2.336
Stdev	0.249	0.269	0.301	0.130	0.207	0.373	0.218	0.191
2860/2940	1.060	1.072	1.002	1.058	1.050	1.006	1.124	1.063
Stdev	0.034	0.044	0.020	0.113	0.033	0.051	0.045	0.038

1075 cm^{-1}	Urethane ether	1703 cm^{-1}	Bonded carbonyl
1105 cm^{-1}	Aliphatic ether	1730 cm^{-1}	Unbonded carbonyl
1175 cm^{-1}	New peak (carbonyl containing)	2860 cm^{-1}	Asymmetrical PTMEG CH ₂ stretch
1220 cm^{-1}	Amide III	2940 cm^{-1}	Symmetrical PTMEG CH ₂ stretch

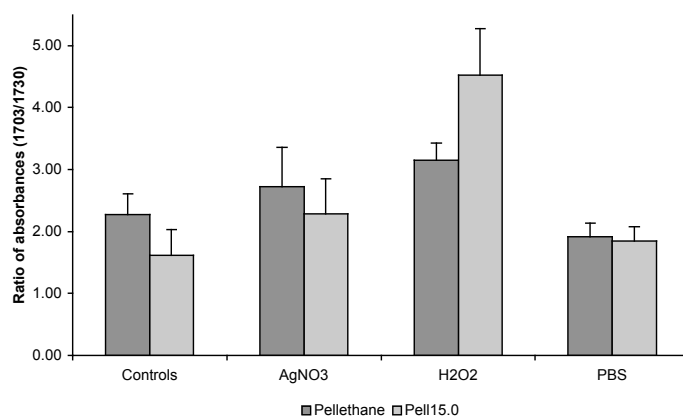


Figure 6.8: Ratios of absorbance \pm standard deviation ($n = 4$) ($1703 \text{ cm}^{-1}/1730 \text{ cm}^{-1}$) for Pellethane and Pell15.0

A minor decrease in asymmetrical PTMEG CH₂ stretch compared to symmetrical PTMEG CH₂ stretch (2860 cm⁻¹/2940 cm⁻¹) (Table 6.4) was observed, with a concomitant increase in the hydrogen-bonding index (ratio of bonded to unbonded carbonyl, 1703 cm⁻¹/1730 cm⁻¹) for all degraded specimens (except samples degraded in PBS) compared to their control samples (Figure 6.8) (only significant (p<0.01) for Pell15.0 degraded in hydrogen peroxide). This finding was consistent with that of Stokes et al. [26]. The hydrogen-bonding index of Pell15.0 was also found to be consistently slightly lower than that of Pellethane, except in hydrogen peroxide where that of Pell15.0 was significantly higher (p=0.01) than Pellethane. This is consistent with the removal of carbamate hydrogens and substitution of 4-pentenoyl pendent groups. The ratios of the aliphatic ether (1105 cm⁻¹) to amide III (1220 cm⁻¹) are presented in Figure 6.9.

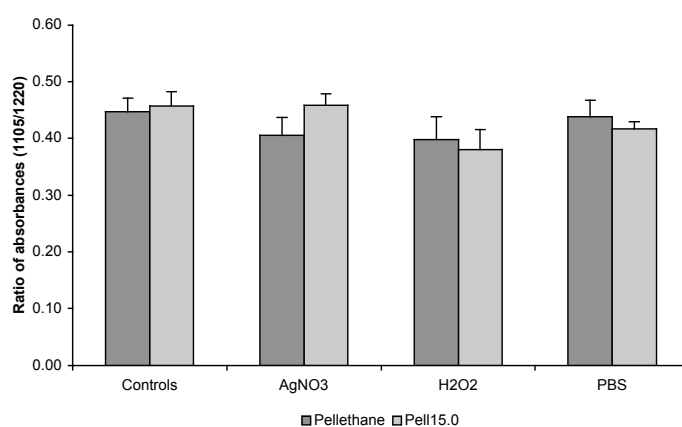


Figure 6.9: Ratio of absorbance \pm standard deviation ($n = 4$) (1105 cm⁻¹/1220 cm⁻¹) for Pellethane and Pell15.0

On average, the ratios (1105cm⁻¹/1220 cm⁻¹) remained relatively constant for both Pell15.0 and Pellethane when compared to each other and to their control samples. It seems therefore that the aliphatic ether and amide III changed simultaneously and consistently during degradation when compared to their controls. This has been reported by Stokes et al. [26] to be a result of permanent re-ordering of the polyurethanes' conformation due to the absorption of the degradation media and degradation occurring in both phases (see discussion in §6.4.1).

The ratios of the urethane ether (1075 cm⁻¹) to amide III (1220 cm⁻¹) are presented in Figure 6.10. The ratios of Pell15.0 were significantly higher than those of Pellethane, for the samples degraded in hydrogen peroxide (p=0.01) and in PBS (p=0.02). An increase in the ratios was observed throughout for both degraded Pellethane and Pell15.0 compared to their controls, although it was only significant in the case of hydrogen peroxide and silver nitrate (p<0.01).

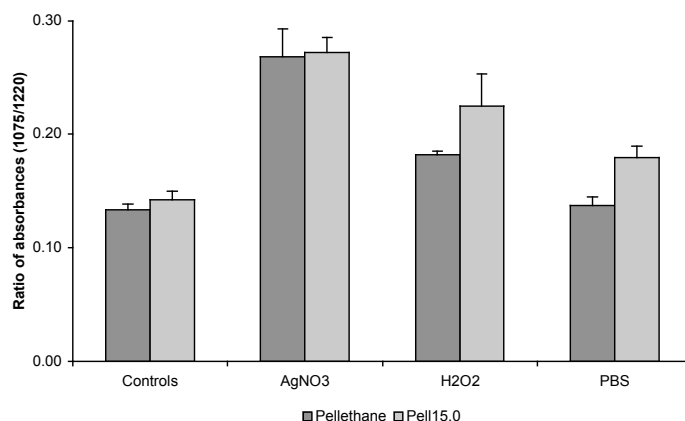


Figure 6.10: Ratios of absorbance \pm standard deviation ($n = 4$) ($1075\text{ cm}^{-1}/1220\text{ cm}^{-1}$) for Pellethane and Pell15.0

It appears that oxidative degradation by silver nitrate leads to better hydrogen bonding and more carbonyl formation in deference to hydrogen peroxide degradation. Degradation in Pell15.0 was slightly greater; diffusion into the hard segments is facilitated, indicating that much of the ratio is due to changes in the hard segment, especially at the periphery.

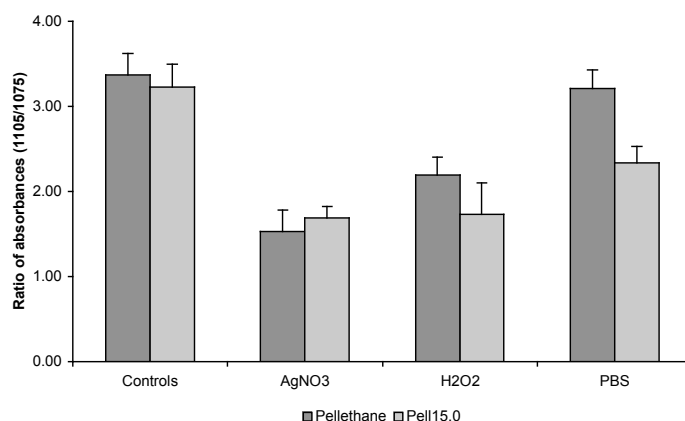


Figure 6.11: Ratio of absorbance \pm standard deviation ($n = 4$) ($1105\text{ cm}^{-1}/1075\text{ cm}^{-1}$) for Pellethane and Pell15.0

The ratios of the aliphatic ether (1105 cm^{-1}) to urethane ether (1075 cm^{-1}) are presented in Figure 6.11. A significant decrease ($p < 0.01$) in this ratio was observed in all the samples, when compared to their respective controls, with the exception of Pellethane degraded in PBS. This observation was found to be consistent with the results obtained by Stokes [26], who attributed it to ether soft segment oxidation. It is however interesting to note though that the loss in aliphatic ether compared to urethane ether ($1105\text{ cm}^{-1}/1075\text{ cm}^{-1}$) was lower for Pell15.0 for all but one sample (AgNO₃) when compared to Pellethane, although only significantly lower for Pell15.0 degraded in PBS ($p < 0.01$) (Figure 6.8). This is

also in agreement with the findings of Stokes et al. [26], who concluded that the primary site of attack must be the “more vulnerable, less ordered” soft segment.

The appearance of a new carbonyl-containing peak at 1175 cm^{-1} , which was observed for Pellethane, degraded in silver nitrate (AgNO_3) and hydrogen peroxide (H_2O_2), but only in one case for Pell15.0 (AgNO_3). It has been suggested [26, 30] that this is a result of coordination of the ether oxygen with a metal ion (although the author is not in full agreement with this explanation), although it has been reported [26] also to occur in an in vitro study with hydrogen peroxide. This finding is consistent with the suggested oxidation mechanism proposed by Stokes et al. [26] and the author suggests that it stems from competitive oxidation occurring in both phases.

Stokes et al. [26] observed significant changes on the surfaces of his samples, but finally concluded that the changes are due to reversible changes in the polyurethane conformation and should not be confused with irreversible changes due to degradation.

6.4.4 X-ray photoemission spectroscopy

Polyurethanes are very mobile polymers and XPS may not be the most suitable analytical technique, due to the surface rearrangement in the high vacuum environment [28]. This technique was never the less used (although results cannot be directly extrapolated to the biological environment) to provide additional/supportive information.

A summary of the XPS results obtained for degraded Pellethane and Pell15.0 is presented in Table 6.5. The high-resolution C_{1s} spectra (narrow scans) could be deconvoluted into two major peaks, at 284.7 eV (hydrocarbon, C-C) and 286.2 eV (ether, C-O) [6, 22, 30], as well as a small but broad peak at 288.4 - 289.4 eV (C=O). The O/C and N/C ratios of Pellethane (control) were found to be consistent with reported values [30].

Table 6.5: Summary of XPS results for Pellethane and Pell15.0

Conc (%)	Controls		H_2O_2		PBS	
	Pellethane	Pell15.0	Pellethane	Pell15.0	Pellethane	Pell15.0
C	88.6	82.7	85.2	78.9	83.6	80.7
O	9.4	14.0	12.9	17.2	13.3	16.3
N	1.4	2.0	0.8	2.9	1.7	1.5
Si	0.6	1.3	1.1	1.0	1.4	1.5
O/C	0.11	0.17	0.15	0.22	0.16	0.20
N/C	0.02	0.02	0.01	0.04	0.02	0.02
Area (%)	Pellethane	Pell15.0	Pellethane	Pell15.0	Pellethane	Pell15.0
C-C	79.74	72.50	87.95	73.80	88.78	80.85
C-O	18.78	24.10	7.54	22.72	6.97	15.10
C=O	1.48	3.40	4.51	3.48	4.26	4.05

Since the 286.2 eV peak is indicative of the soft segment, and the small, broad tail near 288.4 - 289.4 eV is primarily related to the hard segment, their ratio represents the relative contribution from the soft and hard segments [22]. It was apparent that the

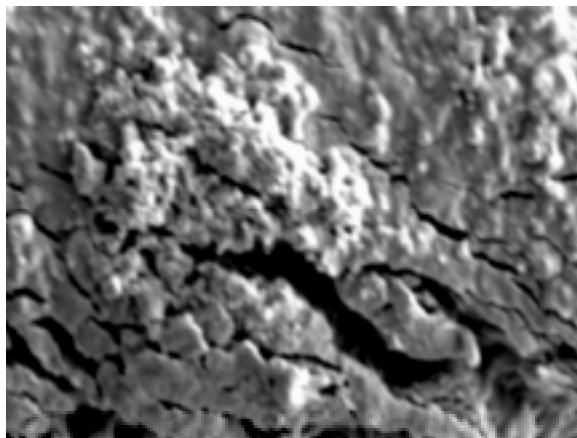
polyether soft segment was enriched at the surfaces of the control samples (Pellethane & Pell15.0). This was confirmed by the very small surface N/C atomic ratio observed.

A significant increase in the O/C ratio (more severe in Pellethane) was observed after the respective polyurethane samples were subjected to hydrogen peroxide degradation, indicating either oxidation of the surface [6, 22, 30] or rearrangement of the polar phases to the surface aqueous media. From the calculated percentages for the 286.2 eV (C-O) peak area tabulated in Table 6.5, a significant disappearance of ether from the surface was also noted, especially for Pellethane samples, when compared to their control. The same observations were made when samples were incubated in PBS. Here previous mechanical data showed very little change, therefore this must be mainly attributed to surface rearrangement to higher polarity.

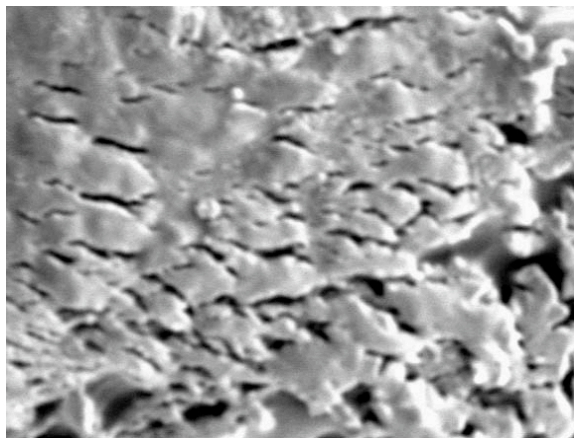
Thus it was concluded from the XPS results that rearrangement occurred at surfaces with probable degradation as well in the oxidized samples. This effect was generally more pronounced in Pellethane samples incubated in both hydrogen peroxide and PBS, because the hard segments are freer to rearrange.

6.4.5 Scanning electron microscopy

Significant surface degradation of Pellethane in both silver nitrate and hydrogen peroxide was seen within 8 weeks (Figure 6.12).



AgNO₃, x5000



AgNO₃, x5000

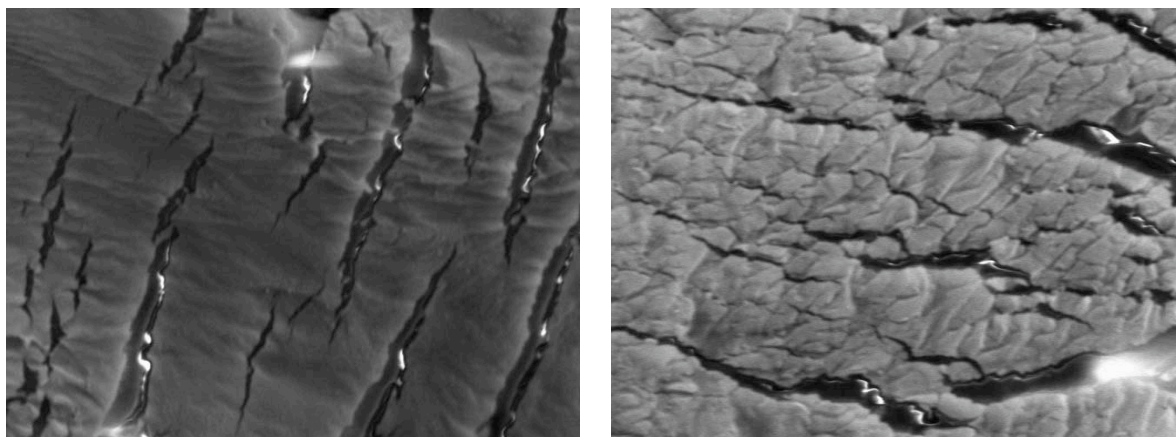
H₂O₂, x4000H₂O₂, x4000

Figure 6.12: Scanning electron micrographs for Pellethane showing severe surface degradation in the presence of silver nitrate and hydrogen peroxide after 8 weeks

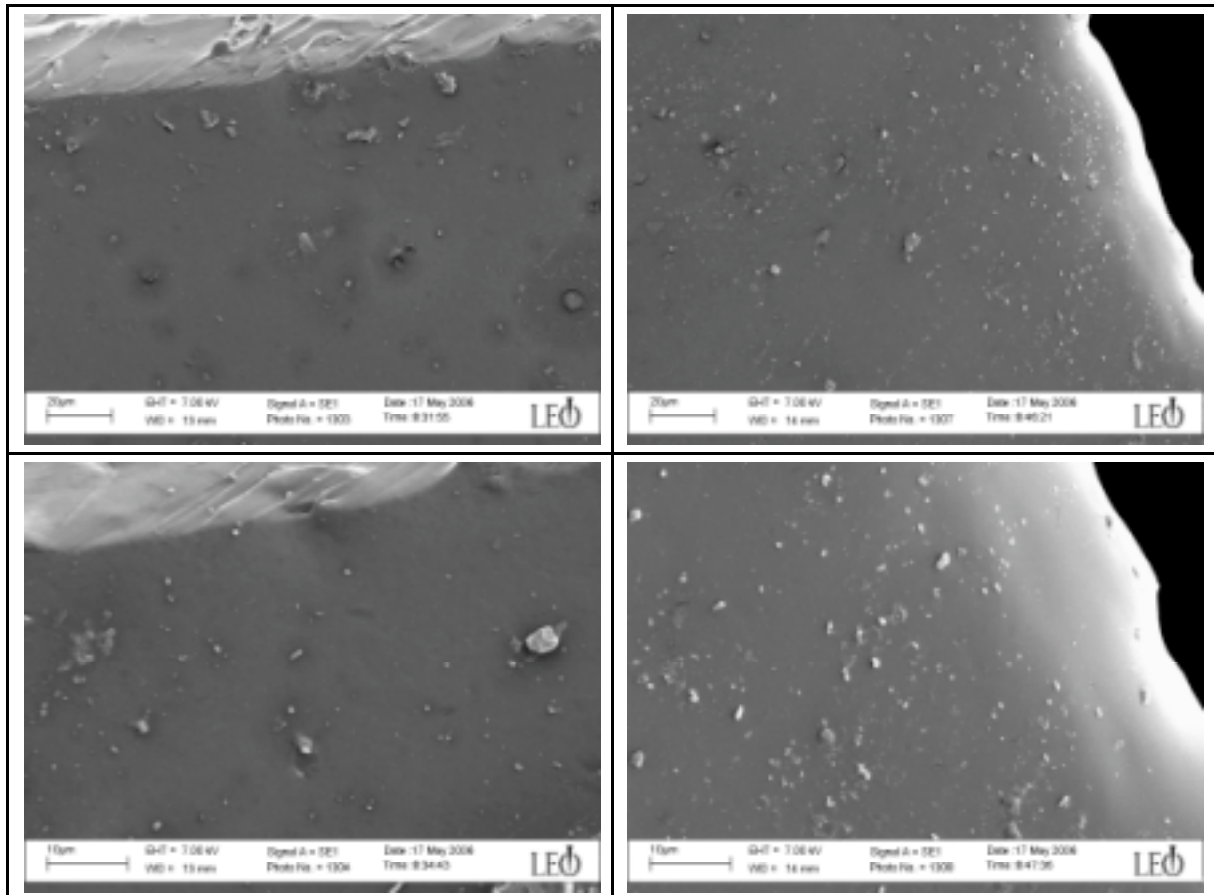
The cracks had rough, often “spiculated” walls, suggestive of a craze origin [31]. Severe cracking (deep cracks that have opened up) was especially observed in the Pellethane samples degraded in hydrogen peroxide.

Typical SEM images of Pellethane and Pell15.0 (non-degraded controls and samples incubated in the various media) are presented in Figure 6.13 at x2000 (above) and x5000 (below) magnifications, respectively.

The smooth surfaces of the control samples (a & b) are clearly evident at x2000 and at x5000 magnifications. The surface of the Pell15.0 sample (d) incubated in silver nitrate has a “wrinkled” appearance (only in a few cases was the onset of small cracks observed), while the surface of the Pellethane sample (c) shows severe surface degradation (formation of deep cracks) [31]. It is proposed that degradation of the Pell15.0 sample is mostly as a result of internal degradation of the hard segment, while the degradation of Pellethane is accelerated by rearrangement.

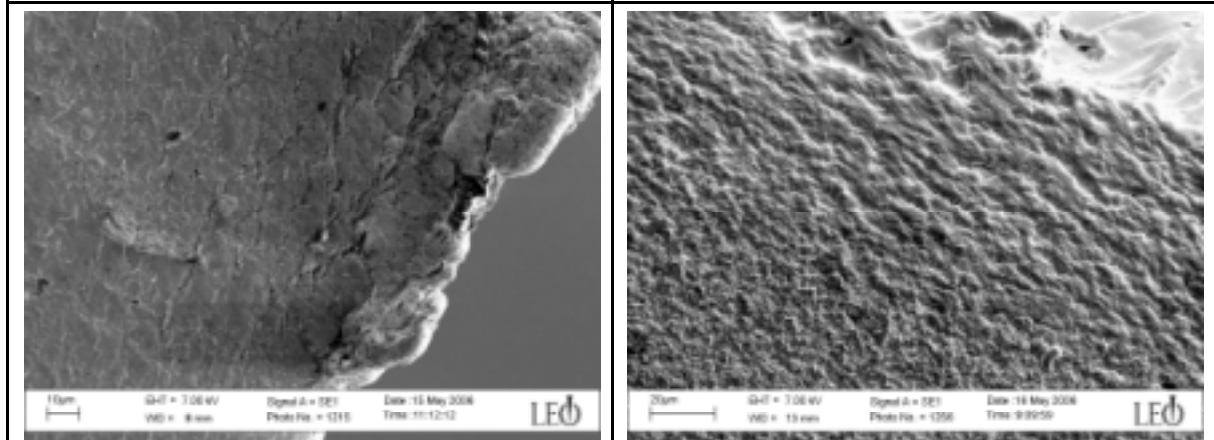
Hydrogen peroxide incubation resulted in the degradation of the Pellethane sample (e) with the very distinct appearance of shallow “mud” cracks [27, 31-33]. This is especially evident at the higher magnification (x5000). The Pell15.0 sample shows some degree of cracking and some pit formation. This could be a result of a leaching product [31], or possibly low molecular mass degradation products. The author suggests further that this is due to degradation-assisted rearrangement of the phases to give hydrophilic surfaces.

Visually no distinct difference could be detected between the Pellethane (g) and Pell15.0 (h) samples incubated in PBS, apart (possibly) from the onset of some “wrinkles” in the former. No cracks were observed in any of the samples incubated in PBS, which suggests that a necessary requirement for crack formation is both an oxidative/hydrolyses medium and rearrangement.



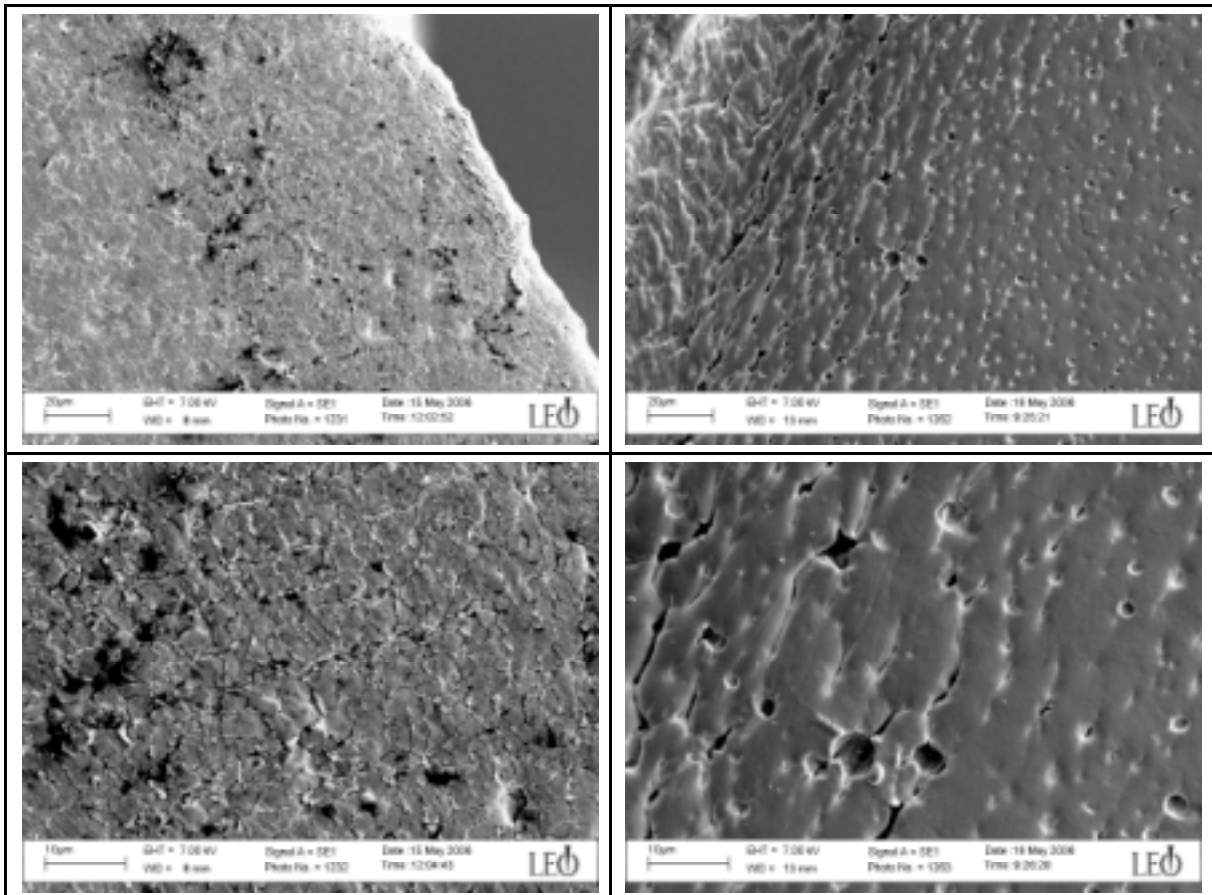
a) Pellethane (Control) x2000(above), x5000(below)

b) Pell15.0 (Control) x2000(above), x5000(below)



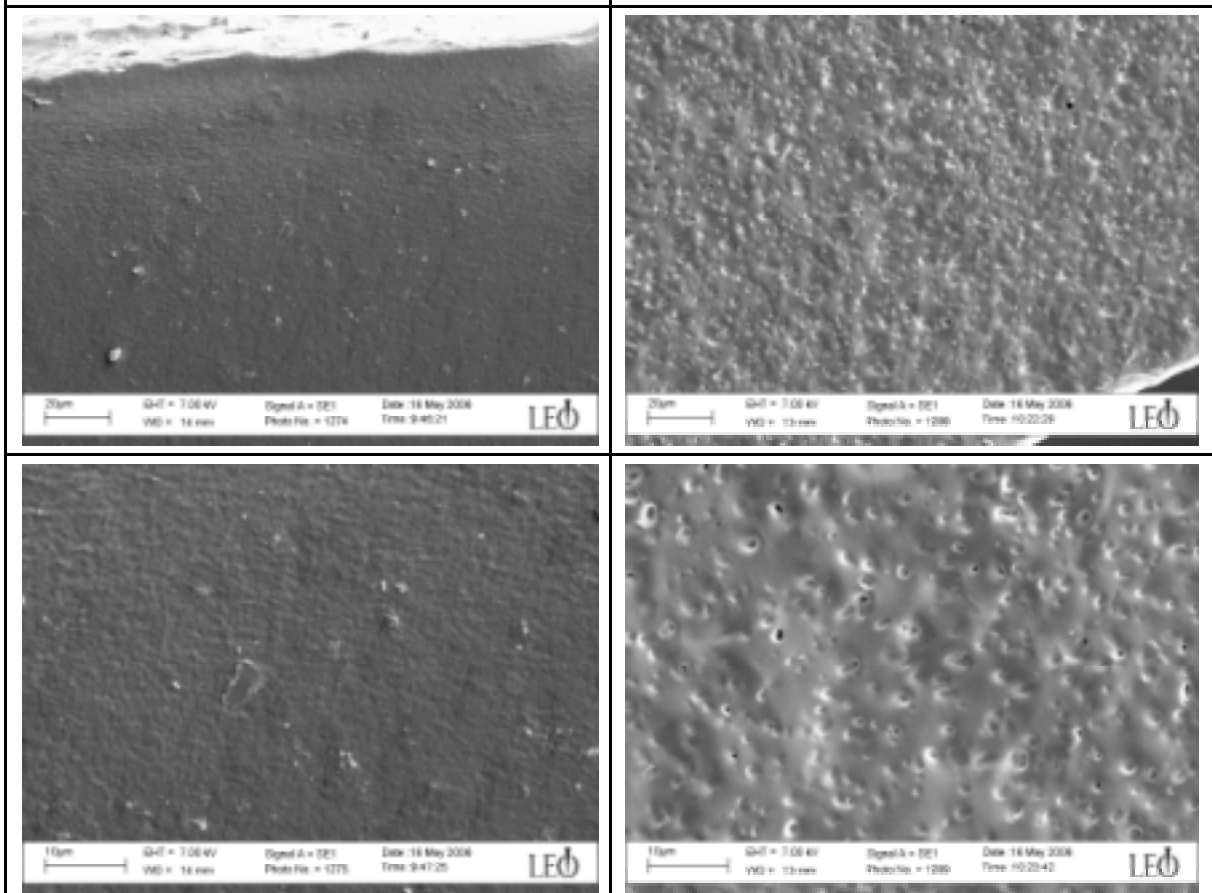
c) Pellethane (AgNO₃) x2000(above), x5000(below)

d) Pell15.0 (AgNO₃) x2000(above), x5000(below)



e) Pellethane (H₂O₂) x2000(above), x5000(below)

f) Pell15.0 (H₂O₂) x2000(above), x5000(below)



g) Pellethane (PBS) x2000(above), x5000(below)

h) Pell15.0 (PBS) x2000(above), x5000(below)

Figure 6.13: Scanning electron micrographs for Pellethane and Pell15.0, degraded and control samples, at x2000 and x5000 magnification

Figure 6.14 shows the average scores for the degraded Pellethane and Pell15.0 samples with the 95% confidence interval for the average, calculated from the scores given by the independent blinded observers.

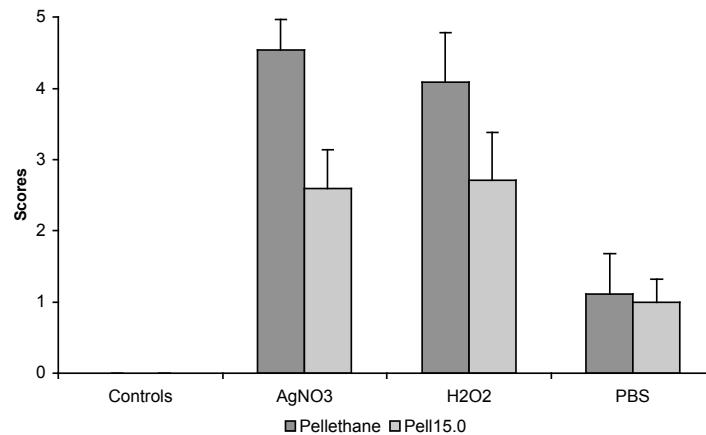


Figure 6.14: Scoring results \pm the 95% confidence interval of SEM images of degraded and control samples of Pellethane and Pell15.0

Significantly higher degradation was observed for the Pellethane sample degraded in silver nitrate ($p < 0.01$) and hydrogen peroxide ($p = 0.05$) when compared to the Pell15.0 samples. Although the difference between the Pellethane and Pell15.0 samples degraded in hydrogen peroxide is bordering on statistical significance on a 95% level there is a clear trend that Pell15.0 performed much better than Pellethane. No significant difference was observed between the Pellethane and Pell15.0 samples incubated in PBS. These results, and as presented in Figure 6.13, were verified using a non-parametric test method (bootstrap) and similar results were obtained.

The results suggest that rearrangement alone cannot form cracks, and that crosslinking of the hard phase restricts rearrangement. This implies that degradation of the hard phase enhances rearrangement (surface analysis) while there is also a contribution from the hard section peripheral and soft section oxidative degradation. Such degradation is essential to form surface cracking.

6.5 Conclusions

Degradation of both the Pellethane and the Pell15.0 samples was evident from their measured tensile properties (e.g. hysteresis and NRS) when compared to their respective controls. Pellethane and Pell15.0 samples degraded in silver nitrate, hydrogen peroxide and

PBS resulted in an increase in the hysteresis and NRS, although PBS had the least influence on the afore-mentioned mechanical properties. The hysteresis and NRS of Pell15.0 was better by at least 27.5% and 21.0%, respectively, when compared to Pellethane.

Chemically induced disruption (degradation) of Pellethane, incubated in silver nitrate and hydrogen peroxide, is clearly evident from the decrease in hard phase integrity (T_2). The opposite effect was observed for the Pell15.0 samples. It can be concluded that it is due to the restriction of chain movement (and thus melting) as a result of the imparted oxidative stable crosslinks.

FT-IR results confirmed the degradation of the “more vulnerable, less ordered” soft phase in both the Pellethane and Pell15.0 samples when compared to their respective controls. It can further be concluded from the FT-IR results that the formation of the new carbonyl containing peaks observed for both Pellethane (2 cases) and Pell15.0 (1 case) stems from competitive oxidation occurring in both the soft and hard phases.

XPS results confirmed the degradation of the surface ether soft phase in both Pellethane and Pell15.0 although this effect was more pronounced in the former, because the hard phases are freer to rearrange.

Significant surface degradation of Pellethane in both silver nitrate and hydrogen peroxide was seen within 8 weeks. The surface degradation was significantly higher for Pellethane when compared to Pell15.0, degraded in the above-mentioned solutions, although it was found not to be statistically significant for samples degraded in hydrogen peroxide, although there is a clear trend.

6.6 References

1. Cury, A., K. Stokes, P. Cahalan, and P. Slaikou, *Biostability considerations for implantable polyurethanes*. Life Support Syst., 1987. **5**(1): p. 25-39.
2. Stokes, K., A. Cury, and P. Urbanski, *Autooxidative degradation of implanted polyether polyurethane devices*. J. Biomater. Appl., 1987. **1**(4): p. 411-448.
3. Stokes, K., W. Berthelsen, and M. Davis, *Metal catalyzed oxidative degradation on implanted polyurethane devices*. ACS Division of Polymeric Materials: Science and Engineering, 1985. **6**: p. 159-169.
4. Cury, A., P. Slaikou, P. Cahalan, K. Stokes, and C. Hobot, *Factors and interactions affecting the performance of polyurethane elastomers in medical devices*. J. Biomater. Appl., 1988. **3**: p. 130-176.
5. Cury, A., P. Slaikou, P. Cahalan, and K. Stokes, *Medical applications of implantable polyurethanes: current issues*. Prog. Rub. & Plas. Tech., 1987. **3**(4): p. 24-37.
6. Takahara, A., A. Cury, R. Hergenrother, and S. Cooper, *Effect of soft segment chemistry on the biostability of segmented polyurethanes. I. In vitro oxidation*. J. Biomed. Mater. Res., 1991. **25**(3): p. 341-356.
7. Santerre, J., R. Labow, D. Duguay, D. Erfle, and G. Adams, *Biodegradation evaluation of polyether and polyester-urethanes with oxidative and hydrolytic enzymes*. J. Biomed. Mater. Res., 1994. **28**(10): p. 1187-1199.

8. Santerre, J., R. Labow, and G. Adams, *Enzyme-biomaterial interactions: effect of biosystems on degradation of polyurethanes*. J. Biomed. Mater. Res., 1993. **27**(1): p. 97-109.
9. Petrovic, Z., Z. Zavargo, J. Flynn, and W. Macknight, *Thermal degradation of segmented polyurethanes*. J. Appl. Polym. Sci., 1994. **51**: p. 1087-1095.
10. del Guerra, R., L. Lelli, C. Tonelli, T. Trombetta, M. Cascone, M. Taveri, P. Narducci, and P. Giusti, *In vitro biocompatibility of fluorinated polyurethanes*. J. Mater. Sci.: Mater. Med., 1994. **5**: p. 452-456.
11. Labow, R., D. Erfle, and J. Santerre, *Neutrophil-mediated degradation of segmented polyurethanes*. Biomaterials, 1995. **16**: p. 51-59.
12. Schubert, M., M. Wiggins, J. Anderson, and A. Hiltner, *Role of oxygen in biodegradation of poly(etherurethane urea) elastomers*. J. Biomed. Mater. Res., 1997. **34**(4): p. 519-530.
13. Guignot, C., N. Betz, B. Legendre, A. Le Moel, and N. Yagoubi, *Degradation of segmented poly(etherurethane) Tecoflex induced by electron beam irradiation: characterization and evaluation*. Nucl. Instr. and Meth. B, 2001. **185**: p. 100-107.
14. Martin, D., L. Poole-Warren, P. Gunatillake, S. McCarthy, G. Meis, and K. Schindhelm, *New methods for the assessment of in vitro and in vivo stress cracking in biomedical polyurethanes*. Biomaterials, 2001. **22**: p. 973-978.
15. Wu, L., B. You, D. Li, and F. Qian, *The in vitro and in vivo stability of poly(urethaneurea)s as biomedical materials*. Polym. Degrad. Stab., 2000. **70**: p. 65-69.
16. Salacinski, H., N. Tai, R. Carson, A. Edwards, G. Hamilton, and A. Seifalian, *In vitro stability of a novel compliant poly(carbonate-urea)urethane to oxidative and hydrolytic stress*. J. Biomed. Mater. Res., 2001. **59**: p. 207-218.
17. Tanzi, M., D. Mantovani, P. Petrini, R. Guidoin, and G. Laroche, *Chemical stability of polyether urethanes versus polycarbonate urethanes*. J. Biomed. Mater. Res., 1997. **36**(4): p. 550-559.
18. Thomas, V., T. Kumari, and M. Jayabalan, *In vitro studies on the effect of physical cross-linking on the biological performance of aliphatic poly(urethane urea) for blood contact applications*. Biomacromolecules, 2001. **2**: p. 588-596.
19. Tang, Y., R. Labow, and J. Santerre, *Enzyme induced biodegradation of polycarbonate-polyurethanes: dose dependence effect of cholesterol esterase*. Biomaterials, 2003. **24**: p. 2003-2011.
20. Salacinski, H., M. Odlyha, G. Hamilton, and A. Seifalian, *Thermo-mechanical analysis of a compliant poly(carbonate-urea)urethane after exposure to hydrolytic, oxidative, peroxidative and biological solutions*. Biomaterials, 2002. **23**: p. 2231-2240.
21. Labow, R., E. Meek, and J. Santerre, *Hydrolytic degradation of poly(carbonate)-urethanes by monocyte-derived macrophages*. Biomaterials, 2001. **22**: p. 3025-3033.
22. Hsu, S.-h. and T.-b. Huang, *The susceptibility of poly(ether)urethanes to enzymatic degradation after oxidative pretreatment*. Polym. Degr. & Stab., 2000. **67**: p. 171-178.
23. Ogawa, R., J. Watanabe, and K. Ishihara, *Domain-controlled polymer alloy composed of segmented polyurethane and phospholipid polymer for biomedical applications*. Sci. & Tech. of Advanced Materials, 2003. **20**: p. 1-8.
24. Hughes-Dillon, K. and L. Schroeder, *Stress cracking of polyurethanes by absorbed steroids*. Polym. Degr. & Stab., 1998. **60**: p. 11-20.
25. Yamada, S., S. Yaguchi, and K. Matsuda, *N-acylation of amides with acid anhydrides by way of dual activation using MgBr.OEt₂*. Tetrahedron Lett., 2002. **43**: p. 647-651.
26. Stokes, K., P. Urbanski, and J. Upton, *The in vivo auto-oxidation of polyether polyurethane by metal ions*. J. Biomater. Sci., Polym. Ed., 1990. **1**(3): p. 207-230.
27. Pinchuk, L., *A review of the biostability and carcinogenicity of polyurethanes in medicine and the new generation of 'biostable' polyurethanes*. J. Biomater. Sci., Polym. Ed., 1994. **6**(3): p. 225-267.
28. Lamba, N., K. Woodhouse, and S. Cooper, *Polyurethanes in Biomedical Applications*. 1998, Boca Raton: CRC Press.
29. Khan, I., N. Smith, E. Jones, D. Finch, and R. Cameron, *Analysis and evaluation of a biomedical polycarbonate urethane tested in an in vitro study and an ovine arthroplasty model. Part I: materials selection and evaluation*. Biomaterials, 2005. **26**: p. 621-631.

30. Simmons, A., J. Hyvarinen, R. Odell, D. Martin, P. Gunatillake, K. Noble, and L. Poole-Warren, *Long-term in vivo biostability of poly(dimethylsiloxane)/poly(hexamethylene oxide) mixed macrodiol-based polyurethane elastomers*. *Biomaterials*, 2004. **25**: p. 4887-4900.
31. Stokes, K., *Polyether polyurethanes: biostable or not?* *J. Biomater. Appl.*, 1988. **3**: p. 228-259.
32. Szycher, M., *Biostability of polyurethanes: A critical review*, in *Blood Compatible Materials and Devices*, C. Sharma, Editor. 1991, Technomic: Lancaster, PA. p. 33-85.
33. Coury, A., *Biostable Polymers as Durable Scaffolds for Tissue Engineered Vascular Prostheses.*, in *Tissue engineering of vascular prosthetic grafts*, Zilla P. and Greisler H., Editors. 1999, R.G. Landes: Texas. p. 469-480.

Chapter 7

Electrospinning of tubular constructs

Abstract

Electrospinning offers a method by which to produce structures suitable to mimic extracellular matrices, and form tissue-engineered scaffolds. This has become a key manufacturing method in the engineering of cardiovascular devices. Pellethane[®] 2363-80AE and the novel modified polyurethane, Pellm15.0 (Chapter 4) was used to study the electrospinning of tubular constructs. An ultraviolet light (UV) initiator, ω,ω -dimethoxy- ω -phenylacetophenone, was included in the Pellm15.0 solution. A suitable set-up was devised and the polymer successfully crosslinked, in situ, by a “reactive electrospinning” method, whereby the fibers are crosslinked during the electrospinning process. The fiber and wall thicknesses of the tubes manufactured using Pellethane were accurately controlled by changing the concentration of the polymer solution and spinning times. Tubular constructs ($n = 4$) with comparable fiber and wall thicknesses ($3.1 \pm 0.7 \mu\text{m}$ and $80.7 \pm 12.0 \mu\text{m}$) for Pellethane and ($3.3 \pm 1.1 \mu\text{m}$ and $78.1 \pm 9.0 \mu\text{m}$) for Pell15.0 were obtained respectively. The measured porosity for Pellethane (69.8% & 63.4%), determined by gravimetric and apparent volume methods, was however significantly higher than for Pell15.0 (44.7% & 40.0%). In conclusion, a novel “reactive electrospinning” technique was used to manufacture crosslinked tubular constructs with fiber and wall thicknesses comparable to those of scaffolds manufactured from Pellethane using a standard electrospinning technique.

7.1 Introduction

The design and manufacture of artificial matrices or scaffolds that mimic the supramolecular structure and biological functions of the extracellular matrix (ECM) is a pivotal issue in tissue engineering and the development of artificial organs [1].

The process of electrospinning has received much attention in biomedical engineering, especially over the last few years, because of the ability it offers to fabricate a wide variety of artificial extracellular matrixes and scaffolds [2] consisting of fibers ranging in thickness from several microns to 100 nm or less.

Electrospinning was therefore chosen as the method of choice for polyurethane processing in this study. Pellethane[®] 2363-80AE and Pellm15.0 were used to electrospin tubular constructs (ID = 1.6 mm). A set-up had first to be devised to initiate *in situ* crosslinking of Pellm15.0, while simultaneously electrospinning on a rotating/translating mandrel.

Constructs with similar fiber and wall thicknesses could be obtained by changing the polyurethane concentration and spinning times, respectively. The resulting porosities of the scaffolds could be determined using well-known techniques, including the Archimedes and apparent volume methods [3].

7.2 Polyurethane processing

The type of processing and processing conditions have a significant influence on the eventual chemical stability of the polyurethane-based prostheses. Processing is an important consideration, as residual stresses imparted during e.g. extrusion processing by inappropriate stretching could accelerate *in vivo* surface micro-fissuring [4]. A number of processing techniques (solvent casting, extrusion etc.) will briefly be discussed here, categorized according to the dimensionality of the resulting product.

Coatings and adhesives are defined as one-dimensional (1-D) processes because the most important dimension is usually the thickness of the respective coating or adhesive [5]. Coatings may be applied using solution-dip or spray-coating techniques (at room temperature) or hot-melt, fluidized bed and electrostatic powder coating (at elevated temperatures) or, alternatively, solvent coating techniques. Solvent casting is another example of 1-D processing.

Two-dimensional (2-D) fabrication processes include extrusion, laminations, and the production of fibers. During extrusion the polyurethane is forced through a die that shapes it into a long shape of constant cross section. Pacemaker leads are commonly manufactured by extrusion. Lamination techniques are used to produce composite

materials, which can be formed during extrusion or by forming the structure around a mandrel. Fibers can also be produced by melt and solvent spinning.

Three-dimensional (3-D) fabrication processes include sheet forming, vacuum forming, post forming, cold forming, weaving, knitting and machining [5]. Some of these processes are used to form polyurethanes into foams, tubing, balloons, and bladders. Non-porous tubing is formed by extrusion or solvent casting, in which the latter is used to e.g. produce anisotropic vascular prosthesis. Porous tubing, used as vascular grafts, is fabricated by electrospinning a polymer from solution onto a rotating/translating mandrel or by phase inversion and extraction techniques. Solvent casting methods have also been used for the processing of intra-aortic balloons [5].

Attention will now be focused on electrospinning and in the following section more background information will be given, followed by a summary of some achievements in applications in the medical industry to date.

7.3 Electrospinning

Electrospinning is not a new process; the application of a static electric field to move fluids is over 500 years old, with patents dating back to as early as the beginning of the 20th century [6].

Polymeric fibers ranging in thickness from 100 nm - 30 μm are produced, which is at least one or two orders of magnitude smaller than the ones obtained through conventional fiber production methods like melt or solution spinning [2]. It is therefore no wonder that electrospun materials have found wide application in the medical field, where they are used in the manufacturing of vascular grafts and prosthetic blood vessels.

The polymeric material is usually fed from a small reservoir (e.g. a syringe) through a capillary (often polyethylene or Teflon) with a conducting tip. This tip forms the one electrode and the target, which can be a mandrel or flat plate, forms the other electrode. When the high-voltage direct current (DC) supply is turned on, the electrode imparts an electric charge to the polymer solution and a jet is ejected from the suspended liquid meniscus (Taylor cone) at the capillary-end when the applied field strength overcomes the surface tension of the liquid [7].

Process parameters, such as the strength of the applied electric field, flow rate, polymer concentration, distance between the capillaries and the target have been found to influence the average fiber diameter, but these parameters are highly dependent on the polymer under investigation [2, 8-12].

Set-ups using one polymer solution or blends of polymer solutions are common practice. More recently however, electrospinning devices have been developed where two

or more polymer solutions have been electrospun simultaneously, in a side-by-side fashion [7].

Accomplishments in the electrospinning of medical devices, including materials and procedures, have been pronounced; especially achievements gained over the last 2 - 3 years. Some will briefly be discussed in the next section (see also Table F.1, Appendix F for a non-exhaustive list of the most recent advances in electrospinning).

7.4 Historical

A variety of natural and synthetic materials, each containing examples of degradable and non-degradable materials, have been electrospun into flat sheets or tubular scaffolds.

Flat sheets were spun mainly to investigate human biocompatibility [8, 13-18] for general wound dressing applications [17, 19-23] and, more specifically, facial [24], liver [25], neural [24], bone [26-29] and cardiac applications [30, 31], in which case the collecting set-ups were simple flat areas or rotating disks.

A number of different materials, both natural (collagen type 1, gelatin type B, alpha-elastin, tropo-elastin and chitosan) and synthetic (poly(caprolactone), poly(ethylene glycol), poly(lactide), poly(glycolic acid), poly(D,L-lactide-co-glycolide) and poly(ethylene oxide)), have been electrospun using different voltages (10 - 20 kV), flow rates (1 - 10 ml/h), average distance between electrodes (150 mm), and mainly using 1,1,1,3,3,3-hexafluoro-2-propanol (HFIP) as solvent, to obtain flat sheet structures with a wide range of fiber thicknesses (40 nm - 10 μ m). A number of different cells (e.g. human embryonic palatal mesenchymal, interstitial, endothelial and smooth muscle cells) were seeded onto these flat sheet structures and the attachment and proliferation of the cells were investigated.

In general, the scaffolds supported the attachment, proliferation and infiltration of the cells used in the respective studies [8, 13-18]. In one specific study [13] however, interstitial and endothelial cells did not infiltrate or attached to the electrospun scaffolds fabricated from poly(glycolic acid) and poly(lactide).

A number of authors have also electrospun flat sheet scaffolds for general use in wound-dressing applications [17, 19-23], while others have investigated their use in more specific applications, e.g. facial [24], liver [25], neural [24], bone formation [26-29] and cardiac [30, 31].

Silk, a natural and non-degradable material, has been used by some researchers [19, 20, 26] with great success in wound-healing applications, while the fabrication of degradable scaffolds has been extensively investigated using both natural (collagen type 1 and fibrinogen) [21, 22] and synthetic (e.g. poly(caprolactone), poly(D,L-lactide-co-glycolide) and poly(ethylene-b-lactide)) [17, 21-25, 27-31] polymers.

A wide range of process conditions and solvents has been used, depending on the specific polymer and its application. The flat sheets were again seeded with different cells (e.g. cardiac myocytes, smooth muscle and endothelial cells) and the attachment and proliferation studied.

The release of DNA [17], an antibiotic (Mefoxin) [23] and Ibuprofen from electrospun flat sheets [32, 33] has also been studied. A composite poly(lactide-co-glycolide)/DNA scaffold was fabricated for therapeutic application in gene delivery for tissue engineering [17]. The release of plasmid DNA was sustained over a period of 20 days, with maximum release occurring at 2 hours. Results indicated that DNA released directly from these electrospun scaffolds was indeed intact, capable of cellular transfection, and successfully encoded the protein β -galactosidase.

Kim et al. [23] demonstrated the successful incorporation and sustained release of an antibiotic (Mefoxin) from a electrospun poly(lactide-co-glycolide) scaffold without the loss of structure and bioactivity. The morphology and porosity of the electrospun flat sheet was found to be dependent on the drug concentration, which was attributed to the change in ionic strength of the polymer solution.

Alternative electrospinning techniques used to manufacture tubular scaffolds [1, 34-37], comprising one or more layers [1, 34] have been much more complicated, consisting of rotating and translating mandrels or even "side-by-side" spinning set-ups [37].

Mainly synthetic materials, degradable (e.g. poly(caprolactone) and poly(D,L-lactide-co-glycolide)) and non-degradable materials (e.g. poly(vinyl chloride and poly(ethylene oxide)) including non-degradable polyurethanes (Cardiomat 610 and Estane[®] 5750). In a selected case [1] the synthetic polymers were used in combination with natural polymers (e.g. collagen type 1 and gelatin).

Inoguchi et al. [35] fabricated vascular grafts using poly(L-lactide-co- ϵ -caprolactone) with an inner diameter of 2.5 mm and wall thicknesses ranging between 50 - 340 μ m in an effort to determine a correlation between wall thickness (controlled by spinning time) and mechanical response (e.g. compliance). The compliance increased with a decrease in wall thickness, approaching that of a native artery [35].

Vaz et al. [34] fabricated a bi-layered tubular scaffold composed of a stiff and oriented poly(lactide) outside fibrous layer and a pliable and randomly oriented poly(caprolactone) fibrous inner layer. Control over the level of fiber orientation of the different layers was achieved through the rotation speed of the collecting mandrel.

Simultaneous electrospinning of poly(vinyl chloride) and a polyurethane (Estane[®] 5750), in a "side-by-side" fashion, was also demonstrated [37]. The two solutions were placed in separate syringes, but in one syringe pump. The tips of the respective syringe needles were however connected to form one end of the electrode, thus mixing the

solutions just before it was electrospun. Fibers (0.1 - 5 μm) were obtained at a working distance of 150 mm and a voltage of 14 kV.

Kidoaki et al. [1] fabricated a bi-layered tubular construct composed of a thick polyurethane (Cardiomat 610) outer layer and a thin type 1 collagen inner layer as a “prototype scaffold of artificial grafts”. Cardiomat and collagen were dissolved in tetrahydrofuran and 1,1,1,3,3,3-hexafluoro-2-propanol (HFIP), respectively, and then spun at distances and voltages of 150 - 300 mm and 9 - 16 kV to produce fibers with thicknesses in the range of 0.2 - 2 μm .

7.5 Theoretical

The structure and architecture of scaffolds are crucial parameters in the design of cardiovascular prostheses as those features have a great influence on the healing response. The mechanical and biological functionality of the scaffolds are influenced by architectural parameters such as porosity, pore size, surface area to volume ratio, cross sectional area, strut/wall thickness and permeability [38]. A number of techniques can be used to evaluate and calculate these parameters, including theoretical assessment, scanning electron microscopy (SEM) analysis, flow and mercury porosimetry, gas pycnometry, adsorption and, more recently, micro computed tomography (CT) [3].

7.5.1 Determination of porosity by apparent volume method

In this method, scaffolds are weighed and the volumes (V_g) of the material obtained by dividing the mass by the material density. The apparent scaffold cube volume (V_a) on the other hand is calculated from its linear measurements (wall thickness and length), and the porosity is then calculated using Eq. 7.1 [3].

$$\text{Porosity} = \left(1 - V_g / V_a\right) \times 100\% \quad (7.1)$$

7.5.2 Determination of porosity by Archimedes method

In the gravimetric method, a scaffold is pre-weighed (M_{dry}), then soaked in water, under vacuum (to remove trapped air), then submerged under water (at ambient pressure) and weighed (M_{sub}). After the sample is removed from the water it is weighed again (M_{wet}) and the porosity then calculated according to Eq. 7.2 [3].

$$\text{Porosity} = \left(M_{\text{wet}} - M_{\text{dry}}\right) / \left(M_{\text{wet}} - M_{\text{sub}}\right) \quad (7.2)$$

7.6 Experimental

7.6.1 Materials

Pellethane[®] 2363-80AE (Pellethane) was obtained from Dow Chemicals (USA). Modified Pellethane (15%) was synthesized as described in Chapter 4 and dissolved in tetrahydrofuran (THF) (Merck, Cat: AB009731). ω,ω -Dimethoxy- ω -phenylacetophenone (DMPA) (Aldrich Cat: 19,611-8) was used as UV initiator in selected experiments.

7.6.2 Methods

7.6.2.1 Electrospinning set-up

The electrospinning apparatus (see Figure 7.1) consisted of a high-voltage power supply (maximum voltage potential of 35 kV), an infusion pump (Vial medical SE 400B), a syringe fitted with a stainless-steel blunt-ended 15G needle, and a circular mandrel (1.6-mm diameter) which was made to rotate and translate during fabrication of the grafts to ensure even deposition of fibers.

An ultraviolet light source (315 - 400 nm) was fixed at a distance of 500 mm directly above the rotating mandrel, to initiate the crosslinking reaction of Pell15.0 (Figure 7.1). Note that the syringe is actually orthogonal to the mandrel (current depiction is for clarity only).

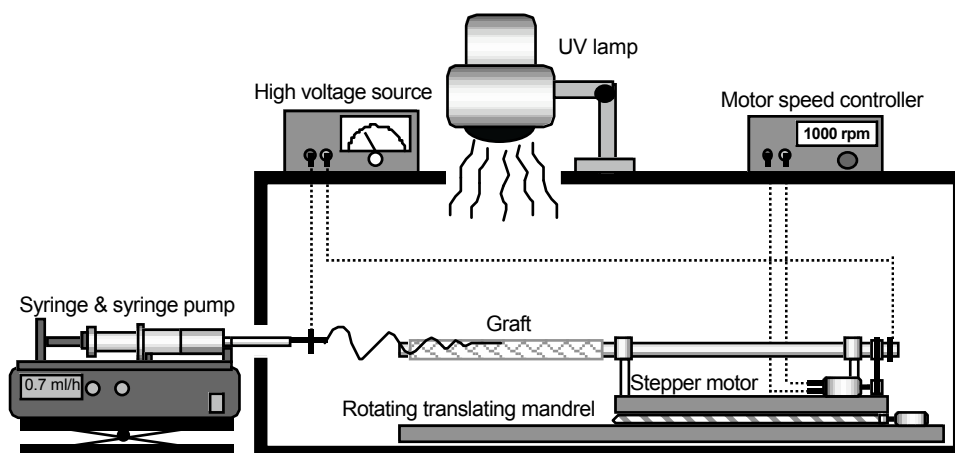


Figure 7.1: Illustration of electrospinning set-up

A 1-ml syringe was horizontally fixed on the infusion pump and the polymer solution pumped through a polyethylene tube and the needle. The polymer solution was electrostatically drawn from the tip of the needle by applying a high voltage between the rotating mandrel and the tip of the needle. The flow rate of the solution, applied voltage and distance between the needle tip and the mandrel were set to 0.7 ml/h, 15 kV and 11 and 15 cm for Pellethane and Pell15.0, respectively. The distance to the ground of the rotating mandrel and the tip of the nozzle were set at 185 mm.

7.6.2.2 Electrospinning procedure

Pellethane and Pellm15.0 were dissolved in THF to obtain solutions ranging in concentration from 16.5% to 18.0% (wt%). DMPA (2.0 wt%) was pre-dissolved in THF and then added to the Pell15.0 solution to obtain a final polymer concentration of 18.0% (wt%).

The polyethylene tubing was primed and the syringe then completely filled with polymer solution. The distance between the tip of the nozzle and the ground was then set to 185 mm. The distance between the nozzle tip and mandrel was then set to either 110 mm (Pellethane) or 150 mm (Pell15.0). The ultraviolet light, syringe pump and rotating/translating mandrel were then switched on. The high-voltage power supply was switched on last and carefully set to the desired setting (15 kV). The wall thickness was achieved by spinning for times ranging between 5 - 30 min.

The tubular constructs (40 mm in length) were then left in ethanol for approximately 1 - 2 min to swell, which allowed their successful removal from the mandrel. They were then dried in vacuo for 24 h at room temperature and analyzed.

Test pieces were cut off the electrospun Pellethane (control) and Pell15.0 grafts and placed in 50 ml of tetrahydrofuran to test whether crosslinking had been achieved.

7.6.2.3 Scanning electron microscopy

A macroscopic evaluation of the electrospun tubes was conducted using a scanning electron microscope (SEM) (Yeol, JSM 5200). Test pieces were cut with a sharp blade, mounted on aluminum stubs, sputter coated with gold-palladium (AuPd) and viewed in the SEM at an accelerating voltage of 25 kV.

7.6.2.4 Architectural and structural evaluation

The concentricity along the length of the tubes was inspected using a light microscope (Leica, MZ 75). Two pieces (3 mm in length) were then cut off on both ends and used to determine the average fiber and wall thicknesses, respectively, using SEM analyses. Three areas were randomly selected on both end pieces for fiber thickness determination while the other two pieces were used, as a whole, to determine the wall thickness of the respective grafts.

The SEM images were analyzed using ImageJ (v1.36) software. At least 300 counts were made per tube and the average fiber thickness calculated, while the wall thickness was measured on at least 30 places on the circumference of the tube, at both ends.

7.6.2.5 Porosity determination

Two non-destructive methods (a gravimetric and a volume method) were used to determine the porosity of the scaffolds.

(A) Archimedes method

The dry mass (M_{dry}) of the tube ($n = 4$) was recorded. It was then placed in a small test tube filled with water, and the entrapped air removed under vacuum. The tube was removed from the test tube and placed in water, and the submerged mass (M_{sub}) recorded (Figure 7.2). It was subsequently taken out of the water, quickly dab-dried and weighed (M_{wet}). The measured values were used to compute the porosity (Eq. 7.2).

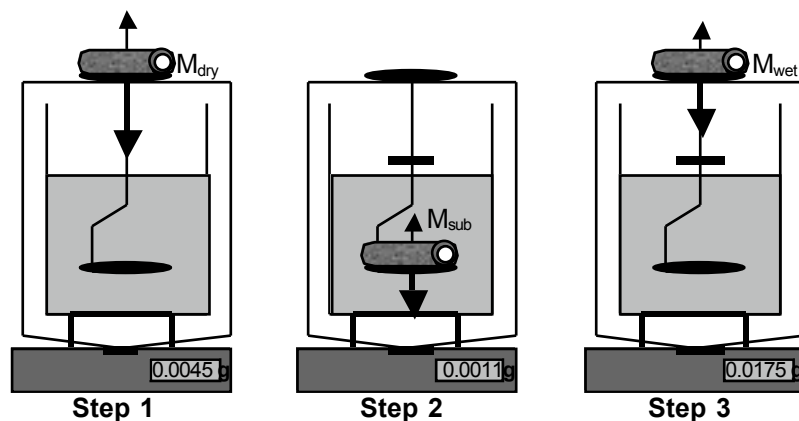


Figure 7.2: Illustration of gravimetric method used for porosity determination of electrospun grafts

(B) Apparent volume method

The length and diameter of each tube ($n = 4$) were recorded and used with the average fiber and wall thickness (obtained as described in §7.3.2.4) to calculate the volume of the polymer scaffold (V_g) and the apparent scaffold cube volume (V_a). Eq. 7.1 was used to calculate the porosity.

7.7 Results and discussion

Pellethane and Pellm15.0 were successfully electrospun on a 1.6-mm rotating/translating mandrel. Tubes, at least 35 - 40 mm in length, and of even concentricity, were obtained. The control samples of Pellethane immediately dissolved when placed in 50 ml THF, while the one manufactured from Pell15.0 only swelled slightly, indicating successful crosslinking.

Pellm15.0 was thus successfully crosslinked *in situ* by a “reactive electrospinning” technique. To the best of the authors’ knowledge this is the first time that a polyurethane material has ever been electrospun in such a manner, to date.

7.7.1 Fiber and wall thickness

It was found possible to electrospin Pellm15.0 at a polymer concentration of 18.0% (w/w) and an average fiber thickness of $3.3 \pm 1.1 \mu\text{m}$ ($n = 4$) was obtained. A typical scanning electron microscope image, showing fiber thickness and orientation, is presented in Figure 7.3. A fairly even fiber thickness distribution was obtained.

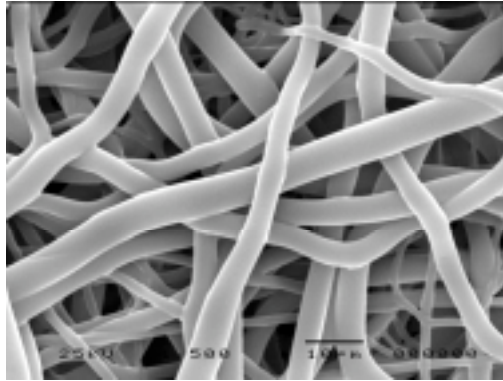


Figure 7.3: SEM (x1500) analysis of outer wall of electrospun Pell15.0

Pellethane at a concentration of 18.0% resulted in a much larger average fiber thickness when compared to Pell15.0. The fiber thickness could however be controlled, by changing the polymer concentration, as is illustrated in Figure 7.4, with the exact values tabulated in Table 7.2

Table 7.2: Change in fiber thickness of Pellethane with change in polymer concentration

Concentration (%)	18.00%	17.00%	16.65%	16.58%	16.50%	16.00%
Fiber thickness (μm)	7.9 ± 4.0	7.4 ± 3.6	3.7 ± 1.2	3.1 ± 0.7	2.8 ± 0.9	1.9 ± 0.8

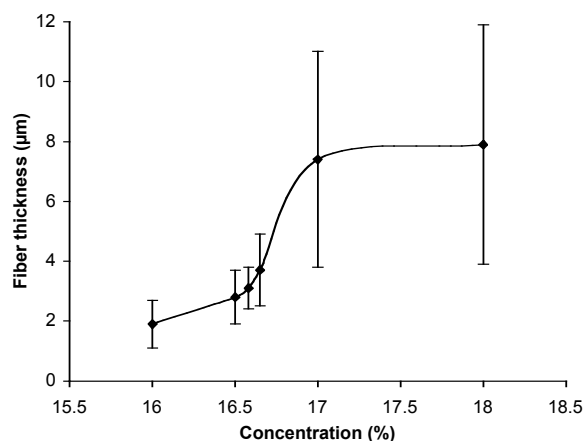


Figure 7.4: Change in fiber thickness with change in Pellethane concentration

At the higher Pellethane concentrations (>17.0%) thicker fibers were obtained with much wider fiber thickness distributions when compared to fibers obtained from lower concentrations (<16.6%). Similar nonlinear increases in fiber thickness and distributions with an increase in polymer concentration, using different polymers (e.g. poly(L-lactide-co- ϵ -caprolactone and Gelatin) and solvents (e.g. acetone and HFIP), have been reported [8, 12, 13, 31, 39].

A Pellethane concentration of 16.58% (w/w) resulted in fibers with a comparable average fiber thickness and standard deviation ($3.1 \pm 0.7 \mu\text{m}$) (Figure 7.4) to that of Pell15.0.

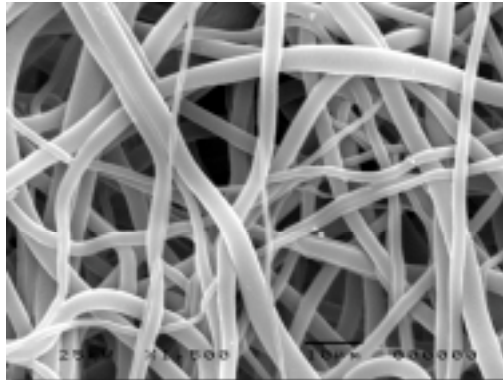


Figure 7.5: SEM (x1500) analysis of outer wall of Pellethane

A visual inspection of the SEM pictures obtained indicated that the tubes obtained from Pell15.0 might be more densely packed (i.e. lower porosity) compared to the tubes obtained from Pellethane (Figure 7.5). Porosity calculations confirmed this initial qualitative observation, and will be discussed further in §7.4.2.

Concentric tubes were obtained using Pellethane and Pell15.0. See Figure 7.6a for a typical result.

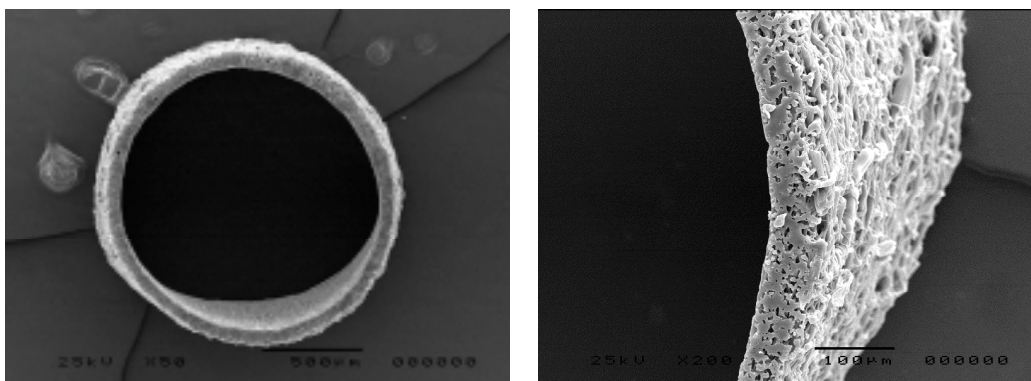


Figure 7.6(a)&(b): SEM analysis showing (a) concentricity (x50) of the tube and (b) part of Pell15.0 tube wall (x150)

Pell15.0, electrospun for 30 min, resulted in tubes ($n = 4$) with an average wall thickness of $78.05 \pm 9.0 \mu\text{m}$ (Figure 7.6b).

The thickness of the wall of the tubes electrospun using Pellethane was found to be very sensitive to the time of spinning. Tubes with much thicker walls compared to tubes electrospun using Pell15.0 were obtained at a spinning time of 6.5 min (Table 7.3).

Table 7.3: Change in wall thickness of Pellethane with spinning time

Time (min)	6.5 min	5.5 min	5.0 min
Wall thickness (μm)	125.1 ± 13.8	83.3 ± 16.3	80.7 ± 12.0

Tubes electrospun for 5 min had wall thicknesses of $80.7 \pm 12.0 \mu\text{m}$ (Figure 7.7), which was comparable to those obtained using Pell15.0. See Table 7.4 for a summary of the fiber and wall thicknesses for grafts ($n \geq 4$) electrospun using Pellethane and Pell15.0, respectively.

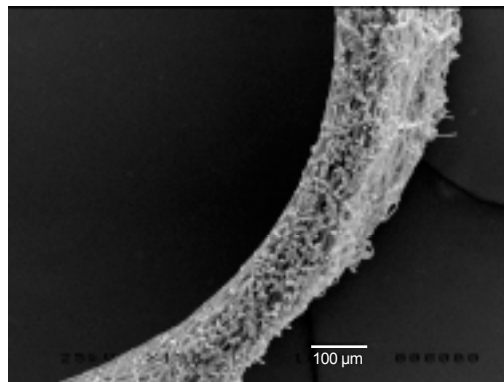


Figure 7.7: SEM ($\times 150$) analysis of wall cross section of electrospun Pellethane

Tubes with very similar fiber and wall thicknesses were obtained. The fairly high standard deviation in wall thickness calculated for the tubes electrospun using Pellethane can be mainly attributed to the sensitivity to spinning times, and is thus a result of slight tube-to-tube variation.

Table 7.4: Summary of fiber and wall thicknesses of tubular scaffolds electrospun from Pellethane and Pell15.0

	Pellethane	Pell15.0
Fiber thickness (μm)	3.1 ± 0.7	3.3 ± 1.1
Wall thickness (μm)	80.7 ± 12.0	78.1 ± 9.0

7.7.2 Porosity evaluation

The results obtained from the two methods used to determine the porosities of the electrospun constructs, namely Archimedes and apparent volume, compared reasonably well. The tubes electrospun using Pell15.0 had a significantly lower porosity than the ones manufactured using Pellethane (Table 7.5).

Table 7.5: Summary of measured and calculated porosities of electrospun constructs

	Pellethane	Pell15.0
Archimedes (%)	69.8	44.7
Apparent volume (%)	63.4	40.0

The difference in porosity between the electrospun Pellethane and Pell15.0 constructs can be explained by the dielectric properties of Pell15.0. These are different to Pellethane as a result of the introduction of the pendent groups. Secondly, the addition of DMPA in the Pellm15.0 solution could also slightly change the viscosity and surface tension of the solution [23], while the resulting change in conductivity (presence of the ionized DMPA molecules) will change the charge density of the jet, resulting in changes in the fibrous morphology [23].

7.8 Conclusions

Pellm15.0 could be successfully crosslinked by a “reactive electrospinning” technique. The concentration and spinning time of Pellethane could be used to control the fiber and wall thicknesses very accurately. Tubular constructs (1.6 mm ID) with comparable wall and fiber thicknesses could be obtained, but the porosity of the Pellethane tubes were found to be much higher compared to the tubes electrospun using Pell15.0, most probably due to differences in dielectric properties of the polyurethanes and ionic strength of the solutions.

7.9 References

1. Kidoaki, S., I. Kwon, and K. Matsuda, *Mesoscopic spatial designs of nano- and microfiber meshes for tissue-engineering matrix and scaffold based on newly devised multilayering and mixing electrospinning techniques*. *Biomaterials*, 2005. **26**: p. 37-46.
2. Srinivasan, G. and D. Reneker, *Structure and morphology of small-diameter electrospun aramid fibers*. *Polym. Int.*, 1995. **36**: p. 195-201.
3. Ho, S. and D. Hutmacher, *A comparison of micro CT with other techniques used in the characterization of scaffolds*. *Biomaterials*, 2005. **27**: p. 1362-1376.
4. Szycher, M., *Biostability of polyurethanes: A critical review*, in *Blood Compatible Materials and Devices*, C. Sharma, Editor. 1991, Technomic: Lancaster, PA. p. 33-85.

5. Lamba, N., K. Woodhouse, and S. Cooper, *Polyurethanes in Biomedical Applications*. 1998, Boca Raton: CRC Press.
6. Pedicini, A. and R. Farris, *Mechanical behaviour of electrospun polyurethane*. *Polymer*, 2003. **44**: p. 6857-6862.
7. Taylor, G., *Disintegration of water drops in electric field*. *Proc. R. Soc. London, Ser A*, 1964. **280**: p. 383.
8. Li, M., M. Mondrinos, M. Gandhi, F. Ko, A. Weiss, and P. Leikes, *Electrospun protein fibers as matrices for tissue engineering*. *Biomaterials*, 2005. **26**: p. 5999-6008.
9. Doshi, J. and D. Reneker, *Electrospinning process and applications of electrospun fibers*. *J. Electrostatics*, 1995. **35**: p. 151-160.
10. Fong, H., I. Chun, and H. Reneker, *Beaded nanofibers formed during electrospinning*. *Polymer*, 1999. **40**: p. 4585-4592.
11. Deitzel, J., J. Kleinmeyer, J. Hirvonen, and N. Tan, *Controlled deposition of electrospun poly(ethylene oxide) fibers*. *Polymer*, 2001. **42**: p. 8163-8170.
12. Demir, M., I. Yilgor, E. Yilgor, and B. Erman, *Electrospinning of polyurethane fibers*. *Polymer*, 2002. **43**: p. 3303-3309.
13. Telemeco, T., C. Ayres, G. Bowlin, G. Wnek, E. Boland, N. Cohen, C. Baumgartner, J. Mathews, and D. Simpson, *Regulation of cellular infiltration into tissue engineering scaffolds composed of submicron diameter fibrils produced by electrospinning*. *Acta Biomater.*, 2005. **1**: p. 377-385.
14. Bhattarai, N., D. Edmondson, O. Veiseh, F. Matsen, and M. Zhang, *Electrospun chitosan-based nanofibers and their cellular compatibility*. *Biomaterials*, 2005. **26**: p. 6176-6184.
15. Shin, N., O. Ishii, T. Sueda, and J. Vacanti, *Contractile cardiac grafts using nanofibrous mesh*. *Biomaterials*, 2004. **25**: p. 3717-3723.
16. Badami, A., M. Kreke, M. Thompson, J. Riffle, and A. Goldstein, *Effect of fiber diameter on spreading, proliferation, and differentiation of osteoblastic cells on electrospun poly(lactic acid) substrates*. *Biomaterials*, 2006. **27**: p. 596-606.
17. Luu, Y., K. Kim, B. Hsiao, B. Chu, and M. Hadjiargyrou, *Development of a nanostructured DNA delivery scaffold via electrospinning of PLGA and PLA-PEG block copolymers*. *J. Control. Release*, 2003. **89**: p. 341-353.
18. Min, B.-M., Y. You, J.-M. Kim, S. Lee, and W. Park, *Formation of nanostructured poly(lactic-co-glycolic acid)/chitin matrix and its cellular response to normal human keratinocytes and fibroblasts*. *Carboh. Polym.*, 2004. **57**: p. 285-292.
19. Min, B.-M., L. Jeong, Y. Nam, J.-M. Kim, J. Kim, and W. Park, *Formation of silk fibroin matrices with different texture and its cellular response to normal human keratinocytes*. *Int. J. Biol. Macromol.*, 2004. **34**: p. 223-230.
20. Min, B.-M., G. Lee, S. Kim, Y. Nam, T. Lee, and W. Park, *Electrospinning of silk fibroin nanofibers and its effect on the adhesion and spreading of normal human keratinocytes and fibroblasts in vitro*. *Biomaterials*, 2004. **25**: p. 1289-1297.
21. Rho, K., L. Jeong, G. Lee, B.-M. Seo, Y. Park, S.-D. Hong, S. Roh, J. Cho, W. Park, and B.-M. Min, *Electrospinning of collagen nanofibers: Effects on the behaviour of normal human keratinocytes and early-stage wound healing*. *Biomaterials*, 2006. **27**: p. 1452-1461.
22. McManus, M., E. Boland, H. Koo, C. Barnes, K. Pawlowski, G. Wnek, D. Simpson, and G. Bowlin, *Mechanical properties of electrospun fibrinogen structures*. *Acta Biomater.*, 2006. **2**: p. 19-28.
23. Kim, K., Y. Luu, C. Chang, D. Fang, B. Hsiao, B. Chu, and M. Hadjiargyrou, *Incorporation and controlled release of a hydrophilic antibiotic using poly(lactide-co-glycolide)-based electrospun nanofibrous scaffolds*. *J. Control. Release*, 2004. **98**: p. 47-56.
24. Lee, Y., J. Lee, I.-G. An, C. Kim, D. Lee, Y. Lee, and J.-D. Nam, *Electrospun dual-porosity structure and biodegradation morphology of Montmorillonite reinforced PLLA nanocomposite scaffolds*. *Biomaterials*, 2005. **26**: p. 3165-3172.
25. Chua, K.-N., W.-S. Lim, P. Zhang, H. Lu, J. Wen, S. Ramakrishna, K. Leong, and H.-Q. Mao, *Stable immobilization of rat hepatocyte spheroids on galactosylated nanofiber scaffold*. *Biomaterials*, 2005. **26**: p. 2537-2547.

26. Li, C., C. Vepari, H.-J. Jin, H.-J. Kim, and D. Kaplan, *Electrospun silk-BMP-2 scaffolds for bone tissue engineering*. *Biomaterials*, 2006. **27**: p. 3115-3124.
27. Yoshimoto, H., Y. Shin, H. Terai, and J. Vacanti, *A biodegradable nanofiber scaffold by electrospinning and its potential for bone tissue engineering*. *Biomaterials*, 2003. **24**: p. 2077-2082.
28. Li, W.-J., R. Tuli, C. Okafor, A. Derfoul, K. Danielson, D. Hall, and R. Tuan, *A three-dimensional nanofibrous scaffold for cartilage tissue engineering using human mesenchymal stem cells*. *Biomaterials*, 2005. **26**: p. 599-609.
29. Riboldi, S., M. Sampaolesi, P. Neuenschwander, G. Cossu, and S. Mantero, *Electrospun degradable polyesterurethane membranes: potential scaffolds for skeletal muscle tissue engineering*. *Biomaterials*, 2005. **26**: p. 4606-4615.
30. Zong, X., H. Bien, C.-Y. Chung, L. Yin, D. Fang, B. Hsiao, B. Chu, and E. Entcheva, *Electrospun fine-textured scaffolds for heart tissue constructs*. *Biomaterials*, 2005. **26**: p. 5330-5338.
31. Mo, X., C. Xu, M. Kotakie, and S. Ramakrishna, *Electrospun P(LLA-CL) nanofiber: a biomimetic extracellular matrix for smooth muscle cell and endothelial cell proliferation*. *Biomaterials*, 2004. **25**: p. 1883-1890.
32. Nair, L.S., S. Bhattacharyya, and C.T. Laurencin, *Development of novel tissue engineering scaffolds via electrospinning*. *Expert. Opin. Biol. Ther.*, 2004. **4**(5): p. 659-668.
33. Jiang, H., D. Fang, B. Hsiao, B. Chu, and W. Chen, *Preparation and characterization of ibuprofen-loaded poly(lactide-co-glycolide)/poly(ethylene glycol)-g-chitosan electrospun membranes*. *J. Biomater. Sci. Polym. Ed.*, 2004. **15**(3): p. 279-296.
34. Vaz, C., S. Tuijl, C. Bouten, and F. Baaijens, *Design of scaffolds for blood vessel tissue engineering using a multi-layering electrospinning technique*. *Acta Biomater.*, 2005. **1**: p. 575-585.
35. Inoguchi, H., I. Kwon, E. Inoue, K. Takamizawa, Y. Maehara, and K. Matsuda, *Mechanical response of compliant electrospun poly(L-lactide-co-e-caprolactone) small-diameter vascular grafts*. *Biomaterials*, 2006. **27**: p. 1470-1478.
36. Stitzel, J., J. Liu, S. Lee, M. Komura, J. Berry, S. Soker, G. Lim, M. Van Dyke, R. Czerw, J. Yoo, and A. Atala, *Controlled fabrication of biological vascular substitute*. *Biomaterials*, 2006. **27**: p. 1088-1094.
37. Gupta, P. and G. Wilkes, *Some investigations on the fiber formation by utilizing a side-by-side bicomponent electrospinning approach*. *Polymer*, 2003. **44**: p. 6353-6359.
38. Lin, A., T. Barrows, S. Cartmell, and R. Guldberg, *Microarchitecture and mechanical characterization of oriented porous polymer scaffolds*. *Biomaterials*, 2003. **24**: p. 481-489.
39. Deitzel, J., J. Kleinmeyer, D. Harris, and N. Tan, *The effect of processing variables on the morphology of electrospun nanofibers*. *Polymer*, 2001. **42**: p. 261-272.

Chapter 8

Conclusions and recommendations for future research

8.1 Introduction

The main goal of this project was to chemically modify existing medical grade polyurethanes using functional groups capable of undergoing crosslinking reactions, in order to improve their chemical stability and mechanical properties. A model compound, with the same hard segment structure of an academic standard polyurethane (Pellethane[®] 2363-80AE), was first used to find a suitable pendant group, and then to optimize the chemistry. The process variables involved in the modification and crosslinking reactions of the polyurethanes were optimized and the chemical stability evaluated in an *in vitro* degradation assay. Porous tubular constructs were subsequently successfully electrospun and crosslinked.

8.2 Conclusions

There were seven major objectives, as set out in Chapter 1, and to which the following conclusions were drawn.

8.2.1 Background and theoretical considerations of polyurethanes as biomaterial

After carrying out a literature survey of polyurethanes as biomaterial the following were found:

- Thermoplastic polyurethanes offer a great variety in terms of chemical and physical properties and are therefore attractive candidate biomaterials.
- Polyurethanes have however not yet demonstrated long-term biostability, and they also suffer from large energy losses (hysteresis) when subjected to continuous cyclic loading, due to the weak nature of virtual crosslinking.

8.2.2 Potential modification of the carbamate nitrogen with an acyl chloride

- The carbamate nitrogen of polyurethanes is a weak nucleophile. The lone electron pair is compromised by back donation into the aromatic p system and because of delocalization into the carbonyl.
- Acyl chlorides of the type R(CO)X (where X is a leaving group) are very reactive towards nucleophilic substitution.

The following model compound was proposed, with which to study the proposed reaction between the carbamate nitrogen and an acyl chloride

8.2.3 Model compound synthesis and optimization of acylation chemistry

- A urethane model compound, based on the same hard segment structure as Pellethane[®] 2363-80AE, was successfully synthesized, purified and characterized.
- Acylation of the model compound with hexanoyl chloride was achieved by either nucleophilic or electrophilic enhancement. Higher conversions were obtained using the former.
- Characterization of the resulting product showed successful acylation at the proposed reaction site (the carbamate nitrogen).
- The success of hexanoyl chloride coupling could be emulated with 4-pentenoyl chloride, thereby introducing an unsaturated C=C bond for potential future crosslinking.
- Although the coupling could be achieved by either nucleophilic or electrophilic enhancement, the former was again found to be the more effective method.
- The formation of the desired acylated product was confirmed by spectroscopic analyses.

8.2.4 Modification of existing polyurethanes

- Pellethane was purified (using ethanol at room temperature) and then successfully modified with 4-pentenoyl chloride.
- The chemistry was successfully transferred from the model compound to a medical grade polyurethane.
- A maximum degree of modification of 20.0% was obtained. It was also found possible to accurately ($R^2 = 0.99$) and reproducibly control the degree of

modification between 4.5% to 20% by changing the sodium hydride and 4-pentenoyl chloride concentrations, respectively.

- PurSil® 35-80A, a second medical grade polyurethane, with a different chemical structure and stoichiometry to that of Pellethane, was also successfully modified with 4-pentenoyl chloride.
- The degree of modification was accurately ($R^2 = 0.99$) controlled between 11.5% and 18.5% (maximum) by changing the sodium hydride and 4-pentenoyl chloride concentrations, respectively.

8.2.5 Optimization of the degree of modification and crosslinking

- Successful crosslinking of two novel modified polyurethanes (so-called Pellx and Purx) was achieved using an ultraviolet light (UV) source, a heat source (120 °C) and gamma irradiation (only UV was investigated as method of crosslinking for Purx).
- The swelling indices, used to calculate the molecular weight between crosslinks, were used to optimize the initiator concentrations used in the crosslinking experiments.
- The lowest swelling indices, i.e. lowest molecular weight between crosslinks, were obtained for Pell15.0 and Pur18.5, respectively.
- The best mechanical properties (lowest hysteresis and creep) were also obtained for Pell15.0 and Pur18.5, with respective improvements of up to 42.5% in hysteresis and 44.0% in creep for Pell15.0.
- The use of crosslinking enhancing monomers (e.g. MbA) resulted in lower swelling index values, but had a detrimental effect on the hysteresis due to long linking groups (bridges) and even more disruption of the hydrogen bonding in the hard phase.

8.2.6 In vitro chemical stability assay

- Degradation of both Pellethane and Pell15.0 was evident from the measured and determined mechanical (e.g. tensile and dynamic mechanical analysis) and chemical properties (Fourier infrared spectroscopy, X-ray photoemission spectroscopy and environmental scanning electron microscopy).
- The hysteresis and non-recovered strain of Pell15.0 was better by at least 27.5% and 21.0%, respectively, when compared to Pellethane.

- It is concluded that Pell15.0 retained hard phase integrity due to the oxidative stable crosslinks when compared to Pellethane.
- Degradation of the “more vulnerable, less ordered” soft phases of Pellethane and Pell15.0 was confirmed by Fourier-transform infrared spectroscopy and X-ray photoemission spectroscopy.
- Significant surface degradation of Pellethane incubated in silver nitrate and hydrogen peroxide was confirmed by environmental scanning electron microscopy. Less surface degradation was observed for Pell15.0 in both the above-mentioned degradation media, and significantly so lower in silver nitrate.

8.2.7 Manufacturing of tubular constructs

- Pellm15.0 was successfully crosslinked by a “reactive electrospinning” technique.
- The concentration and spinning time of Pellethane was used to control the fiber and wall thicknesses very accurately.
- Tubular constructs (1.6 mm ID) with comparable wall and fiber thicknesses, but with different porosities, were obtained.
- The difference in porosity can be attributed to, differences in dielectric properties of the polyurethanes and ionic strength of the spinning solutions.

8.3 Major contributions

In summary, the major contributions of this study are:

- A model urethane compound could be used to find a suitable modification reagent (4-pentenoyl chloride), confirm the intended carbamate nitrogen as successful reaction site, and to optimize the chemistry.
- The chemistry could be successfully transferred and two medical grade polyurethanes, Pellethane® 2363-80AE and PurSil® 35-80A, were subsequently modified with 4-pentenoyl chloride. The degree of modification could be accurately controlled ($R^2 = 0.99$) between 4.5% to 20.0% and between 11.5% to 18.5% for the respective polyurethanes.
- Crosslinking of the two novel modified polyurethanes could be achieved, using an ultraviolet light source, a heat source and gamma irradiation, resulting in improvements in hysteresis and creep of up to 42.5% and 44.3%, respectively, for Pell15.0.

- It could be concluded from an *in vitro* degradation study that Pell15.0 exhibited significant resistance to surface degradation, as studied with scanning electron microscopy, and retained hard phase integrity due to the oxidative stable crosslinks, when compared to Pellethane.
- Small-diameter tubular constructs, with similar fiber and wall thicknesses, could be electrospun from Pellethane and the 15% modified Pellethane using a standard electrospinning technique in the case of the former and, in the latter, a novel “reactive” electrospinning technique for the *in situ* crosslinking of the novel material, while simultaneously forming the tubular constructs.

Patent and presentation emanating from this research:

1. D. Bezuidenhout, J.P. Theron, P. Zilla, *Modification of thermoplastic polyurethanes*, U.S. Patent application Serial No. 11/388 and U.S. Provisional Patent Application Serial No. 60/664,767.
2. J.P. Theron, D. Bezuidenhout, J.H. Knoetze, R.D. Sanderson, P. Zilla, *Modification of polyurethanes with latent crosslinkable groups for use in cardiovascular prostheses*, 8th UNESCO/IUPAC conference on macromolecules, Mauritius, **2005**

Results of this very extensive research conducted in to the development of crosslinkable, thermoplastic polyurethanes should certainly make a meaningful contribution in the field of the manufacturing of new synthetic cardiovascular prostheses.

8.4 Recommendations for future research

On completion of this study, certain recommendations can be made:

- The scale up of the modification reactions should be studied. A bench-scale pilot plant with different size reactors could be designed and built to accommodate such a study. Successful scale-up would ensure that more material would be available, as required for extrusion.
- Pacemaker leads could then be extruded and evaluated subcutaneously in a sheep model.
- Tubular constructs could be implanted in a rodent model, and/or tubes with larger inside diameter (e.g. 4.4 mm) could be electrospun and optimized *in vitro*, whereafter they could be evaluated *in vivo* in a circulatory model, e.g. a femoral arterial baboon model.

Appendices

Appendix A

Raw materials and properties of polyurethanes

Table A.1: List of commonly used raw materials in polyurethane synthesis [1]

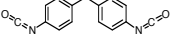
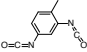
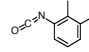
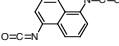
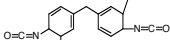
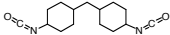
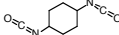
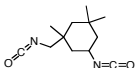
Structure of compound	Name	Abbreviation
Diol extenders		
HO-R-OH	generic diol	DO
HO-(CH ₂) ₂ -OH	ethane diol	EDO
HO-(CH ₂) ₄ -OH	butane diol	BuDO
HO-(CH ₂) ₆ -OH	hexane diol	HDO
Diamine extenders		
H ₂ N-R-NH ₂	generic diamine	DA
H ₂ N-(CH ₂) ₂ -NH ₂	ethylene diamine	EDA
Aromatic diisocyanates		
O=C=N-R ₁ -N=C=O R ₁ = aromatic	generic aromatic diisocyanate	ArDI
	methylene bis(p-phenyl isocyanate)	MDI
	2,4 toluene diisocyanate	2,4 TDI
	2,6 toluene diisocyanate	2,6-TDI
	1,5-naphthalene diisocyanate	NDI
	methylene bis (toluene isocyanate)	TODI
Aliphatic diisocyanates		
O=C=N-R ₂ -N=C=O R ₂ = aliphatic	generic aliphatic diisocyanate	AIDI
	methylene bis(4,4-cyclohexyl isocyanate)	HMDI
	1,4-cyclohexane diisocyanate	CHDI
	3-isocyanatomethyl-3,5,5-trimethylcyclohexyl isocyanate (isophorone diisocyanate)	IPDI
Polyester diols		
HO-[R-C(=O)-O-R-O] _n -H	generic polyester diol	PesD
HO-(CH ₂) ₅ -C(=O)-O-(CH ₂) ₂ -O-C(=O)-(CH ₂) ₅ -OH	polyethylene adipate glycol	PEA
HO-(CH ₂) ₄ -O-C(=O)-(CH ₂) ₄ -O-C(=O)-H	polycaprolactone	PCL
Polyether diols		
HO-[R-O] _n -H	generic polyether diol	PED
HO-[CH ₂ -CH ₂ -O] _n -H	poly(ethyleneoxide) glycol	PEO
HO-[CH ₂ -CH(CH ₃)-O] _n -H	polypropylene oxide glycol	POPG
HO-[CH ₂ -CH ₂ -CH ₂ -CH ₂ -O] _n -H	poly(oxytetramethylene) glycol	PTMEG
Polycarbonate diols		
HO-(CH ₂) ₆ -O-C(=O)-O-(CH ₂) ₆ -OH	polyhexamethylene carbonate glycol	PHMC
Polysiloxane diols		
HO-(CH ₂) ₄ -[Si(CH ₃) ₂]-O-Si(CH ₃) ₂ -(CH ₂) ₄ -OH	hydroxybutyl terminated poly(dimethylsiloxane)	PDMS
Hydrocarbon diols		
HO-[C(CH ₃) ₂ -CH ₂] _n -OH	hydroxy-terminated polyisobutylene	PIB
HO-[CH ₂ -CH ₂ -CH ₂ -CH ₂] _n -[CH ₂ -CH(CH ₂ CH ₃)] _m -OH	hydrogenated polybutadiene	PBD

Table A.2: Listing and properties of medical grade polyurethanes [1]

AROMATIC POLYETHER URETHANES																								
#	Name	Producer	Isocyanate	Soft Segment	Extender	Shore	γ_w	T_g	T_{mh}	M_w ($\times 10^3$)	M_n ($\times 10^3$)	σ_b (MPa)	E_v (MPa)	ϵ_b (%)	E_{100} (MPa)	ρ (g/cm ³)	Ref							
1	Pellethane® 2363	Dow	MDI	PTMEG	BDO	90A-55D												[2-6]						
						55D		156	81	35-48														
						55DE																		
						65D																		
						75D																		
						80A																		
						80AE																		
						90A																		
						90AE																		
						90A																		
2	Vialon® 510X	Becton Dickenson	MDI	PTMEG	BDO													[3, 4]						
3	Cardiomat® 610 Complex	Kontron	MDI	PED	DO	80A					27.6	8.1*	500					[4]						
4	Erythrothane®	Biosearh	ArDI	PED	DO													[4]						
5	Renathane®	Renal Syst's	ArDI	PED	DO													[4]						
6	SRI series	Stanford Res.	MDI	PED	DO													[4]						
7	Estane® 5714	Inst. BF Goodrich	MDI	PED	DO													[3, 4]						
8	Texin®	Mobay (Bayer)	MDI	PED	DO													[4]						
9	Techothane®	Thermedics	MDI	PTMEG				-51										[7, 8]						
	TT-1074A					75A	81		220	100		41.3		550	3.4	1.10								
						85A																		
						85A																		
						94A																		
						54D																		
						64D																		
						69D																		
						74D																		
						75D																		
						82D																		
10	Tecoplast® TP-470	Thermedics																[8]						
11	Elasthane®	PTG	MDI	PTMEG	BDO													[9]						
	55D					55D																		
						74D																		
						74D																		
						85A																		
12	Chronothane® 80A	CT Biomaterials	MDI	PTMEG														[10]						
	80A					80A																		
						80A-75D																		
13	Elast-Eon® 1	Elastomedic	ArDI	PHMO														[11]						

AROMATIC POLYETHER URETHANE UREAS																		
#	Name	Producer	Isocyanate	Soft Segment	Extender	Shore	γ_w	T_g	T_{mh}	M_w ($\times 10^3$)	M_n ($\times 10^3$)	σ_b (MPa)	E_v (MPa)	ϵ_b (%)	E_{100} (MPa)	ρ (g/cm ³)	Ref	
1	Biomer® SolG	Ethicon	MDI	PTMEG	EDA/DAC	75A		-73	295	157	31-41	2.8-5.5	600-800					[3, 12, 13]
2	Biomer® ExtG	Ethicon	MDI	PTMEG	water	75A												[4]
3	Mitrathane®	Polymedica	MDI	PTMEG	EDA						28-35	12.4Flx						[3, 14]
4	Surethane®	Cardial Con Sys	MDI	PTMEG	DA													[4]
5	SRI series	Stanford Res	MDI	PED	DA													[4]
6	Mod.PUU	Mercor	ArDI	PED	DA/Surf.													[4]
7	Univ. Utah	Univ. Utah	MDI	POPG	EDA													[4]
8	Lycra	DuPont	MDI	PTMEG	DA													[4]
9	Biospan®	PTG	MDI	PTMEG	DA													[3, 9]
	70A					70A		-65	180	180	41	41.3	5.9	850				
						TM5												

AROMATIC POLYCARBONATE POLYURETHANES																							
#	Name	Producer	Isocyanate	Soft Segment	Extender	Shore	γ_w	T_g	T_{mh}	M_w ($\times 10^3$)	M_n ($\times 10^3$)	σ_b (MPa)	E_v (MPa)	ϵ_b (%)	E_{100} (MPa)	ρ (g/cm ³)	Ref						
1	Chronoflex® AR	Cardiotech Inc. (Polymedica)	MDI	PCDO	EDA/DAC	75A	86	-34	240	140		51.7						[3, 7, 10, 12]					
2	Bionate® (Corethane)	PTG (Corvita)	MDI	PHECD	BD	80A	81	-18	240	130	45-52	48.1	400-490	570	6.8	1.19			[3, 5, 7, 9]				
						80A																	
						90A																	
						90A																	
						55D	96	-78.3	140	75	48-59	62.0	365-440	380	18.3	1.21							
	75D																						

3	Chronoflex® C 80A 55D 75D	Cardiotech Inc. (Polymedica)				80A 55D 75D											secant 5.3-8.6 12.8-15.2 36.5-39.3	[10]
---	------------------------------------	---------------------------------	--	--	--	-------------------	--	--	--	--	--	--	--	--	--	--	---	------

ALIPHATIC POLYETHER URETHANES

#	Name	Producer	Isocyanate	Soft Segment	Extender	Shore	γ_w	T_g	T_{mh}	M_w ($\times 10^3$)	M_n ($\times 10^3$)	σ_s (MPa)	E_v (MPa)	ϵ_s (%)	E_{100} (MPa)	ρ (g/cm ³)	Ref
1	Tecoflex® EG-80A EG-85A EG-93A EG-100A EG-60D EG-65D EG-68D EG-72D	Thermedics	HMDI	PTMEG	BDO	72A 77A 87A 94A 51D 60D 63D 72D	81	-70				40.0 42.7 53.1 56.5 57.2 57.2 57.2 55.8	580-800	660 550 390 370 360 360 350 310	2.1 4.1 6.9 11.0 12.4 15.2 17.9 23.4	1.04 1.05 1.08 1.09 1.09 1.10 1.10 1.11	[3, 4, 7, 8]
2	Techophilic® HP-60D-20 HP-60D-35 HP-60D-60 HP-93A-100 SRI series	Thermedics				43D 42D 41D 83A						Dry/wet 61.3/35.1 53.7/33.7 57.1/21.3 15.1/9.6		Dry/wet 430/390 450/390 500/300 1040/620		1.12 1.12 1.15 1.13	[8]
3	Southern RI	Stanford Res. Inst.	HMDI	PED	DO												[4]
4	Akzo	Southern Res. Inst.	IPDI	PTMEG	BDO												[4]
5		Akzo	AIDI	PED	DO												[4]

ALIPHATIC POLYETHER URETHANE UREAS

#	Name	Producer	Isocyanate	Soft Segment	Extender	Shore	γ_w	T_g	T_{mh}	M_w ($\times 10^3$)	M_n ($\times 10^3$)	σ_s (MPa)	E_v (MPa)	ϵ_s (%)	E_{100} (MPa)	ρ (g/cm ³)	Ref
1	SRI series	Stanford Res. Inst.	HMDI	PED	DA												[4]

ALIPHATIC POLYCARBONATE POLYURETHANE

#	Name	Producer	Isocyanate	Soft Segment	Extender	Shore	γ_w	T_g	T_{mh}	M_w ($\times 10^3$)	M_n ($\times 10^3$)	σ_s (MPa)	E_v (MPa)	ϵ_s (%)	E_{100} (MPa)	ρ (g/cm ³)	Ref
1	Chronoflex® AL 80A 55D 65D	Cardiotech Inc. (Polymedica)	HMDI???	PCDO	EDA/DAC	80A 55D 65D						37.9 57.9 62.1		585 325 300	4.5 20.0 22.1		[3, 10]
2	Carbothane® PC-3570A PC-3575A PC-3585A PC-3595A PC-3555D PC-3572D	Thermedics	HMDI	PCDO	BD	73A 84A 95A 60D 71D	96	-29	140	75		36.5 41.4 49.0 50.3 58.6		470 410 380 370 360	2.1 4.1 6.9 10.3 22.8	1.15 1.15 1.15 1.15 1.15	[7, 8]

SILOXANE URETHANE COPOLYMERS

#	Name	Producer	Isocyanate	Soft Segment	Extender	Shore	γ_w	T_g	T_{mh}	M_w ($\times 10^3$)	M_n ($\times 10^3$)	σ_s (MPa)	E_v (MPa)	ϵ_s (%)	E_{100} (MPa)	ρ (g/cm ³)	Ref
1	Cardiothane® 51	Avcothane	MDI	PED	DO PDMS	72A					43		580				[4]
2	Rimplast®	Petrarch	AIDI	PED	DO PDMS												[4]
3	Elasteon® 2 85A	Aortec (Elastomedic)	ArDI	PDMS		80A-55D 85A						28±0.7	33	580±5	10±0.3		[11]
4	Elasteon® 3 70A H-0 H-20 H-20 opt H-50 H-80	Aortecbio (Elastomedic)		PDMS/PHMO		65A-80A 70A 89A 85A 85A 82A 82A 85A		-41 NA/-46				25±1 13±1 16±1 25.5 15±2 18±1 28±2	7.0±0.6 38±4 24±1 25±2 23±3 20±1 17±1	490±11 225±35 393±50 460 361±60 473±25 472±25	5.0±0.1	[2, 11, 15]	

Appendix B

Solubility of selected polyurethanes

Solvent	δ_d	δ_p	δ_h	δ_t	ElastEon [®] 2A	ElastEon [®] 2D	Pellethane [®] 2363-80AE	PurSil [®] 35-80A
Acetic acid	14.5	8.0	13.5	21.4	3	4	2	2
Acetic anhydride	16.0	11.7	10.2	22.3	4	4	4	4
Acetone	15.5	10.4	7.0	20.0	3	3	3	2
Acetonitrile	15.3	18.0	6.1	24.4	4	4	4	4
Acrylonitrile	16.0	17.4	6.8	24.8	4	4	3	3
n-Amyl alcohol	16.0	4.5	13.9	21.7	4	4	4	3
Aniline	19.4	5.1	10.2	22.5	3	3	2	2
Benzene	18.4	1.0	2.1	18.5	3	4	3	3
Benzaldehyde	19.4	7.4	5.3	21.4	2	3	2	2
Benzyl alcohol	18.4	6.3	13.7	23.8	2	3	2	2
n-Butanol	16.0	5.7	15.8	23.1	3	4	4	3
Butyl acetate	15.8	3.7	6.3	17.4	3	4	3	3
sec Butyl alcohol	15.8	5.7	14.5	22.2	4	4	3	3
Chlorobenzene	18.6	4.3	4.1	19.5	2	3	3	3
Chloroform	17.8	3.1	5.7	18.9	2	3	2	2
m-Cresol	18.0	5.1	12.9	22.7	1	1	1	1
Cyclohexane	16.7	0.0	0.0	16.7	4	4	4	4
Cyclohexanone	17.8	6.3	5.1	19.6	1	2	1	1
Dichloroethane	19.0	7.4	4.1	20.9	3	3	3	3
Diethyl ether	14.5	2.5	5.1	15.8	3	3	4	3
Diethylene glycol	16.2	14.7	20.5	30.0	2	3	3	2
N,N dimethyl acetamide	16.8	11.5	10.2	22.7	1	1	1	1
N,N dimethyl formamide	17.4	13.7	11.3	24.8	1	1	1	1
Dimethyl sulfoxide	18.4	16.4	10.2	26.7	2	1	2	2
1,4-Dioxane	19.0	1.8	7.4	20.4	1	2	1	1
Ethanol	15.8	8.8	19.4	26.5	4	4	4	4
Ethyl acetate	15.8	5.3	7.2	18.1	3	4	3	3
Hexane	14.9	0.0	0.0	14.9	4	4	4	4
Methyl chloride	18.2	6.3	6.1	20.2	3	3	2	2
Methyl ethyl ketone	16.0	9.0	5.1	19.0	2	3	2	2
N-methyl-2-pyrrolidone	18.0	22.2	7.1	22.9	1	1	1	1
Nitrobenzene	20.0	8.6	4.1	22.2	4	4	3	2
Nitroethane	15.8	18.8	5.1	25.1	4	4	4	4
n-Propanol	16.0	6.8	17.4	24.5	4	4	4	4
Propylene glycol	16.8	9.4	23.3	30.2	4	4	4	4
Pyridine	19.0	8.8	5.9	21.8	1	1	1	1
Tetrahydrofuran	16.8	5.7	8.0	19.4	1	2	1	1
Toluene	18.0	1.4	2.0	18.2	4	4	3	3
Triethanolamine	17.2	15.6	21.3	31.5	4	4	4	4
Trimethyl phosphate	16.8	16.0	10.2	25.3	4	4	4	4
1 = Good solvent	2 = Good swelling agent				3 = Poor swelling agent			4 = Non-solvent

Appendix C

Determination of solvent solubility parameters

C.1 Theoretical background

Focus will first be placed on cohesive energy and then solubility of polymers, in order to provide the necessary background to the methods used to predict the solubility parameters of the polyurethanes. The very comprehensive book by Van Krevelen [16] will be used as reference.

C.1.1 Cohesive energy

The cohesive energy (E_{coh}) of a substance in a condensed state is defined as the increase in internal energy per mole (ΔU) of substance if all the intermolecular forces are eliminated (Eq C.1). The solubility parameter (δ) of the polymer is defined as the square root of the cohesive energy density in the amorphous state at room temperature (Eq. C.2) [16].

$$E_{coh} = \Delta U \quad (C.1)$$

$$\delta = \left(\frac{E_{coh}}{V} \right)^{1/2} \equiv e_{coh}^{1/2} \quad (C.2)$$

,where V is the specific volume and e_{coh} is the cohesive energy density in the amorphous state. For liquids of low molecular mass, the cohesive energy is closely related to the molar heat of evaporation ΔH_{vap} (at a given temperature, T).

$$E_{coh} = \Delta U_{vap} \approx \Delta H_{vap} - RT \quad (C.3)$$

Therefore, for low molecular mass substances E_{coh} can easily be calculated from the heat of evaporation, which is unfortunately not possible for polymers, as polymers cannot evaporate. Indirect methods therefore have to be used, where the molar attraction constant F (at 298K) is defined as:

$$F = (E_{coh} V(298))^{1/2} \quad (C.4)$$

C.1.2 Solubility

The thermodynamic criteria of solubility are based on the free energy of mixing ΔG_M . Two substances are mutually soluble if ΔG_M is negative. By definition,

$$\Delta G_M = \Delta H_M - T\Delta S_M \quad (C.5)$$

where ΔH_M is the enthalpy of mixing; ΔS_M is the entropy of mixing. As ΔS_M is generally positive, there is a limiting positive value of ΔH_M below which dissolution is possible.

Hildebrand tried from as early as 1916 to correlate solubility with cohesive properties of solvents, but it was only in 1949 that he proposed the term solubility parameter (δ). According to Hildebrand, the enthalpy of mixing can be calculated by

$$\Delta h_M = \phi_i \phi_j (\delta_i - \delta_j)^2 \quad (C.6)$$

where Δh_M is the enthalpy of mixing per unit volume; ϕ_i and ϕ_j are the volume fractions of components i and j; δ_i and δ_j are the solubility parameters of components i and j.

Eq. C.6 predicts that $\Delta H_M = 0$ if $\delta_i = \delta_j$, so that two substances with equal solubility parameters should be mutually soluble due to the negative entropy factor, as in accordance with the general rule that chemical and structural similarity favors solubility. As the difference between δ_i and δ_j increases, the tendency towards dissolution decreases.

It may be concluded then that as a requirement for the solubility of a polymer (1) in a solvent (2), the value $(\delta_1 - \delta_2)^2$ has to be as small as possible.

In the derivation of Eq. C.6 only dispersion forces between structural units have been taken into account. For liquids and amorphous polymers, however, the cohesive energy is also dependent on the interaction between polar groups and on hydrogen bonding.

The cohesive energy (E_{coh}) may thus be divided into three parts, corresponding with the contributions of the dispersion forces (E_d), polar forces (E_p) and hydrogen bonding (E_h), and given by:

$$E_{coh} = E_d + E_p + E_h \quad (C.7)$$

with the corresponding equation for the solubility parameter

$$\delta^2 = \delta_d^2 + \delta_p^2 + \delta_h^2 \quad (C.8)$$

The equivalent of Eq. C.6 then becomes

$$\Delta h_M = \phi_i \phi_j [(\delta_{di} - \delta_{dj})^2 + (\delta_{pi} - \delta_{pj})^2 + (\delta_{hi} - \delta_{hj})^2] \quad (C.9)$$

Values of δ_d , δ_p and δ_h cannot be determined directly and therefore have to be determined using indirect methods. One such a method was proposed by Hansen [16].

C.2 Indirect determination of solubility parameters

C.2.1 Method of Hansen

Hansen presumed the applicability of Eqs. C.8 and C.9 so that the solubility parameters can be represented in three-dimensional vector space and may be depicted by the point $(\delta_p, \delta_d, \delta_h)$ in the centre of a solubility sphere.

$$\delta_t^2 = \delta_d^2 + \delta_p^2 + \delta_h^2 \quad (\text{C.10})$$

The solubility parameters of the polyurethanes (Pellethane[®] 2363-80AE and PurSil[®] 35-80A) were calculated (Eq. C.10) using the results presented in Appendix B.

$$\delta_{\text{Pellethane}} = 21.8 \text{ MPa}^{1/2}$$

$$\delta_{\text{PurSil}} = 24.2 \text{ MPa}^{1/2}$$

C.3 Group contribution methods

It is impossible to predict solubility parameter components from the chemical structure, since the polar and hydrogen-bonding properties are so complicated that it does not obey simple rules. The solubility parameter can at best be described as a very rough estimate [16]. A further complicating factor lies in the fact that the exact molecular structure of the polymers has to be known.

The limited available information on Pellethane (Table A.2, Appendix A) was used to deduce a very rough first approximation of its structure, based on the type, molecular mass and stoichiometry possible of the respective raw materials and the published average molecular mass of the polymer chains.

Two methods by which to estimate a solubility parameter have been published viz. that of Hoftyzer and Van Krevelen (HVK) (1976) and that of Hoy (1985). In both methods the same basic assumption is made, namely that of Hansen [16]:

$$E_{\text{coh}} = E_d + E_p + E_h \quad (\text{C.7})$$

$$\delta^2 = \delta_d^2 + \delta_p^2 + \delta_h^2 \quad (\text{C.8})$$

C.3.1 Method of Hoftyzer and Van Krevelen

The solubility parameter components may be predicted from group contributions, using the following equations [16]:

$$\delta_d = \frac{\sum F_{di}}{V} \quad (\text{C.11})$$

$$\delta_p = \frac{\sqrt{\sum F_{pi}^2}}{V} \quad (\text{C.12})$$

$$\delta_h = \sqrt{\frac{\sum E_{hi}}{V}} \quad (\text{C.13})$$

The group contributions, F_{di} and F_{pi} , to the dispersion and polar components of the molar attraction coefficient can simply be added. The “F-method” is however not applicable to the calculation of δ_d as the hydrogen bonding energy E_{hi} per structural group is approximately constant, thus leading to the form of Eq. C.13. The group contributions F_{di} , F_{pi} and E_{hi} (Eqs. C11 - C13) for a number of structural groups can be found in the literature [16]. The solubility parameter of Pellethane was calculated to be $19.11\text{MPa}^{1/2}$.

C.3.2 Method of Hoy

Hoy’s method is in many respects different from that of Hoftyzer and Van Krevelen. A number of auxiliary equations are used (Eqs. C.14 - C.16)

$$\alpha = \frac{777\Delta_T}{V} \quad (\text{C.14})$$

$$\bar{n} = \frac{0.5}{\Delta_T} \quad (\text{C.15})$$

$$\bar{B} = \frac{277}{n} \quad (\text{C.16})$$

where α is the molecular aggregation number, describing the association of the molecules; \bar{n} is the number of repeating units per effective chain segment of the polymer; Δ_T is the Lyderson correction for non-ideality; B is the base value. Expressions for the components of δ are given in Eqs. C.17 - C.20

$$\delta_t = \frac{F_t + \bar{B}}{V} \quad (\text{C.17})$$

$$\delta_p = \delta_t \left(\frac{1}{\alpha} \frac{F_p}{F_t + \bar{B}} \right)^{1/2} \quad (\text{C.18})$$

$$\delta_h = \delta_t \left(\frac{\alpha - 1}{\alpha} \right)^{1/2} \quad (\text{C.19})$$

$$\delta_d = \left(\delta_t^2 - \delta_p^2 - \delta_h^2 \right) \quad (\text{C.20})$$

where F_t is the molar attraction function; F_p is its polar component; V is the molar volume of the structural unit of the polymer; δ_t is the molar attraction contribution to the solubility parameter. Published values for Δ_T , B, F_t , F_p , and V [16] were used to calculate a solubility parameter of $24.01\text{MPa}^{1/2}$ for Pellethane.

Appendix D

Crosslinking of novel modified polyurethanes

Table D.1: Molecular mass between crosslinks (M_c) for Pellx

Mc (g/mol)	Pell4.5	Pell6.5	Pell8.5	Pell12.5	Pell15.0
UV Initiation					
Mc (Hoy)	8443±405	6638±216	3603±16	3075±170	2309±63
Mc (Ideal)	7921±390	6120±205	3357±15	2866±157	2157±59
Heat initiation					
Mc (Hoy)	11118±527	8196±510	7176±378	4789±289	2807±38
Mc (Ideal)	10523±519	7684±488	6709±359	4461±270	2618±35

Table D.2: Molecular mass between crosslinks (M_c) for Purx

Mc (g/mol)	Pur11.5	Pur15.0	Pur18.5
Mc (Ideal)	16417±228	12011±618	7701±423
Mc (Hansen)	17332±241	12672±654	8107±448

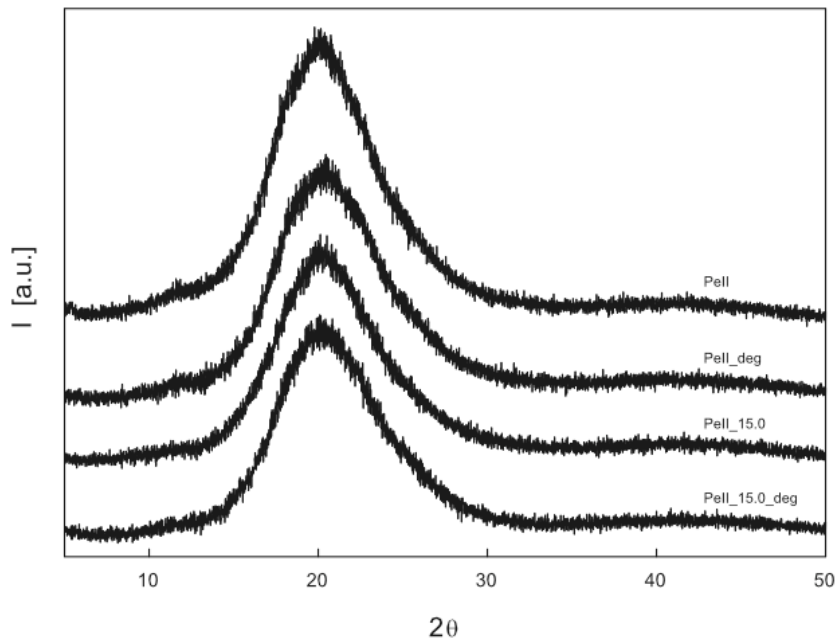


Figure D.1: Wide angle X-ray scattering analysis of Pellethane (Pell) and Pell15.0 (Pell_15.0) control samples compared to Pellethane (Pell_deg) and Pell15.0 (Pell_15.0_deg) degraded in hydrogen peroxide

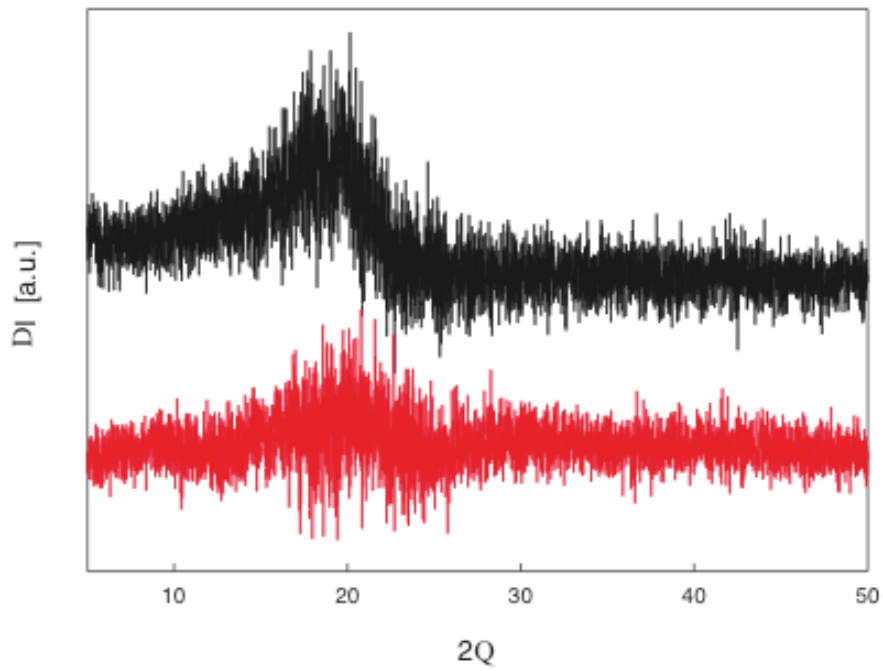


Figure D.2: Wide angle X-ray scattering results of Pellethane (PelI)-Pellethane degraded in hydrogen peroxide (PelI_deg) [Top] and PelI15.0 (PelI_15.0)-PelI15.0 degraded in hydrogen peroxide (PelI_15.0_deg) [Below]

Appendix E

Listing of polyurethane in vitro degradation studies

Table E.1: Chronological listing of polyurethane in vitro degradation studies

Material	Sample	Solutions	Test conditions	Analysis	Results	Reference
Polyester urethane Polyether urethane Polyacrylate Castor oil urethane Polyester-ether urethane Ricinoleate urethane	Films	Humidity	50, 71, 85, 100 °C 95% humidity	Shore hardness	Polyester urethanes found to be hydrolytically unstable.	[17]
Pellethane® 80A (Dow Chemicals)	Pacemaker leads	3% H ₂ O ₂	37 °C, 60 days	EDAX, FT-IR, SEM	Cracks were observed after 30 days and were severe after 60 days.	[18]
Pellethane® 80A Pellethane® 55D (Dow Chemicals)	ASTM (D-1708) Microtensile specimens	1. PtCl ₂ , HNO ₃ , NaClO, AgNO ₃ , FeCl ₃ 2. Cu ₂ Cl ₂ , Cu(OAc) ₂ , Ni(OAc) ₂ , Co(OAc) ₂ 3. H ₂ O (control)	ASTM (D-1708) 0.1 M solutions 90 °C, 35 days	FT-IR, Tensile	Degradation rate of Pellethane® 80A higher than 55D because of the higher ether content of Pellethane® 80A.	[4]
Pellethane® 80A, 90A, 55D, 75D (Dow Chemicals) MedAdhere® 2110 (Medtronic)	Pre-stressed tubing (0 – 500%) 0.25-0.9 mm thick	1. PtCl ₂ , NaClO, AgNO ₃ , FeCl ₃ Cu ₂ Cl ₂ , Cu(OAc) ₂ , Ni(OAc) ₂ , Co(OAc) ₂ 2. AgNO ₃ /lactic acid, lactic acid, Ringer's solution 3. H ₂ O (control)	ASTM (D-1708) 0.1 M solution 90 °C, 35 days	FT-IR, Tensile	Ether containing urethanes (Pellethane) degraded in oxidation media, but not in HCl and NaOH (non-oxidizing acid and base).	[19]
Pellethane® 80A, 55D (Dow Chemicals) Techoflex® EG80A (Thermedics) Biomer® (Ethicon) Cardiothane® -51 (Avcothane) MedAdhere® 2110 (Medtronic)	1. Flat films 2. Whole pacemaker leads 3. Tubing (1.75 × 2.0 mm)	1. AgNO ₃ 2,3. Co salt/ H ₂ O ₂	1. ASTM (D-1708) 0.1 M solution 90 °C, 35 days 2,3. 3% solution 37 °C, 6 months	FT-IR, Tensile	Susceptibility to degradation directly proportional to oxidation potential of metal ions and ether content of polyurethane.	[20]
Poly(ethylene terephthalate) Nylon 66 Poly(methyl methacrylate)	As a precipitate	Trypsin, chymotrypsin, papain and esterase	37 °C, 15 days	Thermal analyses FT-IR	pMMA not affected by enzymes, only hydrolytically unstable bonds.	[21]
Pellethane® 80A, 55D (Dow Chemicals)	Flat films (0.089 mm)	Ringer's solution H ₂ O (control)	ASTM (D-1708) 37, 90 °C, 6 months	Tensile	Loss in tensile strength, especially at elevated temperatures.	[22]

Material	Sample	Solutions	Test conditions	Analysis	Results	Reference
MDI/PEO(1000)/BD MDI/PTMO(1000)/BD MDI/PBD(2000)/BD MDI/HPBD(2100)/BD MDI/PDMS(1350)/BD Biomer® (Ethicon) Biostable® PUR (Medtronic) Pellethane® 80A (Dow Chemicals)	Flat films (0.20 mm)	1. AgNO ₃ 2. AgNO ₃ /lactic acid sodium salt 3. H ₂ O (control)	75 °C, 10, 30 days	Tensile, GPC, DSC, XPS	High resistance could be obtained from aliphatic polyol soft segment, high linear & saturated hydrocarbon content.	[13]
PUU-PCLG PUU-PEO/PPO	Pre-stressed tubing (400%) (0.178 mm ID x 0.204 mm OD) Flat films (0.30 mm)	1. PMN 2. HOCl 3. ONOO ⁻	1. 37 °C, 3 hr 2. 25 °C, 24 hr 3. 25 °C, 24 hr	FT-IR, GPC	HOCl or PMN cause degradation of aliphatic ester and peroxy nitrite of the aliphatic ether.	[23]
TDI/PTMO/ED TDI/PCL/ED TDI/PTMO-PEO/ED MDI/PTMO/ED MDI/PTMO(650)/BD MDI/PTMO(1000)/BD MDI/PTMO(2000)/BD MDI/PTMO(1000)* ¹ /BD MDI/PTMO(2000)* ¹ /BD MDI/PTMO(1250)* ¹ /BD MDI/PTMO(2000)* ¹ /BD (*fluorinated diols included) Cardiothane® (control) (Avcothane)	Glass tubes coated (0.01 mm)	0.25 ml CE (1 u/ml) 0.05 ml CB (2 u/ml) 0.5 ml CO (10 u/ml) 0.025 ml XO (0.025 u/ml) Cholesterol esterase Horseradish peroxidase	37 °C, 28-30 days	FT-IR, DSC, ESCA, SEM	Biodegradation process result of multitude of biologically mediated components acting synergistically. Process enhanced by e.g. material dissolution.	[24]
MDI/PTMO/ED (4.2)* MDI/PTMO/ED (3.0) TDI/PTMO/ED (6.8) TDI/PCL/ED (7.5) TDI/PCL/ED (7.5) MDI/PTMO/ED (3.0)* MDI/PTMO/BD (15.0) TDI/PTMO-PEO/ED(8.5) TDI/PTMO/ED (6.8) TDI/PCL/ED (2.9) * (c.p.m. mg ⁻¹ x 10 ⁻⁵) Pellethane® 80A Pellethane® 55D (Dow Chemicals)	Flat films	Thermal	0 - 450 °C	TGA	Hydrolytic enzyme CE responsible for degradation of urethane-urea linkages in soft segment.	[25]
	Porous membranes	1. Activation of PKK to KK (thrombogenicity) 2. Neutral red Kenacid blue (Cytotoxicity) 3. HUVEC	1. 37 °C, 3 min. 2. 37 °C, 5 days 3. 37 °C, 7 days	1. 2. 3. SEM	Different results obtained depending on method used.	[26]
	Membranes	Human neutrophil cell culture	37 °C, 5% CO ₂ , 100% humidity	Elastase activity	PU's containing PCLG instead of PTMO showed lowest thrombogenicity and best cytocompatibility.	[27]
		1. PtCl ₂ , AgNO ₃ , FeCl ₃ 2. Cu ₂ Cl ₂ , Cu ₂ (OAc) ₂ , Ni(OAc) ₂ , Co(OAc) ₂ 3. H ₂ O (control)	ASTM (D-1708) 0.1 M solution 90 °C, 35 days	FT-IR, Tensile	Elastase as contributor to PU degradation. Polyester urea-urethane (TDI/PCL/ED) showed the highest cell-mediated degradation.	[28]
					Degradation rate of Pellethane® 80A higher than 55D (higher ether contents).	[29]

Material	Sample	Solutions	Test conditions	Analysis	Results	Reference
Uncoated Pellethane catheter (BN 508159, 508384) Coated Pellethane catheter (BN 301972, 302247) Topecon catheter (Ohmeda Inc.) MDI/PTMO(2000)/BD	Catheter	Various clinically used drugs	37 °C, 24 hours	UV spectroscopy	Uptake of the drugs by Topecon was lower than the Pellethane catheters, because of higher proportion of hard segment.	[29]
Pellethane® 80AE (Dow Chemicals) Corethane® 80A (Corvita)	Flat films (0.5 mm) Flat films	20% H ₂ O ₂ / 0.1M CoCl ₂	37 °C, 12 days	FT-IR, GPC, SEM, O ₂ permeability, Tensile DSC, GPC, FT-IR	Surface phenomena resulting from an autooxidation mechanism. Degradation of Pellethane strongly influenced by aging media. Poly(carbonate urethane) (Corethane®) presents greater chemical stability than does the ether-containing Pellethane.	[30] [5]
Pellethane® 80A Pellethane® 55D (Medical Profiles)	Tubing, circumferentially stretched (0 – 250%)	1. Cholesterol 2. Cholesteryl acetate 3. Cortisone	37 °C, 12 days	SEM, DSC	Polar steroids have strong interactions with especially Pellethane® 55D. Environmental stress cracking observed for both polymers at moderate strains.	[31]
PEUU/PDMS PEUU Biospan® (PTG, Corvita)	Blood sacks	Saline buffer solution	37 °C, 30-60 days	GPC, Tensile, DMA	PDMS modified PEUU showed greater resistance to degradation.	[32]
Poly(ether)urethanes (PEU) chain extended with: 1. 1,4-butane diol 2. 2-butene-1,4-diol	0.5 mm films	10% H ₂ O ₂ /0.05M CoCl ₂ enzyme (papain)	37 °C, 1 week	ATR-IR, XPS, AFM	PEU, chain extended with 2-butene-1,4-diol less susceptible to enzymatic (oxidative) degradation.	[33]
Poly(carbonate) urethane Poly(ester-urea) urethane	Polymer coated slips	Activated human monocyte-derived macrophages	37 °C, 1 week 37 °C, 1 month	SEM, Radiolabeled release	Poly(carbonate) urethanes are less susceptible to oxidative degradation than poly(ether) urethanes, but are hydrolytically unstable.	[34]
Poly(ether urethane) (Pulse-Tech) Poly(carbonate urethane urea) (CPU)	Porous graft	1. Cholesterol esterase 2. 1.63M t-butyl hydroperoxide/0.10M CoCl ₂ 3. 0.10M glutathione/1.63M t-butyl hydroperoxide/0.10M CoCl ₂ 4. Plasma 5. H ₂ O (control)	1. 37 °C, 70 days 2, 3. 70 days 4. 37 °C, 70 days 5. 37 °C, 70 days	ESEM, GPC, Compliance, Tensile	Poly(carbonate urethane urea) far greater chemical stability than Poly(ether urethane) grafts.	[35]
Pellethane® 80A, 55D (Dow Chemicals)	Pre-strained dumbbell (150%) (1 mm) Pre-strained tubing (150-300%) (1.8 mm O.D.)	1. Human plasma 2. 10% H ₂ O ₂ / 0.1M CoCl ₂	1. 37 °C, 7 days 2. 50 °C, 10, 20 days	SEM	Pellethane® 80A underwent considerable stress cracking compared to Pellethane® 55D.	[36]
Tecoflex® (Thermedics)	Flat sheet (0.01 mm)	Sterilization	25 – 1000 kGy (5 MGy h ⁻¹)	FT-IR, TG, SEC	Small oxidized components detected (toxicity concern).	[37]

Material	Sample	Solutions	Test conditions	Analysis	Results	Reference
HMDI/PTMEG/HTPBD/HDA (?:0%:42.5%:57.5%) (?:0%:32.1%:67.9%) (?:21.3%:21.3%:21.3%) (?:16.1%:16.1%:16.1%) MyoLink®	Flat sheets	1. Rabbit blood 2. Mouse fibroblast cells 3. Calcium phosphate 4. Human blood	1. 37 °C, 1 min. 2. 37 °C, 1 days 3. 37 °C, 30 days 4. 22 °C, 1 h	1. Hemolysis 2. Cytocompatibility 3. Calcification 4. Blood compatibility	PUU resulted in higher calcification and WBC consumption. PEU opposite effect.	[38]
(poly(carbonate-urea) urethane) Pulse-Tec® (poly(ether)urethane)	Compliant vascular grafts (100 mm long, 5 mm ID)	1. Plasma fractions I-IV 2. A ₂ (PLA) 3. Cholesterol esterase 4. H ₂ O ₂ /CoCl ₂ 5. t-butyl peroxide/CoCl ₂ 6. Glutathione/ t-butyl peroxide/CoCl ₂	37 °C, 70 days	1. Thermo-mechanical analyses 2. Dynamical mechanical analyses	MyoLink more resistant to degradation than Pulse-Tec and only degraded in glutathione/ t-butyl peroxide/CoCl ₂ .	[39]
Poly(MPC-co-EHMA) (MPC) Tecoflex® EG-60D (SPU) (Thermedics Inc.)	0.2 mm films	Immunoglobulin	37 °C, 60 min.	Protein adsorption (micro-BCA method)	Lower protein adsorption was found in a blend of MPC and Tecoflex® than with just the Tecoflex®.	[40]
HDI/PCN/BD = 3:1:2 HDI/PCN/BD = 2:1:1 HDI/PCN/BD = 3:2:1 HDI/PCN/BD = 4:3:1 HDI/PCN/BD = 3:2:1 MDI/PCN/BD = 3:2:1 HMDI/PCN/BD = 3:2:1	Small tubes (3 mm ID)	16, 80, 160 or 400 units/ml cholesterol esterase	pH = 7.0, 25 °C	Contact angle, Radiolabeled analyses,	Hydrolytic action of the enzymes used had the most pronounced effect on the PU manufactured from HMDI.	[41]
Corethane® 80A (Corvita) Pellethane® 80A (Dow Chemicals) ChronoFlex® AL-80A (CardioTech Inc.) PHMO-PU (CSIRO)	1. Flat sheets 2. Pre-strained (200%) 3. ASTM D-638 4. ASTM D-638	1. PBS (pH = 7.4) 2. H ₂ O ₂ / CoCl ₂ 3. 3% H ₂ O ₂ + Co 4. SBF	37 °C, 3 months	Tensile (ASTM D-638), DSC, FT-IR, ESEM	Corethane® 80A displayed best overall resistance to hydrolysis, ESC, MIO and calcification. Pellethane was the least stable.	[42]
Pellethane® 80A Pellethane® 55D (Dow Chemicals)	1. Flat sheets 2. ASTM D-638	0.05M CoCl ₂ 1.63M H ₂ O ₂	25 °C, 20 – 60 days	Tensile, SAXS	Solvent-cast Pellethane® 80A samples failed significantly earlier than heat pressed samples when compared to Pellethane® 55D.	[43]

Abbreviation	Description	Abbreviation	Description	Abbreviation	Description
AFM	Atomic force microscopy	FT-IR	Fourier transform infrared	PDMS	Poly(dimethylene siloxane)
AgNO ₃	Silver nitrate	GPC	Gel permeation chromatography	PEO	Poly(ethylene oxide)
ASTM	American standard test method	HCl	Hydrochloric acid	PHMO	Poly(hexamethylene oxide)
BD	Butane diol	H ₂ O	Water	PKK	Prekallikrein
CB	Cathepsin B	H ₂ O ₂	Hydrogen peroxide	pMMA	Poly(methyl methacrylate)
CE	Cholesterol esterase	HOCl	Hypochlorous acid	PMN	Neutrophils

Co	Cobalt	HPLC	High pressure liquid chromatography	PPO	Polypropylene glycol
CO	Colagenase	HTPBD	Hydroxy-terminated polybutadiene	PtCl ₂	Platinum chloride
Co(OAc) ₂	Cobalt acetate	KK	Kallikrein	PTMO	Poly(tetra methylene oxide)
Cu ₂ Cl ₂	Copper(II) chloride	MDI	4,4-methylenebis(phenylisocyanate)	PUU	Poly(urethane urea)
Cu(OAc) ₂	Copper acetate	MPC	2-methacryloylethyl phosphorylcholine	SAXS	Small-angle X-ray scattering
DSC	Differential scanning calorimetry	NaOH	Sodium hydroxide	SEM	Scanning electron microscopy
ED	Ethylene diamine	Ni(OAc) ₂	Nickel acetate	SPU	Segmented polyurethane
EDAX	Electron dispersive analysis by X-ray	ONOO ⁻	Peroxynitrite	TDI	2,4-toluene diisocyanate
ESCA	Electron spectroscopy for chemical analyses	PBD	Poly(butane) diol	TGA	Thermal gravimetric analysis
ESEM	Environmental scanning electron microscope	PCL	Poly(caprolactone)	WBC	White blood cells
EHMA	2-ethylhexyl mechacrylate	PCLG	Poly(caprolactone diol)	XO	Xanthine oxidase
FeCl ₃	Ferrous(III) chloride	PCN	Polycarbonate	XPS	X-ray photoemission spectroscopy

Appendix F

Electrospinning of cardiovascular and other medical devices

Table F.1: Summary of some recent articles on electrospinning of cardiovascular and other medical devices

Material	Description	M _w (g/mol)	Conc (wt%)	Solvent	Volt (kV)	Dist (mm)	Flow (ml/h)	Caplry (mm)	Thick (μm)	Fibre (μm)	Results	Ref
PCL	Fiber collected on wire rings. Flat sheet. Scaffolds coated with collagen type 1. Seeded with cells.	80 kDa	10	CHCl ₃ MeOH	12		6	1	10	0.25	Thin fibers obtained. Neonatal rat cardiomyocytes attached well to the scaffold. Bio-engineered patch.	[44]
PANi	PANi blended with protein, gelatin and co-electrospun. Flat sheet. Seeded with cells		3-8	HFIP	10	100			0.5-1	200-300	H9c2 rat cardiac myoblast cells attached & proliferated on scaffold. Confluent layer.	[45]
PEG-PLA	Flat sheet. Influence of fiber thickness investigated. Seeded with cells.	10.5 kDa	8.2-25.9	HFIP	15	150	1.5	22G		0.14-2.1	MC3T3-E1 osteoprogenitor cells adhered and proliferated. Cell density increased with fiber diameter.	[46]
Collagen type1/ Elastin/ PLGA	Vascular graft. Seeded with cells. Higher PLGA conc used than in other studies.		15	HFIP	25	150	3	18G	1000	0.72	Changing ratio of respective materials improved physical properties. Biocompatibility was favorable.	[47]
Collagen type1	Flat sheet. Seeded with cells. Wound healing.		8	HFIP	15-20	215	0.12	0.84	0.46	0.2	Human oral keratinocytes adhered and proliferated. Wide pore size distribution.	[48]
Silk-BMP-2/ nHAP/ hMSCs	Flat sheet. nHAP and hMSCs included with silk and BMP-2. Bone regeneration		8		12	215	0.12	1.5		0.5-0.6	Incorporation of BMP-2 and nHAP enhanced bone formation significantly.	[49]
Fibrinogen	Flat sheets for wound healing. Mechanical properties investigated.			HFIP	22	100	1.8	18G		0.12-0.6	Porous structures obtained with good mechanical properties for wound dressing.	[50]
PLA PLGA	Flat sheet. Cardiac tissue engineering application. Seeded with cells.	75000		ACA	30	150	6			1	Cardiac myocytes preference to hydrophobic surfaces. PLA scaffolds promoted better cell adhesion.	[51]
Chitosan/ PEO	Flat sheet.	190 kDa 900 kDa	<2	DMF DMSO	20-25	17-20		0.5		0.04	Promoted attachment of human osteoblasts and chondrocytes.	[52]
PEUU	Flat sheet and tubes. Co-electrospinning with SMC.		5-12	HFIP	10	230	1.5	1.2	300-500		Microintegration and alignment of SMC possible into degradable scaffold.	[53]

Material	Description	M _w (g/mol)	Conc (wt%)	Solvent	Volt (kV)	Dist (mm)	Flow (ml/h)	Caplry (mm)	Thick (µm)	Fibre (µm)	Results	Ref
DegraPol	Flat sheets. Scaffold for skeletal muscle tissue engineering.		30	CHCl ₃	18				100	10	Murine and rat myoblast cell line and human satellite cells showed adhesion and proliferation to degradable scaffolds.	[54]
PELA	Dual porosity scaffold for facial application.	110000		CHCl ₃	25		1				MMT and NaCl incorporated to achieve nano- and microporosity respectively during electrospinning.	[55]
PU (Pellethane® 2102-75A)	Flat sheet. Fiber alignment and direction evaluated using HLF.		20	DMF		200		18G		0.5-0.84	Aligned structure led to increased ECM production and was more sensitive to strain in the longitudinal direction.	[56]
Silk fibroin	Flat sheet. Wound dressing. Seeding of cells		8	FA	15	70	1.5				Silk fibroin matrix promoted cell adhesion and spreading of collagen type 1.	[57]
PLCL	Small diameter vascular graft		2	CHCl ₃	20	200	5	0.8	50-340	0.7-0.8	Compliant small-diameter graft spun from PLCL. Thin wall thickness simulated compliance of native artery well.	[58]
PLA	Flat sheets. Fibrous scaffolds for neural tissue engineering. Seeding of cells	300000	2 5	DCM DMF	12	100	1	18G		0.15-0.5 0.8-3	Neural stem cells elongated and their neurite outgrew along the fiber direction.	[59]
Collagen type 1 ST-gelatin	Bilayered vascular graft.		1-7 2.5-10	HFIP HFIP	9.6-16 7.3-11	150 50	5 3	0.8 0.8		0.2-2	Multilayering and mixing electrospinning devised to design a mesoscopically ordered structure.	[60]
PU PEO PLGA PLGA/Chitin	Flat sheet. Biodegradable composite matrix for tissue engineering.		15	THF CHCl ₃ HFIP	25	300	3	0.8 0.8 0.84			Simultaneous electrospinning process introduced. Attachment and spreading of human keratinocytes promising. 3-D structure obtained with PLGA/Chitin	[61]
Silk fibroin	Flat sheet. Cell culture of human keratinocytes and fibroblasts. Wound dressing and tissue engineering.		3-15	FA	15	70		0.495		0.03- 0.12	Wide pore size distribution. Silk fibroin promoted cell adhesion and spreading.	[62]
PLCL	Flat sheet. Biocompatibility of the PLCL scaffold investigated.		3-9	Acetone	9-15	130	2	0.4-1.2		0.5-1.5	SMC and EC adhered and proliferated well on the PLCL scaffold.	[63]
PLGA PLA-PEG DNA	Flat sheet. Therapeutic application in gene delivery for tissue engineering.		35	DMF	25	150	1.2	20G		0.38-1.1	Electrospinning of plasmid DNA/polymer solution possible.	[64]

Material	Description	M _w (g/mol)	Conc (wt%)	Solvent	Volt (kV)	Dist (mm)	Flow (ml/h)	Caplry (mm)	Thick (µm)	Fibre (µm)	Results	Ref
PLGA-Mefoxin	Flat sheet. Wound healing. Controlled release of antibiotics.		33	DMF	23-27	150	1.2	0.7		0.17-0.58	Mefoxin incorporated and released from scaffold without the loss of structural integrity.	[65]
PLA	Flat sheets. Control of biodegradability.	90000	30-50	DMF	23-27		1.2	0.7			Good hydrophilic and mechanical properties obtained.	[66]
PCL	Flat sheets. Candidate scaffold for bone regeneration. Seeded with cells	80000	10	CHCl ₃	13		6	1		0.2-0.6	Mesenchymal stem cells penetrated scaffold and surface covered after 1 week.	[67]
PLA PCL	Bilayered tubular scaffold. Blood vessel engineering.	76 kDa 80 kDa	12.5	CHCl ₃	13	200	10.6-1.2	26G	600	1-6	Multilayering electrospinning achieved. Support attachment, spread and growth of mouse fibroblast and human myofibroblasts.	[68]
Gelatin type B Collagen type 1 Alpha-elastin Tropoelastin PCL	Flat sheets. Generation of biomimetic scaffolds made of natural polymers for tissue engineering. Multi-filament yarn		8.3 8.3 20 20 9	HFIP CHCl ₃ / MeOH	10 15	150 150	1-10 0.1	18G 16G		0.2-0.5 0.2-0.5 0.5-4.2 1.1-9.7 1.26	Good control over fiber thickness. Scaffolds support attachment and growth of HEPM cells. Fibers are 3-D suspended between two grounded rings.	[69] [70]
PCL	Flat sheets. Scaffold for cartilage tissue engineering using hMSCs.	80000		FHF/DMF	12	200	0.4	18G	1000	0.7	Electrospun PCL candidate scaffold for cell-based tissue engineering approaches to cartilage repair.	[71]
PCLEEP	Flat sheets. Galactose ligand surface influences attachment etc of rat hypocytes in culture.	70760	21.5	Acetone	17	80	0.3	27		0.3-1.5	PCLEEP promotes hepacyte aggregates within fiber mesh suggesting application in liver tissue engineering.	[72]
PLGA	Flat sheets. Nano-surface structure for improved degradation.	18000 - 23000	5	Acetone EA DCM CHCl ₃	3-9	10-20	0.01-10	0.05-0.5			Different nano-surface structures with change in solvent and flow rate.	[73]
PEO PAA PVA PU PCL	Investigation into governing parameters in electrospinning	600000 250000 10000 80000	1-10	THF DCM DMF Water EtOH	10-100		0.02-0.6				Voltage, flow rate, concentration, molecular weight and nozzle-to-ground distance key parameters. Volume charge density follows power law dependence on above-mentioned parameters.	[74]
PU	Flat sheets. Mechanical properties.		7	DMF	20		0.24	1			Different mechanical response than bulk material. Molecular orientation within fiber and strain-induced during spinning.	[75]

Material	Description	M _w (g/mol)	Conc (wt%)	Solvent	Volt (kV)	Dist (mm)	Flow (ml/h)	Caplry (mm)	Thick (µm)	Fibre (µm)	Results	Ref
Estane® PVC/ PVDF	Simultaneous spinning side-by-side fashion.	135900 Da	20,25	DMAc	14	150	3	0.7		0.1-5	Bicomponent spinning in side-by-side fashion demonstrated.	[76]
PLCL	Flat sheet. Aligned fibers to mimic medial layer in native artery.	250000 Da	25,20 5	Acetone	15 20	200 150	3 1			0.1-5 0.55	Able to control fiber thickness. Fiber aligned scaffold. Directional growth of SMC along fiber orientation.	[77]
Collagen type 1 PGA PLA PGA/PLA	Infiltration of interstitial cells into e-spun scaffolds.			HFIP	20	125			200-250	0.5-1	Only scaffolds prepared with collagen showed rapid, and dense, infiltration of interstitial and EC.	[78]

Abbreviation	Description	Abbreviation	Description	Abbreviation	Description
ACA	Acetic acid	FA	Formic acid	PEG	Poly(ethylene glycol)
BMP-2	Bone morphogenic protein 2	Fiber	Fiber thickness	PELA	Poly(ethylene-b-lactide)
Caplry	Capillary	Flow	Flow rate	PEO	Poly(ethylene oxide)
CHCl ₃	Chloroform	HEPM	Human embryonic palatal mesenchymal	PEUU	Poly(ester urethane)urea
Conc	Concentration	HFIP	1,1,1,3,3,3-hexafluoro-2-propanol	PGA	Poly(glycolic acid)
Da	Dalton	HLF	Human ligament fibroblast	PLA	Poly(lactide)
DCM	Dichloromethane	hMSCs	Human mesenchymal stem cells	PLGA	Poly(D,L-lactide-co-glycolide)
Dist	Distance	ID	Inside diameter	PLCL	Poly(L-lactide-co-caprolactone)
DMAc	N,N-dimethyl acetamide	MeOH	Methanol	PU	Polyurethane
DMF	N,N-dimethylformamide	M _w	Molecular weight	PVA	Poly(vinyl alcohol)
DMSO	Dimethyl sulfoxide	nHAP	Hydroxyapatite	PVC	Poly(vinyl chloride)
DNA	Deoxyribose nucleic acid	PAA	Poly(acrylic acid)	PVDF	Poly(vinylidene fluoride)
EA	Ethyl acetate	PANi	Polyaniline	Ref	Reference
EC	Endothelial cells	PCL	Poly(caprolactone)	SMC	Smooth muscle cells
E-spun	Electrospun	PCLEEP	Poly(caprolactone-co-ethyl ethylene phosphate)	ST-gelatin	Styrenated gelatin
EtOH	Ethanol			Volt	Voltage

Appendix G

Communication of wide-angle X-ray scattering results

-----Original Message-----

From: Fernando Ania [<mailto:emfernando@iem.cfmac.csic.es>]

Sent: 26 July 2006 12:40 PM

To: Fourie, Aneli <aef2@sun.ac.za>

Cc: "Baltá Calleja, F.J."

Subject: Results

Dear Prof. Sanderson,

Please find attached the first results on the Polyurethane samples that you sent us. Fig. 1 shows the WAXS scans of the four samples and, as you can see, there is no clear evidence of crystalline peaks in any of the polymers. It means that, from the point of view of X-ray scattering, the crystallinity is negligible. This result does not exclude the possible presence of small amounts of crystallites, not contributing to the coherent scattering, which could be possibly detected by other methods such as DSC.

Not having any details of the materials, just the reference names, I have tried to compare (Fig. 2) the Pell and Pell_15.0 samples with their "deg" (degraded?) counterparts. By subtraction, one observes a certain excess scattering in the 2theta range 18-21° of the former polyurethanes, which could account for the presence of such small amounts of crystallites.

I hope that these measurements can be useful and do not hesitate to ask in case

you need any further explanations.

Best regards,

Fernando Ania

Dr. Fernando Ania

Instituto de Estructura de la Materia, C.S.I.C.

Serrano 119, 28006-Madrid , Spain

Fax: +34 915642431

Phone: +34 915619400

Appendix H

Summary of Bootstrap method

The Bootstrap method is a non-parametric test method, commonly used in statistical comparisons between two data sets, where it is suspected that the standard assumptions of e.g. normality and equal variance are violated [79].

The logic flow diagram of the Bootstrap method, as published by Efron and Tibshirani [79], for the comparison of two such data sets, \underline{x}_1 and \underline{x}_2 of size n_1 and n_2 , respectively (n_1 not necessarily equal to n_2) is presented in Figure H.1.

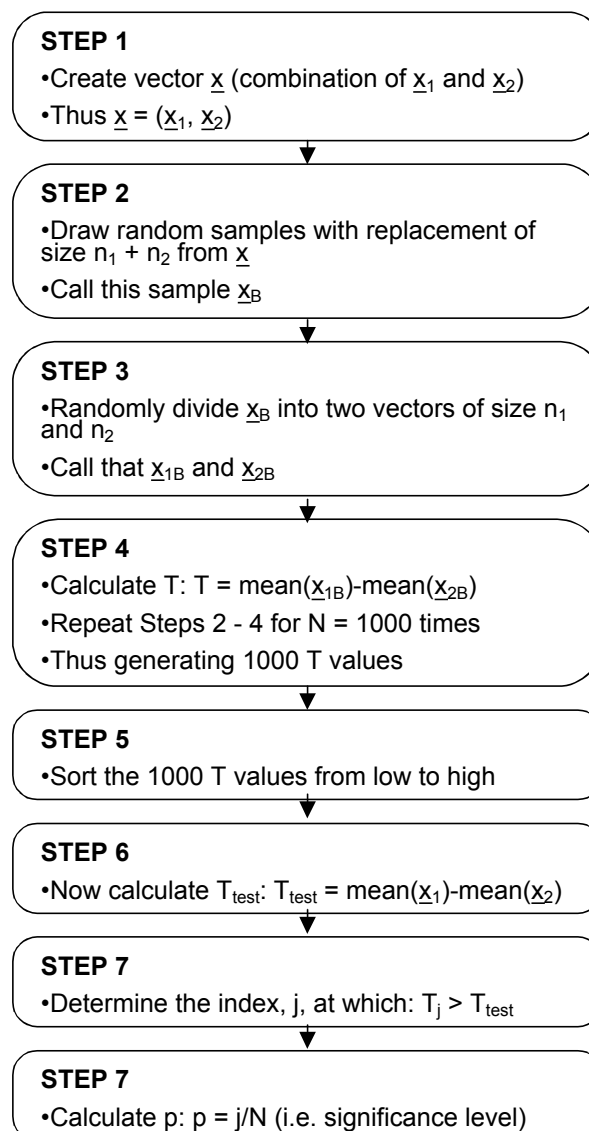


Figure H.1: Flow diagram of the Bootstrap method

References

1. Bezuidenhout, D., *Porous Polymeric Superstructures as In-growth Scaffolds for Tissue-engineered Vascular Prosthesis*, PhD dissertation. 2001, University of Stellenbosch: Stellenbosch.
2. Martin, D., L. Warren, P. Gunatillake, S. McCarthy, G. Meis, and K. Schindhelm, *Polydimethylsiloxane/polyether-mixed macrodiol-based polyurethane elastomers: biostability*. *Biomaterials*, 2000. **21**: p. 1021-1029.
3. Zdrahala, R. and I. Zdrahala, *Biomedical applications of polyurethanes: a review of past promises, present realities, and a vibrant future*. *J. Biomater. Appl.*, 1999. **14**(1): p. 67-90.
4. Coury, A., P. Slaikeu, P. Cahalan, and K. Stokes, *Medical applications of implantable polyurethanes: current issues*. *Prog. Rub. & Plas. Tech.*, 1987. **3**(4): p. 24-37.
5. Tanzi, M., D. Mantovani, P. Petrini, R. Guidoin, and G. Laroche, *Chemical stability of polyether urethanes versus polycarbonate urethanes*. *J. Biomed. Mater. Res.*, 1997. **36**(4): p. 550-559.
6. www.dowchemicals.com, *Typical physical properties of Pellethane*. [accessed: 8 June 2006].
7. Yang, M., Z. Zhang, C. Hahn, G. Laroche, M. King, and R. Guidoin, *Totally implantable artificial hearts and left ventricular assist devices: selecting impermeable polycarbonate urethane to manufacture ventricles*. *J. Biomed. Mater. Res.*, 1999. **48**(1): p. 13-23.
8. www.thermedics.com, *Medical grade resins- A selection guide*. Thermedice Inc [accessed: 8 June 2006].
9. www.polymertech.com, *The polymer technology group*. [accessed: 8 June 2006].
10. www.cardiotech-inc.com, *Polyurethane biomaterials from CT biomaterials*. [accessed: 8 June 2006].
11. www.elastomedic.com, *Guide to Elast-Eon medical polymers*. [accessed: 15 August 2001].
12. Reed, A., J. Potter, and M. Szycher, *A solution grade biostable polyurethane elastomer: ChronoFlex AR*. *J. Biomater. Appl.*, 1994. **8**(3): p. 210-236.
13. Takahara, A., A. Coury, R. Hergenrother, and S. Cooper, *Effect of soft segment chemistry on the biostability of segmented polyurethanes. I. In vitro oxidation*. *J. Biomed. Mater. Res.*, 1991. **25**(3): p. 341-356.
14. Gilding, D., A. Reed, I. Askill, and S. Briana, *Mitrathane. A new polyether urethane urea for critical medical application*. *Trans. Am. Soc. Artif. Intern. Organs.*, 1984. **30**: p. 571-576.
15. Gunatillake, P., G. Meijs, S. McCarty, and R. Adhikari, *Poly(dimethylsiloxane)/Poly(hexamethylene oxide) mixed macrodiol based polyurethane elastomers. 1. Synthesis and properties*. *J. Appl. Polym. Sci.*, 2000. **76**: p. 2026-2040.
16. Van Krevelen, D., *Properties of polymers*. 1990, Amsterdam: Elsevier Science.
17. Gahimer, F. and F. Nieske, *Hydrolytic stability of urethane and polyacrylate elastomers in the human environment*. *J. Elast. Plast.*, 1969. **1**: p. 266-280.
18. Stokes, K., W. Berthelsen, and M. Davis, *Metal catalyzed oxidative degradation on implanted polyurethane devices*. *ACS Division of Polymeric Materials: Science and Engineering*, 1985. **6**: p. 159-169.
19. Coury, A., K. Stokes, P. Cahalan, and P. Slaikeu, *Biostability considerations for implantable polyurethanes*. *Life Support Syst.*, 1987. **5**(1): p. 25-39.
20. Stokes, K., A. Coury, and P. Urbanski, *Autooxidative degradation of implanted polyether polyurethane devices*. *J. Biomater. Appl.*, 1987. **1**(4): p. 411-448.
21. Smith, R., C. Oliver, and D. Williams, *The enzymatic degradation of polymers in vitro*. *J. Biomed. Mater. Res.*, 1987. **21**: p. 991-1003.
22. Coury, A., P. Slaikeu, P. Cahalan, K. Stokes, and C. Hobot, *Factors and interactions affecting the performance of polyurethane elastomers in medical devices*. *J. Biomater. Appl.*, 1988. **3**: p. 130-176.
23. Sutherland, K., J. Mahoney, A. Coury, and J. Eaton, *Degradation of biomaterials by phagocyte-derived oxidants*. *J. Clin. Invest.*, 1993. **92**(5): p. 2360-2367.

24. Santerre, J., R. Labow, and G. Adams, *Enzyme-biomaterial interactions: effect of biosystems on degradation of polyurethanes*. J. Biomed. Mater. Res., 1993. **27**(1): p. 97-109.
25. Santerre, J., R. Labow, D. Duguay, D. Erfle, and G. Adams, *Biodegradation evaluation of polyether and polyester-urethanes with oxidative and hydrolytic enzymes*. J. Biomed. Mater. Res., 1994. **28**(10): p. 1187-1199.
26. Petrovic, Z., Z. Zavargo, J. Flynn, and W. Macknight, *Thermal degradation of segmented polyurethanes*. J. Appl. Polym. Sci., 1994. **51**: p. 1087-1095.
27. del Guerra, R., L. Lelli, C. Tonelli, T. Trombetta, M. Cascone, M. Taveri, P. Narducci, and P. Giusti, *In vitro biocompatibility of fluorinated polyurethanes*. J. Mater. Sci., Mater. Med., 1994. **5**: p. 452-456.
28. Labow, R., D. Erfle, and J. Santerre, *Neutrophil-mediated degradation of segmented polyurethanes*. Biomaterials, 1995. **16**: p. 51-59.
29. Coury, A., R. Levy, C. McMillin, Y. Pathak, B. Ratner, F. Schoen, D. Williams, and R. Williams, *Degradation of Materials in the Biological Environment*, in *Biomaterials Science: An Introduction to Materials in Medicine.*, B. Ratner, et al., Editors. 1996, Academic Press: San Diego. p. 243-281.
30. Schubert, M., M. Wiggins, J. Anderson, and A. Hiltner, *Role of oxygen in biodegradation of poly(etherurethane urea) elastomers*. J. Biomed. Mater. Res., 1997. **34**(4): p. 519-530.
31. Hughes-Dillon, K. and L. Schroeder, *Stress cracking of polyurethanes by absorbed steroids*. Polym. Deg. & Stab., 1998. **60**: p. 11-20.
32. Wu, L., B. You, D. Li, and F. Qian, *The in vitro and in vivo stability of poly(urethaneurea)s as biomedical materials*. Polym. Deg. Stab., 2000. **70**: p. 65-69.
33. Hsu, S.-h. and T.-b. Huang, *The susceptibility of poly(ether)urethanes to enzymatic degradation after oxidative pretreatment*. Polym. Deg. & Stab., 2000. **67**: p. 171-178.
34. Labow, R., E. Meek, and J. Santerre, *Hydrolytic degradation of poly(carbonate)-urethanes by monocyte-derived macrophages*. Biomaterials, 2001. **22**: p. 3025-3033.
35. Salacinski, H., N. Tai, R. Carson, A. Edwards, G. Hamilton, and A. Seifalian, *In vitro stability of a novel compliant poly(carbonate-urea)urethane to oxidative and hydrolytic stress*. J. Biomed. Mater. Res., 2001. **59**: p. 207-218.
36. Martin, D., L. Poole-Warren, P. Gunatillake, S. McCarthy, G. Meis, and K. Schindhelm, *New methods for the assessment of in vitro and in vivo stress cracking in biomedical polyurethanes*. Biomaterials, 2001. **22**: p. 973-978.
37. Guignot, C., N. Betz, B. Legendre, A. Le Moel, and N. Yagoubi, *Degradation of segmented poly(etherurethane) Tecoflex induced by electron beam irradiation: characterization and evaluation*. Nucl. Instr. and Meth. B, 2001. **185**: p. 100-107.
38. Thomas, V., T. Kumari, and M. Jayabalan, *In vitro studies on the effect of physical cross-linking on the biological performance of aliphatic poly(urethane urea) for blood contact applications*. Biomacromolecules, 2001. **2**: p. 588-596.
39. Salacinski, H., M. Odlyha, G. Hamilton, and A. Seifalian, *Thermo-mechanical analysis of a compliant poly(carbonate-urea)urethane after exposure to hydrolytic, oxidative, peroxidative and biological solutions*. Biomaterials, 2002. **23**: p. 2231-2240.
40. Ogawa, R., J. Watanabe, and K. Ishihara, *Domain-controlled polymer alloy composed of segmented polyurethane and phospholipid polymer for biomedical applications*. Sci. & Tech. Adv. Mater., 2003. **20**: p. 1-8.
41. Tang, Y., R. Labow, and J. Santerre, *Enzyme induced biodegradation of polycarbonate-polyurethanes: dose dependence effect of cholesterol esterase*. Biomaterials, 2003. **24**: p. 2003-2011.
42. Khan, I., N. Smith, E. Jones, D. Finch, and R. Cameron, *Analysis and evaluation of a biomedical polycarbonate urethane tested in an in vitro study and an ovine arthroplasty model. Part I: Materials selection and evaluation*. Biomaterials, 2005. **26**: p. 621-631.
43. Taylor, J., P. Laity, S. Freeburn, S. Wong, K. Norris, P. Khunkamchoo, M. Cable, G. Andrews, A. Johnson, and R. Cameron, *Effect of processing route and acetone pre-treatment on the biostability of pellethane materials used in medical device applications*. Biomaterials, 2005. **26**: p. 6467-6476.
44. Shin, N., O. Ishii, T. Sueda, and J. Vacanti, *Contractile cardiac grafts using nanofibrous mesh*. Biomaterials, 2004. **25**: p. 3717-3723.

45. Li, D., Y. Guo, Y. Wei, A. MacDiarmid, and P. Lelkes, *Electrospinning polyaniline-contained gelatin nanofibers for tissue engineering application*. *Biomaterials*, 2006. **27**: p. 2705-2715.
46. Badami, A., M. Kreke, M. Thompson, J. Riffle, and A. Goldstein, *Effect of fiber diameter on spreading, proliferation, and differentiation of osteoblastic cells on electrospun poly(lactic acid) substrates*. *Biomaterials*, 2006. **27**: p. 596-606.
47. Stitzel, J., J. Liu, S. Lee, M. Komura, J. Berry, S. Soker, G. Lim, M. Van Dyke, R. Czerw, J. Yoo, and A. Atala, *Controlled fabrication of biological vascular substitute*. *Biomaterials*, 2006. **27**: p. 1088-1094.
48. Rho, K., L. Jeong, G. Lee, B.-M. Seo, Y. Park, S.-D. Hong, S. Roh, J. Cho, W. Park, and B.-M. Min, *Electrospinning of collagen nanofibers: Effects on the behaviour of normal human keratinocytes and early-stage wound healing*. *Biomaterials*, 2006. **27**: p. 1452-1461.
49. Li, C., C. Vepari, H.-J. Jin, H.-J. Kim, and D. Kaplan, *Electrospun silk-BMP-2 scaffolds for bone tissue engineering*. *Biomaterials*, 2006. **27**: p. 3115-3124.
50. McManus, M., E. Boland, H. Koo, C. Barnes, K. Pawlowski, G. Wnek, D. Simpson, and G. Bowlin, *Mechanical properties of electrospun fibrinogen structures*. *Acta Biomater.*, 2006. **2**: p. 19-28.
51. Zong, X., H. Bien, C.-Y. Chung, L. Yin, D. Fang, B. Hsiao, B. Chu, and E. Entcheva, *Electrospun fine-textured scaffolds for heart tissue constructs*. *Biomaterials*, 2005. **26**: p. 5330-5338.
52. Bhattarai, N., D. Edmondson, O. Veiseh, F. Matsen, and M. Zhang, *Electrospun chitosan-based nanofibers and their cellular compatibility*. *Biomaterials*, 2005. **26**: p. 6176-6184.
53. Stankus, J., J. Guan, K. Fujimoto, and W. Wagner, *Microintegrating smooth muscle cells into biodegradable, elastomeric fiber matrix*. *Biomaterials*, 2006. **27**: p. 735-744.
54. Riboldi, S., M. Sampaolesi, P. Neuenschwander, G. Cossu, and S. Mantero, *Electrospun degradable polyesterurethane membranes: potential scaffolds for skeletal muscle tissue engineering*. *Biomaterials*, 2005. **26**: p. 4606-4615.
55. Lee, Y., J. Lee, I.-G. An, C. Kim, D. Lee, Y. Lee, and J.-D. Nam, *Electrospun dual-porosity structure and biodegradation morphology of Montmorillonite reinforced PLLA nanocomposite scaffolds*. *Biomaterials*, 2005. **26**: p. 3165-3172.
56. Lee, C., H. Shin, I. Cho, Y.-M. Kang, I. Kim, K.-D. Park, and J.-W. Shin, *Nanofiber alignment and direction of mechanical strain affect the ECM production of human ACL fibroblast*. *Biomaterials*, 2005. **26**: p. 1261-1270.
57. Min, B.-M., L. Jeong, Y. Nam, J.-M. Kim, J. Kim, and W. Park, *Formation of silk fibroin matrices with different texture and its cellular response to normal human keratinocytes*. *Int. J. Biol. Macromol.*, 2004. **34**: p. 223-230.
58. Inoguchi, H., I. Kwon, E. Inoue, K. Takamizawa, Y. Maehara, and K. Matsuda, *Mechanical response of a compliant electrospun poly(L-lactide-co-e-caprolactone) small-diameter vascular grafts*. *Biomaterials*, 2006. **27**: p. 1470-1478.
59. Yang, F., R. Murugan, S. Wang, and S. Ramakrishna, *Electrospinning of nano/micro scale poly(L-lactic acid) aligned fibers and their potential in neural tissue engineering*. *Biomaterials*, 2005. **26**: p. 2603-2610.
60. Kidoaki, S., I. Kwon, and K. Matsuda, *Mesoscopic spatial designs of nano- and microfiber meshes for tissue-engineering matrix and scaffold based on newly devised multilayering and mixing electrospinning techniques*. *Biomaterials*, 2005. **26**: p. 37-46.
61. Min, B.-M., Y. You, J.-M. Kim, S. Lee, and W. Park, *Formation of nanostructured poly(lactic-co-glycolic acid)/chitin matrix and its cellular response to normal human keratinocytes and fibroblasts*. *Carbohydrate Polym.*, 2004. **57**: p. 285-292.
62. Min, B.-M., G. Lee, S. Kim, Y. Nam, T. Lee, and W. Park, *Electrospinning of silk fibroin nanofibers and its effect on the adhesion and spreading of normal human keratinocytes and fibroblasts in vitro*. *Biomaterials*, 2004. **25**: p. 1289-1297.
63. Mo, X., C. Xu, M. Kotakie, and S. Ramakrishna, *Electrospun P(LLA-CL) nanofiber: a biomimetic extracellular matrix for smooth muscle cell and endothelial cell proliferation*. *Biomaterials*, 2004. **25**: p. 1883-1890.
64. Luu, Y., K. Kim, B. Hsiao, B. Chu, and M. Hadjiargyrou, *Development of a nanostructured DNA delivery scaffold via electrospinning of PLGA and PLA-PEG block copolymers*. *J. Control. Release*, 2003. **89**: p. 341-353.

65. Kim, K., Y. Luu, C. Chang, D. Fang, B. Hsiao, B. Chu, and M. Hadjiargyrou, *Incorporation and controlled release of a hydrophilic antibiotic using poly(lactide-co-glycolide)-based electrospun nanofibrous scaffolds*. J. Control. Release, 2004. **98**: p. 47-56.
66. Kim, K., M. Yu, X. Zong, J. Chiu, D. Fang, Y.-S. Seo, B. Hsiao, B. Chu, and M. Hadjiargyrou, *Control of degradation rate and hydrophilicity in electrospun non-woven poly(D,L-lactide) nanofiber scaffold for biomedical application*. Biomaterials, 2003. **24**: p. 4977-4985.
67. Yoshimoto, H., Y. Shin, H. Terai, and J. Vacanti, *A biodegradable nanofiber scaffold by electrospinning and its potential for bone tissue engineering*. Biomaterials, 2003. **24**: p. 2077-2082.
68. Vaz, C., S. Tuijl, C. Bouten, and F. Baaijens, *Design of scaffolds for blood vessel tissue engineering using a multi-layering electrospinning technique*. Acta Biomater, 2005. **1**: p. 575-585.
69. Li, M., M. Mondrinos, M. Gandhi, F. Ko, A. Weiss, and P. Lelkes, *Electrospun protein fibers as matrices for tissue engineering*. Biomaterials, 2005. **26**: p. 5999-6008.
70. Dalton, P., D. Klee, and M. Moller, *Electrospinning with dual collection rings*. Polymer, 2005. **46**: p. 611-614.
71. Li, W.-J., R. Tuli, C. Okafor, A. Derfoul, K. Danielson, D. Hall, and R. Tuan, *A three-dimensional nanofibrous scaffold for cartilage tissue engineering using human mesenchymal stem cells*. Biomaterials, 2005. **26**: p. 599-609.
72. Chua, K.-N., W.-S. Lim, P. Zhang, H. Lu, J. Wen, S. Ramakrishna, K. Leong, and H.-Q. Mao, *Stable immobilization of rat hepatocyte spheroids on galactosylated nanofiber scaffold*. Biomaterials, 2005. **26**: p. 2537-2547.
73. Berkland, C., D. Pack, and K. Kim, *Controlling surface nano-structure using flow-limited field-injection electrostatic spraying (FFESS) of poly(D,L-lactide-co-glycolide)*. Biomaterials, 2004. **25**: p. 5649-5658.
74. Theron, S., E. Zussman, and A. Yarin, *Experimental investigation of the governing parameters in the electrospinning of polymer solutions*. Polymer, 2004. **45**: p. 2017-2030.
75. Pedicini, A. and R. Farris, *Mechanical behaviour of electrospun polyurethane*. Polymer, 2003. **44**: p. 6857-6862.
76. Gupta, P. and G. Wilkes, *Some investigations on the fiber formation by utilizing a side-by-side bicomponent electrospinning approach*. Polymer, 2003. **44**: p. 6353-6359.
77. Xu, C., R. Inai, M. Kotaki, and S. Ramakrishna, *Aligned biodegradable nanofibrous structure: a potential scaffold for blood vessel engineering*. Biomaterials, 2004. **25**: p. 877-886.
78. Telemeco, T., C. Ayres, G. Bowlin, G. Wnek, E. Boland, N. Cohen, C. Baumgartner, J. Mathews, and D. Simpson, *Regulation of cellular infiltration into tissue engineering scaffolds composed of submicron diameter fibrils produced by electrospinning*. Acta Biomater., 2005. **1**: p. 377-385.
79. Efron, B., and R.J. Tibshirani, *An Introduction to the Bootstrap*. 1993, London: Chapman & Hall/CRC.